

**HOW THE COASTAL GLACIAL SYSTEMS OF THE WESTERN
ROSS SEA IN ANTARCTICA RESPOND TO HOLOCENE CLIMATE
VARIABILITY- RECONSTRUCTION BASED ON GEOLOGICAL
AND GEOPHYSICAL RECORDS FROM TWO CASE STUDIES:
EDISTO INLET FJORD AND ROBERTSON BAY**

by

Francesca Battaglia

A thesis submitted in partial fulfilment of the requirements for the degree of

PhD in Science and Management of Climate Change

at

Cà Foscari University of Venice



XXXIII Cycle

2021/2022

Tutor

Laura De Santis

Istituto Nazionale di Geofisica e Oceanografia (OGS)

Co-Tutor

Florence Colleoni

Istituto Nazionale di Geofisica e Oceanografia (OGS)

Co-Tutor

Christina Riesselman

Otago University, Dunedin, NZ

ABSTRACT

Existing continental-scale reconstructions of the retreat of the Antarctic ice sheet (AIS) during the last deglaciations show that the AIS has experienced substantial changes after the last glacial maximum (LGM, ~ 21 kiloyears ago, ka). The last deglaciation is the most recent, large-scale climate warming interval during which northern and southern hemispheres ice sheets retreated and sea level rise at a non-uniform rate. The Antarctic ice sheet is the main source of uncertainties upon future sea level rise, but little is known about its last deglaciation chronology and factors triggering ice sheet retreat. In the Ross Sea, where the ice sheet has mostly advanced up to the continental shelf edge, the deglacial history remains, however, still debated. In this area, the ice sheet was located below sea level and as such was sensitive not only to atmospheric warming, but also to ocean warming. Therefore, the Ross Sea geological record is particularly suitable to reconstruct rates, mechanism and forcing factors of past ice sheet retreat. These information are crucial to predict future scenario. Marine data compilations indicate that retreat was not simultaneous between the east and the western Ross Sea. This has generally been attributed to differences in pinning areas in seafloor bathymetry. In the western Ross Sea, marine data suggest that the ice sheet had retreated from the continental shelf edge to a mid-shelf position inside the Pennel and Joides basins, by 15 ka, and 13 ka respectively. But the location of the ground line along the coast of Victoria Land is unknown and tentatively located offshore to approximately 8 ka. To fill this knowledge gap, additional marine data from this area are needed. The coastal fjords of North Victoria Land (NVL) are ideal environments to retrieve highly resolved archives as they act as natural sediment traps.

To better understand the significance of these recent changes, I have assimilated a database of new and published marine sedimentary records spanning the Holocene Epoch (the last 11.5 kyrs). The study area includes 2 coastal embayments: Edisto Inlet Fjord and Robertson Bay in the NVL, with expanded sedimentary packages and well-dated cores. Multi-proxy analysis, including, geophysics, sedimentology and geochemistry was conducted at each site to reconstruct glacial history at millennial-scale resolution.

I combine multibeam, reflection seismic data, and oceanographic measurements with the southernmost, first evidence of an expanded, ultrahigh resolution, Holocene sedimentary

section deposited in the Edisto Inlet fjord (North Victoria Land, NVL). I find that post-glacial sedimentation resulted in an up to 130-meters-thick undisturbed diatom ooze (mainly), locally redistributed by bottom currents over confined drifts-moats in the inner part of the fjord. This line of evidence indicates that the Edisto fjord was not carved by grounding ice after the Holocene Climatic Optimum anymore and was subject to seasonal sea-ice free conditions with regular warm water intrusions. Those findings support an early retreat of coastal glaciers by ca. 11 ka from the NVL continental shelf after this period.

In Robertson Bay, the second case study, a protected embayment west of Cape Adare and adjacent to the outlet glaciers of the Transantarctic Mountains, I reported the first geophysical and morphological characterization of the Bay. I compared radiocarbon dates with lithological and geochemical proxies to provide a first-order constraint of the ice sheet retreat in the western Ross Sea. This findings from core BAY05_32c suggest that ice was extended in Robertson Bay during the LGM but the glacio-marine diamicton dated 17.5 ka shows that the ice sheet was no grounded anymore by that time. The multiproxy approach allowed me to study seabed landforms, ice extent, ocean stratification and primary productivity from the Holocene to the present.

The geological and paleoceanographic reconstruction presented in this thesis indicates that, to improve projections of further climate change, global climate models require regional observations for accurate representation of the Antarctic marginal marine environment.

ACKNOWLEDGMENTS

I am immensely grateful to my supervisors Laura De Santis, Florence Colleoni and Christina Riesselman for their guidance, support, and friendship over the last four years. I would like to thank them for their knowledge, enthusiasm, inspiration and careful feedback that has helped me to become a better scientist and encouraging me to aim high. I will be forever grateful for the opportunity to contribute to Antarctic science.

Financial support for this project was provided by several projects of the Italian National Research Program in Antarctica (PNRA), PNRA18_00100 EDISTHO, PNRA16_00016 WHISPERS, PNRA16_00293 GLEVORS and PNRA18_00002 ANTIPODE.

I'm grateful also to the Project STREAM of the Ministry of Foreigner Affairs International Collaboration (MAECI).

I am also grateful to Olivia Truax for her willingness to share her knowledge of palaeoceanographic proxies during the second half of this project. Thank you for answering my questions while I was learning how to interpret my data.

Thanks a lot, to Luca Baradello for helping me with the data processing and I also thank Vedrana Kovacevic, Laura Ursella, Manuel Bensi, Daniela Accettella, Tommaso Tesi, Leonardo Langone, Ester Colizza, Fiorenza Torricella and Dr. Joohan Lee for sharing their knowledge and data.

I would like to thank Ritika for being an incredible friend as we made the decision to undertake this PhD project. Thanks also for all the nightly conversations, for always being there and for your amazing moral support.

I would like to thank Ilaria, for being a friend and also my problem solver when I was panicking with a thousand questions, and for sharing the passion for the polar sciences.

I want to thank my long-time friends Andrea, Domenico, Sergio, Gabriele, Federica, Monica for always inspiring me to follow my passion and for the endless transatlantic videocall.

I would like to thank all the PhD students at Cà Foscari University and OGS for a fun and supportive research journey. Special thanks to Nessim for your enthusiasm and for being a great friend in and out of our office.

I would also like to thank the many people who welcomed me to Dunedin and supported me throughout the last two years and helping to feel home in your beautiful country. To the friends and family at 4 Wycolla Avenue, to Sam, Jack, Fran, Nico, Carline, thanks for all the laughter, cooking Italian classes vs kiwi “culinary style”, dinners, parties and hangovers. This experience would not be the same without you.

More satisfying than submitting this thesis is the knowledge that I have made friends for life.

And to my Family, Mum, Dad and my sisters thank you for everything else. Thank you for believing in me and encouraging me in all of my pursuits. Thank you for being there each and every day. Like a Ph.D., life is full of beauty and opportunity, but it can also be adverse, messy and complicated. Thank you for teaching me that life is about living in the moment, and above all about being true to yourself. This thesis is for you.

TABLE OF CONTENTS

Abstract	i
Acknowledgments	iii
List of Figures	x
List of Abbreviations	xii
Declaration	1
1 Introduction	
1.1 Antarctica’s role in the global environment.....	2
1.2 Rationale	4
1.3 Research objectives.....	6
1.4 Regional setting	7
1.5 Oceanographic setting.....	13
1.5.1 Sea ice	17
1.6 Sedimentation in polar environment.....	18
1.6.1 Continental shelf	20
1.6.2 Continental slope	22
1.7 Fjords: formation and sediment dynamics.....	26
1.7.1 Broader context.....	28
1.7.2 Glacio-marine sedimentary process.....	29
1.7.3 The polar fjords.....	31
1.7.3.1 Antarctic fjords	32
1.8 Glacial processes and landforms.....	33
1.8.1 Marginal moraines	36
1.8.2 Glacial striations	36
1.8.3 Meltwater channels	37
1.8.4 Glacial lineations	37
1.8.5 Drumlins	38
1.8.6 Crag and tail.....	39
1.8.7 Grounding zone features	39
2 Research Context	
2.1 Ice Sheets, ice shelves and climate change.....	40

2.2 The Antarctic contribution to sea level rise	41
2.3 Mass loss from Antarctica	43
2.3.1 Mechanism of rapid mass loss from AIS	45
2.4 The importance of Antarctic ice shelves.....	47
2.5 The Ross Ice shelf, West Antarctica.....	48
2.5.1 Variations since the Last Glacial Maximum	49
2.5.2 Future prospects	49

3 Methodology

3.1 Introduction	51
3.2 Project goals.....	51
3.3 Geophysical methods.....	52
3.3.1 Bathymetric survey	52
3.3.2 Data acquisition and processing.....	53
3.3.3 Seismic reflection method	53
3.3.3.1 The Sub-Bottom profiler	57
3.3.3.2 SBP acquisition and processing	57
3.3.3.3 Processing data	58
3.4 Tool for paleo - reconstructions	61
3.4.1 Marine sediment cores	61
3.4.1.1 Marine sediment cores database	61
3.4.2 Diatom ecology	63
3.5 Geochemistry	66
3.5.1 The carbon isotopes proxy	66
3.5.2 The nitrogen isotopes proxy	67
3.5.3 Robertson Bay C and N analysis	68
3.5.4 Carbon to nitrogen ratio (C:N).....	69
3.5.5 The biogenic silica proxy	69
3.5.5.1 Biogenic silica (BiS) concentration method	71
3.6 Chronology	74
3.6.1 Antarctic radiocarbon chronology	74
3.6.2 Challenges of dating Antarctic sediment.....	74
3.6.3 Recent advance in Antarctic radiocarbon dating	74
3.6.4 Marine reservoir effect	76

3.6.5 Radiocarbon calibration	77
3.6.5.1 Ramped Pyrolysis (RP) radiocarbon method	78
3.6.5.2 Ramped Pyrolysis split analysis	78
3.6.5.1 RP delayed results due to Covid-19 pandemic	79
3.6.6 Edisto Inlet and Robertson Bay radiocarbon calibration	79

4 Edisto Inlet Fjord

4.1 Introduction.....	82
4.2 Study Site.....	84
4.3 Data and methods.....	86
4.3.1 Geophysics data	86
4.3.2 Sediment cores	87
4.3.3 Sedimentological analysis.....	88
4.3.3.1 Grain size analysis	89
4.3.3.2 Diatoms analysis	89
4.3.4 Oceanographic data.....	90
4.4 Results.....	91
4.4.1 Seismic facies	91
4.4.2 Bathymetry and submarine landforms	96
4.4.3 Stratigraphic data	98
4.4.3.1 Cores description.....	100
4.4.3.2 Lithostratigraphic facies	102
4.4.3.3 Correlation between seismic data and sediment core.	107
4.4.4 Sediment drifts.....	109
4.4.4.1 Sediment drifts formation.....	110
4.5 Discussion	113
4.5.1 Evidence of past glacial dynamics.....	113
4.5.2 Post – LGM progressive opening of the Fjord	114
4.5.3 Preserved Late Holocene high resolution sedimentary record...116	
4.5.4 Edisto Inlet post LGM evolution	117
4.6 Conclusions.....	121

5 Robertson Bay

5.1 Introduction.....	122
-----------------------	-----

5.2 Regional setting.....	124
5.3 Oceanography	125
5.4 Data and Methods	127
5.4.1 Multibeam bathymetry and Sub-Bottom profiles.....	127
5.4.2 Sedimentological analyses	130
5.4.2.1 Grain size analysis	130
5.4.2.2 Diatom relative abundance	130
5.4.2.2.1 Diatom Paleocology	131
5.4.3 Geochemical analyses	131
5.4.4 Chronology	132
5.5 Results.....	133
5.5.1 Glacial landforms	133
5.5.1.1 Description of glacial landforms.....	135
5.5.2 Seismic facies	140
5.5.3 Seismo - stratigraphy	143
5.5.4 Stratigraphic data	148
5.5.4.1 Cores description	149
5.5.4.1.1 Lithostratigraphic facies	149
5.5.5 Geochemical Proxies	150
5.5.5.1 Core 29c	150
5.5.5.2 Core 32c	151
5.6 Discussion.....	153
5.6.1 Interpretation of glacial landforms.....	153
5.6.2 Core BAY05_29c and 32c proxy data reconstruction	158
5.6.3 Robertson Bay Post – LGM evolution	162
5.7 Conclusions.....	166

6 Conclusions and future work

6. Conclusions.....	170
6.1 Edisto Inlet Fjord	171
6.2 Robertson Bay.....	171
6.3 Evolution post LGM: comparison between Edisto Inlet Fjord and Robertson Bay.....	173
6.4 Forward look.....	175

7 Bibliography 176

Appendices

Appendix A – Grain size data

Appendix B - Bulk radiocarbon dates tables

Appendix C - Geochemical data sets

Appendix D - Published paper: Baradello, L., Battaglia, F. & Vesnaver, A. Fast method to transform chirp envelope data into pseudo-seismic data. *Mar Geophys Res* 42, 14 (2021).

LIST OF FIGURES

<i>Number</i>	<i>Page</i>
1.1 Geography map of the North Victoria Land in the western Ross Sea.	6
1.2 Antarctica. From USGS Landsat Image Mosaic of Antarctica (LIMA).	8
1.3 Basic differences between EAIS and WAIS.....	10
1.4 Scheme of an ice stream and ice stream processes	11
1.5 LIMA Antarctica Maps.....	12
1.6 Sea Ice maximum and minimum concentration around Antarctica	14
1.7 Oceanic Currents around Antarctica.....	15
1.8 Water masses in Southern Ocean.....	16
1.9 Ice streams, Ice sheet and Ice shelf.....	19
1.10 Ice velocities	20
1.11 Ice sheet advances and retreats following glacial and interglacial phases.....	22
1.12 Classification scheme for submarine bottom flow types	23
1.13 Sediment drift types and inferred bottom-current paths	26
1.14 A fjord carved by glaciers with steep rock walls.....	27
1.15 Schematic evolution of a valley resulting from glacial erosion.....	28
1.16 Processes Affecting Tidewater Glaciers	29
1.17 Transport mechanisms within fjords	31
1.18 Sediment delivery systems (SDS) within glacial environments	34
1.19 Cartoon of the transition and distribution of glacial geomorphic features	35
2.1 Geography of the Antarctic continent.....	41
2.2 Changes in ice volume for WAIS, EAIS, Antarctic Peninsula and AIS.....	44
2.3 Bed elevation of the Antarctic continent	46
3.1 Multibeam echo sonar (MBES).....	52
3.2 Principal mechanism behind SBPs	55
3.3 Filter cleaning outgoing Chirp pulse	57
3.4 Example of raw data and after electrical clean and amplitude recovery	59
3.5 Example of gained data and after deconvolution and sea waves correction.....	60
3.6 Diagram of the oceanographic controls on nutrient availability to diatoms	68
3.7 Silica cycle in the marine environment.	70
3.8 Photos of the procedure used during the analysis of biogenic silica	71
3.9 Comparison of ¹⁴ C ages from bulk AIOM, RP, carbonate	75
4.1 Map of Edisto Inlet	85
4.2 Multibeam swath bathymetry of Edisto Inlet Fjord and cores location.....	88
4.3 Seismic facies classification	91
4.4 Chirp record showing the general seismic stratigraphy in Edisto Inlet fjord	92
4.5 Chirp profile with evidence of thrust faults within the seismic facies EII.....	93

4.6 Isopach map showing the thickness variations of the seismic unit EI.....	94
4.7 SBP track lines show an elongated sediment drift thick 130 m.....	95
4.8 3D representation of the outer fjord showing the seafloor landforms	96
4.9 3D multibeam swath bathymetry of the deepest depression in Edisto Inlet	97
4.10 XRay, Photo, MS and lithofacies of the core:CH41, 14c, 18c, 20c.....	105
4.11 Xray and MS curve of the core BAY05-22c, GC-03 and GC-04.....	106
4.12 SBP showing core HLF17-01location and MS	107
4.13 Location of core 18c with MS, gran size and ¹⁴ C plotted on the SBP	108
4.14 Multibeam map shows the position of the sediment drifts	110
4.15 Vertical transect of the currents from the vmADCP above SBP	111
4.16 Oceanographic properties in the Edisto Inlet.....	112
4.17 Cartoon of the Post-LGM Progressive opening phases of Edisto Inlet	120
5.1 Map of Robertson Bay and the Adare Peninsula.....	124
5.2 Satellite image of Terra Nova Bay polynya from NASA	126
5.3 Schematic of the movement of water masses in the Ross Sea.....	127
5.4 Bathymetric map of Robertson Bay, SBP and cores location	128
5.5 Geographic Map of Robertson Bay with geophysics dataset and cores	129
5.6 Geographic Map of Robertson Bay highlighted the 2 sectors in RB.....	133
5.7 3D Bathymetric data collected from sector 1 of Robertson Bay (RB)	134
5.8 Relief shaded bathymetric map of Robertson Bay with mapped landforms ...	138
5.9 3D swath bathymetry of submarine elongate ridges.....	139
5.10 SBP showing two lateral moraines	139
5.11 SBP showing two cross- sections of the elongated ridges.	140
5.12 Seismic Facies Classification.....	142
5.13 SBP showing elongated ridges, depressions and stratified basin	143
5.14 SBP with location and seismic facies of the sediment cores 29c and 32c	144
5.15 SBP showing lateral moraine and stratified basin filled in RB	146
5.16 Elongated drifts and confined drifts recognized in Robertson Bay	147
5.17 Physical properties, grain size, BSi, TOC of the core 20c and 32c	148
5.18 Core 29c, weight percent biogenic silica, $\delta^{13}\text{C}$, and C:N ratio,.....	151
5.19 Core 32c, weight percent biogenic silica, $\delta^{13}\text{C}$, and C:N ratio	152
5.20 Summary results figure core 29c ¹⁴ C, MS, BSi, $\delta^{13}\text{C}$, ADA	157
5.21 Summary results figure core 32c ¹⁴ C, MS, BSi, $\delta^{13}\text{C}$, ADA	158
5.22 Holocene environmental trends in Robertson Bay core 32c.....	160
5.23 Holocene environmental trends in Robertson Bay core 29c.....	161
5.24 Proposed paleoenvironmental evolution model of Robertson Bay.....	165

LIST OF ABBREVIATIONS

AABW Antarctic Bottom Water	MICI Marine ice cliff instability
AASW Antarctic Surface Water	MISI Marine ice sheet instability
AACC Antarctic coastal current	MS Magnetic susceptibility
ACC Antarctic circumpolar current	NVL North Victoria Land
ADA Absolute diatom abundance	PDB Pee Dee Belemnite
AIS Antarctic Ice Sheet	PNRA Programma Nazionale di Ricerca in Antartide
AP Antarctic Peninsula	RB Robertson Bay
BSi Biogenic silica	R/V Research Vessel
CDW Circumpolar Deep Water	RIS Ross Ice Shelf
C:N Carbon to Nitrogen ratio	SBP Sub Bottom Profile
CO₂ Carbone dioxide	TAM The Transantarctic Mountains
CRS <i>Chaetocerus</i> resting spore	TOC Total organic carbon
CTD Conductivity-Temperature-Depth	WAIS West Antarctic Ice Sheet
DEM Digital elevation model	¹⁴ C Carbon -14
EAIS East Antarctic Ice Sheet	$\delta^{13}\text{C}$ Ratio of carbon-13 to carbon 12
GMSL Global mean sea level	$\delta^{15}\text{N}$ Ratio of nitrogen-15 to nitrogen-14
GZW Grounding zone wedge	$\delta^{18}\text{O}$ Ratio of oxygen-18 to oxygen-16
HSSW High salinity shelf water	
ISW Ice shelf water	
IPCC Intergovernmental Panel on Climate Change	
MBES Multibeam echo sounder	
MSGIs Mega scale glacial lineations	
mCDM Modified Circumpolar Deep Water	

DECLARATION

This dissertation is my own work and contains six chapters, Chapter 1 outlines the main thesis objectives with a description of the rationale behind each objective and a general introduction of Antarctica. Chapter 2 provides the research background and theoretical context for the main chapters; Chapter 3 provides the methods and the collected data used for the thesis; Chapter 4 and 5 present the two-case study Edisto Inlet Fjord and Mac Robertson Bay like stand-alone papers each with their own introduction, method, results, discussion and conclusion sections.

Chapter 6 synthesizes the preceding chapters, summarizes the main results, and concludes with recommendations for further work.

This thesis contains published material. The contents of Chapter 3 appear in Baradello, L., Battaglia, F. & Vesnaver, A. Fast method to transform chirp envelope data into pseudo-seismic data. *Mar Geophys Res* 42, 14 (2021). <https://doi.org/10.1007/s11001-021-09436-y>

Chapter 1

1. INTRODUCTION

1.1 Antarctica's role in the global environment

During the past decade there has been a great increase in interest and awareness of global climate change. The warming of the Earth's climate has been observed in air and ocean temperatures with effects such as melting of sea ice and glaciers and consequently a rise of global average sea level (Comiso et al., 2008). However, better understanding of the environmental impacts from a changing climate and of the climate system's response to different forcing is needed. In this context, a long-term perspective of the past environmental evolution of the ocean and terrestrial system is required. However, a perspective reaching beyond that provided by instrumental records (Moberg et al., 2005) can only be obtained from geological archives.

To understand how human activities are influencing the environmental changes and what mitigation policies of greenhouse gas emissions must be implemented, we must understand what are the natural mechanisms that control the climate.

Climate change is affecting all parts of the Earth and some of the impacts in Antarctica are among the most pronounced on the planet.

Antarctica is a keystone to understand the past and present status of the Earth system, as well as to predict future figures of our planet as viewed from the polar region. The Antarctic region is composed by an ice-covered continent and it is surrounded by the Southern Ocean. It has been only partially explored, since the International Geophysical Year (1957-58) requiring innovative technological development and significant logistic effort involving all scientific branches of bioscience, physical sciences, geosciences, oceanography. Scientific challenges in the Antarctic include reconstructing the signature of the presence of the ice sheets, ice shelves, glaciers, and sea-ice in and around the continent during its past evolution. In this concern, particularly the cryosphere system is likely to be influenced by temporal spatial variations in the atmospheric and ocean changes, and continuous researches of their variability provide direct evidence of climate change.

The Antarctic ice sheet plays a pivot role in global sea-level and thermoaline circulation changes. Presently, much of the cold and dense bottom water that feeds the Southern Oceans is produced in large polynyas of the Ross and Weddell Seas, seaward of the largest fringing ice shelves of the West Antarctic Ice Sheet (WAIS). Models predict that destabilization of the WAIS, caused by atmospheric and oceanic warming, may result in large melt water discharges to the Southern Ocean. Such discharges have the potential to disrupt global thermohaline circulation and increase global sea levels, with important implications for Earth's climate system (Jacobs et al., 2002; Shepard et al., 2004; Steig et al., 2009).

Monitoring change in the climate, cryosphere and biosphere of Antarctica is therefore a critical element in understanding and predicting future global change.

Much of what is known about the evolution of Antarctica's cryosphere in the geologic past is derived from ice-distal deep-sea sediment records. Advanced Piston Corer in ocean drilling technology and climate proxy methods have made it possible to retrieve and interpret high-quality ice-proximal sedimentary sequences from Antarctic's margins and the Southern Ocean. These records contain a wealth of information about the individual histories of the East and West Antarctic Ice Sheets and associated temperature change in the circum Antarctic seas that are only obtainable via geologic drilling. For example, studies of Antarctic drill cores from the Ross Sea (Naish et al., 2007; Naish et al., 2009) provide evidence of dynamic climate variability on both short and long timescales over the past 35 million years. Integrated discoveries from recovered ice proximal records and distal deep-sea geochemical records (e.g. Naish et al., 2009; McKay et al., 2012) are improving the understanding of the links between past Antarctic ice-volume fluctuations and oceanographic changes necessary for understanding Earth's long-term climate evolution.

Marine seismic surveys are means for mapping subsurface geologic structures and stratigraphy over large areas (Bart, P.J. and L. De Santis. 2012). Marine geophysical studies e.g. Bartek, L et al (1997); Viseras et al (1999); Escitia et al (2000); Rebesco et al (2006); Hockmuth et al. (2019), show how the continental margin of Antarctica has been influenced for tens of millions of years by glacial processes and resulted in the development of a morphology very different from the one of low latitude continental margins (Bartek, L et al 1997). In particular, the shelf is over deepened and landward dipping due to glacial erosion largely affecting the internal sectors and by ice loading depressing the subglacial and ice proximal areas. The sediments are generally filling tectonic basins and are transported and deposited at and beyond the continental margin. Large trough-mouth fans develop at the ocean termination of main ice streams. A fully protected large-scale marine reserve in the

Ross Sea, in particular, offers science a unique natural laboratory to study the impacts of climate change free from the influence of other types of human activity.

Exploring the Antarctic time capsule is so the key for reconstructing the Antarctic ice sheet and ocean history over the past millions of years. The Antarctic ice sheet evolution history has experienced a large array of global climate and environmental changes since its onset, such as changes in atmospheric carbon dioxide concentration, which affects atmospheric and ocean temperature and consequently marine productivity of the Southern Ocean and Antarctic Bottom water formation (AABW), the main driver of global ocean circulation, and sea level change due to increase and decrease of Antarctic ice sheet.

In efforts at investigating these issues, Antarctic paleoenvironmental studies provide essential information to understand the trends and impacts of global climate change.

Continuous records of paleoenvironmental changes can be obtained from marine sediments, geophysics data, lake sediments and ice cores.

This thesis reports an integrated morpho-bathymetric and seismo-stratigraphic analysis for paleoclimatic reconstruction based on geophysical, geological and paleo climatic information from the Edisto Inlet fjord and Robertson Bay along the Ross Sea continental shelf.

The multidisciplinary approach has allowed the discovery of a Holocene sedimentary record of great paleoclimatic importance.

1.2 Rationale

The study of late Quaternary sequences at high latitude allows to more directly reconstructing the fluctuations of the ice sheet, from maximum to minimum extension reached during glacials and interglacials. This information is needed to estimate the contribution of the ice sheet to global sea level changes. Information on glacier variations in Antarctica is limited and sometimes contradictory, mainly related to different ice sheet evolution in different ice catchment/drainage areas and also due the lack of enough data and difficulty in dating glacial sediments. However, if the behaviour of the glaciers during the recent past can be better understood, it helps to evaluate their sensitivity to climatic changes, so that their contribution to the sea level variation may be more realistically predicted (Baroni and Hall 2004).

Understanding sediment type and spatial distribution is critical for studies reconstructing glacial and ice-sheet behaviour based on paleo-records (e.g., Naish et al. 2009; Anderson et al. 2011; Fernandez, Anderson, Wellner et al. 2011; Stokes et al. 2015). Previous studies in the western Ross Sea continental shelf document that interglacial phases are characterized by deposition of diatom mud (Tolotti et al 2013; Kim et al 2020; Khim et al 2021). The presence of this type of sediment in the geological record is interpreted as representing the establishment of seasonally sea ice open climatic conditions. However interglacial diatom mud deposits are difficult to find, because they have been mostly eroded by grounding ice sheet, during subsequent glacial expansion, remolded by icebergs or swept by bottom currents. Coastal bays and deep fjords are potentially good candidates to preserve expanded geological records of past interglacials. This is the case in all the Antarctic margins as it was shown by ODP Leg 178 (Domack et al., 2001) and IODP Expedition 318 (Escutia et al., 2011; Behrens et al., 2022) These basins do exist as well in the Ross Sea and can have the same potential as past environmental change recorders e.g Prothro et al. 2018 and Wellner et al. 2014 show that the sediment deposited after the LGM in the Ross Sea, are located mainly in inner shelf basins (where it is preserved from the action of icebergs and of strong bottom currents impinging the continental margin).

Tidewater glaciers generally respond more rapidly to climatic fluctuations than large ice sheet because they have small drainage areas and high accumulation rates (Anderson 1999). Rapid sediment accumulation generally is observed in temperate and subpolar fjords and coastal bays where tidewater glaciers are debouching and into which they carved deep depressions during maximum expansion. These depressions are now filled with high-resolution sedimentary record, deposited after glacier retreat. These sedimentary records can be used as a tool to reconstruct environmental changes during past glacial and interglacial times. Environmental variations are reflected in the cyclic alternations between glacial facies (mainly diamicton and silty-clay mudstone with ice rafted debris - IRD) and open marine facies (biogenic-rich, silty-clay mudstone). However, characteristics of a single bay can be widely variable, from the number and type of glaciers draining into the same bay and of processes carrying and depositing sediment in and out of the bay. Numerous factors control sedimentation in fjords, including climate, seafloor topography, bay geometry, oceanographic regime, the presence of sea ice, the size of drainage areas and proximity to sediment sources (Griffith & Anderson 1989; Domack & McClennen 1996; Ashley & Smith 2000). Each of these contributes differently to the distribution of sediment along the bays. Therefore, when applying any model of sediment distribution in a fjord or in a bay

environment, one must take into account how local versus regional variations of bay systems variations affect sediment distribution.

1.3 Research Objectives

The aim of this study is to reconstruct the response of the East Antarctic Ice Sheet to warming associated with deglaciation and the Holocene climatic optima at the interface between the Ross Sea and the Southern Ocean by investigating the dynamics of small glacial systems along its periphery.

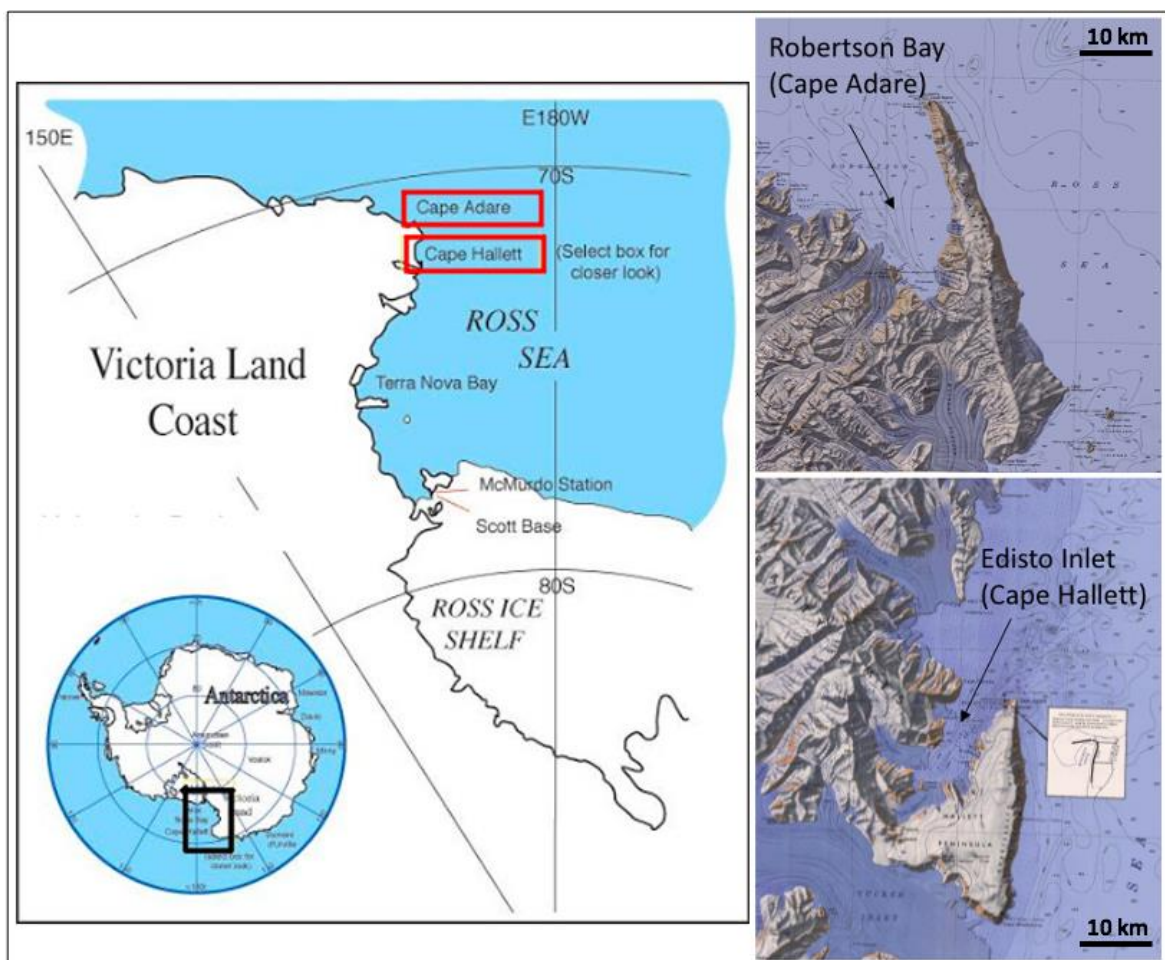


Figure 1.1: Geography map of the North Victoria Land in the western Ross Sea. Location and topographic map of the study areas Edisto Inlet Fjord and Robertson Bay. (1:250,000-scale topographic maps have been published by the U.S Geological Survey in cooperation with the National Science Foundation).

The study areas include the Edisto Inlet Fjord and Robertson Bay (Figure 1.1), located along the North Victoria Land in the western Ross Sea. Their location, at the immediate termination of the EAIS close to the continental shelf margin, where water masses forming

in the Ross Sea polynya mix with ocean waters, makes the Edisto inlet Fjord and Robertson Bay key sites for investigating the effects on the glaciomarine depositional environment where to retrieve highly resolved archives as they act as natural sediment traps.

This can be addressed by aiming at three key objectives:

The first objective is to understand the dynamics of sedimentary processes in the fjords and map the areas with the highest vulnerability related to the last deglaciation phase.

I performed that Integrating bathymetric and seismic data with the purpose to defining the geometry and spatial distribution of depositional and erosional features. The aim was to infer sedimentary processes and their variation during past glacial advance and retreat and current circulation changes in the Edisto Inlet and Robertson Bay.

The second objective is to investigate which were/are the boundary climatic, oceanographic, geological conditions that determine the response of depositional systems to climatic changes in the North Victoria Land coastal bays (in the Holocene and may be earlier) and in the North western Ross Sea continental margin since the Pliocene.

The third objective is to collect observations to perform models for reconstructing the North Victoria Land coastal bays evolution, and the north western Ross Sea margin evolution.

1.4 Regional Setting

Isolated from the other continents by the Antarctic Ocean and its strong circumpolar current, Antarctica is the southern-most continent, and the only one entirely characterized by a polar climate. It covers an area of about 14 million km², contains 30 million Km³ of ice and is located southern of the Antarctic Circle. The Antarctic Ice Sheet, the largest single mass of ice on Earth, covers more or less the 98% of the continent itself (Ingólfsson et al., 1998) (Figure 1.2).

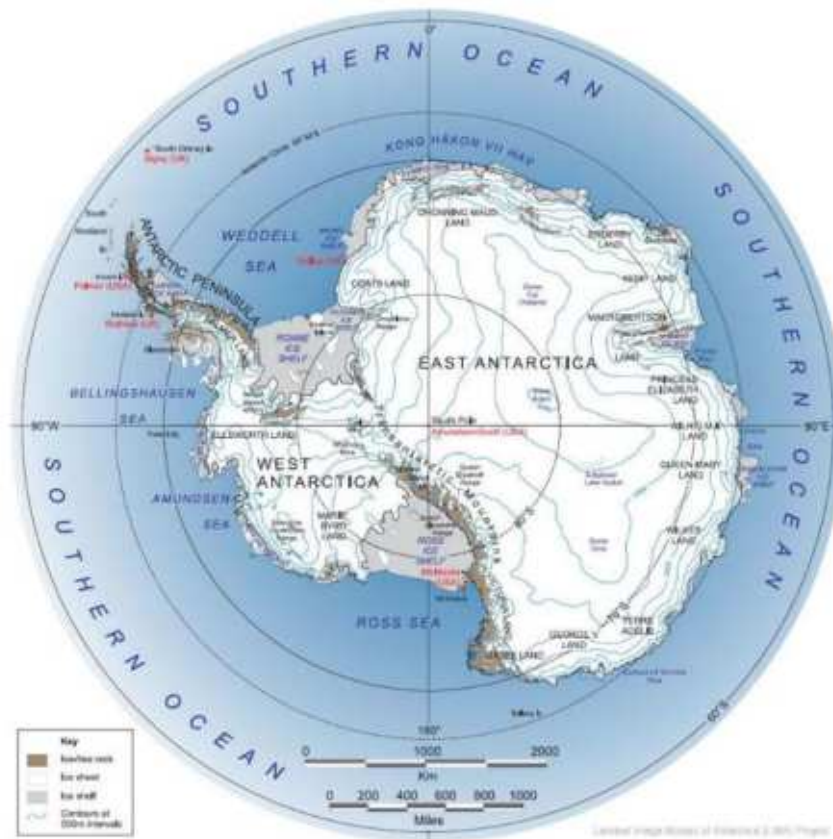


Figure 1.2: Antarctica. From USGS Landsat Image Mosaic of Antarctica (LIMA).

The Antarctic continent played a key role in the regulation of climate, oceanography, sea level changes during glacial and interglacial phases that characterized most of the Cenozoic Era. The white continent has not always been frozen: during the Cretaceous Era, its position was further north, where nowadays we can find South America. The tectonic evolution of Antarctica in the Cenozoic was characterized by the igneous activity that was formed as a result of simultaneous continental rifting and subduction processes acting during the final stages of the southward drift of Gondwana towards the South Pole.

There are many theories about its formation one of the most accredited is that it could be the result of modifications to the Drake Passage, the body of water between South America and Antarctica, which deepened about 35 million years ago and triggered a radical change in ocean currents. The growing separation between Antarctica and South America has created a powerful underwater current called the Antarctic Circumpolar Current (ACC). The ACC prevented the warmer waters of the North Atlantic and Central Pacific from moving towards Antarctica, isolating it and allowing ice sheets to form.

The Transantarctic Mountains (TAM) appear to be the major structural and morphological

partition line, also due to their partial coverage by the Antarctic Ice Sheet. The principal mountain range started to raise at the end of Mesozoic, above the Paleozoic Ross orogenesis. It extends for almost 3500 km, strongly affecting the Antarctic morphology. TAM results to be a clear separation between East and West side of Antarctica. Two main parts are identifiable: East Antarctic Ice Sheet (EAIS) and West Antarctic Ice Sheet (WAIS), gone through a distinct evolution resulting in differences in size, shape and dynamism (Anderson et al., 1999; Curtis M.L. 2001; Jordan et al 2020; Storey et al 2021). An ice sheet is generally defined as a mass of ice that covers a total area of more than 50000 km² (Bates J.A. et al., 1987), consisting mainly of continental ice, of meteoric origin. The EAIS, although it has large areas where the ice sheet is marine-based, covers much of the continental area, so it is considered more stable, although some recent studies and models from the marine sediment record, and glaciological modelling strongly supports the hypothesis of the 14-million-year stability of the EAIS, the main ice mass on Earth (Cook et al., 2013; Andrè, 2017; Sangiorgi et al., 2018; Wilson et al., 2018). Anyway, East Antarctic Ice Sheet presents about 9 times the volume of the western one, as an average thickness of 2226m compared with the WAIS maximum of 1306m, reaches a higher elevation (over 4000m), and a maximum thickness of 4776m. The WAIS is mostly marine-based, and it would speed up the ice flow after the ice sheet collapse, increasing considerably sea level. It covers a continental archipelago, and therefore is anchored on sparse bedrock pinning points, but still results as more vulnerable and unstable than EAIS, in case of sea level rise that will foster detachment of the ice sheet from the bottom and its subsequently rapid melting/disintegration (Joughin et al., 2014) (Figure 1.3). Indeed, the marine WAIS instability hypothesis presumes that atmospheric and oceanic warming could result in increased melting and recession at the grounding line on such a reverse slope gradient. This would activate flotation, basal melting, increased iceberg production, and further retreat within a positive feedback loop (Andrè, 2017).

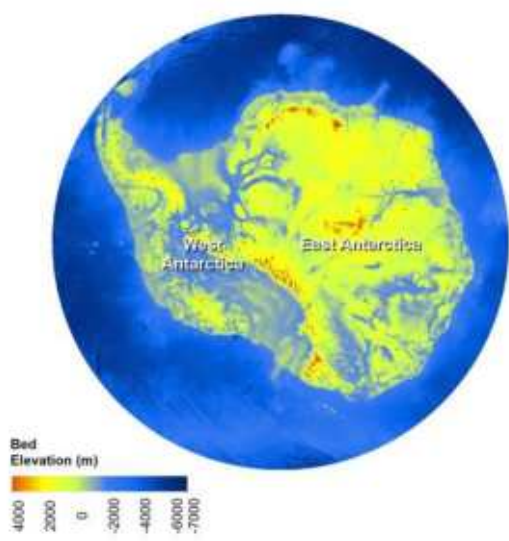
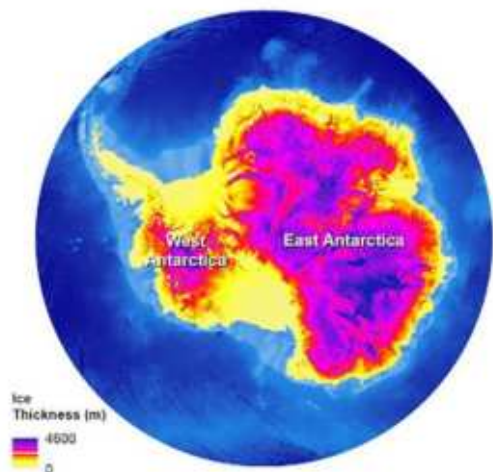
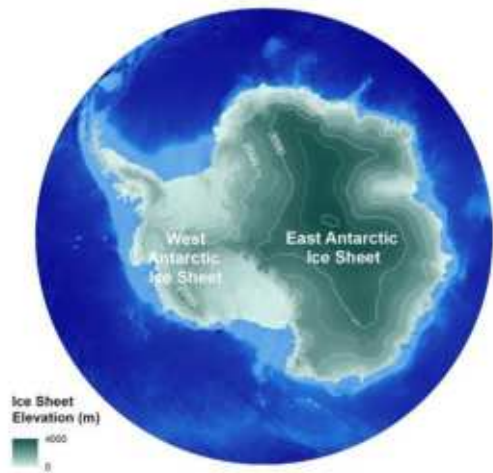


Figure 1.3: Basic differences between EAIS and WAIS: ice elevation, thickness, bedrock elevation (From BedMap2).

One fundamental but also controversial problem in Antarctica, indeed, concern mass balancing and ice sheet stability. The mass balance is defined as the net result of mass gains above the ice sheet (snow deposition) and mass loss by melting (either at the glacier surface or under the floating ice shelves or ice tongues) and by ablation caused by calving processes (production of icebergs) (Hanna et al. 2013).

An essential role in regulating mass balance is played by ice streams, both for the water volume and the sediment volume they transport, flowing through the ice sheet. Ice streams are corridors of fast-flowing ice within an ice-sheet and they can reach a velocity of 500 m/year (Whillans I.M. Et al., 1993, Scheuchl et al., 2012) discharging ice and sediments into the sea. Even if they represent only 10% of the volume of the ice sheet, ice streams present considerable dimensions, up to 50 km in width, 2000 m in thickness and hundreds of km in length (Bennett, 2003) (Figure 1.4).

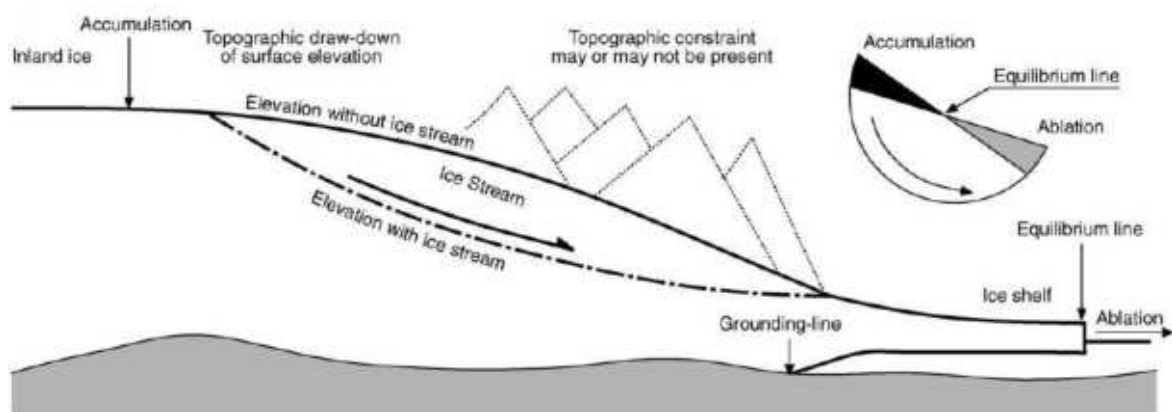


Figure 1.4: Scheme of an ice stream and ice stream processes (From Bennett, 2003).

Ice streams are fed by complex inflows that extend up to 1000 km towards the inner ice sheet (Bamber J.L. et al., 2000). Ice stream differs from outlet glacier because is bordered by ice instead of rocks, and from shelf ice because it is not floating (Bentley, 1987). Satellite data reveal widespread, patterned, enhanced flow with tributary glaciers reaching hundreds to thousands of kilometres inland, over the entire continent (Rignot et al., 2011). Because of all these characteristics, ice streams behaviour and their stability have an important role in the study of the ice sheet dynamics and mass balance (Bennett M.R., 2003).

Ice sheet mass balance results in Rignot et al 2019 reveal that in the Antarctic ice sheet from 1979 to 2017 mass loss was dominated by sectors of the Amundsen / Bellingshausen Sea in West Antarctica (159 ± 8 Gt / a), Wilkes Land, East Antarctica (51 ± 13 Gt / y) and the western and north-eastern peninsula (42 ± 5 Gt / year) During the whole period, the mass

loss was concentrated in areas closest to warm, salty, deep circumpolar deep waters (CDW), that is, consistent with the increase in the westerlies polars pushing CDW towards Antarctica to melt its floating ice shelves, destabilize glaciers and raise sea levels.

Drainage from the EAIS and WAIS are divergent mainly toward Ross, Ronne-Filchner, Amery, Larsen C, Riiser-Larsen, Finbul, Shackleton, George VI, West, Wilkins, and Totten ice shelves (Figure 1.4). The biggest and largest ice steams draining WAIS flow into Weddell, Ross and Amundsen Sea (Figure 1.5).

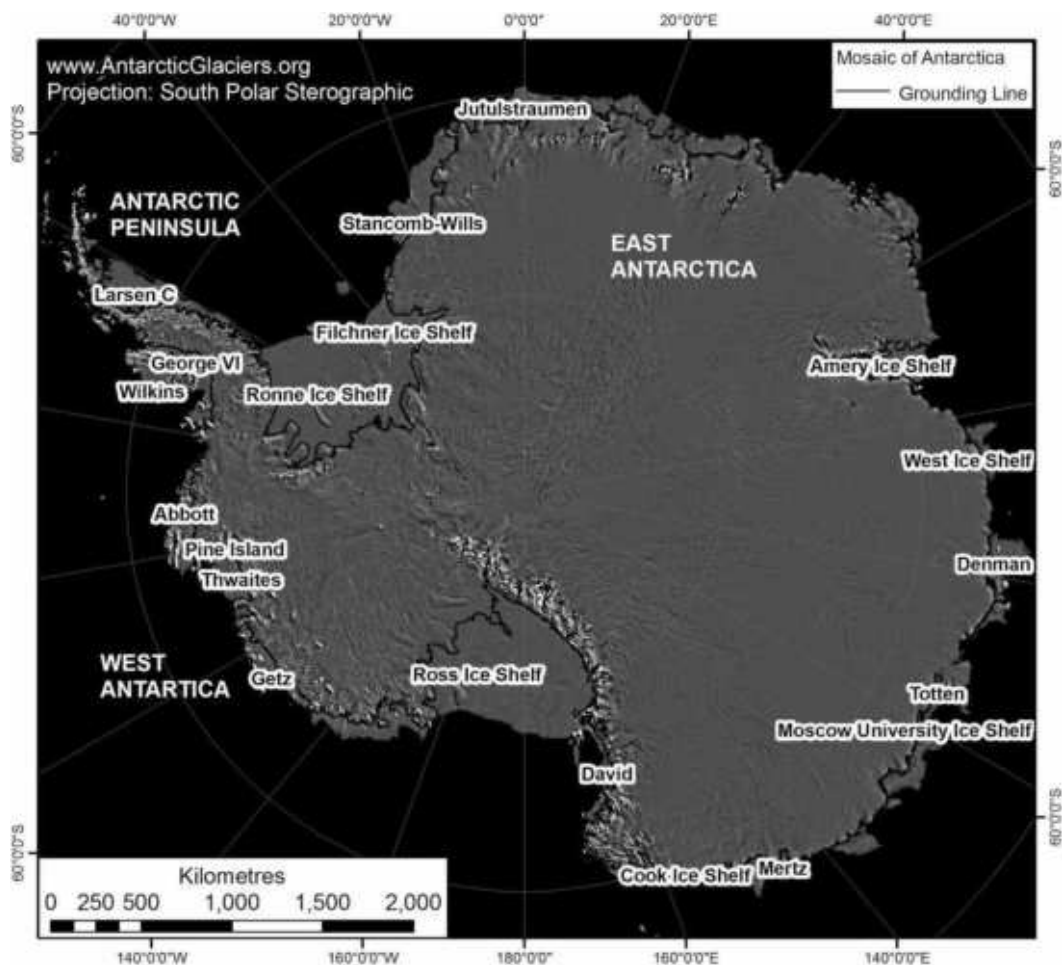


Figure 1.5: LIMA Antarctica Maps.

Another important element in the Antarctic system is given by the presence of thick floating ice shelves, bordering the seaward termination of the ice sheet: in some places, the ice shelf is strongly anchored to submerged banks, which play a key role buttressing the ice sheet. Ice shelves can be divided in three main categories: ice shelves fed by glaciers, ice shelves created by sea ice and local snowfall, and composite ice shelves (Jeffries, 2002). The withdrawal of the ice shelf in some coastal areas accelerates the icebergs calving from

glaciers and ice streams; this phenomenon affects the reduction in the ice sheet volume and size. A significant ice shelf retreat occurs on the Larsen Ice Shelf, on the eastern side of the Antarctica Peninsula, but all West Antarctic shelves can also be susceptible to fast melting and disintegration. In recent decades, reductions in the thickness and extent of floating ice shelves have destabilized inland ice flow, triggering retreat, acceleration and drawdown of many marine-terminating ice streams (The IMBIE Team, 2018).

1.5 Oceanographic Setting

The Southern Ocean surrounds Antarctica. It is the only region where the thermohaline circulation, can continue barely disturbed all around the globe. In this point of view, the ocean circulation becomes closest to the situation in the atmosphere without any boundary constraint. The Antarctic Circumpolar Current (ACC) is the major ocean current that flows clockwise from west to east around Antarctica. An alternative name for the ACC is the West Wind Drift. The ACC is the dominant circulation feature of the Southern Ocean and has a mean transport estimated at 100-150 Sverdrup (Sv, million m^3/s), or possibly even higher, making it the largest ocean current. The current is circumpolar due to the lack of any landmass connecting with Antarctica and this keeps warm ocean waters away from Antarctica, enabling that continent to maintain its huge ice sheet. Antarctica presents an unlimited communication with all oceans: the hydrology of all ocean basins cannot be understood without considering the dynamics of processes occurring on the Antarctic margin.

The presence/absence of the sea ice is very important in the entire climate system. The extension of the sea ice around Antarctica changes seasonally significantly: in austral winter it covers the whole Southern Ocean up to about 65°S to a maximum of about $18 \times 10^6 \text{ km}^2$ in September, while in summer it decreases drastically until a minimum of about $3 \times 10^6 \text{ km}^2$ in February in some areas (Comiso et al., 2011) (Figure 1.6).

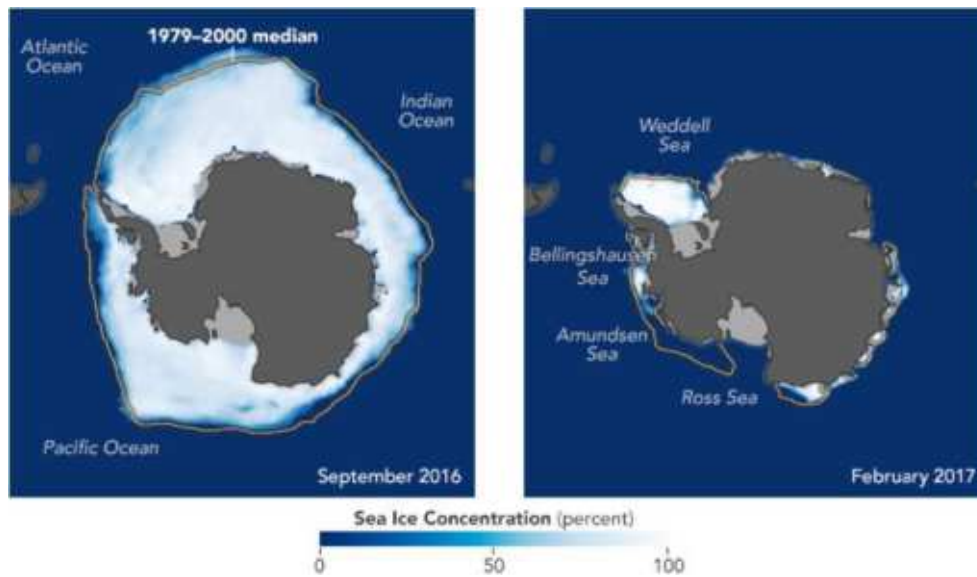


Figure 1.6: Sea Ice maximum and minimum concentration around Antarctica. (From NASA Earth Observatory maps by Joshua Stevens, based on AMSR2-E data from NSIDC).

The sea ice covering the ocean changes the surface albedo, insulates the ocean from heat loss, and provides a barrier to the exchange of momentum and gases such as water vapor and CO₂ between the ocean and atmosphere (IPCC, 2013). The volume, thickness and extension of sea ice also influences atmospheric circulation (above all the wind intensity) and oceanic circulation, triggering heat transfer mechanisms between high and medium latitudes on a global scale. The Southern Ocean is divided into zones, with different vertical distribution of temperature, salinity and currents direction. Fronts with very different water properties separate these zones (Patterson S.L. and Whitworth T., 1990).

Fronts and areas include from North to South: the Subtropical Front, the Sub-Antarctic Zone, the Sub-Antarctic Front, the Polar Frontal Area and the Polar Front. The Subantarctic Front (SAF) and the Southern ACC Front (SACC) are the northern and southern edges of the ACC. Four masses of oceanic water are recognized south of the Polar Front: cold Antarctic Surface Water (ASW), warm Deep Water (DW), warm Circumpolar Deep Water (CDW) and cold Antarctic Bottom Water (AABW). SACC is determined as the southernmost extent of Circumpolar Deep Water (temperature of about 2 °C at 400 m). This water mass flows along the shelf break of the western Antarctic Peninsula and thus marks the most southerly water flowing through Drake Passage and therefore circumpolar. The bulk of the transport is carried in the middle two fronts. The circulation near the continental edge presents variations in density and salinity as the currents originate from the mixing of different waters: water masses produced in coastal areas and polynya, which are cold and relatively less salty (with a temperature that varies between 1.5 ° and 1.9 ° C), mix with oceanic, warmer and saltier

waters. The Antarctic Divergence is a region of divergent flows of superficial waters and roughly corresponds to the Antarctic Circumpolar Trough, which separates two zones of atmospheric circulation from Antarctica. South of the Antarctic Divergence, the Antarctic Circumpolar Current (ACC) is directed toward east and some low-pressure atmospheric cells create several vortexes.

Near the continent, instead, prevails a current directed toward West, called East Wind Drift (Freeman, 2016, Deacon, 1937). This superficial flow creates two wide closed vortexes, the Ross Sea Gyre and the Weddell Sea Gyre (Figure 1.7).

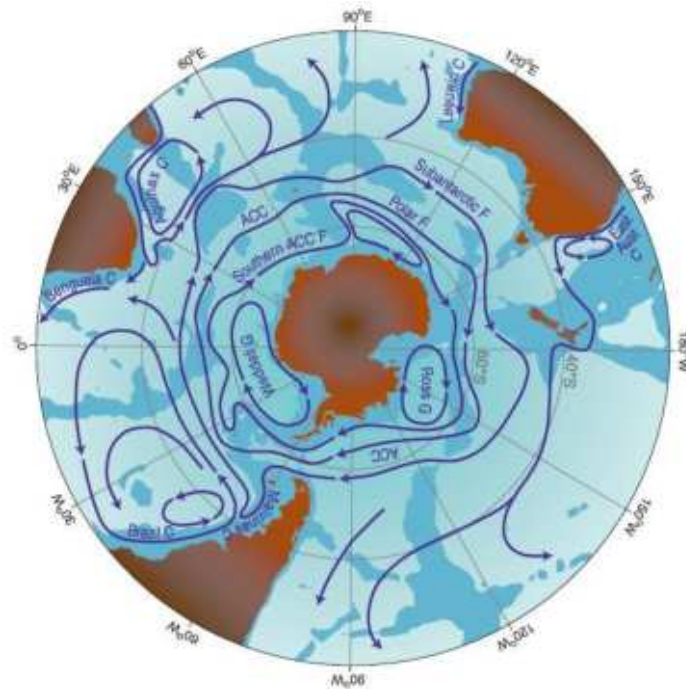


Figure 1.7: Oceanic Currents around Antarctica (From Rintoul, 2011)

The Antarctic Divergence is also an area characterized by upwelling. This phenomenon is caused by vertical water shifts in Warm Deep Water, in response to the flow of the Antarctic Surface Water. Recognizing and characterizing the Antarctic circumpolar currents has a high impact also on a global level, due to its interaction with the so-called great ocean conveyor belt. This belt represents the wide circuit of marine currents that redistribute the heat from one ocean to another and from the deep layers to superficial ones.

The characteristics of water masses along the Antarctic continental shelves vary considerably from one location to another. Water masses can be modified by different factors such as the residence time of shelf waters, the contributions from basal melting of ice shelves, the tidal forcing and the flow interactions with bathymetry (Gordon et al., 2009,

Whitworth and Orsi, 2006, Shapiro et al., 2003, Jacobs, 2004, Padman et al., 2009, Budillon et al., 2011).

The Ross Sea presents four main water masses: Ice Shelf Water (ISW), High Salinity Shelf Water (HSSW), Modified Circumpolar Deep Water (MCDW, modified starting from Circumpolar Deep Water) and Antarctic Bottom Water (AABW). A fifth current (the Antarctic Surface Water, AASW) affects the most superficial portion of water (Figure 1.8).

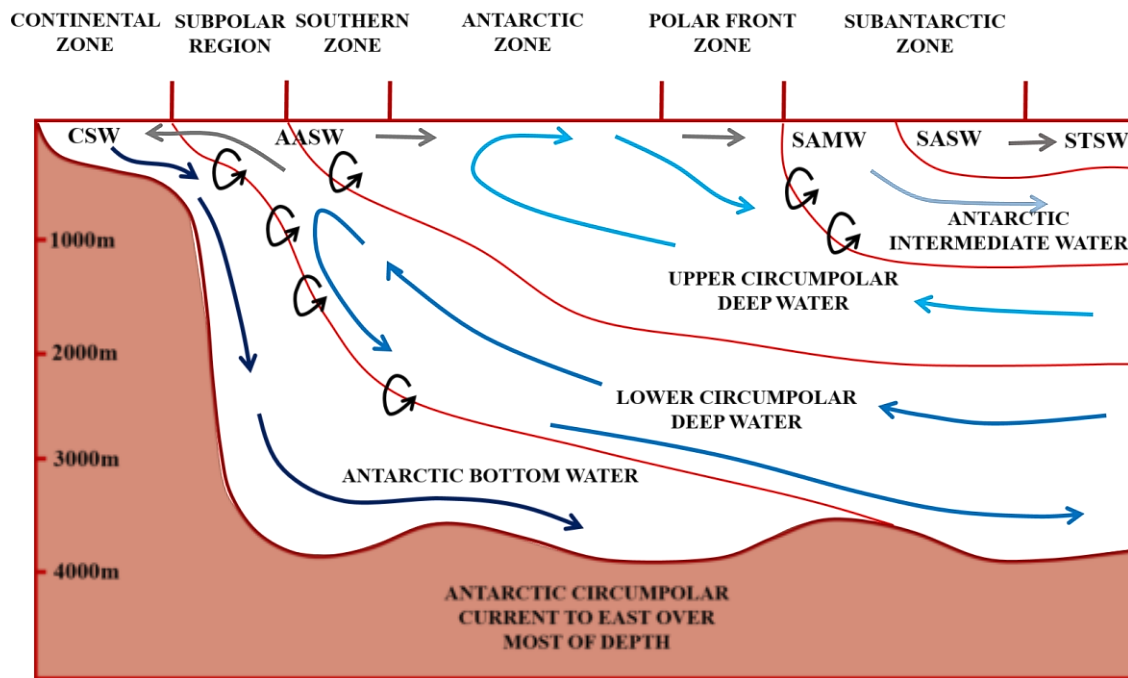


Figure 1.8: Water masses in Southern Ocean. Continental Shelf Water (CSW), Antarctic Surface Water (AASW), Subantarctic Mode Water (SAMW), Subantarctic Surface Water (SASW), Subtropical Surface Water (STSW) (Modified after Speer et al., 2000)

Antarctic Surface Water (AASW; $\gamma^n < 28.00 \text{ kg/m}^3$, and $S < 34.30$) occupies the upper ocean and is strongly modified by atmospheric forcing, sea ice formation and melting, and mixing with the waters below the AAS and, following seasonal variations in temperature and salinity, in relation to the phenomenon of freezing and thawing.

Ice Shelf Water (SW) is defined by $\gamma^n > 28.27 \text{ kg/m}^3$ and $\theta < -1.851 \text{ }^\circ\text{C}$: SW is found below the surface freezing point, below AASW on the shelf, preferentially in the deep troughs.

The Antarctic Bottom Water (AABW) is defined by $\gamma^n > 28.27 \text{ kg/m}^3$ and $\theta > -1.851 \text{ }^\circ\text{C}$. This range of γ^n excludes lighter water that can traverse the sill of the Drake Passage. Water with the same properties of AABW is called Modified Shelf Water (MSW) when it is found at depths of 700 m.

High Salinity Shelf Water (HSSW; defined as $\gamma^n > 28.27 \text{ kg/m}^3$, $\theta \approx -1.851\text{C}$; $S > 34.7$) is mainly formed in the TNB Polynya by salt release during sea ice formation. From this primary source, HSSW spreads along the seabed, filling the depressions of the Ross Sea.

One branch moves northward along the DT where it reaches the shelf break to contribute to AABW formation through mixing. Another branch moves southward under the Ross Ice Shelf.

Mixing of meltwater from the ice shelf base produces water that is potentially supercooled. Therefore, with the given salinity, these waters present temperature less than the surface freezing point. This High Salinity Shelf Water (HSSW, $\theta < -1.931\text{C}$) exits the sub-ice-shelf cavity near the dateline meridian and moves northward, reaching the shelf break near 75°S just to the east of the date line. A large volume of Low Salinity Shelf Water (LSSW, defined as $\gamma^n > 28.27 \text{ kg/m}^3$, $\theta \approx -1.80^\circ\text{C}$; $S \approx 34.47$) is present at inter-mediate depths in the central eastern Ross. Its formation appears to be due to the interaction between AASW and colder waters in the subsurface layers, after several freezing (melting) cycles of the surface water. Modification of incoming Circumpolar Deep Water (CDW; $\gamma^n > 28.00 \text{ kg/m}^3$, $\theta > 1.21^\circ\text{C}$) produces *Modified Circumpolar Deep Water* (MCDW; $28.00 < \gamma^n < 28.27 \text{ kg/m}^3$). Inflow of MCDW across the continental shelf is the primary source of heat and salt and nutrients to the Ross Sea continental shelf. This inflow appears to be strongly influenced by the topography of the banks and troughs along the shelf break (Budillon et al., 2011).

In the last five decades, in the Southern Ross Sea water masses changed in temperature, depth, volume and salinity. The HSSW was affected by a freshening of > 0.1 during this period (Jacobs et al., 2002), while RSBW decreased in volume.

1.5.1 Sea Ice

The growth and decay of Antarctic sea ice is one of the greatest seasonal surface changes on Earth. In winter, sea ice extends hundreds of kilometers out to latitudes $\sim 60^\circ\text{S}$ in the Pacific and 55°S in the Atlantic and Indian oceans but retreats to within a few kilometers of the Antarctic coast during spring and summer (Comiso and Nishio, 2008). Sea ice extent exerts a significant control on Southern Hemisphere climate by regulating heat and gas exchange between the atmosphere and the ocean, increasing planetary albedo, controlling stratification, influencing AABW formation via brine rejection, and impacting primary productivity (Godfred-Spenning and Simmonds, 1996; Pezza et al., 2012; Raphael, 2003;

Yuan and Martinson, 2000). The main factors controlling the formation of sea ice include seasonal insolation, SST (must be colder than -1.86°C for sea ice to form), salinity, and surface wind speed, which advects ice away from the site of formation (Ackley and Sullivan, 1994; Pezza et al., 2012). During sea ice formation salty brine is rejected as freshwater freezes into sea ice. Cold, salty water formed during sea ice production sinks to form shelf water (SW) or, in areas of intense sea ice production and brine rejection, HSSW. Sea ice dynamics in the Antarctic impact the state of global climate in turn because they exert a control on equatorward heat transport by the atmosphere and the ocean (Fogwill et al., 2015; Purkey and Johnson, 2013).

1.6 Sedimentation in a polar environment

In a glacial context, like the polar one, the ice dynamic and the processes derived from that (erosion, transport, subsidence and isostatic rebound induced by ice loading and unloading) play a central role on deposits position, geometry and characteristics of a high latitude continental margin(Cofaigh et al 2003; Passchier et al 2019; Van Weering et al 2008; Batchelor, et al 2015; Menzies et al 2018). They can strongly affect deposits position, geometry and characteristics of a high latitude continental margin.

Glacial deposits are often associated with typical sedimentary successions of terrestrial (river, lake, and desert) and marine (deltaic, turbiditic, contouritic) environments. Sometimes it is hard to discern a glacial system deposit from others with similar facies, especially if there are no elements that prove their origin. The study of glacial deposits, therefore, requires particular attention, like detailed vertical profiles, lithostratigraphic data and information about lateral variability and geometries. The most important element in the study of glacial depositional environment and processes is certainly the glacier. A glacier is defined as a dynamic body that is rheologically similar to a very high-density fluid that flows by gravity. The glaciers present various sizes, and the most imposing ones are currently found in Antarctica, where they form the terminations (ice streams) of the ice sheets (Figure 1.9). They are characterized by alternating movements of expansion and retreat, which reflect glacial and interglacial periods, or local conditions.

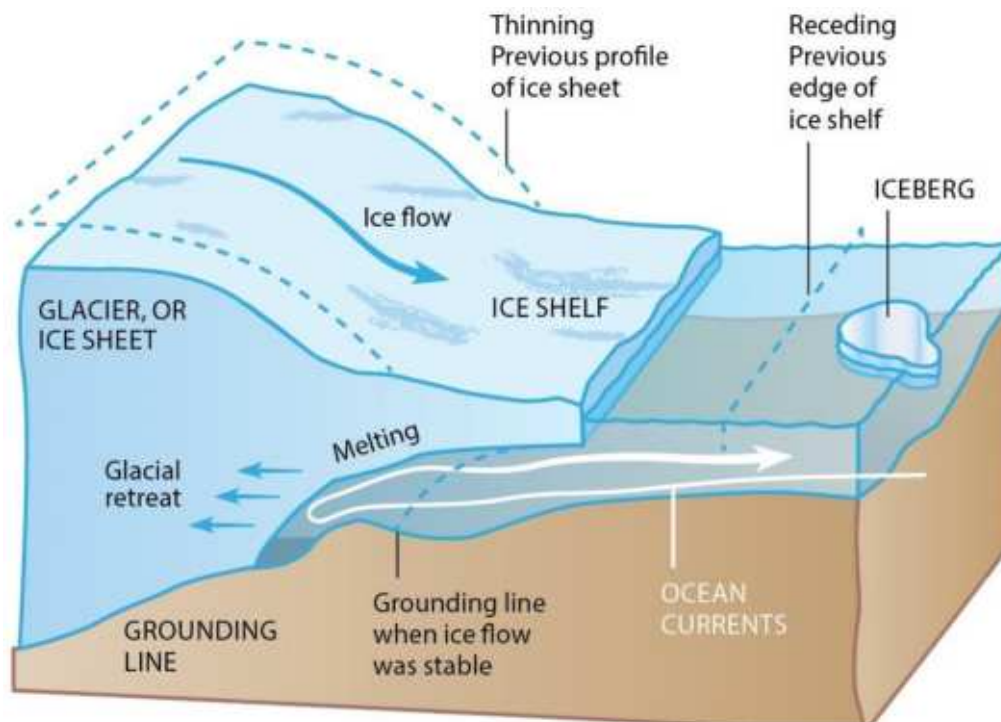


Figure 1.9: Ice streams, Ice sheet and Ice shelf (National Snow and Ice Data Centre, NASA).

Some models assume the presence of a saturated layer of sediments, at the base of the ice streams, which lubricates and increase their outflow towards the sea. The melt water, present at the base of ice sheets and ice streams, can be conveyed into a sub-glacial drainage system, which in some cases is directly connected to the sea (Kyrke-Smith et al., 2013, Christoffersen et al., 2006, Joughin et al., 2002).

The distribution and characterization of sediments depends mainly on the influence of the morphology and depositional processes related to the dynamics of ice and currents (Anderson J.B. 1999; Van Weering et al 2008; Rebesco et al 2008; Menzies et al 2018). Studies related to direct investigations (Jenkins et al., 2010) and modeling (Alley et al., 1989) of the conditions that exist at the base of ice streams prove evidence of sedimentary material eroded and incorporated by ice. Ice creates a deformed and saturated layer of water, where the ice stream can slide. This layer, at the interface between bedrock and ice, increases the ice streams speed flow towards the sea (Alley et al., 1989) (Figure 1.10). If the rate of sliding increases without a gain in the ice accumulation, the ice sheet became thinner and collapses, causing the sea level rise (Alley and Whillans, 1991).

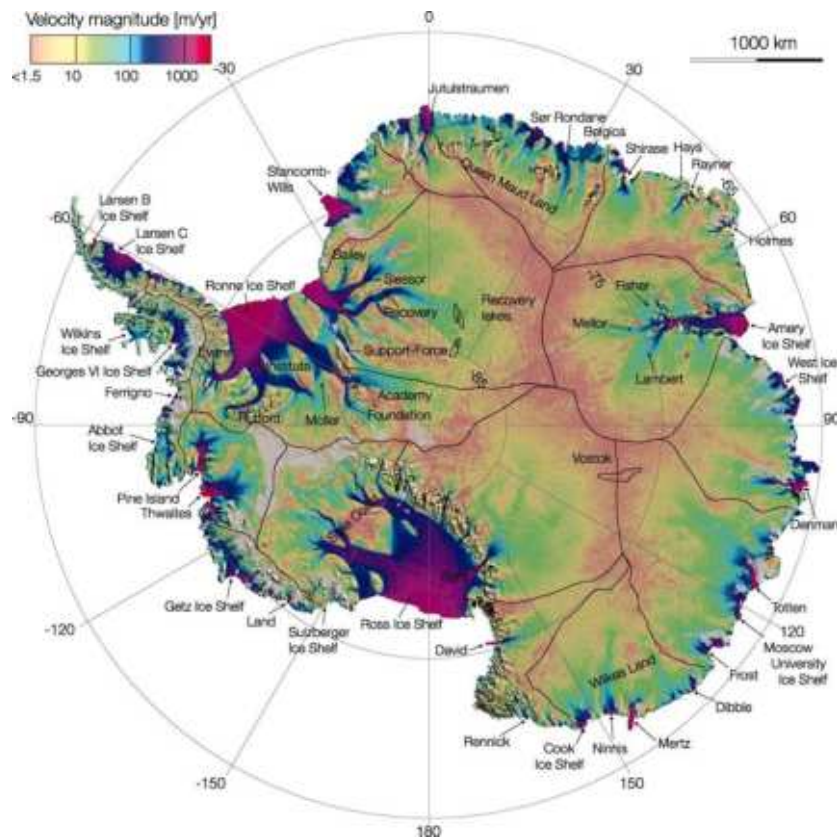


Figure 1.10: Ice velocities (from Rignot et al., 2011).

1.6.1 Continental Shelf

A continental shelf is generally a portion of a continental margin submerged under the sea. Continental shelves constitute about 8% of the entire area covered by oceans. Much of the low and mid latitude continental shelves are at maximum 200 meters deep and were exposed above the sea level during glacial periods, when the global sea level fall. The Antarctic continental shelf is typically about 500 m deep, and the distance from the Antarctic ice sheet or coastline to the shelf break varies from tens (in East Antarctica or the West Antarctic Peninsula) to hundreds of kilometres (in the Ross or Weddell Seas) (Heywood et al., 2014). The particular morphologic character of high-latitude continental shelves (great depth, rugged topography, and landward- sloping profile) may be attributed both to glacial erosion and deposition or, in large part, to isostatic down-warping of the continental shelf itself, in response to the weight of the adjacent ice sheet (Anderson, 1999).

During the advance, the glacier performs a double action: on one side, it erodes the rocky substratum (or sediments previously accumulated) at its base and along its flanks; on the other it incorporates and drags sediment in the same direction of its advance. This combined

action is called “bulldozer effect”. Bulldozer effect gives rise to hiatuses in sedimentary sections deposited during glacial epochs. Sometimes, a part of sediment accumulated during the previous interglacial period, is also removed (Lisitzin, 2003).

The eroded sediment, incorporated at the base of the ice and transported on the glacier front, is finally deposited at its maximum expansion point, beyond the so-called grounding line. The grounding line is the point that divides the area where the ice is resting on the substrate, from the area where the ice floats in the water. More properly is better to refer to ‘grounding zone’, that means where the ice sheet marine margins cease to be in contact with the seafloor (Dowdeswell and Fugelli, 2012). It is important to map the repositioning of the grounding line, in order to understand better the marine ice sheet dynamic. In fact, the transition zone can help to determine the rate at which ice flows out of the grounded part of the ice sheet (Schoof, 2007).

The glacial sediment deposited along the grounding line, can be lodgment till, a heterogeneous and massive deposit, or can be coarse-grained material, if outwash melt water is present (Powell, 1990). The coarser sediments are deposited immediately close to the grounding line, while the fine sediment is transported as plume and deposited in ice distal areas.

At the grounding line, during stationary phases between the ice advance and retreat (O'Brien et al 1999; McMullen et al., 2006; Dowdeswell et al 2012), a till delta can be deposited (Alley et al., 1989). After retreat of the ice, the deposition of pelagic and hemipelagic sediments drapes the seabed, creating Grounding Zone Wedges (GZW) (O'Brien et al 1999; Bart and De Santis, 2012, Dowdeswell et al 2012; Batchelor et al 2015; (Figure 1.11).

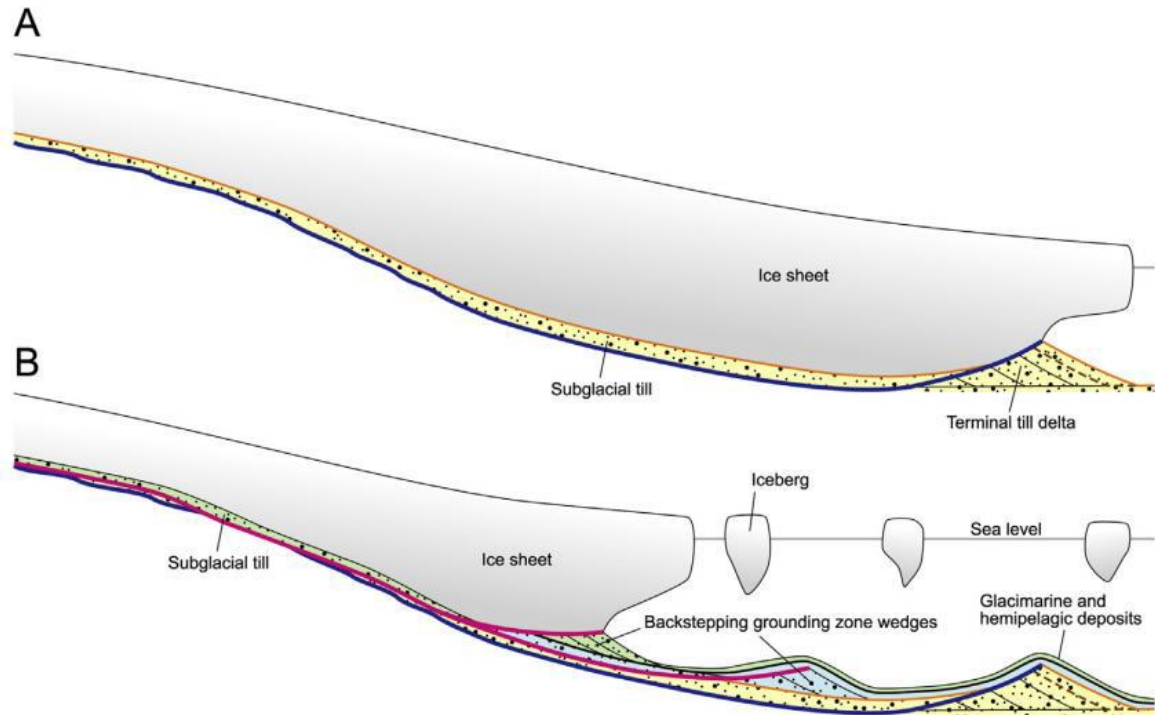


Figure 1.11: Ice sheet advances and retreats following glacial (A) and interglacial (B) phases. (From Zecchin et al., 2015)

1.6.2 Continental Slope

The advance of the ice sheet on the continental shelf, during repeated glaciations, with erosion of the inner continental shelf and deposition on the outer continental shelf caused the progressive over-deepening and landward dipping profile of the shelf (Evans et al 2009; Reinardy et al 2015; Peters et al 2016; Bart et al 2016).

One of the peculiar morphological characteristics of the Antarctic margin is the presence of large marine glacial troughs. Those troughs were eroded and dug by ice streams repeatedly (up to over 1000 meters in the inner shelf). During glacial advance across the glacial troughs, the ice mass transported and accumulated sediments up to the maximum limit of the glacier's advance, sometime at the shelf edge. In this case, the sediments were dumped directly to the slope, where they formed large trough-mouth fans. This glacial form is generally described in the literature as set of more episodes of glacial advance and retreat (Bart, 2001).

Depending on slope angle and roughness and on sediments characteristics, sediment downslope flows may present different rheology (fluidal versus plastic) and may have

laminar, mixed or turbulent behaviour producing deposits with different geometry, texture and internal structure Figure 1.12 (Haughton et al., 2009).

FLOW TYPE		FLOW STRUCTURE	BEHAVIOUR	DEPOSITS
DEBRIS FLOW	COHESIVE		 Laminar Flow	
COMPOSITE/ CO-GENETIC FLOWS	MIXED		 	
HIGH-DENSITY TURBIDITY CURRENT	NON-COHESIVE		 Turbulent Flow	
LOW-DENSITY TURBIDITY CURRENT				

Figure 1.12: Classification scheme for submarine bottom flow types and structures linked to their deposits. (From Haughton et al., 2009)

Gravitational flows also generate mixed sediments of glacial and glacio-marine deposits. When a sufficient amount of water is added to the glacial sediment dropped to the upper slope, in fact, dilution triggers turbulence and the release of coarse sediments, generating turbidity currents. Thick turbidites were recognized in areas far from the shelf, up to abyssal areas, along the Antarctic perimeter (Wright, Anderson and Fisco, 1983, Rodriguez and Anderson, 2004; Escutia et al., 2005, Barker et al., 1998). These kind of deposits were also recovered by ODP Leg 188 from the Prydz Bay continental slope (O'Brien et al., 2001), IODP Expedition 318 also recovered glaci-marine debris flows derived from the shelf at site U1356 (Escutia et al., 2011).

The subglacial sediments that are deposited by grounding ice near the shelf edge and that rapidly and massively flow downslope may preserve a similar composition of till sediments. The highly cohesive nature of till gives a high inclination to polar margins respect to those at mid latitude (Larter and Barker, 1989). The seismic facies of this type of deposit is lens-shape, chaotic or massive with sharp erosive base, and is interpreted as debris flow. This deposit can be interlayered with stratified sediments deposited by hemi-pelagic settling or turbidity flows. Debris flows were recognized on Antarctic continental margins in western Bellingshausen Sea (Hillebrand et al., 2005, O' Cofaigh et al., 2005), northern Antarctica Peninsula (Nelson et al., 2009, Diviacco et al., 2006), northern Victoria Land (Hauber et al., 2018).

Sediments can be affected by alongslope currents, too. In this case, they are interpreted as contourites. Contourites are defined as 'sediments deposited or substantially reworked by the persistent action of bottom currents (Stow et al., 2002, Rebesco, 2005, 2014).

Usually, landslides deposits present a seismic transparent, or chaotic, non-laminated facies. It is possible to identify, inside the chaotic deposit, some continuous reflectors, that represent faults. High sedimentation rates occur in a glacial temperate setting, or in a wet basal ice sheet condition. In fact, there are the main factor for the collapsing and sliding material. The gravitational deposits distribution is closely linked to the amount of sediments discharged through melt waters. In some cases, like on the Wilkes Land western margin, the trigger mechanism is the occurrence of earthquakes, intensified by isostatic variations that occur after the sheet retreat (Donda et al., 2007).

The presence of bottom currents is also an important factor influencing the deposition on the continental slope. Geostrophic currents move at a constant depth, along bathymetric contour lines, in thermal and density equilibrium, where Coriolis force compensates density/gravitational gradient. Any cause that can break the potential vorticity constraint causes the downslope flows or even the cascading process (an irregular bathymetry, a canyon, an intersection of dense water). Currents tend to cascade if their density increases (due to salinity or suspended material increment). Their speed range between 1cm to 20cm/s (Hollister and Heezen, 1972). In some cases, they can reach 3m/s.

Bottom currents can therefore re-suspend and entrain the fine-grained sediment component, transporting it and re-depositing in drift contouritic deposits (contourite drifts). Contourite drifts can be found at different depths, and present many different shapes, the most common

has an asymmetric mounded shape with an elongated side on current direction (Rebesco et al. 2004). Seismically contourite drifts present laminated sigmoidal facies. In some cases, the facies appear internally completely homogeneous; in other cases, there are indistinct, discontinuous and parallel laminations, with sub horizontal irregular erosional surfaces, and thinner layers and lenses of coarse grain size material. Turbidite, contourite and hemipelagic deposits can be found also in Antarctica in the continental rise and shelf of the Wilkes Land (Escutia et al., 2002), in the northern Weddel Sea (Maldonado et al. 2005), and East Antarctica (Close D.I 2010).

Cross-laminations are rarely present only in silt or fine sand deposits. Contourite drifts are generally composed by fine sediment (mud, silt) with silicoclastic, biogenic, and vulcanoclastic components. Usually, they can form slowly and in calm environment. The variation of their internal and external facies indicates a change in the bottom circulation, differently from the gravitational deposits, usually caused by episodic and local currents (Figure 1.13).

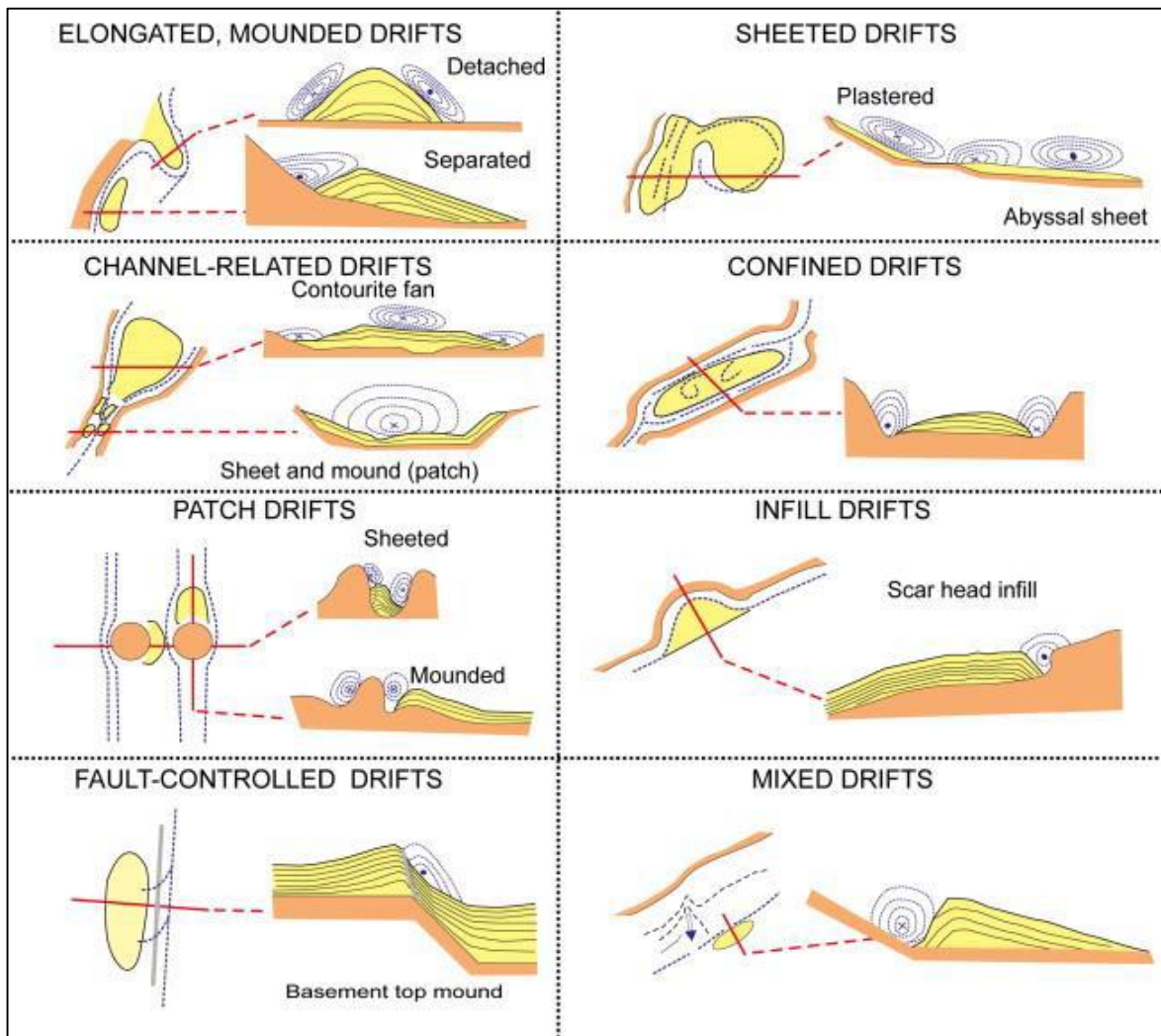


Figure 1.13: Sediment drift types and inferred bottom-current paths (From Rebesco et al., 2014)

1.7 Fjords: formation and sediment dynamics

A fjord is a deep elongated estuary which has been formed by erosion of land-based ice in the course of century. Fjords are found mainly in Norway, Greenland, New Zealand, Canada, Chile and Antarctica (Meier et al., 1994; Straneo et al., 2013, Wellner al 2001; Munoz et al 2016) they are sculpted by glaciers and set in deep U-shaped valleys and are found in places where the present or past glaciation extended below present sea level (Koechlin, R. 1947). The depth of the fjord depends on the erosive power of the glacier that formed it. Thus, a glacier of outstanding size will give rise to a fjord of equal importance. Sediments and rocky debris transported by the glacier are deposited on the bottoms of fjords and break up the regularity of their beds.

As the glacier excavates its way into the ground it leaves its two walls, which may retain their vertical cross-section or may by degrees, according to the nature of the rock, become less steep by weathering (Fig 1.14).

Fjords are commonly characterized by energetic tides and show a steep fjord-head delta that is fed by sediment-laden rivers and streams that drain the diminished glacier that eroded the valley (e.g. Farmer and Freeland, 1983; Syvitski et al., 1987; Syvitski and Farrow, 1989).



Figure 1.14: A fjord carved by glaciers with steep rock walls (Nesje, A. 2009).

A fjord is formed when a glacier recedes, having carved its typical U-shaped valley, and the sea fills the resulting valley floor.

This forms a narrow and steep cove (sometimes deeper than 1300 meters) connected to the sea. The terminal moraine pushed down from the valley by the glacier is left underwater at the fjord entrance, causing the water at the neck of the fjord to be shallower than the main body of the fjord behind it.

As a result of the glacial processes that formed the fjord, a main feature of most (not all) fjords is a sill (e.g. a moraine) at the mouth, or sometimes additional sills that separate multiple basins (Fig 1.15). However, sills can also be predefined by the underlying bedrock.

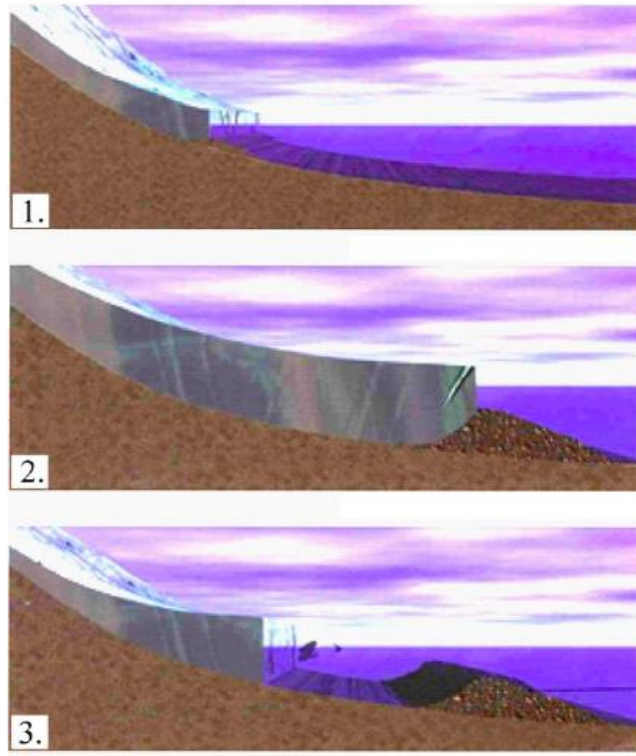


Figure 1.15: Schematic cross-sectional evolution of a valley resulting from glacial erosion (from Harbor 1992)

1.7.1 Broader context

Large, recent fluctuations in the termini of outlet glaciers draining the significant portion of the Greenland and Antarctic Ice Sheets provide considerable impetus for understanding the processes controlling the stability of these ice masses on much shorter (< 100 yr) time scales. Modern fjords constitute ideal natural laboratories for illuminating these underlying processes, as many retreating tidewater glaciers are relatively accessible for oceanographic studies. Moreover, they produce relatively large meltwater and sedimentary signals (e.g., Hallet et al., 1996; Koppes and Hallet, 2002) that are related to subglacial processes on diverse time scales ranging from events lasting minutes to many decades (e.g., Cowan et al., 1988; Jaeger and Nittrouer, 1999a). In addition, studies of sedimentary processes along the ice-ocean interface will help refine poorly constrained parameters, such as the sediment production rate, to more accurately model ice behavior over cycles of advance and retreat (Nick et al., 2007). Establishing a direct link between ice behavior, the formation of sediment shoals, and ice-proximal sediment deposits will help increase the accuracy and resolution of interpretations from glacial marine sediment archives on longer time scales (Cowan et al., 1988; Anderson et al., 2002; Andresen et al., 2011).

1.7.2 Glaciomarine Sedimentary Process

Sediment deposits near tidewater glacier termini merit close attention because the dynamics of these glaciers are at least partially modulated by the sediments they produce, and the sediments also contain valuable information about past glacier behavior. These glaciers frequently discharge into nearly closed fjords, forming a well-preserved sediment record of glacier fluctuations, associated climatic changes, erosion, and sediment-transfer events (Cowan et al., 2010). A number of studies have related known environmental conditions to sedimentary signatures in fjord seabeds (e.g., sedimentary structure, seismic stratigraphy, accumulation rates) (e.g., Griffith and Anderson, 1989; Domack et al., 1993; Cowan et al., 1997; Milliken et al., 2009), and a continuing research objective is to increase the accuracy and resolution of such paleoenvironmental interpretations (Figure 1.16). Studies of fjords from Svalbard, Alaska, Patagonia, and Antarctica stress the first-order importance of climate in controlling glaciomarine sedimentation by determining the thermal regime of the glacier and the amount of meltwater produced (Griffith and Anderson, 1989; Powell, 1991; DaSilva et al., 1997).

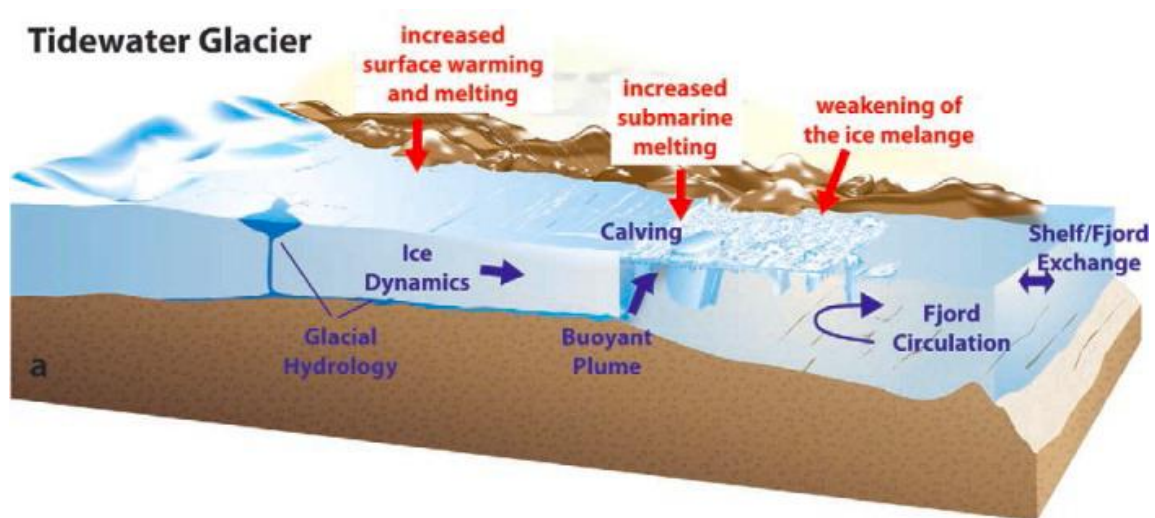


Figure 1.16: Processes Affecting Tidewater Glaciers Several mechanisms controlling the recent retreat of glaciers worldwide have been proposed (shown in red). Specific processes that need further direct study are highlighted in blue (from Straneo et al., 2013).

For the relatively well studied temperate tidewater glaciers of Alaska, glacial meltwater transports the majority of glacially derived sediment to fjords (Powell and Molnia, 1989;

Cowan and Powell, 1991; Syvitski, 1989). If the density of the sediment-rich fresh water exceeds the density of the ambient seawater, the fresh water will move seaward as a gravity flow, driven by its excess density (Figure 1.17) (Mulder et al., 2003). If the freshwater density is low, meltwater delivered at the base of the glacier will rise buoyantly as a turbulent plume, mix with the ambient seawater (Powell and Molnia, 1989; Syvitski, 1989), and sediment suspended in the plume will settle to the seabed (Cowan and Powell, 1990, 1991; Hunter et al., 1996a). The large meltwater discharge in temperate glacimarine systems results in some of the highest rates of grounding-line sediment accumulation worldwide; they can exceed tens of meters per year (e.g. Molnia, 1983; Cowan and Powell, 1991). These rates have been shown to decrease rapidly with distance from the terminus (e.g., Powell and Molnia, 1989; Cowan and Powell, 1991). Fjord sediments from temperate glaciers commonly comprise interlaminated sands, muds, and ice rafted debris, and often preserve a high-resolution history of glacier behavior and sediment production over a range of timescales (tidal, diurnal, seasonal, individual event) (e.g., Mackiewicz et al., 1984; Domack et al., 1994; Cowan et al., 1997; 1999; Jaeger and Nittrouer, 1999). In polar and subpolar settings, controls on sedimentation are believed to be somewhat different. The production of sediment by glacial erosion is expected to decrease progressively as surface melt vanishes, because little or no water reaches the bed from the glacier surface to facilitate glacier sliding, erosion, and the transport of sediment. Significant sediment production by bedrock erosion likely vanishes as soon as the basal ice temperature drops below the melting point (e.g., Cuffey et al., 1999). Thus, in polar regions, rates of sediment production are likely to nearly vanish as surface temperatures drop well below 0°C (Griffith and Anderson, 1989; Hooke and Elverhøi, 1996; Powell et al., 1996). For subpolar glaciers, the majority of sediment is thought to be transported through fjords in bottom and intermediate-depth plumes of cold water, which appear to originate at the grounding line (e.g., Domack and Williams, 1990; Domack et al., 1994).

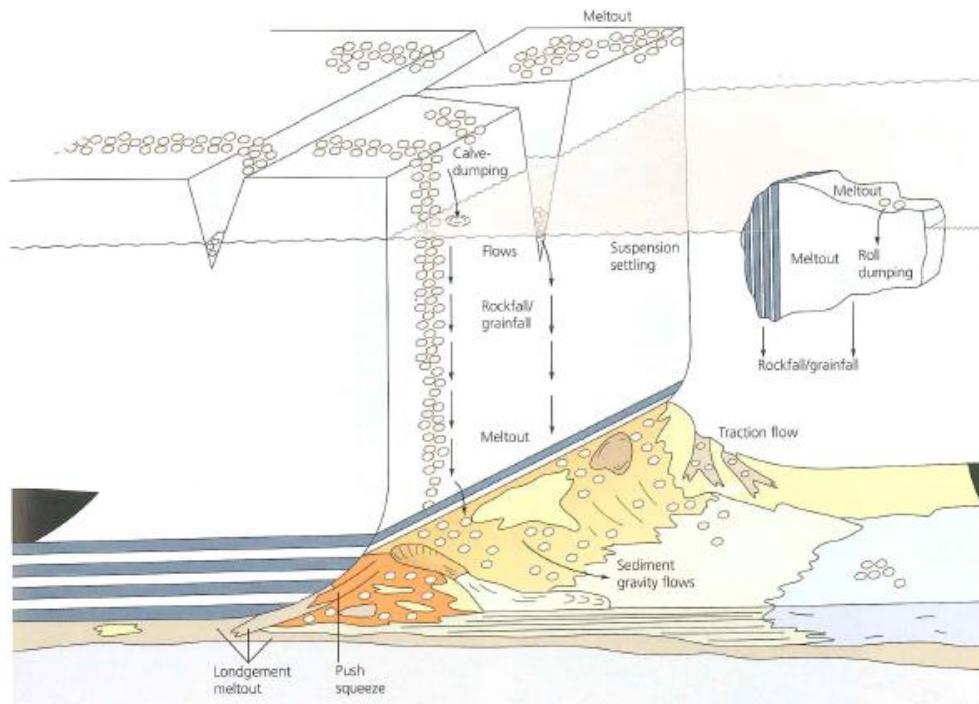


Figure 1.17: Glacimarine Sedimentary Processes Glaciers deliver sediment and mechanisms transport within fjords (from Benn and Evans, 2014).

1.7.3 The Polar Fjords

Polar fjord types such as the Lallemand Fjord on the Antarctic Peninsula, or fjords found in Greenland and the Canadian Arctic are almost always covered by sea ice or contain ice shelves and glaciers.

One objective of contemporary glacimarine research is to understand the fidelity of recent and past climate-change signals preserved in the sedimentary record, and how these records are altered by time and changing boundary conditions (e.g., Milliken et al., 2009; Koppes et al., 2010; Fernandez et al., 2011; Simms et al., 2011). Climate controls the extent and thermal regime of glaciers, as well as the amount of meltwater produced (e.g., Griffith and Anderson, 1989; DaSilva et al., 1997), with increased meltwater generally promoting glacier erosion by reducing the basal effective pressure (e.g., Cuffey and Paterson, 2010). When abundant, glacial meltwater transports the majority of glacially derived sediment to fjords, where most of this sediment remains trapped (e.g., Powell and Molnia, 1989; Cowan and Powell, 1991; Hallet et al., 1996; Hunter et al., 1996a). The large meltwater discharge in temperate glacimarine systems results in proximal rates of sediment accumulation that can

reach tens of meters per year (e.g., Molnia, 1983; Cowan and Powell, 1991). In colder settings, the production of sediment by glacial erosion is expected to decrease progressively as surface melt vanishes, because little or no water reaches the bed from the glacier surface to facilitate sliding, erosion, and sediment transport. Moreover, significant sediment production likely vanishes as soon as the basal ice temperature drops below the freezing point (e.g., Cuffey et al., 1999). Thus, for polar and subpolar regions, subglacial sediment production and delivery to fjords are both expected to drop with decreasing air temperature, especially as it drops below 0°C (Griffith and Anderson, 1989; Hooke and Elverhøi, 1996; Powell et al., 1996).

1.7.3.1 Antarctic Fjords

Fjords act as natural sediment traps, preserving histories of glacial landscape erosion within semi-enclosed basins (Jaeger & Koppes, 2016, Y.P. Munoz & J.S. Wellner 2016). In fjords fed by tidewater glaciers, sediment accumulation rates vary from millimeters to centimeters per year (typical of polar and subpolar fjords in Antarctica, Greenland, and Svalbard; e.g., Boldt et al., 2013; Andrews et al., 2016; Elverhøi & Seland, 1983;) to meters per year (typical of temperate fjords in Alaska and Patagonia; e.g., Powell & Molnia, 1989; Jaeger & Nittrouer, 1999).

Presently, fjords of the West Antarctic Peninsula (WAP), exhibit slow accumulation rates of ~1–20 mm/year (Boldt et al., 2013), characteristic of subpolar fjords fed by cold-based glaciers. Because of this slow accumulation, WAP fjords can be biologically productive and support high abundances of pelagic and benthic biota under conditions of relatively low turbidity and sedimentation (Eidam et al 2019; Grange & Smith, 2013; Pan et al., 2019). However, this region has experienced rapid environmental changes since the mid-20th century including atmospheric and sea-surface warming, widespread glacial retreat, and reduced annual sea-ice duration (Cook et al., 2005, 2014, 2016; Chapman & Walsh, 2007; Ducklow et al., 2007; Meredith & King, 2005), although very recently, air temperatures have cooled slightly (Turner et al., 2016). Based on modeled climate and erosion dynamics, WAP glacial sediment yields are expected to increase in the coming decades (e.g., Koppes et al., 2015; Turner et al., 2016), which could cause greater sediment inputs and greater stresses on pelagic and benthic communities.

However, paleoclimate and oceanographic reconstructions, especially from the fjords of the western Ross Sea, as well as the circulation and processes impacting their exchange with the shelf and wider ocean, are scarce.

To understand recent and potential shifts for the sedimentation patterns in a global and historical context, reliable data are needed about accumulation rates over decades to centuries as well as an understanding of sediment delivery by glaciers, in contrast to temperate systems. Fjord accumulation rates are often obtained from seismic records (Fernandez et al., 2016; Harris et al., 1999), which are key for obtaining millennial-scale data, but cannot resolve more rapid fluctuations in sediment delivery, for example, related to recent warming (e.g., Chapman & Walsh, 2007; Meredith & King, 2005).

In this study, a large dataset of geophysical, geological and geochemical proxies are used to have a comprehensive view of sediment dynamics of the North Victoria Land fjords and provide context for evaluating AIS retreat after the LGM.

1.8 Glacial processes and landforms

Glacial geomorphology studies describe the product of the action of glaciers on the earth's surface, most of the areas today characterized by this morphology were created by the movement of large continental glaciers during the Quaternary glaciations forming complex delivery sediment systems (SDS) (Alley et al., 1997; Evans, 2014).

Sediment deposition takes place as a function of the dynamics of the ice, the type of glacial mass, the geology and sedimentology of the basement and subsoil, the temporal and spatial variability of erosion, thermal and hydrological regimes and topography. Once sediments are produced by erosion, their transport and subsequent deposition within the glacial system require a different classification in supraglacial, englacial, subglacial and proglacial subenvironments. Fig. 1.18 illustrates the numerous and complex paths of these delivery systems.

The influence that ice dynamics have on sediment deposition depends on the basal thermal conditions of the ice.

It was once thought that little or nothing was transported under basal ice conditions, but today we have some evidence showing that limited transport occurs as a slow deformation (Alley et al., 1997; Gulley et al., 2009; Batchelor and Dowdeswell, 2014; Dowdeswell et al., 2015; Livingstone et al.; Hogan et al., 2019).

Most of the sediments transported and deposited by the ice masses reflect the geology of the substrate that is eroded through the mechanism of abstraction or ablation (Alley et al., 2019).

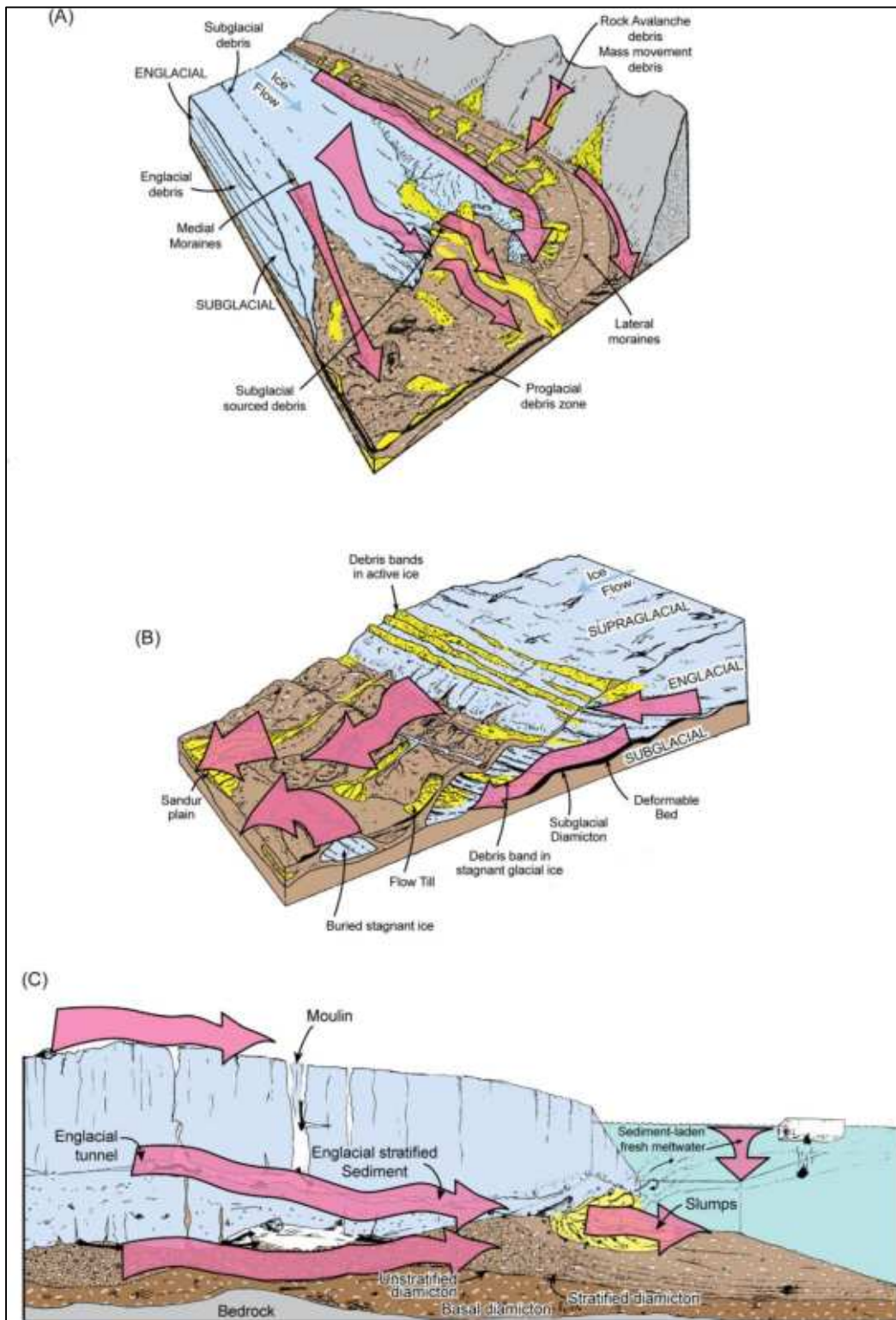


Figure 1.18: Sediment delivery systems (SDS) within glacial environments (A) SDS within valley glacial systems, (B) SDS within marginal ice sheet systems, and (C) SDS within subaqueous glacial environments (Menzies, J., & Ross, M., 2020).

In the past decades, these morphologies were considered individual with their characteristics and origin of formation, today, most of these forms are considered as a series or subset of bedforms that have many similarities not only in sediment content but also forming in comparable environments, albeit, sometimes in different environmental or glacio-dynamic conditions (Stokes et al., 2013a; Ely et al., 2018).

Glacial geomorphic maps provide direct information on past ice trajectories and inter-ice flows, which has important implications for the reconstruction of former ice sheets.

The reconstruction of the latter is based precisely on the study of glacial morphologies, as well as on the dynamics of the ice flow and the location of paleo ice flows.

Glacial flows generally consist of geomorphological shapes that indicate the direction of the ice flow by forming patterns often of similar size (Clark, 1993).

Glacial geomorphic features are classified according to the shape, size and nature of the substrate on which they are formed (Benn and Evans, 1998). Every detail is the result of the glacial processes that have affected the environment. The various characteristics can be further classified into three regional zones with reference to the continental shelf: internal shelf, med-shelf and outer shelf (Wellner, et al., 2001, 2006) (Figure 1.19).

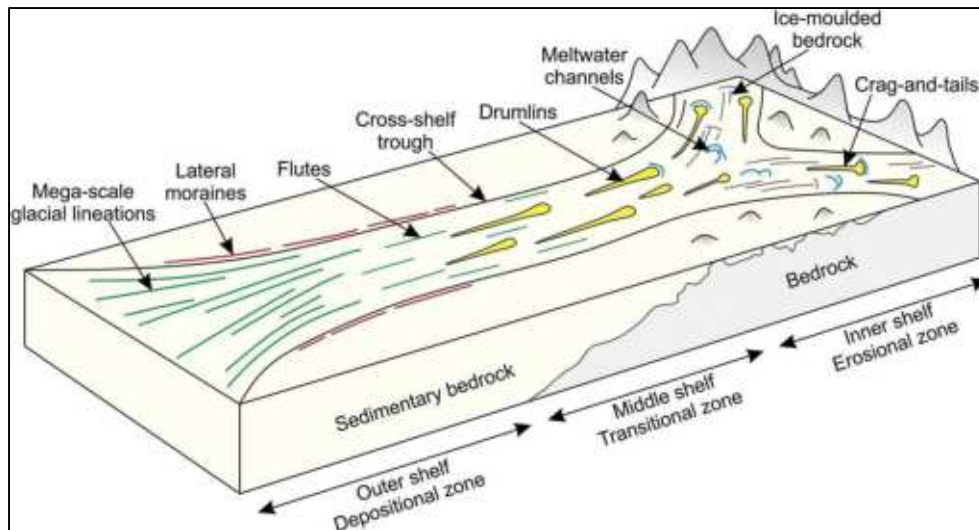


Figure 1.19 Schematic cartoon of the transition and distribution of glacial geomorphic features that takes place as ice flows from an interior ice-sheet drainage basin into a cross-shelf trough (modified from Wellner et al. 2001, 2006).

The inner shelf is generally composed of crystalline bedrock with rugged, irregular bathymetry, and characterized by erosional features, including glacial troughs (Wellner et al 2001, 2006; Napieralski et al 2007).

The mid shelf marks the transition from crystalline bedrock to a sedimentary substrate, wherein a combination of erosional and depositional features are often seen.

The outer shelf is characterized by a prograding sedimentary substrate and depositional landforms that tend to be highly elongate (Wellner, et al., 2006). Specific characteristics of some geomorphic features, such as attenuation and elongation of a landform, may be used to estimate ice flow velocity (Stokes and Clark, 1999; Briner, 2007). Estimating ice flow velocity is an important component in the modeling and calculation of ice flux (Pritchard, et al., 2009).

1.8.1 Marginal Moraines

Moraines that form transverse to the ice flow direction, but not formed subglacially, may be the result of push from advancing ice or the upward squeezing of sediments at ice margins or accumulate at the ice frontal margin as end, recessional, or terminal moraines (Bennett and Boulton, 1993; Krüger, 1996; Evans and Hiemstra, 2005). Such moraines can vary in height from a few meters to several tens of meters and commonly have an asymmetric transverse profile.

The sediment content of most marginal moraines reflects a wide diversity of sediment facies characteristic of supraglacial, englacial and subglacial environments. In addition, lateral and medial moraines commonly contain a large percentage of mass movement sediments which, in the case of valley glaciers, mirrors the surrounding geology of the mountainous terrain in which the valley glacier resides.

1.8.2 Glacial Striations

Glacial striations are a series of long, parallel lines or grooves scratched on a rock surface by rock fragments deposited at the base of a moving glacier from glacial abrasion (Klassen, R.A. 1994). Glacial striations generally represent glacier movement using rock fragments and grains of sand, embedded in the base of the glacier (Ray et al 2021). Large amounts of coarse gravel and boulders carried under the glacier provide the abrasive power to cut

trough-like glacial ruts. Finer sediments at the base of the moving glacier also scour and smooth the rock surface further. The ice itself is not a material hard enough to change the shape of the rock, but because the ice has rock embedded in the basal surface it can effectively abrade the bedrock.

1.8.3 Meltwater channels

Meltwater channels for definition are erosional features, cut into rock and sediment by flowing water beneath or close to ice-sheet margins. The channel may form on the surface of, within, beneath, along the margins of or downstream from the ice mass.

A subglacial meltwater channel instead is a channel beneath an ice mass, such as ice sheets and valley glaciers, roughly parallel to the main ice flow direction. These meltwater channels can have different sizes, ranging from very small channels of a metre deep and wide to big valleys which can be up to a kilometre wide (Röthlisberger, H.,1972). The dimensions of these channels are regulated by several factors: water temperature, meltwater volume, debris content in the water, ice wall closure rates (governed by the ice thickness) and squeezing of fluidized sediment (Van der Meer et al 2003, Simkins et al 2018).

1.8.4 Glacial Lineations

Mega-scale glacial lineations (MSGLs) and flutings are elongate, ice-molded, linear, sediment ridges that occur in patterns with variable length and spacing, can be several meters to over 10 m high and extend many kilometers in length (Clark, 1993). These landforms have been observed forming in situ, subglacially, in the Rutford Ice Stream (West Antarctica) by King, et al. (2009). These lineations occur as a result of active depositional and hydrological processes operating at the ice-bed interface on decadal time scales. While flutings are indicative of ice flow direction, the only certain indicator of fast flowing ice streams is the presence of MSGLs. This observation is based on their exceptional length and elongation (characteristics highly reflective of streaming ice flow), but also because of their composition of dilatant, deformation till over stiffer lodgment till (Clark, 1993; Stokes and Clark, 1999). Deformation till is a softer, water saturated and hence more malleable, glacial till that is defined by its ability to deform under glacial pressure. Hence, MSGLs are molded

and shaped by streaming ice, though the precise mechanism by which this occurs remains a hotly contended issue. MSGs vary widely in terms of length, ranging from minimum lengths of 1 km to more than 80 km (Stokes and Clarke, 1999; Spagnolo, et al., 2014). Where MSGs are preserved with no modification, the deglacial mechanism is inferred as ice-sheet thinning, followed by lift-off and retreat through rapid iceberg calving (Dowdeswell, et al., 2008).

1.8.5 Drumlins

Elongated landforms aligned parallel to ice flow are common on subglacial beds. They have been classified in different ways based on their morphology. Drumlins are oval-shaped hills intermediate forms, varying in size from a few meters to over 200 m in height and can stretch a few meters long to over a kilometer (cf. Spagnolo et al., 2014; Hillier et al., 2016; Ely et al., 2018) with streamlined tails of sediment (Clark, et al., 2009). Their varied morphology can deviate considerably from the classical tear-shaped, particularly when they are in a transition zone with MSGs.

Drumlins are definitive characteristics of glaciated landscapes, and nearly as scientifically confounding as they are ubiquitous. Drumlins are thought to form in the onset zone of an ice stream trunk, where ice flow is still relatively slow (Wellner et al., 2001; King, et al., 2009) at the transition between crystalline basement and sedimentary substrate, upstream of the MSGs. In some cases, as drumlins get elongated, they essentially "transform" into MSGs, making the distinction between the two morphologies be arbitrary (Graham et al., 2009; Stokes et al., 2013b; Spagnolo et al., 2014; Stokes, 2017).

Like all subglacial features, drumlin formation in situ has been largely inaccessible to direct observation beyond borehole measurements and geophysical surveys. The first in situ observation of drumlins and MSGs forming beneath an ice stream was published by King et al. (2007). The study revealed that both features form on decadal scales (7 years) in a mixed environment of erosion and deposition.

1.8.6 Crag and Tail

The Crag and Tail are landform consisting of a small rocky hill (crag) from which extends a tapering ridge of unconsolidated debris (tail).

Craggs are formed when a glacier or ice sheet passes over an area that contains a particularly resistant rock formation (often granite, a volcanic plug or some other volcanic structure). The force of the glacier erodes the surrounding softer material, leaving the rocky block protruding from the surrounding terrain (Nitsche et al 2016). The crag is a residual feature left by selective glacial erosion, while the tail is drift-deposited by ice on the lee side of the obstacle.

1.8.7 Grounding Zone Features

Grounding zones are geomorphic indications of still-stands, or periods of stability, of an ice sheet or glacier (Bart and Anderson, 1996; Dowdeswell, et al., 2008, Batchelor et al 2015). Their presence implies episodic or slow ice-sheet retreat, while their absence implies fast retreat. They are typically recognized in map-view by arcuate or wedge-shaped geometry, perpendicular to ice flow, as they indicate the position of the former grounding line. These features are also recognized as marking the transition from grounded ice sheet to floating ice shelf (Rebesco, et al., 2014). In seismic profile, they are characterized by acoustically chaotic or transparent units, owing to their general composition of till and/or diamicton. Grounding zone wedges are considerably variable in terms of size and geometry. Determination of till volume in a grounding zone wedge (GZW) can be calculated to infer the duration of still-stand (Howat and Domack, 2003).

Chapter 2

2. RESEARCH CONTEXT

2.1 Ice sheets, ice shelves and climate change

The AIS (Antarctic Ice Sheet) is a vast, $\sim 14 \times 10^6 \text{ km}^2$ expanse of glacial ice resting on a continental land mass (Bindschadler et al., 2011). Formation of the AIS began 34 million years ago via the gradual accumulation of snow and ice in mountains and the continental interior (Zachos et al., 1996; Lear et al., 2000; Pagani et al., 2011).

The ice deforms under its own weight and flows as a viscous fluid towards the coast (Fretwell et al., 2013). Flow from the ice sheet interior is organized into ice streams and glaciers characterized by relatively fast flow speeds ($> 10 \text{ ma}^{-1}$). Ice reaching the coast may spread to form floating ice shelves in coastal embayments or calve off to form icebergs. The transitional region between grounded ice (resting on bedrock or the seafloor) and floating ice is known as the grounding line or grounding zone. The grounding line retreats and advances in response to changes in ice thickness and flow speeds. Changes in grounding line position are a useful indicator of changes in external or internal forcing of the ice sheet–ice shelf system (Konrad et al., 2018; Jenkins et al., 2018).

Three glaciologically distinct regions comprise the AIS: the East Antarctic Ice Sheet (EAIS, $\sim 11.5 \times 10^6 \text{ km}^2$), the West Antarctic Ice Sheet (WAIS, $\sim 2.0 \times 10^6 \text{ km}^2$), and the Antarctic Peninsula ($\sim 5.2 \times 10^5 \text{ km}^2$) (Bindschadler et al., 2011) (Fig.2.1). Large areas of the continental landmass underlying the WAIS lie below sea level and the ice margin is in direct contact with the ocean, while much of the EAIS lies on bedrock elevated above sea level (with the exception of some marine-terminating sectors such as Wilkes Land and George V Land). The marine nature and smaller thickness of the WAIS means that the ice sheet is more vulnerable to climate warming and more prone to unstable retreat of the grounding line along inland deepening slopes (Weertman, 1974; Schoof, 2007). The WAIS and EAIS contain a global sea level equivalent of 3 to 5 m, and approximately 53 m, respectively (Fretwell et al., 2013).

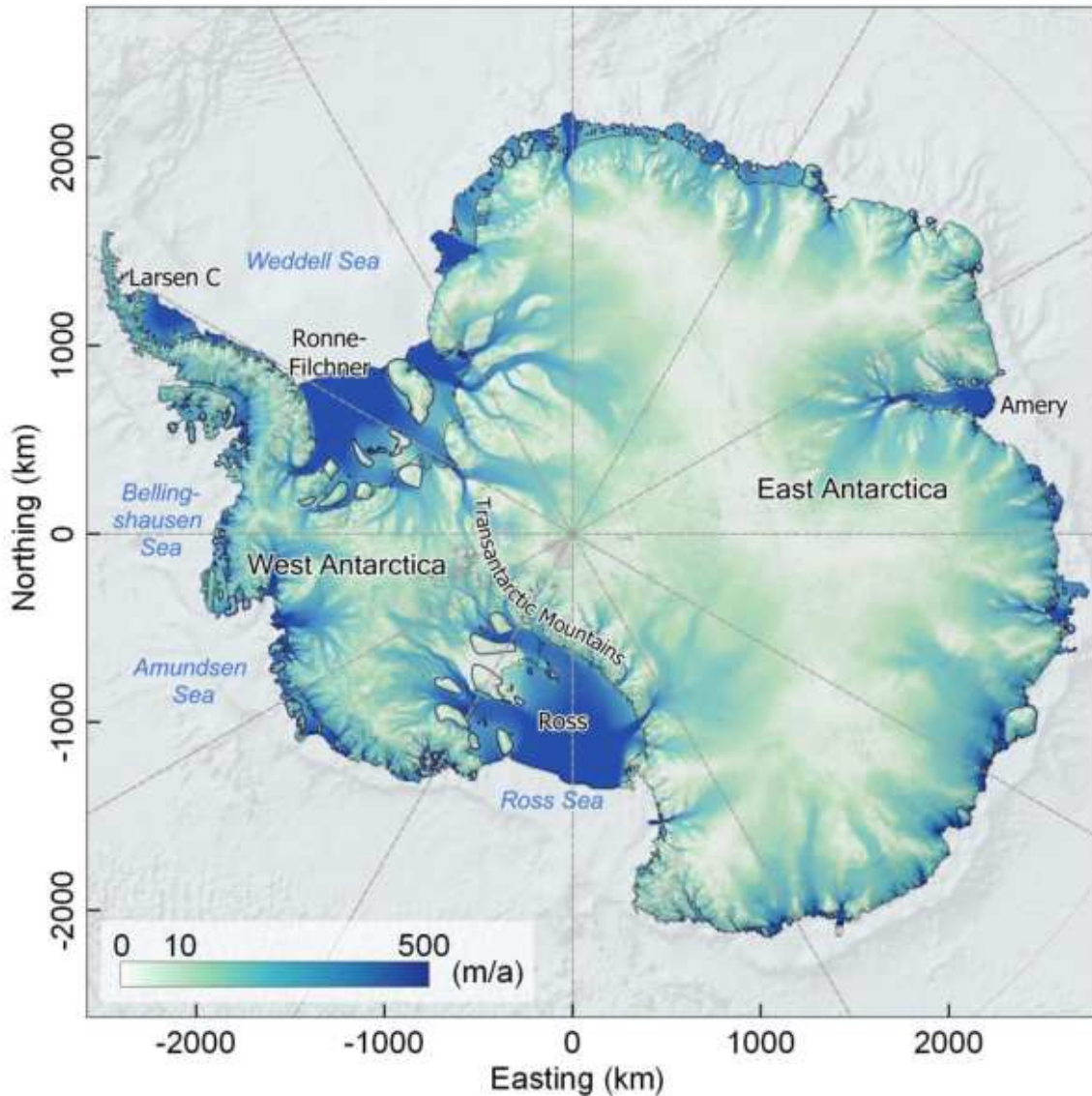


Figure 2.1: Geography of the Antarctic continent. Ice flow speeds from Rignot et al. (2011) demonstrate tributary flow. The grounding line and ice shelf boundaries are from Bindschadler et al. (2011), pinning point perimeters are from Matsuoka et al. (2015) and the IBSCO bed DEM is from Arndt et al. (2013). Prominent ice shelves are labelled.

2.2 The Antarctic contribution to sea level rise

Exchanges of mass between the cryosphere and ocean are the principal control on global mean sea level (GMSL) over multicentennial timescales. In general terms, large-scale mass loss from the Antarctic and Greenland Ice Sheets increases GMSL, while large-scale mass gain decreases GMSL. During the last century, mass loss from non-polar mountain glaciers and ocean thermal expansion were the two largest contributors to sea level rise (Church et al., 2013), however, the sea level rise contribution from polar ice sheets has since overtaken the mountain glacier contribution (Cazenave, 2018). The average rate of global sea level rise

from 1993 to present (detected via the satellite altimeter observational record) is $\sim 3 \text{ mm a}^{-1}$ (Nerem et al., 2010; Dieng et al., 2017; Ablain et al., 2017), in comparison to $\sim 1.2 \text{ mm a}^{-1}$ during the 20th century (Hay et al., 2015), and a background rate of tenths of millimeters per year during the late Holocene (Church et al., 2013). The rate of sea level rise is projected to increase to between 4 and 12 mm a^{-1} by 2100 as mass loss from the AIS and Greenland Ice Sheet accelerates (Church et al., 2013).

Of all sources of GMSL, the future contribution from the AIS is the most uncertain (Kopp et al., 2017; Garner et al., 2018; Robel et al., 2019). This uncertainty arises from the non-linear dynamic response of the ice sheet to oceanic and atmospheric warming (i.e., the potential for unstable, runaway grounding line retreat), the challenges inherent in simulations of regional-scale Antarctic meteorology, the simplified representation of physical processes in numerical ice sheet models used to make projections, and a short satellite observation record of ice sheet variability (~ 30 years) to validate the predictive capabilities of models (Kopp et al., 2017; Bamber et al., 2019). The sea level rise assessment in the Intergovernmental Panel on Climate Change (IPCC) Fifth Assessment Report (AR5) predicts a mean likely sea level contribution from the AIS of 4 cm by 2081-2100 (with an uncertainty bound of -6 to 12 cm) (Church et al., 2013). These projections, however, are regarded as conservative because non-linear, irreversible collapses of marine sectors are not accounted for in coupled ice sheet–climate models. Irreversible and rapid retreat of marine ice sheet sectors could increase sea level well beyond the range predicted by the IPCC (DeConto and Pollard, 2016; Bamber et al., 2019; Robel et al., 2019). More recent projections of the AIS contribution to GMSL rise exceed IPCC projections but vary widely depending on the physical processes incorporated into numerical ice sheet models. Coupled climate–ice sheet model simulations performed by DeConto and Pollard (2016) indicate an AIS sea level rise contribution of $>1\text{m}$ by 2100 when accounting for non-linear, rapid grounding line retreat driven by marine ice sheet and ice cliff instabilities in a ‘business as usual’ (RCP8.5) greenhouse gas emissions scenario. Other process-based models that do not account for marine ice cliff instabilities (currently an ill-constrained process) predict an AIS sea level contribution of 15 to 45 cm by 2100 under high emissions scenarios (Levermann et al., 2013; Ritz et al., 2015; Edwards et al., 2019; Bamber et al., 2019).

2.3 Mass loss from Antarctica

Ice sheet mass balance is defined as the net difference between mass gain from snow accumulation and mass loss into the ocean. Mass loss processes include basal melting, iceberg calving, surface meltwater runoff and surface ablation (sublimation). The latter two processes provide a minimal contribution to the AIS net mass balance (Rignot et al., 2013; Paolo et al., 2015) and therefore mass loss predominately occurs by contributions from basal melting and iceberg calving. Rates of mass loss depend on interconnections between climate (atmospheric and ocean warming controls melt rates and the surface mass balance) and ice flow dynamics (changes in the rate of ice flow from the ice sheet interior to the ocean).

The increasing Antarctic contribution to sea level rise principally originates from changes in ice dynamics (i.e., the speed up of outlet glaciers), rather than changes in the volume of snow accumulated in interior basins (Velicogna et al., 2014; Rignot et al., 2019). The rate of net mass loss from the WAIS, EAIS and Antarctic Peninsula has increased over the span of the observational record (Fig. 2.2). Mass loss from AIS has increased by 52% in the last decade (2009-2017) compared to 1999-2009 (Shepherd et al., 2018; Rignot et al., 2019). Antarctic mass loss is spatially variable, with high rates of dynamic mass loss concentrated along the Amundsen Sea sector of the WAIS periphery and the Antarctic Peninsula (McMillan et al., 2014; Paolo et al., 2015; Rignot et al., 2019). Processes responsible for this dynamic ice loss include relatively high basal melt rates and ice shelf thinning due to the incursion of relatively warm Circumpolar Deep Water (CDW) into ice shelf cavities (Dutrieux et al., 2014; Alley et al., 2015; Jenkins et al., 2018). As ice shelves thin, flow buttressing (compression that resists upstream ice flow) is reduced (Fürst et al., 2016), outlet glaciers respond by accelerating and thinning (Hulbe et al., 2008; Thomas et al., 2011; Alley et al., 2015), and the grounding line retreats (Konrad et al., 2018). Rates of mass loss from the EAIS are smaller but are accelerating (Fig. 2.1.2) (Rignot et al., 2019). Margins of the EAIS are undergoing dynamic thinning and outlet glaciers are retreating (Pritchard et al., 2012; Miles et al., 2013), contradicting the traditional notion that the EAIS is stable and insusceptible to changes in ice dynamics. The response time of polar ice sheets to environmental perturbations ranges from diurnal (tide forcing) to millennial (climate forcing) scales and the configuration of Antarctic ice shelves, the grounding line position, and the rate of mass loss observed today are all an integrated response to these perturbations. The long residence time of atmospheric CO₂, the range of time scales involved in the climate

response to CO₂ radiative forcing (Archer and Brovkin, 2008; Archer et al., 2009), and the range of time scales involved in ice sheet response to climate change imply that future changes in ice sheet volume are ‘committed’ according to the accumulated atmospheric CO₂ concentration (Levermann et al., 2013; Zickfeld et al., 2017). Past and present greenhouse gas emissions will continue to drive change in the WAIS over the coming centuries and millennia, regardless of the future emissions pathway (Levermann et al., 2013; DeConto and Pollard, 2016; Zickfeld et al., 2017).

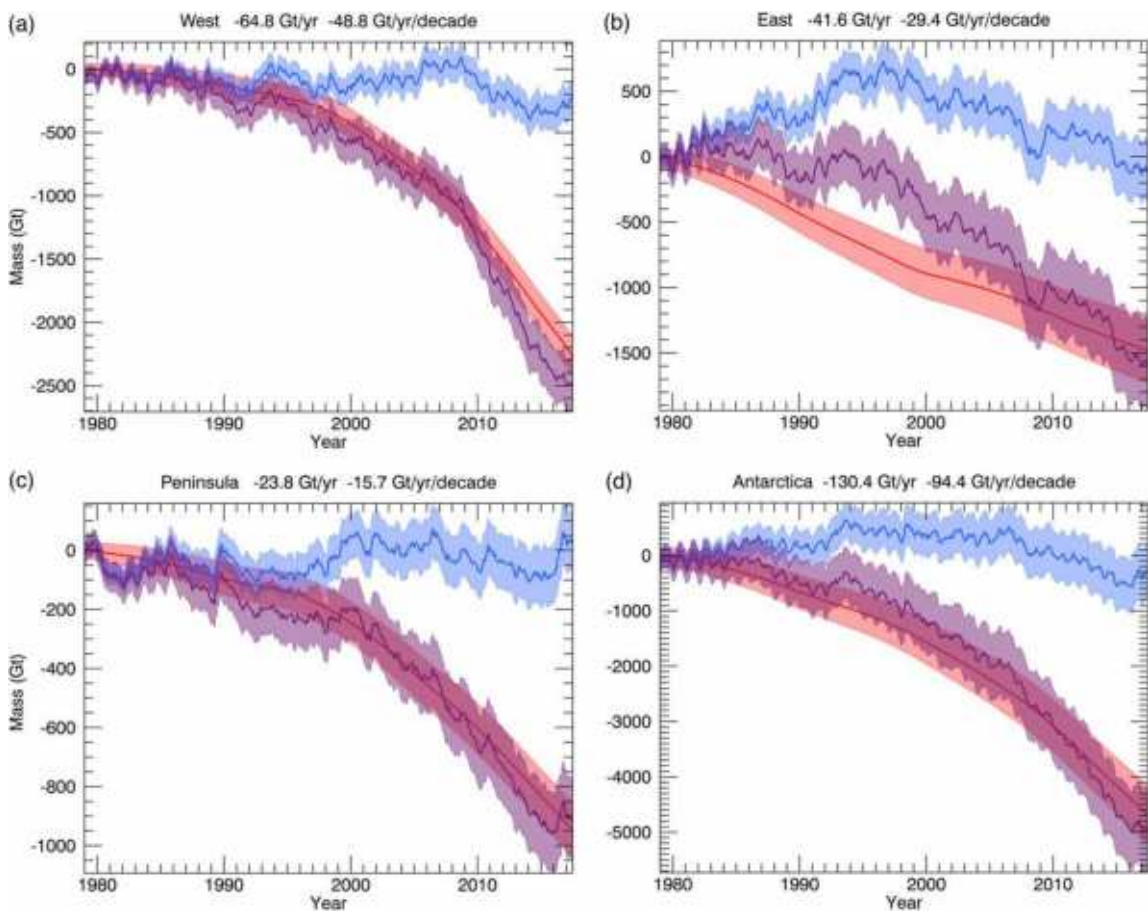


Figure 2.2: Cumulative changes in ice volume over the time period 1979-2017 for (a) the WAIS (b) the EAIS (c) the Antarctic Peninsula and (d) the entire AIS. The purple line represents the total mass change, the blue line represents the surface mass balance, and the red line represents the ice discharge into the ocean. The two numbers above each subfigure report the mean mass loss per year and the acceleration in mass loss per decade. This figure is a reprint of Fig. 3 from Rignot et al. (2019).

2.3.1 Mechanisms of rapid mass loss from the AIS

Ice shelves and ice sheets may exhibit non-linear threshold responses to climate forcing. These processes are inherently difficult to incorporate into numerical models, however correct representation of instability processes in ice sheet models will be needed to project Antarctic's future contribution to sea level rise. Mechanisms of rapid mass loss may result in changes to the ice shelf pinning points and therefore they are described here.

(a) Marine ice sheet instability (MISI)

Both the WAIS and some sectors of the EAIS are grounded below sea level on beds that deepen into the ice sheet interior (so-called “retrograde” slopes) (Fretwell et al., 2013) (Fig. 2.3). Ice sheets situated on submarine basins with grounding lines lying below sea level are sensitive to oceanic forcing via the influx of warmer modified circumpolar deep water into ice shelf cavities. An increase in basal melting due to the incursion of warmer water can change the balance of forces in the ice shelf by reducing the ice thickness and consequently its anchor to bathymetric features or by directly changing the thickness gradient near the grounding line. This, in turn, may initiate unstable grounding line retreat (Weertman, 1974; Schoof, 2007). When ice thins and its grounding line retreats along a landward deepening bed, ice starts to float. The ice flux, which depends on ice thickness and on basal sliding condition, increases, and the grounding line retreats further inland. Unless the grounding line stabilises on a bedrock ridge (Favier et al., 2014) or on a prograde slope (Schoof, 2007), the retreat is irreversible. Satellite records of grounding line retreat and ice sheet numerical model experiments have provided evidence to suggest that Pine Island and Thwaites Glaciers in the Amundsen Sea region may already be undergoing MISI caused by warmer CDW flowing up onto the continental shelf and under the glaciers' terminal ice shelves (Favier et al., 2014; Joughin et al., 2014; Rignot et al., 2014; Seroussi et al., 2017), although the exact set of conditions required to initiate MISI still remains unclear (Pattyn et al., 2018; Waibel et al., 2018). Rapid ice loss via MISI is anticipated to be a main driver of sea level rise beyond the year 2100 (Golledge et al., 2015; DeConto and Pollard, 2016).

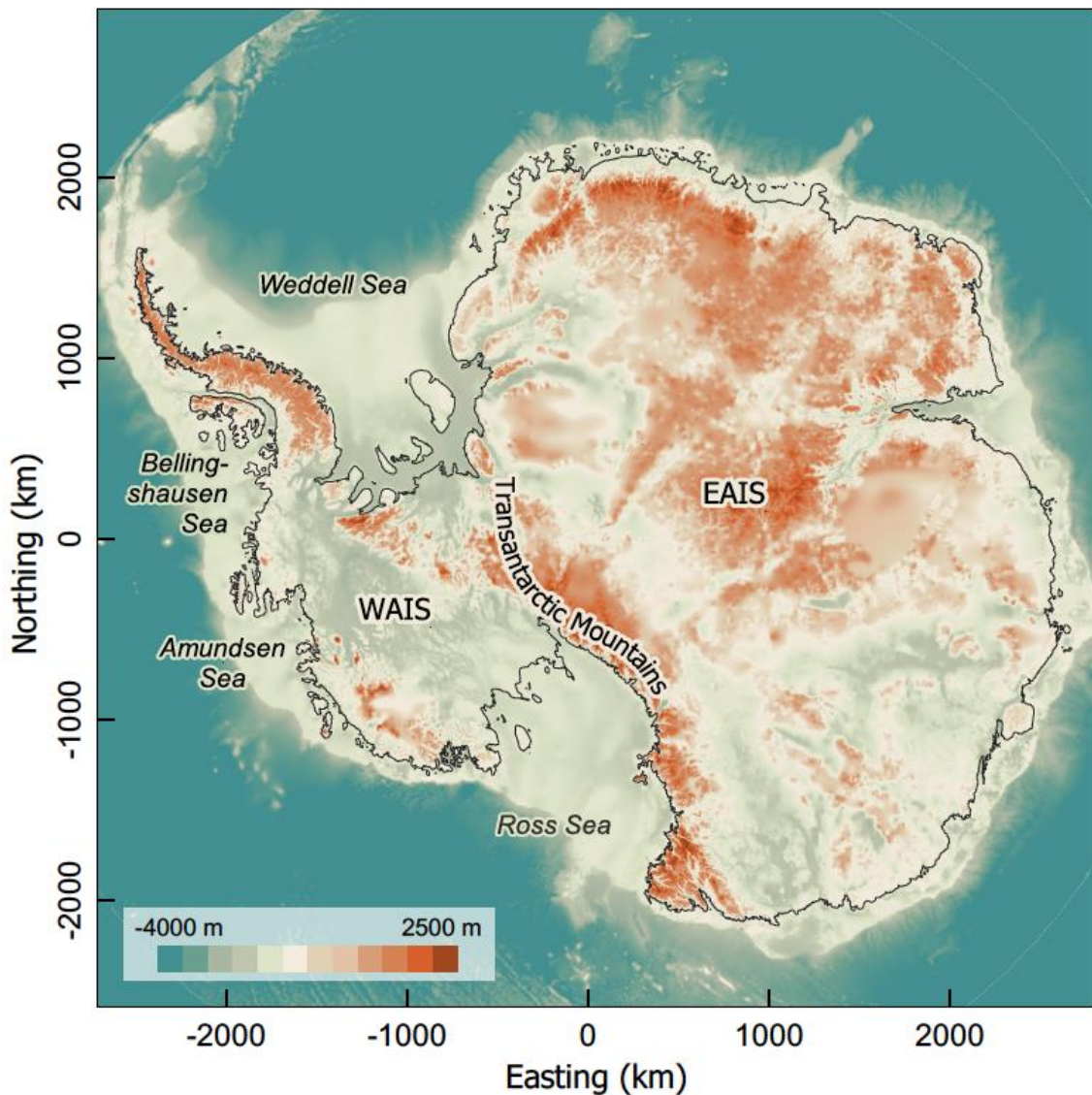


Figure 2.3: Bed elevation of the Antarctic continent. Much of the WAIS lies below sea level. The grounding line (Bindschadler et al., 2011) and pinning point locations (Moholdt and Matsuoka, 2015) are outlined. Bed elevation data are from the Bedmap2 dataset (Fretwell et al., 2013) and overlaid onto the IBSCO bed DEM (Arndt et al., 2013).

(b) Ice shelf hydrofracturing

The rapid disintegration of ice shelves can proceed by hydrofracturing when anomalous high summer temperatures facilitate surface meltwater ponding (Scambos et al., 2000). If the layer becomes saturated (preventing absorption and refreezing of meltwater), excess meltwater fills surface fractures, driving the vertical propagation of the fracture through the full ice shelf thickness (Scambos et al., 2000; Scambos et al., 2009). As large surface meltwater lakes drain, the ice shelf rebounds and new fractures form (MacAyeal and

Sergienko, 2013; Banwell and Macayeal, 2015; Banwell et al., 2019). The combination of relatively warm local air temperatures, meltwater ponding, and eventually hydrofracturing, contributed to the disintegration of the Antarctic Peninsula's Wordie Ice Shelf during the 1980s (Doake and Vaughan, 1991), and the Larsen A and B ice shelves in 1995 and 2002, respectively (Scambos et al., 2000; Banwell et al., 2013). In view of future RIS behaviour, small quantities of meltwater are detected on the shelf surface during the summer (e.g., Kingslake et al., 2017). This meltwater, however, is reabsorbed by the firn layer and does not accumulate into pools over time.

(c) Marine ice cliff instability (MICI)

MICI is a theorized mechanism of self-sustaining rapid ice sheet mass loss, invoked after ice shelf disintegration (Bassis and Walker, 2012; Bassis and Jacobs, 2013). MICI theory posits that the height of an ice cliff above sea level (freeboard) has a maximum limit before structural stability is compromised and the ice cliff collapses. The instability is initiated when tall marine-terminating ice cliffs are exposed following ice shelf disintegration. Mechanical failure of an ice cliff exposes a more expansive ice cliff, initiating further self-sustaining rapid retreat of the grounding line by runaway calving (Bassis and Walker, 2012; Pollard et al., 2015). While MICI provides an explanation for rapid sea level rise during the Pleistocene (Pollard et al., 2015), the only indirect observations of MICI include an absence of marine-terminating glaciers with high ice cliffs exceeding 100 m (implying that expansive ice cliffs must collapse) and geological evidence in the form of iceberg scour marks (Wise et al., 2017). At present, MICI processes are not fully developed in ice sheet models and parameterizations of calving and ice cliff collapse remain highly simplified.

2.4 The importance of Antarctic ice shelves

Ice shelves regulate the AIS contribution to sea level rise through their effects on the dynamics of the grounding line and upstream tributary glaciers. An ice shelf laterally confined within an embayment experiences reduced longitudinal tensile stress (and stretching) relative to an unconfined shelf, and this is transmitted across the grounding line (Dupont and Alley, 2005; Gagliardini et al., 2010). This flow resistance is provided by lateral shearing as ice flows past coastal features and islands, and by localized grounding on

topographic rises on the seafloor (Matsuoka et al., 2015). Together, these resistive stresses reduce the rate of mass flux across the grounding line, a mechanism commonly referred to as ‘flow buttressing’ (defined as a normal force exerted on upstream grounded ice by the ice shelf) (Dupont and Alley, 2005; Fürst et al., 2016). The buttressing potential of an ice shelf reduces with thinning, loss of mechanical contact with pinning points and coastal margins, or a loss of ice shelf extent (Dupont and Alley, 2005; Matsuoka et al., 2015; Fürst et al., 2016). These processes act to increase the net longitudinal (along-flow) tensile stress acting on the ice shelf and grounding line. An increase in the tensile stress generates faster creep rates and speed-up, thinning, and a greater susceptibility to fracture formation and propagation (Gagliardini et al., 2010; Borstad et al., 2013). Perturbations to the ice shelf stress balance are transmitted across the ice shelf and the grounding line. The loss of an ice shelf in both model simulations and observations causes the speed up of tributary glaciers and ice streams, inland thinning, grounding line retreat and ultimately an increase in ice discharged into the ocean (Rignot et al., 2004; Hulbe et al., 2008; Martin et al., 2019).

2.5 The Ross Ice Shelf

The Ross Ice Shelf (RIS, 78° S to 86° S) is Antarctica’s largest ice shelf with an area of 5.01×10^5 km² (Rignot et al., 2013), approximately twice the land area of New Zealand. Ice in the easternmost two-thirds of the ice shelf originates from the WAIS through the Ross ice streams (68 Gt/year), while ice in the westernmost third originates from the EAIS (52 Gt/year), flowing through the glaciated valleys of the Transantarctic Mountains (Thomas et al., 2013). Ice shelf thickness ranges from ~1 km along the Siple, Shirase and Gould Coast grounding lines, where ice enters the shelf, to ~100-200 m at the calving front (Fretwell et al., 2013). While the RIS is relatively stable at present (Pritchard et al., 2012; Campbell et al., 2018), the catchment is vulnerable to marine ice sheet instability (Fretwell et al., 2013, Morlinghem et al., 2020). Small perturbations in grounding line position could initiate relatively fast rates of grounding line retreat, and thus rapidly increase the WAIS sea level rise contribution.

2.5.1 Variations since the Last Glacial Maximum

The flow of the RIS and Ross ice streams varies over interannual to millennial timescales. Externally forced variations in ice flow are driven by the atmosphere or ocean while internally forced variations are driven by the ice sheet-ice shelf system. Internal instabilities alone are not inconsequential and are thought to have the potential to initiate grounding line retreat past a threshold where MISI is invoked (Joughin and Alley, 2011). Any observed changes in ice shelf flow or geometry should be interpreted with the contributions of external and internal forcing in mind (e.g., Campbell et al., 2017).

Since the LGM, the RIS grounding line retreated ~1300 km from near the continental shelf edge to its present-day position (Conway et al., 1999; Anderson et al., 2014). Retreat from the LGM maximum ice extent was episodic and nonuniform (Mosola and Anderson, 2006; Dowdeswell et al., 2008) rather than a sustained, constant retreat of the RIS grounding line. This non-uniform behavior implies that retreat is modulated by a combination of climate forcing, seafloor morphology (Anderson et al., 2014; Matsuoka et al., 2015) and variations in ice discharge from ice streams (Hulbe and Fahnestock, 2007). The RIS grounding line is thought to have retreated in two distinct phases - rapid retreat across the outer continental shelf during the early Holocene, followed by continuous, widespread grounding line retreat until the RIS reached its present-day configuration ~1500- 2000 years ago (Anderson et al., 2014; Yokoyama et al., 2016, Bart et al 2020). Initial, rapid grounding line retreat eventually slowed as the ice remained pinned on shallow stabilizing banks (Yokoyama et al., 2016; Kingslake et al., 2018). The grounding line position has remained relatively stable over the last 1500 years, punctuated with episodes of retreat and readvance (Catania et al., 2006; Kingslake et al., 2018).

2.5.2 Future prospects

The RIS is relatively stable in comparison to the Antarctic Peninsula and Amundsen Sea sector ice shelves that are exhibiting thinning, grounding line retreat and in some cases, have undergone catastrophic collapse (Scambos et al., 2000; Mouginot et al., 2014; Schannwell et al., 2016). Ice shelf collapse on the eastern side of the Antarctic Peninsula appears to have been driven by surface melting (Etourneau et al 2019) while the primary cause of change in

the Amundsen Sea region appears to be sub-shelf melting and thinning due to the intrusion of CDW in ice shelf cavities. CDW is a relatively warmer water mass 3-4 C higher than the freezing temperature (Jacobs et al., 1992; Pritchard et al., 2012) and consequently average basal melt rates for the Amundsen Sea ice shelves can exceed 5 m a^{-1} (Pritchard et al., 2012). In contrast, the RIS is less exposed to CDW due to the presence of colder continental shelf waters that inhibit basal melting (Orsi and Wiederwohl, 2009; Anderson et al., 2019). While present shelf-wide RIS melt rates are relatively low, numerical model simulations project a pattern of greater basal melt rates in the eastern sector of the RIS (near Roosevelt Island) generated by the inflow of warmer water masses from the east Ross Sea (Schodlok et al., 2016, Tinto et al 2019). Feedbacks between climate warming and modifications to ocean dynamics (including the incursion of CDW into ice shelf cavities and warming of CDW) remain a key uncertainty in projections of the WAIS/EAIS response to climate change.

Chapter 3

3. METHODS AND DATA

3.1 Introduction

Mapping the sea floor can help reveal the traces left by the last glacial retreat.

Marine geologists use acoustic methods such as multibeam and sub-bottom profiler for seafloor surveying. These methods can produce high-resolution images of the seabed and sediments beneath the seafloor. Thanks to their ability to visualize both surface forms and deep sediments, acoustic methods are suitable for studying morphology and sediments in marine environments in areas affected by glaciations, such as the continental margin of Antarctica.

The methods used in this thesis include processes and techniques used for the analysis and interpretation of geophysical, sedimentological and geochemical data, description sampling and data collection methods.

3.2 Project Goals

The goal of this project is to analyze and interpret the geomorphological features of the seabed of the two case studies Edisto Inlet Fjord and Robertson Bay in the western Ross Sea in relation to glacial history and paleoceanography using acoustic data acquired with marine geophysical mapping methods, sedimentological data and geochemical analyses.

3.3 Geophysical Methods

3.3.1 Bathymetric survey

Echosounder or depth sensing sonar is used to determine the depth of water under the transducer (bathymetry). It involves the transmission of acoustic waves in water and the recording of the time interval between the emission and the return of an impulse; This measurement is based on the velocity of sound through water and the time from transmission to reception. The depth acquired needs to be corrected for tidal effects and is reduced to Lowest Astronomical Tide (LAT) as a standard. These surveys typically employ an Multibeam echo sounder (MBES) Figure 3.1.

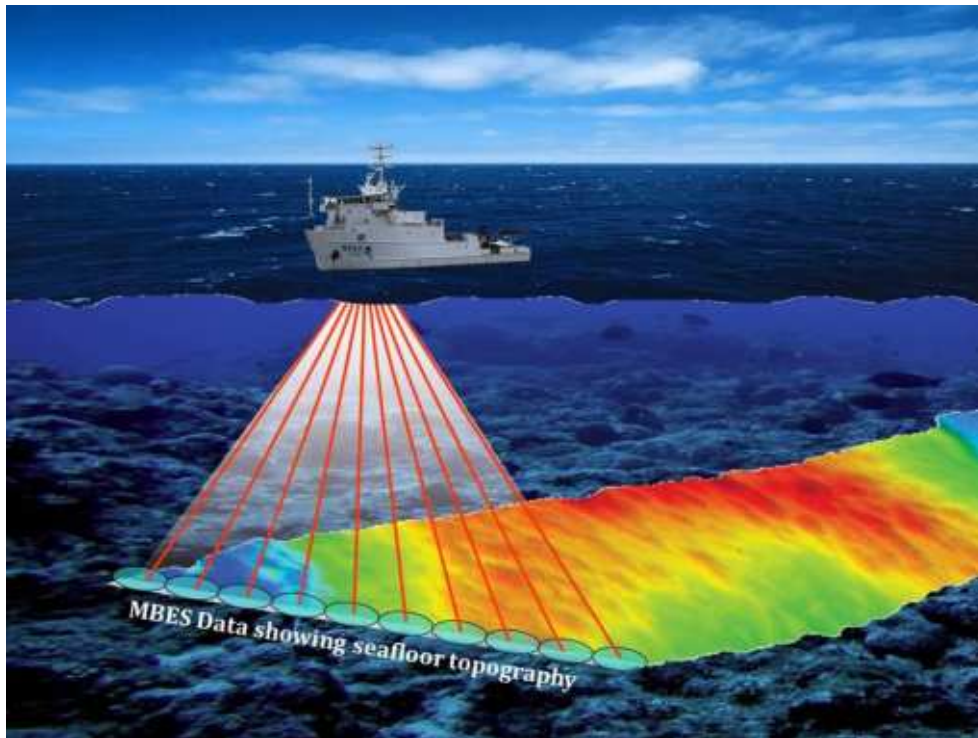


Figure 3.1: Multibeam echo sonar (MBES) is used to map the ocean floor. Image courtesy of New Zealand Institute of Water and Atmospheric Sciences.

MBES have become one of the standard tools for geophysical surveying and seafloor mapping and have been used for a variety of scientific, maritime safety (hydrographic and military operations) and industrial applications. MBES can produce a spatially continuous acoustic image of the seafloor surface by generating a "swath" or "fan" of continuous data points, increasing the resolution of the resulting surfaces. This has revolutionized our ability

to understand the physical processes occurring on the seafloor and the composition and distribution of the substrate, which in turn has greatly improved our knowledge of seafloor ecosystems (Lucieer and Lamarche 2011). Bathymetric morphology mapping will outline the geological features that matter (using changes in seafloor depth information), however in regions where the relief is smaller than the minimum mapping unit (resolution of the grid cell is larger than the feature of interest) backscatter data can be used to assess the boundaries of the geology or sediment structure.

3.3.2 Data Acquisition and Processing

Swath bathymetric data was acquired during the OGS Explora expedition 2017 along the Edisto Inlet fjord, using a Teledyne Reson SeaBat 7150 Multibeam Echo Sounder, which has a system frequency of 12 kHz and 880 beams. These data sets were processed using PDS2000 software, then survey data were manually edited to remove anomalous readings and gridded to create relief maps. The optimal resolution of the data is a 10 m grid.

In Mac Robertson Bay the multibeam swath bathymetry data were collected during a geophysical research expedition aboard the RV/IB Araon. Multibeam soundings were collected in a swath perpendicular to the ship track using a hull-mounted Kongsberg EM122 (Kongsberg Maritime, Kongsberg, Norway), with a swath of 432 beams, operating at a frequency of 12 KHz. Acquired bathymetry data were processed onboard using CARIS (HIPS&SIPS 9.0, Teledyne CARIS, Fredericton, NB, Canada), specialized bathymetry processing software, and the results were plotted using Generic Mapping Tools (GMT 6.1.1, School of Ocean and Earth Science and Technology of University of Hawaii at Manoa, HI, USA) software and gridded to 25x25m. To understand ice flow activity, we compared the submarine landforms to the seafloor lithology based on sub-bottom profiling results.

3.3.3 Seismic reflection method

The “high-resolution sub-bottom profilers such as the chirp sonar used for this study generate a sound wave by passing electricity through a piezo-electric material. This causes the piezoelectric material to expand and contract and doing so transmits sound. The transmitted sound wave is later echoed back from the sea floor or internal reflectors in the

below sea floor to the receiver and the two-way travel time (TWT) is recorded. This can be converted to depth using equation (1):

$$d = v * \frac{TWT}{2} \quad (1)$$

where v is the sound wave velocity (Jakobsson et al., 2016). Acoustic waves obey the same natural laws as light passing through different media and therefore, we can describe the behaviour of sound waves using Snell's Law shown in equation (2):

$$\frac{\sin \theta_1}{v_1} = \frac{\sin \theta_2}{v_2} \quad (2)$$

where θ_1 is the incidence angle, v_1 is the velocity of the incidence wave, θ_2 is the refraction angle and v_2 is the refracted wave velocity (Jakobsson et al., 2016). The wave reflection coefficient (μ_0) is a measure of the strength of the reflected acoustic wave, and is dependent on the acoustic impedance contrast of the lithological layers as is described in equation (3):

$$\mu_0 = \frac{I_2 - I_1}{I_2 + I_1} = \frac{v_2 * \rho_2 - v_1 * \rho_1}{v_2 * \rho_2 + v_1 * \rho_1} \quad (3)$$

where I_1 is the acoustic impedance of the first lithological layer, I_2 is the acoustic impedance of the second layer, v_1 is the acoustic wave velocity in the first layer, v_2 is the velocity in the second layer, ρ_1 and ρ_2 is the bulk density in the first and second layer the beam passes through (Mosher & Simpkin, 1999), see figure (3.2).

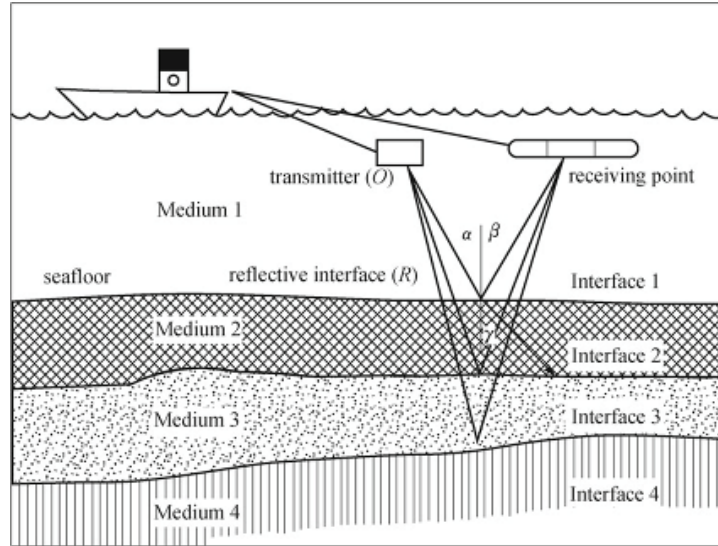


Figure 3.2: Image showing the principle behind SBPs where the incoming signal is both reflected from the sea floor and refracted down the sediments. The refracted beam can also be reflected and refracted as a new sediment layer of different acoustic impedance. Sun et al. (2021)

The area covered by the sound beam is determined by the footprint (Df), which is calculated using equation (4):

$$Df = 2 * H * \tan\left(\frac{\alpha}{2}\right) \quad (4)$$

where H is the distance from sound source to the sea floor and α is the beam angle (Jakobsson et al., 2016). The beam angle is the angle the beam has when leaving the transducer source and is dependent of the interference pattern generated by the apparatus and is determined by the frequency of the sound wave and the length of the transducer (Jakobsson et al., 2016). The beam angle can be calculated using equation (5) below (Jakobsson et al., 2016):

$$\alpha = \frac{60 * \lambda}{\emptyset} \quad (5)$$

from the wavelength of the sound wave (λ) and the transducer length (\emptyset).

The resolution of the data is the minimum distance that two different objects must be separated to be distinguished in the sonar reading as individual objects vertically or horizontally. Resolution in all signal processing is linked to the frequency, whose maximum value is constrained by Nyquist Theorem, which states that the minimum sampling density

must be twice the frequency of the signal. If the sampling density is lower than this, we will experience aliasing, which is a form of signal distortion (Jakobsson et al., 2016). The ability to distinguish the difference between two objects vertically acoustic data is determined by the Rayleigh criterion which states that two objects must be separated a quarter of the wavelength as stated by equation (6):

$$Rv = \lambda * \frac{1}{4} \quad (6)$$

where Rv is vertical resolution and λ is the wavelength (Jakobsson et al., 2016). In vertical resolution consideration must be taken to water depth meaning that for shallower waters with depth less than 100 m the frequency should be higher than 200 kHz with a wavelength shorter than 0.75 cm and for larger depths of more than 1.5 km the frequency should be between 12 kHz and 50 kHz with a wavelength between 12.5 cm and 3 cm (Jakobsson et al., 2016). This is because the energy of a high frequency signal is more easily absorbed in the sea water. With a long wavelength (i.e. low frequency), the beams can reach longer but the resolution will be lower (Jakobsson et al., 2016). The ability to resolve objects horizontally on the sea floor is also determined by the 1st Fresnel zone since everything outside this zone will alternate between constructive and destructive interference. The 1st Fresnel zone radius is determined with equation (7):

$$RF \approx \sqrt{\frac{H*\lambda}{2}} \quad (7)$$

Where RF is the Fresnel zone radius, H is the water depth and λ is the wavelength (Jakobsson et al., 2016). For the multibeam sonar system used here, the horizontal resolution is for a signal of 300 kHz and a water depth at ~40m gives a resolution of 31.6 cm whereas the chirp sonar has a vertical resolution determined by equation (8);

$$Rv_{chirp} = \frac{v}{(2*B)} \quad (8)$$

where v is the sound speed velocity in sea water (approximated to 1500 m/s), B is the bandwidth ranging from 14 kHz if SBP has 2 kHz to 16 kHz range, giving a vertical resolution of about 5 cm”.

3.3.3.1 The Sub-Bottom Profiler

The sub-bottom profilers (SBP) are powerful tools of looking down through the sediment layers. The chirp sonar transmits an FM signal sweeps a range of frequencies spanning from 2 kHz to 16 kHz which enables the chirp to generate a sound pulse stronger than ordinary SBPs (Jakobsson et al., 2016). The behaviour of the transmitted signal obeys the physical laws described in equations (2) and (3) implying that the beams will either reflect or refract when encountering a geological layer of different acoustic impedance. The reflection coefficient in equation (3) is determined by the impedance and sound velocity in the layer which manifests in the produced SBP image (Lurton, 2010). The chirp sonar also makes use of a so-called matched filter (figure 3.3) that matches a compressed transmitted FM signal to the received signal which allows a collapse of the signal leaving an amplified signal to generate higher penetration and resolution (Schock et al., 1989).

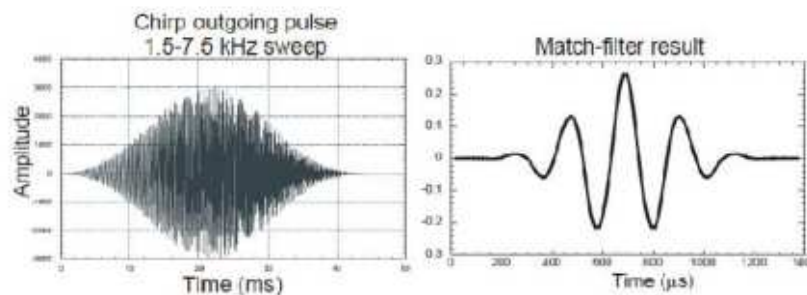


Figure 3.3 Showing the matched filter cleaning the outgoing Chirp pulse when returned to the receiver, figure from Mosher & Simpkin, (1999). Notice the shorter wavelength and lower amplitude.

3.3.3.2 SBP Acquisition and Processing

From 2002 to early 2017 the Italian research vessels *Italica* and *OGS Explora* performed shallow chirp seismic profiles in the continental shelf of the Ross Sea.

Sub-bottom profiles were acquired in the Edisto Inlet fjord entrance with a 3.5 kHz SBP on N/R *Italica* in 2005 and a hull-mounted Benthos CAP-6600 Chirp II Data Sonics on board of N/R *OGS Explora* in 2017 along the entire fjord. The Chirp sweep had frequencies between 2 and 7 kHz with 10 ms length and to reduce the magnitude of the Klauder wavelet side-lobes, a tapering function of 10% was used (Gutowski et al. 2002). The Chirp data were not recorded as envelope format after Hilbert transformation, but in full wave, after the

cross-correlation with sweep, so that the signal/noise ratio could be improved with post-cruise processing (Quinn et al., 1997, Baradello, 2014, Baradello et al., 2021), to attenuate the sea-waves effects and the signal ripples.

The two seismic datasets embrace a wide spectrum of penetration depth (up to ca. 100 meters below the sea floor, assuming a velocity of 1500 m/s) and vertical resolution between 100 and 20 cm, providing a good image of the geological setting beneath the seafloor and good potential for correlation with main density shift detected in the sediment cores.

The analysis of all dataset was conducted by using the IHS Kingdom Suite seismic interpretation software, to perform seismic stratigraphy, correlation of acoustic facies with sediment magnetic susceptibility and grain size logs and to obtain three dimensional, morpho-bathymetric images of the fjord.

Shallow sub-bottom profiling data were collected from a Korea Polar Research Institute (KOPRI) cruise in 2015 in the sampling area, Robertson Bay, using an SBP120 Sub-bottom profiler with an optional extension to the highly acclaimed EM122 multibeam echo sounder. The data were logged in the TOPAS raw format and can be saved in SEG-Y format for postprocessing with a standard seismic package. The data were used to identify seafloor lithology and the thickness of surface sedimentary units (unconsolidated sediments up to 100 m below the seafloor). Additional SBP data was collected with the RV *Italica* in 2005 where the sampling frequency during the campaign survey was 12kHz using a SBP Geopulse Transmitter Mod. 5430 and a Geopulse Receiver Mod. 5210A. Hull transducers (n° 16), with a frequency of 3.5 kHz. Profiles were analyzed using the IHS Kingdom software.

3.3.3.3 Processing Data

All SBP data were processed by L. Baradello using the FOCUS-PARADIGM package on workstation Linux. The raw data show a DC-offset and several high-frequency noises are random along traces, due to spurious electrical currents during surveys (noise bursts). With a low-cut filter, we attenuated the DC and with a 2-D median filter cleaned the noisy electrical discharges (Figure 3.4).

During transmission, the wavefront spreading, and frequency absorption produce a strong amplitude decrease in the signals. After the spherical divergence correction, the amplitude recovery was attained by applying decay curves calculated along time gates.

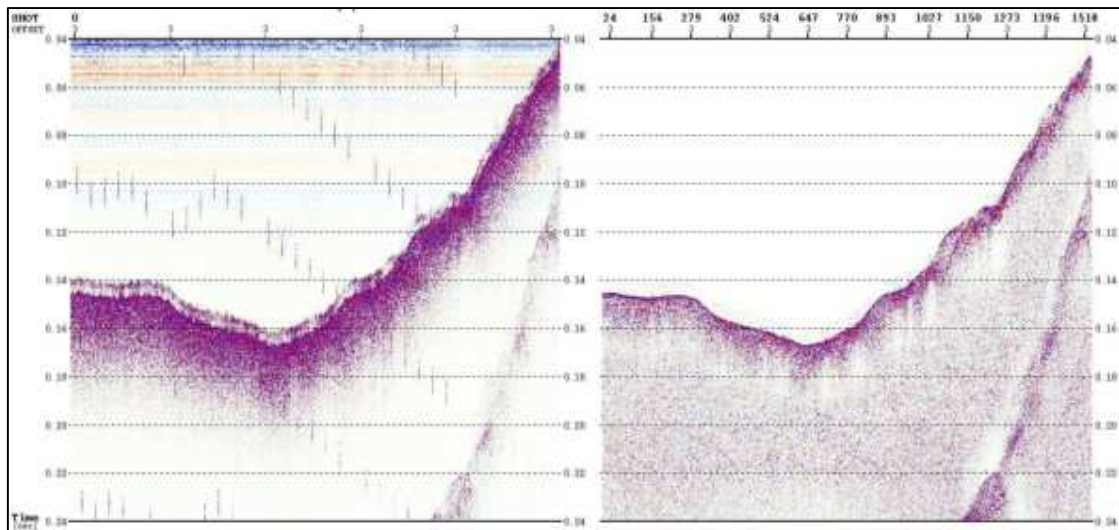


Figure 3.4: Example of row data (left) and after electrical clean and amplitude recovery (right).

In order to improve the interpretability, we focused the processing to attenuate the sea-waves effects and the signal ripples. The sea undulations modify the images of the sea-bottom and underlying sediments, causing often a loss of reflections continuity. We solved this problem applying a Non-Surface-Consistent Static correction (NCS). In a time-window centered around the sea-bottom, it's detected a pilot trace and then evaluated time shifts present in all other input traces. The pilot trace represents a median of traces sliding along the profile.

Data exhibit ringing on reflections, caused by Klauder tails. The Klauder is a zero-phase wavelet and this is not a condition to use the deconvolution (Yilmaz, 2001).

The earth acts on the sweep as a minimum-phase filter, so SBP data reflections could be considered to mixed-phase signals. After several test we found a predictive deconvolution that improves a lot vertical resolution attenuating Klauder lobes (Figure 3.5). The deconvolution parameters were obtained from trace autocorrelation: the second zero is the gap and the operator length is 0.6 – 0.9 ms. Furthermore, not to run into Wiener algorithm issues, a 0.1% of white noise was added.

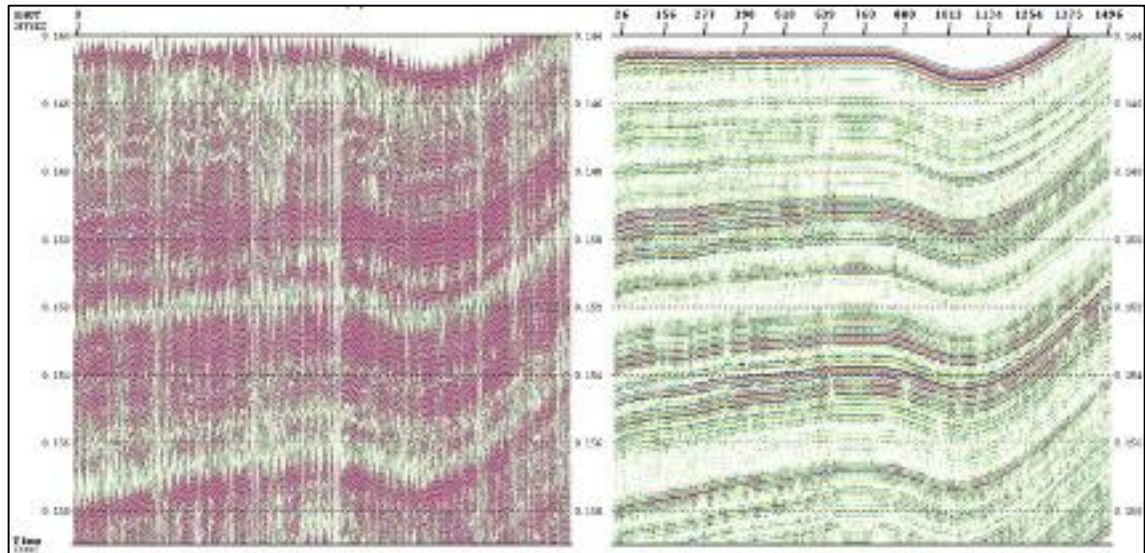


Figure 3.5: Example of gained data (left) and after deconvolution and sea waves correction (right).

To improve the interpretation to enhance the weak reflections, the Hilbert transform was applied and a seismic attribute, the trace envelope, a phase-independent amplitude representation was created (Henkart, 2006).

3.4 Tool for Paleo-reconstructions

3.4.1 Marine sediment cores

Marine sediment cores preserve material derived from the water column and terrestrial sources. Coastal areas of Antarctica, particularly within the Ross Sea, are sites of strong air-ocean-ice interaction, in comparison to the deep ocean, with the potential to preserve continuous records of environmental change (Arrigo et al., 2008; Bendle, 2011). As a result, these regions experience enhanced seasonality and primary production, which on millennial-centennial timescales, provides insight into long-term trends and transient changes in the environment and overall oceanography and climate (Leventer et al., 1993, 2002; Finocchiaro et al., 2005).

3.4.1.1 Marine sediment cores database

The study of **Edisto Inlet Fjord** is focused on 10 sediment cores (BAY05 13c, 14c, 18c, 19c, 20c, 2c, ANTA02-CH41, HLF17-01, RS17-GC03, RS17-GC04) collected during several Italian oceanographic cruises in the framework of PNRA-Projects and located very close or on the SBP seismic profiles. All cores are stored at the Sorting Center of the Italian National Antarctic Museum Section of Trieste (<http://www.mna.it/collezioni/antarctic-marine-sediments-trieste-section>). Some cores have been already published, others have been analysed but not published yet, others are still closed, and only magnetic susceptibility (MS) and X-ray are available. Table 1 summarizes the details of dataset and the available data for each considered core and the bay sector.

Table 1 : PNRA sediment cores dataset available in the Edisto Inlet Fjord

location	tool	PNRA Expedition	coreID	Lat (S)	Long (E)	water depth (m)	recovery (cm)	MS Bartington	MSCL	X-ray	Water content	grain size	TOC	BioSi	¹⁴ C (quantity)	PROJECT	references
sector 1	gravity core	XVII	ANTA02-CH41	72° 17.49'	170° 09.05'	416	406	X		X	X	X	X	X	7	Glaciology and Paleoclimatology	Finocchiaro et al.(2005)
sector 1	gravity core	XX	BAY05-13c	72° 17.64'	170° 08.92'	411	166	X		X						BAY	
sector 1	gravity core	XX	BAY05-14c	72° 17.66'	170°08.92'	411	452	X		X						BAY	
sector 1	gravity core	XX	BAY05-18c	72° 17.85'	170° 05.27'	464	419	X		X	X	X	X	X	2	BAY	
sector 1	gravity core	XX	BAY05-19c	72° 17.68'	170° 07.48'	422	73	X		X						BAY	
sector 1	gravity core	XX	BAY05-20c	72° 18.30'	170° 04.46'	456	445	X		X	X	X	X	X	4	BAY	Mezgec et al. (2017), Di Roberto et al. (2020)
sector 2	gravity core	XX	BAY05-22c	72° 19.17'	170° 04.83'	447	389	X		X	X	X	X		4	BAY	
sector 2	piston core	XXXIII	HLF17-01PC	72° 19.44'	170° 01.58'	465	1465	X		X	X	X	X		13	HOLOFERNE	Tesi et al. (2020)
sector 2	gravity core	XXXIII	IT17RS_GC003	72° 20.60'	170° 01.11'	495	430		X	X					1	GLEVORS	
sector 2	gravity core	XXXIII	IT17RS_GC004	72°19.75'	170° 01.11'	504	406		X	X						GLEVORS	

The BAY Project took place in January 2005 and collected Sub Bottom Profiler, gravity cores and box corer in several bays along the Victoria Land coast.

In **Robertson Bay** 8 gravity cores (for a total of 30 meters) and one box corer were acquired. The choice of the sampling sites has been assisted by the aid of the high-resolution seismic profiles (SBP). The sediment cores, with an average length of about 4 meters, were sectioned into 100 cm lengths and the magnetic susceptibility was measured on board. The cores were then stored at -4° C for the subsequent analysis.

Of the eight cores acquired in Robertson Bay, to date only three have been opened (28c-29c-32c) and preliminary described on board. Of these three, two were chosen for this thesis: the core 29c and the core 32c. On these cores the following analysis were made (Table 2): X-ray analysis (Bartington MS2C), grain size analysis (approximately every 20 cm) (the biogenic component is given mainly by diatoms and spicules), multisensor core logger analysis (density, magnetic susceptibility, p-Wave), magnetic susceptibility was made on board and forams assemblage (R. Melis, not published yet) at University of Trieste. Organic matter characterization (TOC, TIC), Carbone and Nitrogen isotopes ($\delta^{13}\text{C}$; $\delta^{15}\text{N}$) and Biogenic silica concentration (BSi) at University of Otago and Ramped Pyrolysis at the Rafter Radiocarbon Lab AMS facility at GNS in Wellington for radiocarbon dating.

Table 2: summarizes the details of dataset and the available data for these cores:

PNRA Expedition	core ID	tool	PROJECT	Lat (S)	Long (E)	water depth (m)	recovery (cm)	MS Bartington	MSCL	X-ray	Water content	grain size	TOC	BSi	^{14}C (quantity)	Ramped Pyrolysis
XX	BAY05-29c	gravity core	BAY	71° 29' 128	169° 45' 117	524	585	X	X	X	X	X	X	X	4	4
XX	BAY05-32c	gravity core	BAY	71° 24' 296	169° 50' 225	406	468	X	X	X	X	X	X	X	5	5

3.4.2 Diatoms Ecology

Diatoms are an effective proxy for reconstructing past environmental conditions, because they are highly specialized to their environment, abundant, diverse, and readily preserved in high latitude marine sediment (Armand et al., 2005, Crosta et al., 2005; Cunningham et al., 1999). In marine sediment cores variations in diatom assemblage is a useful indicator of paleoenvironmental change; previous studies of modern diatom distributions in the water

column and within surface sediments from Antarctica demonstrate that diatom assemblages found in the sediments accurately reflect spatial variations in productivity, oceanography, and the extent/duration of sea ice cover (Armand et al., 2005; Crosta et al., 2005; Cunningham and Leventer, 1998; Kellogg and Truesdale, 1979; Scott, 2005).

Published data on the ecology and assembly of diatoms by Finocchiaro et al (2005), Mezgec et al (2017) and Tesi et al (2020) were used for the paleo-environmental reconstruction of Edisto Inlet Fjord.

The unpublished datasets for the reconstruction of the paleo-environment in Robertson Bay presented in this thesis were provided by PhD student F. Torricella who performed diatom analysis at the University of Pisa.

Table 3.4.2 A summary of the environmental preferences of diatoms present in relative abundances of greater than 5% in Robertson Bay

Species	Ecological information
<i>Fragilariopsis curta</i>	<i>F. curta</i> abundance increases southward with increasing sea ice cover and decreasing temperature (Gersonde and Zielinski, 2000). <i>F. curta</i> is associated with pack and fast-ice with highest occurrences both within sea and as well as in ice melt influenced waters in the marginal ice zones (Cunningham and Leventer, 1998; Cunningham et al., 1999; Leventer et al., 1996). <i>F. curta</i> is also associated with heavily consolidated winter sea ice conditions (60-90%) and is most abundant in locations with 9- 11 months/year of sea-ice cover and Austral summer February SST temperatures between 0.5 and 1 °C (Armand et al., 2005). Summer sea ice does not appear to play a role in its distribution below 40%: <i>F. curta</i> is equally tolerant of un-consolidated summer sea ice cover and ice free conditions (Armand et. al, 2005)
<i>Fragilariopsis obliquecostata</i>	<i>F. obliquecostata</i> is associated with surface melt pools though it is also found in water beneath sea ice and has been observed in land-fast and pack-ice samples (Armand et al., 2005). Confined to a sea ice environment, highest abundances of <i>F. obliquecostata</i> occur in areas with 7 months/year of sea ice cover and heavily consolidated winter sea ice (65-90%) that remain ice free in the summer with February SSTs between -1 and 0 °C (Gersonde and Zielinski, 2000; Armand et al., 2005).

<i>Thalassiosira antarctica</i>	<i>T. antarctica</i> is a sea ice species associated with low SSTs and a meltwater rich environment through it requires open water to bloom. Blooms are often recorded late in the summer season after sea ice has retreated and/or in association with newly forming sea ice (Cunningham and Leventer, 1998; Cunningham et al., 1999; Leventer et al., 1996). <i>T. antarctica</i> is a major component of assemblages in non-stratified or weakly stratified surface waters and associated with open water primary production. Abundances greater than 10% indicate sea ice duration is greater than 6 months/year and maximum abundances (32%) occur in regions with February SSTs between 0 and 0.5 °C and a maximum sea ice duration of 8.5 months/year (Armand et al., 2005).
<i>Chaetoceros spp.</i>	<i>Chaetoceros spp.</i> is associated with nutrient-rich, wind-mixed surface waters (Beans et al., 2008; Cunningham and Leventer, 1998; Leventer et al., 1996). <i>Chaetoceros</i> resting spore (CRS) formation occurs when stratified surface waters become nutrient depleted; high abundances of CRS relative to <i>Chaetoceros spp.</i> are associated with nutrient limitation and strong spring stratification (Leventer, 1992)
<i>Setae group</i>	<i>Chaetoceros spp.</i> , <i>Corethron spp.</i> , <i>Rhizosolenia spp.</i> , and <i>Proboscia spp.</i> Are often found together in Antarctic coastal environments with nutrient rich mixed surface waters (Beans et al., 2008). Grouped as the setae diatom group (S-DG), Denis et al. (2009) proposed their relative abundance as a proxy for upwelling of mCDW in the Adélie Land region (increased abundance = increased upwelling).

3.5 Geochemistry

3.5.1 The carbon isotopes proxy

In marine sediments, carbon isotopes are an effective proxy for primary production, ocean atmosphere interaction and changes in water mass sources (Berg et al., 2011; Crosta et al., 2002; Villinski et al., 2000). Carbon isotope values are reported in per mil (‰) using standard delta notation:

$$\delta^{13}\text{C} = \frac{(^{13}\text{C}/^{12}\text{C})_{\text{sample}} - (^{13}\text{C}/^{12}\text{C})_{\text{standard}}}{(^{13}\text{C}/^{12}\text{C})_{\text{standard}}} \times 1,000$$

where the reference standard is Pee Dee Belemnite (PDB) carbonate material. The anomalously high ratio of ^{13}C to ^{12}C in PDB (0.0112372), was established as $\delta^{13}\text{C}$ value of zero (Libes, 1992).

In Antarctic settings, the $\delta^{13}\text{C}$ in bulk sediments is an effective proxy for primary production and/or changes in water mass source and structure (Berg et al., 2013; Crosta et al., 2002; Villinski et al., 2000). Diatoms and other phytoplankton biologically discriminate against the heavier ^{13}C isotope relative to ^{12}C . This process causes the stable carbon isotopic signature ($\delta^{13}\text{C}$) of the residual pool of dissolved inorganic carbon (DIC) to become more positive if the carbon pool is not replenished by mixing. Furthermore, the phytoplankton are preserved in the seafloor and record this more positive $\delta^{13}\text{C}$ signature (Hayes, 1993; Henley et al., 2012; Jacot Des Combes et al., 2008). Drawdown of CO_2 via photosynthesis during phytoplankton blooms influence the pCO_2 of the upper water column, and consequently affects CO_2 flux between the atmosphere and ocean. This process is globally important: CO_2 is removed from the atmosphere, incorporated into phytoplankton biomass and sequestered in seafloor sediments, thus influencing global atmospheric temperature (Henley et al., 2012; Villinski et al., 2000).

Carbon is affected by several processes in the water column and post-depositional alteration (Jacot Des Combes et al., 2008; O'Leary et al., 2001; Villinski et al., 2000). Stratification of the water column from spring sea-ice melt results in nutrient depletion in the surface water and reduced primary productivity. Stratification prevents replenishment of the DIC pool,

where phytoplankton preferentially assimilate the lighter ^{12}C carbon and later in the season, when ^{12}C is fractionally consumed, will assimilate ^{13}C . As mentioned previously, this process is reflected in a more positive sedimentary $\delta^{13}\text{C}$ signature. Vital effects including species-specific isotopic fractionation alters $\delta^{13}\text{C}$, and thus changes in $\delta^{13}\text{C}$ can reflect both changes in dominant diatom assemblages and environmental influences (Arrigo et al., 1998; Berg et al., 2013; Henley et al., 2012; O'Leary et al., 2001; Villinski et al., 2000).

3.5.2 The nitrogen isotopes proxy

Nitrogen isotopes are an important tool for evaluating past changes in ocean circulation, large scale N cycling and the biological pump strength (Karsh et al., 2014; Robinson et al., 2008; Robinson et al., 2012). Nitrogen isotope values are reported in per mil (‰) using standard delta notation:

$$\delta^{15}\text{N} = \frac{(^{15}\text{N}/^{14}\text{N})_{\text{sample}} - (^{15}\text{N}/^{14}\text{N})_{\text{standard}}}{(^{15}\text{N}/^{14}\text{N})_{\text{standard}}} \times 1,000$$

where the reference standard material is atmospheric N_2 .

The $\delta^{15}\text{N}$ of sinking organic material reflects relative nutrient utilization as a balance between supply of nitrate (NO_3^-) from ocean water upwelling and uptake by diatoms an essential process to produce biomass. Modern field and laboratory studies demonstrate isotopic fractionation occurs during nitrate assimilation by diatoms, where the lighter ^{14}N isotope is preferentially consumed and imprinted into their organic matter. As NO_3^- is progressively consumed, the ocean water nitrate pool becomes enriched in ^{15}N (Altabet and Francois, 1994; DiFiore et al., 2009; DiFiore et al., 2006; Robinson et al., 2004; Shemesh et al., 2003). Diatoms are exported to the seafloor and record the $\delta^{15}\text{N}$ signature in the geologic archive. Measurements of bulk sediment $\delta^{15}\text{N}$ therefore provide insight into primary productivity and surface water NO_3^- utilisation, whereby a more positive $\delta^{15}\text{N}$ value has been attributed to high nutrient consumption, strengthening of the biological pump and/or a reduction in upwelling nutrients to the surface waters due to stratification (fig. 3.6) (DiFiore et al., 2009; Robinson et al., 2004; Robinson et al., 2012; Shemesh et al., 2003). The degree of nutrient utilisation in surface waters is not the only signal contributing to changes in bulk

sedimentary N isotopic records. Alteration of the $\delta^{15}\text{N}$ signal during sinking and burial has been observed, which can enrich (up to 2-5 ‰) or deplete the sedimentary $\delta^{15}\text{N}$ relative to ocean water $\delta^{15}\text{N}$ (Altabet and Francois, 1994). To circumvent these complications, diatom-bound nitrogen is becoming popular in paleoceanographic studies, as the siliceous frustules of diatoms are physically protected from early-stage diagenesis (Brunelle et al., 2007; Karsh et al., 2014; Robinson et al., 2004; Robinson et al., 2012; Sigman et al., 1999). Despite an improvement to bulk $\delta^{15}\text{N}$, this proxy presents uncertainties of its own. Species-specific nitrate isotopic fractionation is evident in culture studies (e.g. (Granger et al., 2004; Horn et al., 2011)) and sedimentary records (e.g. (Robinson and Sigman, 2008)), due to factors including (but not limited to) varying growth rates and cell volume that must be accounted for (Altabet and Francois, 1994; Brunelle et al., 2007; Horn et al., 2011).

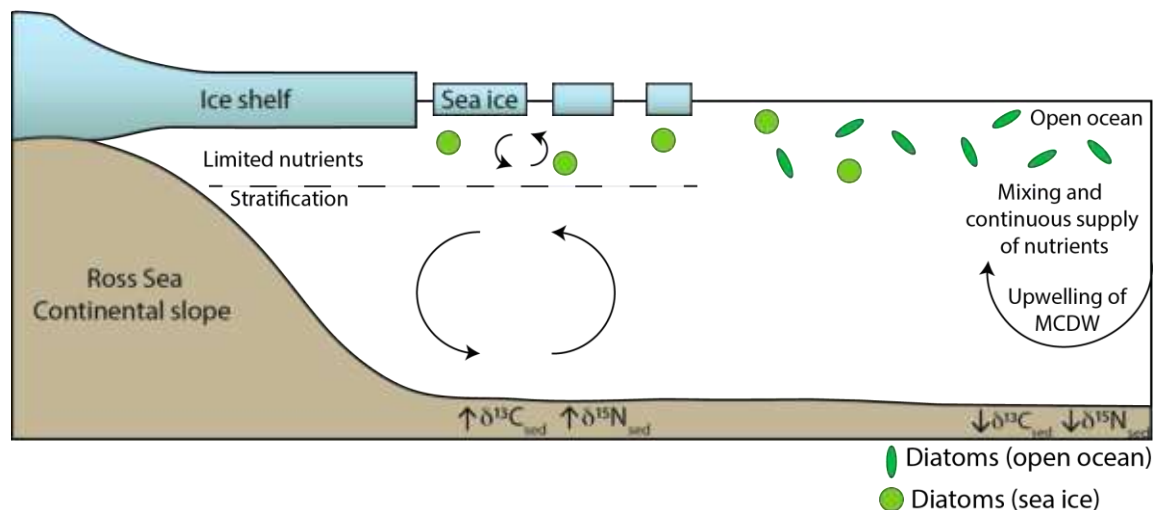


Figure 3.6: Schematic diagram highlighting the oceanographic controls on nutrient availability to diatoms. In stratified waters, diatoms will assimilate the heavy and light isotopes of C and N, thus displaying a more positive $\delta^{13}\text{C}$ and signature. In well mixed waters, diatoms preferentially assimilate the lighter C and N isotopes to display more negative $\delta^{13}\text{C}$ and $\delta^{15}\text{N}$ signatures in the sedimentary record.

3.5.3 Robertson Bay C and N analysis

Sediment samples for bulk carbon analyses were taken from core Bay05-29c and Bay05-32c at 5 cm resolution (211 samples in total). Sample preparation was conducted in the Geochemical Preparation Laboratory, Geology Department, University of Otago. Thirty milligrams of sediment were weighed into silver capsules for carbon and nitrogen concentrations and carbon isotopes (wt% Corg; wt% Norg; $\delta^{13}\text{C}$). To remove carbonate, the

sediment was acidified progressively with 5- 6% sulphurous acid (H₂SO₃) 6 times; 30 µL (x1) 60 µL (x2), 90 µL (x1), 120 µL (x2) until no bubbles were observed. A stepwise addition of acid prevents acid and sediment overflow from the capsule. Between acidifications, samples were loosely covered and dried in a 40°C oven for at least 6 hours. Completely dried samples were folded to enclose the sediment. Replicates were incorporated for every 10th sample, along with two blanks and one internal standard for every analytical run.

Carbon and nitrogen concentrations and carbon isotopes were analysed using a Carlo Erba NA1500 Series 2 Elemental Analyzer interfaced with a DeltaPlus isotope ratio mass spectrometer via a ConFloII device at the Stable Isotope Laboratory at Stanford University, California, USA. Each run was conditioned at the outset with two acetanilide standards. To evaluate internal consistency between analytical runs and correct for instrument drift, each analytical run was calibrated with eight USGS-40 standards dispersed throughout the run. Average standard deviation of replicate analyses is 0,21 for wt% Corg, 0,27 for wt% Norg, and 0,24 for δ¹³C.

3.5.4 Carbon to nitrogen ratio (C:N)

C:N ratios provide insight into the source of organic matter and post depositional alteration within bulk sediment were calculated using C and N concentration data from acidified samples using the following equation:

$$C:N \text{ ratio} = \frac{\text{Wt.\% C} \times \text{atomic mass of C}}{\text{Wt.\% N} \times \text{atomic mass of N}}$$

where atomic mass of C = 12.0107, and atomic mass of N = 14.0067 (Meyer, 1994).

3.5.5 The biogenic silica proxy

The Southern Ocean plays a central role in the global biogeochemical cycle of silicon, with potentially more than half of the removal of Si from the world ocean occurring through the accumulation of biogenic silica in Antarctic sediments (DeMaster, 1981; Lisitzin, 1985; Ledford-Hoffman et al., 1986). This is a direct consequence of the importance of diatoms as primary producers in polar surface waters (eg Priddle et al., 1986). It also involves a close

coupling between the Si cycle and that of carbon, nitrogen, phosphorus and trace elements in the Southern Ocean (Figure 3.7).

Sedimentary biogenic silica (diatom, chrysophyte, radiolarian and sponge spicule concentration) is controlled primarily by four factors: clastic sedimentation rate, aquatic production, post-depositional preservation of siliceous organisms and organic matter sedimentation (McKay et al., 2007). A fraction of the biogenic silica that is deposited from the photic zone redissolves during its transit through the water column. Most of the regeneration of dissolved nutrient silica, however, occurs at the sea floor (Broecker and Peng, 1982). Benthic regeneration of silica depends on a number of processes, including burial and mixing of sediments, dissolution of silica tests, transport of silicic acid through the porous medium, and precipitation of native silicate minerals. The dissolution of biogenic silica affects not only the return of nutrient silicic acid to the overlying water column, but also the integrity of the fossil record of diatoms. The latter is an important consideration when using silica accumulation rates and diatom assemblages preserved in sediment cores to reconstruct past changes in surface water productivity and paleoenvironmental conditions (e.g. Pichon et al., 1987, 1992; Lyle et al., 1988; Shemesh et al., 1989; Birks et al., 1990; Fritz et al., 1991; Bareille et al., 1991; Berger and Herguera, 1992).

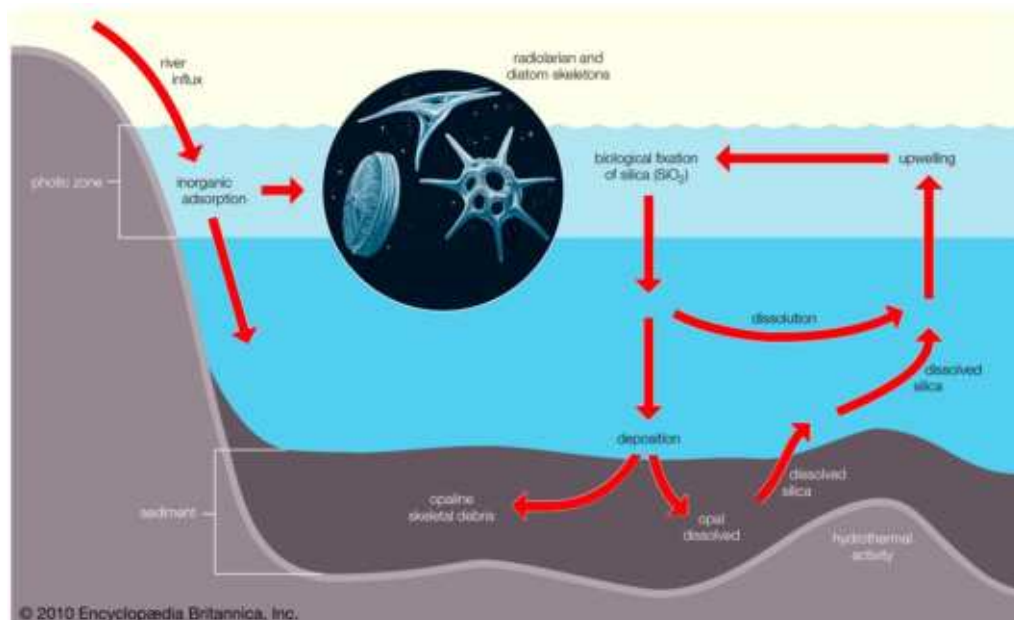


Figure 3.7 Silica cycle in the marine environment. Silicon is commonly found in nature in the form of silicon dioxide (SiO₂), also called silica. It cycles through the marine environment, entering mainly through river runoff. Silica is removed from the ocean by organisms such as diatoms and radiolarians which use a dead form of silica in the cell walls. After death, their skeletons settle through the water column and the silica dissolves again. A small number reach the ocean floor, where they remain, forming a siliceous slime, or dissolve and are returned to the photic zone for ascent. Source Encyclopædia Britannica, Inc.

3.5.5.1 Biogenic silica (BSi) concentration method

The concentration of biogenic silica (wt% BSi), a chemically determined proxy, which measures the amorphous Si content of bulk sediments. There are several techniques to estimate wt% BSi in sediments. This thesis uses a method adapted from Mortlock and Froelich (1989) by David A. Mucciarone at Stanford University Stable Isotope Laboratory. The procedure is designed to give weight percent biogenic silica extracting it from a sediment sample with an alkaline solution and then measuring the dissolved silicon concentration in the extract by molybdate-blue spectrophotometry following the method of Strickland and Parsons (1972) (Figure 3.8).

Average standard deviation of replicate analyses is 0,45 wt% BSi for the core BAY05_29c and 0,46 for the core BAY05_32c.

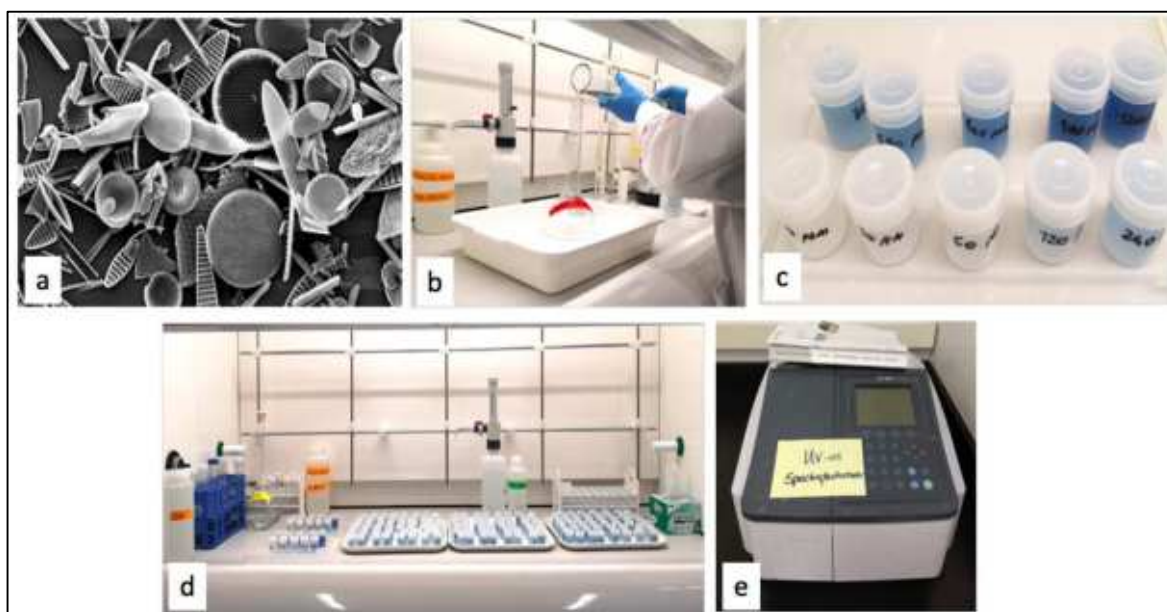


Figure 3.8 Photos taken during the execution of the procedure used during the analysis of biogenic silica at the University of Otago, following the modified method of Mortlock and Froelich (1989). a) diatoms and spongy spicules with shells (frustules) composed of biogenic silica b) preparation of acids and chemical reagents c) two sets of 10 standards with known concentrations d) 12 ml vials sampled and labeled e) spectrophotometer.

Biogenic Silica Analysis Procedure

This procedure is designed to give weight percent biogenic silica using a small amount of sample material. A total of 42 analyses (40 unknowns, 1 blank, 1 standard) can be run using this procedure. This procedure modified from Mortlock and Froelich (1989) uses a 0.1N NaOH solution heated to 85°C to leach the silica from the sediment sample. Aliquots of the leachate are then collected at regular time intervals to measure sequential dissolution.

All BAY05 samples (211 in total) were freeze-dried and homogenized with a mortar and pestle. Eighteen milligrams of sediment were weighed and placed into 50 mL Oak Ridge polypropylene centrifuge tubes and the replication frequency was one every ten samples. Using a Dispensette bottle-top dispenser, each labelled centrifuge tube were filled with 40 mL of 0.1N sodium hydroxide (NaOH) solution, capped and placed in a water bath with constant temperature at 85°C, and shaken every 30 minutes to ensure even dissolution of biogenic silica particles.

Depending on the sample material being analyzed (sediment trap or sediments) the sampling interval may vary. Sediment trap samples are usually sampled at hours 2 and 3. For some marine sediments, samples are collected at hours 2, 3, 4 and 5. Test analysis of Robertson Bay samples established that wt% BSi values calculated from hours 2, 3, and 4 were statistically indistinguishable from values calculated when hour 5 was included, so subsequent runs sampled hours 2, 3, and 4 only.

For the initial sample at hour 2, the centrifuge tubes were removed from the water bath, placed in the centrifuge and spun at 3800 rpm for approximately 3 minutes. Next, 0.25 ml (250 µl) of sample was taken from each tube using a 250 µl pipette and placed in a labelled 12 ml (Fig. 3.8, C and D) vial. 250 ml of Nanopure was added for a total of 0.5 ml (500 µl). After sampling, each centrifuge tube was re-capped, shaken on the vortex to resuspend the sediment, and returned to the water bath. This sample routine was repeated for each subsequent sampling hour.

While the samples were dissolving, two sets of 10 standards with known concentrations ranging from 0,001 to 1,360 were also prepared by adding 0.5 ml (500 µl) of each standard into a 12 ml vial using a 500 µl pipette and then adding 4.5 ml of nanopure water to each of the vials to bring the total volume to 5.0 ml. At the end of hour 4 sampling, we added 2 ml of molybdate reagent, followed after 10 minutes by 3 ml of reducing solution to each of the sample, blank and standards vials. Once reducing solution was added, all the vials were

capped, shaken and left to stand for 3-5 hours before measuring their absorbance on the spectrophotometer at 812 nm.

When all the standards, blanks, and unknowns were analysed, results were entered into the OPAL Program (Vbasic Macro) to obtain a standards curve and calculate weight percent values for the unknown samples. A simple linear regression is used to calculate the slope and intercept on the standard values entered into the program. The weight percent biogenic silica results are calculated using the following equation:

$$\text{Wt. \% SiO}_2 = ([\text{SiO}_2]) * (0.5 \text{ ml/aliquot}) * (\text{volume}) * (60.1 \text{ g Si/mole}) * (0.0001)/(\text{Sample wt.})$$

Where: $[\text{SiO}_2] = ((\text{absorbance} - \text{y intercept})/\text{slope})$

absorbance = reading from spectrophotometer.

aliquot = amount of sample taken from centrifuge tube in ml.

sample wt = weight of sample in mg.

slope = calculated from standards curve.

volume = amount of NaOH solution added to centrifuge tube in ml.

y intercept = calculated from standards curve.

$0.0001 = (1\text{E}-06 \text{ g}/\mu\text{g} * 100\%)$

$60.1 \text{ g Si/mole} = \text{amount of Si in one mole of SiO}_2.$

With this method, a least-squares regression analysis is made on the increase in Si extracted versus time (taking into account the various dilution steps and the amount of sediment used) and extrapolation to the intercept is made to estimate BSi concentration.

3.6 Chronology

3.6.1 Antarctic radiocarbon chronology

Paleoenvironmental records from the Antarctic and Southern Ocean play an important role in identifying the processes that drive the Antarctic system during intervals of rapid change (i.e. Hillenbrand et al., 2017). However, our ability to reconstruct past conditions from marine sediment cores is limited by the accuracy of core chronologies (Rosenheim et al., 2013; Subt et al., 2016). This chapter discusses the specific challenges of dating Antarctic sediments and the methodology used to overcome these challenges to obtain a robust chronology for cores BAY05-29c and BAY05-32c.

3.6.2 Challenges of Dating Antarctic Sediments

Antarctic sediments are difficult to date due to the lack of (or very poor preservation of) foraminifera (CaCO_3), the most reliable source of carbon for ^{14}C dates (Berkman and Foreman, 1996; Licht et al., 1998). As an alternative, the bulk acid insoluble organic matter (AIOM) carbon fraction is frequently used to determine the age of sediments (e.g. Mezgec et al., 2017). However, AIOM fraction ^{14}C dates of Antarctic sediments are influenced by the variable upwelling of old deep waters around the continent, leading to the highest surface-water reservoir ages on Earth (1100-1600 years; Andrews et al., 1999; McKay et al., 2016; Subt et al., 2015). Additionally, Antarctic core-top ages are often much older than can be explained by the ocean reservoir effect alone, because of terrigenous inputs of reworked carbon: the AIOM carbon fraction includes a mix of carbon derived from both contemporaneous primary production that reflects the time of deposition and ancient detrital material (Andrews et al., 1999; Rosenheim et al., 2009; 2013; Subt et al., 2016). Both effects must be corrected for to obtain absolute chronology (Subt et al., 2015).

3.6.3 Recent Advances in Antarctic Radiocarbon Dating

The novel Ramped PyrOx (RP) methodology for ^{14}C analysis corrects for the uncertainties introduced by terrigenous carbon (Subt et al., 2016). Ramped PyrOX exploits the thermochemical stability differences between the fresh autochthonous AIOM and

diagenetically stabilized allochthonous AIOM. During RP, a pre-treated sediment sample is heated in a furnace and CO₂ fractions are collected as the temperature of combustion is slowly increased. The separation of samples into several fractions for radiocarbon dating produces a spectrum of ages, ranging from the youngest (least thermochemically stable) material to the oldest (most thermochemically stable) material with increasing pyrolysis temperature (Figure 3.4.3). Ideally, the first two splits will be statistically indistinguishable, which indicates that no old carbon was combusted at low temperatures; if split one is considerably younger than split two, split one may not have captured contemporaneously deposited carbon alone and therefore reflects a maximum age constraint, not the true age of the sediment (Rosenheim et al., 2008; 2013; Subt et al., 2016; 2017).

RP is more precise than bulk AIOM dating and has proved a reliable method for eliminating the down core age reversals that are sometimes a feature of bulk AIO ¹⁴C chronologies due to changes in the contribution of older contaminant ¹⁴C through time (Rosenheim et al., 2008; 2013; Subt et al., 2016). Subt et al., (2016) found that the age derived from the lowest temperature ramped pyrolysis split can (but does not always) approach CaCO₃ ages from the same or similar depth (Figure 3.9).

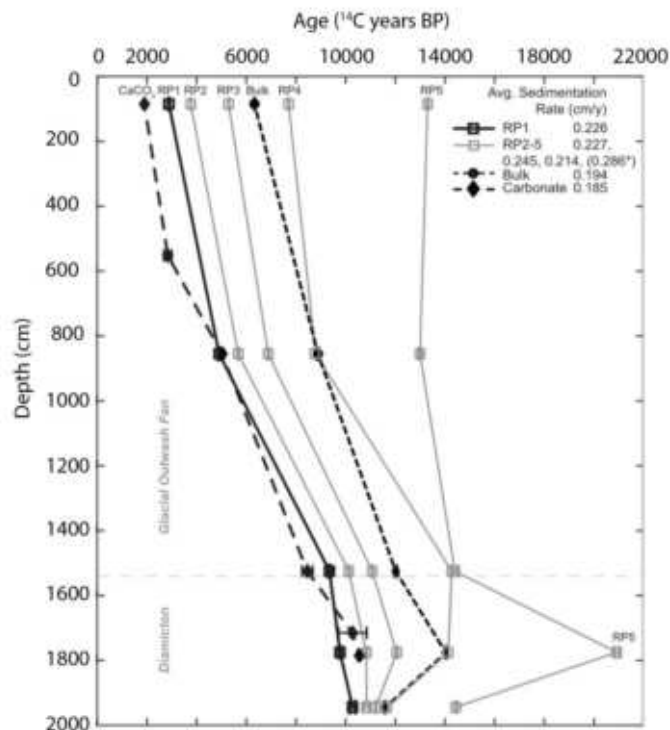


Figure 3.9: Comparison of ¹⁴C ages from bulk AIOM, RP, carbonate. Carbonate ages and low-temperature RP ages (RP-1) increase down core and yield similar results, while bulk AIOM and high temperature RP splits show an age reversal at 1800 cm depth due to contamination by older carbon (Source: Subt et al., 2016).

3.6.4 Marine Reservoir Effect

On Earth, there are two major ^{14}C reservoirs – the atmosphere and the ocean. Independently dated, tree-ring measurements, plant macrofossil data, and speleothems provide a well constrained record of atmospheric ^{14}C concentrations, particularly since 13,900 cal yr BP (Reimer et al., 2013). In comparison, the reconstruction of ocean ^{14}C concentrations is complicated by comparatively fewer marine archives, slow equilibrium time between the atmosphere and ocean, and upwelling of old deep ^{14}C depleted water (Hall et al., 2010). The combined effect of the latter two processes is that marine samples in the surface ocean (e.g. planktonic foraminifera, shells and corals) appear older than coeval terrestrial samples. This offset between contemporaneous marine and terrestrial carbon reservoirs is known as the marine reservoir age (Stuiver and Polach, 1977). A global marine reservoir age is derived by incorporating the atmospheric ^{14}C (IntCal13) into an ocean-diffusion box model to generate a modeled global average of ~400 years for surface waters (Oeschger et al., 1975; Stuiver and Braziunas, 1993). However, significant deviations can occur from the global average, which are a function of climate and oceanographic circulation systems.

Marine radiocarbon data from pre-bomb carbonates from the South Shetland Islands and the Antarctic Peninsula yield an average reservoir age of 1300 ± 100 years (Andrews et al., 1999). Ages between 1100 and 1300 are currently accepted as the Southern Ocean reservoir age; these are used extensively for marine records around the Antarctic continent in locations where the core top cannot be reliably dated (Andrews et al., 1999; Berkman and Forman, 1996; Panizzo et al., 2014). In locations where the core top can be reliably dated, the age at the sediment water interface determines the local reservoir age. When possible, the use of a local reservoir age is desirable because it eliminates potentially significant error associated with regional variations in reservoir ages (Andrews et al., 1999; Subt et al., 2015). The difference in the ocean reservoir ^{14}C and atmospheric ^{14}C is likely to change with temporal changes in reservoir parameters (e.g. input and output fluxes and exchange with the atmosphere; Butzin et al., 2005). However, in most cases a lack of detailed information means the reservoir age is held constant through time (Stuiver et al., 1986).

A standard zero point (0 BP) has been set at 1950 CE on the ^{14}C timescale, and all ^{14}C ages are reported relative to this baseline. The use of 1950 CE reflects the closest decadal date to

the publication of the first series of ^{14}C determinations in December 1949 (Arnold and Libby, 1949). After 1950 AD, nuclear weapons testing in the Northern Hemisphere released large quantities of anthropogenic ^{14}C into the atmosphere, which complicates direct measurement of the natural Antarctic reservoir age. Post-bomb carbonates indicate the Antarctic marine radiocarbon reservoir has been altered by ~500 years during the 20th century due to nuclear explosions and fossil fuel combustion (post-bomb reservoir age = 800 years; pre- bomb reservoir age = 1300 years; Berkman and Foreman, 1996). To date, the most accurate natural reservoir ages are those derived from pre- bomb carbonate samples (Berkman and Forman, 1996; Hall et al., 2010).

3.6.5 Radiocarbon Calibration

Past changes in atmospheric ^{14}C caused by geomagnetic and solar modulation of the cosmic-ray flux and the carbon cycle means that relationship between ^{14}C age and calendar age is not linear (Blaauw, 2010; Reimer et al., 2013b). Radiocarbon dates are converted to calendar ages through comparison to independently dated records (calibration curves) such as ice cores and tree rings (Stuiver and Polach, 1977). Common archives for calibration curves include tree rings, terrestrial macrofossils, corals, forams and speleothems (Reimer et al., 2013a). Three calibration curves exist: the marine calibration curve (Marine13), which represents the hypothetical global marine reservoir (Reimer et al., 2013b), and the Northern (IntCal13) (Reimer et al., 2013b) and Southern (SHCal13) Hemisphere calibration curves (Hogg et al., 2013), which represent the mid-latitude Northern and Southern Hemisphere atmospheric reservoirs respectively. A robust calibration curve requires high-resolution data with accurately quantified uncertainties.

Post-bomb dates (indicated by negative ^{14}C ages) are calibrated with CALIBomb (<http://calib.org/CALIBomb>), an extension to IntCal13 and SHCal13 curves. Four zonal data sets of tropospheric bombs ^{14}C data have been compiled for 1950-2010 AD, with significant geographical differences in ^{14}C due to atmospheric circulation (Hua et al., 2013). To date, there is no post-bomb extension to the Marine13 curve, and thus post-bomb marine ages cannot be calibrated.

3.6.5.1 Ramped Pyrolysis (RP) radiocarbon methodology

To develop a chronology for core BAY05_29c e BAY05_32c, sediment samples for RP radiocarbon analysis were taken from four depths for core 29c and from five depths from core 32c spanning the length of the cores. The uppermost sample was taken between 0 and 1 cm for both cores and the bottom sample was taken between 554 and 555 cm for the core 29c, 30 cm above the base of the core and between 459-460 cm for the core 32c, 8 cm above the base of the core. In core 29c, a sample was taken at 205 cm because of a notable shift in magnetic susceptibility evident in shipboard measurements. A final sample at 405 cm was selected to give an even spacing of dates down core.

The other sample depths for the 32c core are respectively: 144-145 cm, 189-190 cm, 374-375 cm chosen based on changes in the $\delta^{13}\text{C}$ and biogenic silica curves. Both cores have existing bulk AIOM ^{14}C age models, enabling comparison between age models developed using RP and bulk dates.

Samples were pre-treated at the University of Otago and sent to the Rafter Radiocarbon Lab AMS facility at GNS in Wellington for radiocarbon dating in November 2021.

For the pre-treatment the samples were mixed with a magnetic flea in acid with 1 M HCl, room temperature (20 ° C). The amount of acid depends a bit on the amount and carbonate content of sample that is being pre-treated and the surface area the sample is sitting in for treatment. I added enough acid to cover the sample and wait for any bubbling to complete while gently swirling to get it all into solution and adding a bit more acid until the complete evolution of the carbonate occurs. The samples were mixed for one hour and left to stand in acid overnight. The next day they were placed in the centrifuge and rinsed with DI water, and tested for neutrality with the pH strips.

At Rafter, each sample was baked at 500°C and then passed through a CO₂ purification procedure to remove contaminants prior to graphitisation and AMS measurement. GNS scientists corrected AMS measurements using a three-component mixing model of modern blank, dead blank, and sample material, following Santos et al. (2007).

3.6.5.1.1 Ramped Pyrolysis Split Analysis

The purpose of RP is to obtain the age of the youngest carbon within each bulk sediment sample (Subt et al., 2015). Typically, RP split ages become progressively older with

increased pyrolysis temperature in proportion to the amount of reworked carbon incorporated within each split (e.g. Rosenheim et al., 2013; Subt et al., 2015). If the ages of the first two splits are statistically indistinguishable, the age of split 1 likely represents to true age of the sediment with no contribution of detrital carbon; if the split 2 is much older than split 1, the split 1 may be contaminated by older carbon and is therefore considered a maximum age constraint (Rosenheim et al, 2008; Rosenheim, per comms). However, samples of Holocene sediments collected from the Ross Sea sector commonly yield a younger age for split 2 than for split 1 (Parker, 2017; Truax, 2018; Gilmer, 2020). The older age of split 1 is provisionally attributed to an elevated concentration of degradation products containing old carbon, based on the distribution of various organic compounds identified through pyrolysis gas chromatography-mass spectrometry (GCMS), measured at the GNS Rafter Radiocarbon Lab (C. Ginnane, pers. comm.) These compounds are also present in lower concentrations in split 2, suggesting that these dates should be treated as oldest limiting ages rather than true ages.

3.6.5.1.2 RP delayed results due to covid-19 pandemic

Due to lab closures and personnel restrictions caused by the Covid-19 pandemic, the measurement of RP in BAY05 samples suffered severe delays, and results were unfortunately not delivered before the thesis submission deadline. For the thesis, we therefore use only the bulk AIO ^{14}C dates and age model calibrate with the OxCal Bayesian model following Tesi et al 2020, Marine 13 curve.

3.6.6 Edisto Inlet and Robertson Bay radiocarbon calibration

Radiocarbon dating of bulk OC for six cores in Edisto Inlet Fjord (CH41, BAY05 18c, 20c, 22c, HLF17_01 and GC17_03) and 2 cores in Robertson Bay (BAY05 29c, 32c) (total 14C n = 32) and carbonate samples (n = 2) was performed via accelerated mass spectrometry (AMS) at The National Ocean Sciences Accelerator Mass Spectrometry (NOSAMS) of the Woods Hole Oceanographic Institution, USA and at the Poznan Radiocarbon Laboratory (Poland).

The age model was constructed using the median values provided by using the latest version of the OxCal bayesian program. OxCal v4.4.4 Bronk Ramsey (2021), Marine13 marine curve calibration curve (Reimer et al., 2013).

The single dates mentioned in the text (Table 3) refer to the median age in the 2σ calibrated age range.

It has been simulated a calendar ages from each of the calibrated ^{14}C ages and construct an age-depth model through the points for each core (linear interpolation between the dated levels).

When the age mode plots show a sigma posterior 68.3% probability- 1σ (68.3%) and a 95.4% probability - 2σ (95.4%), agreement 100.0%.

In the core Anta02_CH41, BAY05_20c and 32c the limitation of the model due an inversion date showed a negative accumulation rates and a low accuracy, so in that case we used the unmodeled calibrated dates.

Radiocarbon dates were calibrated using data base and a local reservoir age performed by Tesi et al 2020, on the core HLF17_01, which built an age-depth model using ^{14}C ages derived from both carbonate and organic carbon matrices, with additional dates obtained from excess ^{210}Pb and one tephra horizon.

The ΔR_{CaCO_3} based on U/Th dating of coral samples trapped by the fringing Ross Sea ice shelf (Hall et al. 2010), where the ΔR value of the carbonate matrix (ΔR_{CaCO_3}) in the Ross Sea has remained relatively stable over the last 6000 years is $\Delta R_{\text{CaCO}_3} = 791 \pm 121$ yrs.

The ΔR_{oc} for bulk sediment derived by pairing benthic foraminifera with organic carbon from the same horizons, relying on the well constrained ΔR^{CaCO_3} and is $\Delta R_{\text{oc}} = 1320 \pm 135$ years, 1σ .

All the plots curve can be found in the appendix B.

Table 3. Radiocarbon dates and calibrated ages of samples from Edisto Inlet Fjord and Robertson Bay.

Core ID	Depth (cm)	Radiocarbon age ¹⁴ C BP (y)	Error (y)	Calibrated age yr BP modelled median age	Type of sample	ID Lab
ANTA02_CH41	1	1790	± 40	recent	AIO	GX-29188
ANTA02_CH41	35	4490	± 50	2982*	AIO	GX-30574
ANTA02_CH41	71	9400	± 40	8576*	AIO	GX-29991
ANTA02_CH41	232	9970	± 50	9287*	AIO	GX-29189
ANTA02_CH41	300	10920	± 50	10475*	AIO	GX-29190
ANTA02_CH41	369	9130	± 40	8267*	AIO	CX-29992
ANTA02_CH41	402	10070	± 50	9400*	AIO	GX-29191
BAY05-18c	1	2430	± 40	660	AIO	OS-75006
BAY05-18c	67	4940	± 40	3524	AIO	OS-75007
BAY05-18c	175	8070	± 55	7265	AIO	OS-75008
BAY05-18c	284	11500	± 75	11113	AIO	OS-75155
BAY05-18c	345	11550	± 50	11430	AIO	OS-59379
BAY05-18c	353	33500	± 260	35650	AIO	OS-39370
BAY05-20c	2	1760	± 30	recent	AIO	OS-59367
BAY05-20c	140			1254 ^a	Tephra	
BAY05-20c	147	2760	± 40	994*	AIO	OS-59368
BAY05-20c	240	2640	± 30	1409*	mollusc	OS-59019
BAY05-20c	369	4750	± 30	3289*	AIO	OS-59369
BAY05-22c	1	1610	± 35	recent	AIO	OS-65603
BAY05-22c	197	4700	± 45	3329	AIO	OS-65787
BAY05-22c	335	8150	± 60	7296	AIO	OS-65599
BAY05-22c	384	9000	± 55	8152	AIO	OS-65806
RS17-GC03	442	1940	± 55	714	Forams	
HLF17_01	1456	4220	± 50	2623 ^b	Bulk OC	Poz-92969
BAY05_29c	1	1650	± 30	recent	AIO	OS-59350
BAY05_29c	35	2930	± 35	1009	AIO	OS-59351
BAY05_29c	226	3840	± 30	2283	AIO	OS-59366
BAY05_29c	404	5810	± 40	4634	AIO	OS-59352
BAY05_29c	555	7150	± 40	6238	AIO	OS-59353
BAY05_32c	1	2060	± 140	258*	AIO	Poz-140705
BAY05_32c	40	3370	± 60	1626*	AIO	Poz-140706
BAY05_32c	145	3650	± 60	1957*	AIO	Poz-140707
BAY05_32c	190	10470	± 60	9903*	AIO	Poz-140708
BAY05_32c	300	7200	± 80	6297*	AIO	Poz-140709
BAY05_32c	375	16180	± 150	17602*	AIO	Poz-140710

^a Di Roberto et al (2019)

^b Tesi et al (2020)

*calibrated unmodelled median age

Chapter 4

4. EDISTO INLET FJORD

4.1 Introduction

The study of the sedimentary sequences from high latitude, marine, ice proximal and ice-distal areas, combined with the ice core records allow to directly reconstruct the fluctuations of the ice volume and seaward extension during past glacials and interglacials, tied to climate atmospheric and ocean changes. This information is needed to estimate the ice sheet sensitivity to past and future climatic changes and to predict its contribution to global sea level changes. Understanding sediment distribution is critical for studies reconstructing glaciers and ice-sheet behavior based on paleo-records (e.g., De Santis et al. 1999; Perez et al., 2021; Naish et al. 2009; Anderson et al. 1999; Wellner et al. 2001; Stokes et al. 2015). However, this information is limited and sometimes contradictory, mainly due to the lack of enough data and difficulty in dating glacial sediments. Here I present a unique and comprehensive set of data from the Edisto Inlet along the coast of the northern Victoria Land (Antarctica), that is used to reconstruct the environmental conditions occurred after the LGM, contributing to fill the knowledge gap about post-LGM ice retreat from the western Ross Sea.

The data were collected during four campaigns of the Italian Antarctic Program (PNRA) on board the *Italica*, the *OGS Explora* and the *Laura Bassi* research vessels, in fortuitous austral summers with no or limited sea ice cover from 2002 to 2020. Following the pioneering study at the entrance of the fjord (Finocchiaro et al., 2005), multibeam swath bathymetry, sub-bottom seismic profiles, gravity cores and oceanographic data (from CTD, thermosalinographer, ADCP-VM and LADCP) were acquired. The data show for the first time the existence of up to 130 meters thick Holocene stratigraphic section that accumulated inside this Antarctic fjord and sheds light into processes that influenced the marine deposition since the LGM.

Tidewater glaciers generally respond more rapidly to climatic fluctuations than large ice sheet because they have small drainage areas and high snow accumulation rates (Anderson 1999). Rapid and high sediment accumulation is generally observed in temperate and subpolar fjords and coastal bays where tidewater glaciers are debouching and carving deeply the fjord sea floor during frequent ice expansions. Environmental variations are reflected by the alternations between glacial facies (generally silty mudstone with ice rafted debris - IRD) and marine facies (biogenic-rich mud) (E.A. Cowan and R. D. Powell 1990, W. Szczuciński et al 2009, J. A. Howe 2010). Despite climate conditions determining for example the amount of meltwater, of sea ice, of snow precipitations in the catchment area, numerous other factors control sedimentation in fjords, including seafloor bathymetry, bay geometry, oceanographic regime, proximity to sediment sources (Griffith & Anderson 1989; Leventer et al 1996; Ashley & Smith 2000). Paleo environmental reconstructions that take into account all forcing factors are needed when applying any model of sediment distribution in a fjord or in a coastal bay environment, to distinguish local versus regional climate variations. Although a large literature exists about temperate and subpolar fjords, few studies are reported from the Antarctic polar fjords (Shevenell et al 1997; McMinn et al 2001; Minzoni et al 2015). Various studies describe ecosystems and environmental variations from Holocene sediments recovered from inner and mid Antarctic shelf depressions (fig. 1), like the Palmer Deep in the Antarctic Peninsula (Sjunneskog et al., 2002; Rebesco et al., 1998; Cunningham et al., 1999; Domack et al., 1999; 2001; Domack et al 2003; Mosola and Anderson, 2006; McGlannan et al., 2017) and the Adelie Deep to the west of the Mertz Polynya, East Antarctic coast, (Escutia et al., 2014; Crosta et al 2021), acting as natural sediment traps, deeper than iceberg keel scouring (Prothro et al., 2018). These deposits are particularly thick in areas of polynya or in general, where there is high productivity of biogenic material that is entrained and accumulated in sediment drifts by slow, dense water bottom currents (e.g. the Mertz Drift, Harris et al., 2001, Presti et al., 2005; Wellner et al. 2014). The presence of this type of sediment in the geological record is interpreted as representing the establishment of seasonally sea ice open climatic conditions (Finocchiaro et al. 2005, Tesi et al 2020). Its thickness appears to be a function of both biogenic productivity and duration of open marine conditions (Dunbar et al., 1985; Smith et al., 2003; Prothro et al., 2018) established after events of warm ocean current incursions on the continental shelf, triggering ice shelf collapse (e.g. at Pine Island Bay, fig. 1, Hillebrandt et al., 2017; Joughin et al., 2021) and meltwater discharge (e.g. Ashley et al., 2020).

Fjord systems are usually protected from strong external oceanic influence. However, it has been observed that on-going ocean warming is triggering the penetration of North Atlantic warm waters in some of the Greenland fjords where outlet glaciers drain a substantial part of the Greenland ice sheet. The rapid retreat of those glacier fronts due to the oceanic influence can lead to a rapid and large ice mass loss into the ocean (Straneo & Heimbach, 2013, Crosta et al 2021).

The Edisto Inlet fjord presents some similarities with the Greenland fjords where the entering of vigorous oceanic circulation is likely inhibited by a shallow threshold at the fjord entrance, but a tidally-driven circulation can occur. The fjord is located along the coast of the northern Victoria Land, in the western Ross Sea. Here, high salinity shelf water (HSSW) that forms in the Ross Sea polynya due to brine rejection flows northwestward, geostrophically balanced, up to Cape Adare where it mixes with warm Circumpolar Deep Water (CDW) that impinges the continental shelf edge (Silvano et al 2020).

No previous data are reported for circulation inside the coastal fjord. This work provides snapshots of the modern water mass and post-LGM sediment distribution and describes a possible relationship between past circulation and seabed geomorphology.

4.2 Study site

Edisto Inlet (72°19'S 170°16'E) is an NNE-SSW elongated fjord (15 km long and 4 km wide), enclosed between Cape Hallett and Cape Christie along the North Victoria Land coast in the western Ross Sea (Fig 4.1). The Edisto fjord lies within the Hallett Volcanic Province (HVP) (Harrington et al. 1967) of the McMurdo Volcanic Group (Hamilton 1972; Kyle 1990, Late Miocene ~13–5 Ma), with a more recent volcanic activity from Mount Rittman (Di Roberto et al 2019). Its bathymetry shows a step-like profile with a pronounced landward deepening and the fjord is separated from Moubay Bay by a sill approximately 400 m deep. The fjord serves as outlet to four ice-tongue glaciers (Fig 4.1), the three most important being the Manhaul Glacier (16 km long and 7 km wide), flowing down from Mt Humphrey Lloyd; the Arneb Glacier (6 km long and 4 km wide), flowing northwest into Edisto Inlet; and two ice streams converging into the Edisto Glacier (10 km long and 6 km wide). Inferred large calving rates from remote sensing suggest that the Manhaul Glacier has been subject to a major calving event between 1989 and 1999 (Fountain 2017) and that two major calving

events of the Arneb Glacier occurred between 1989-1999 and 2014-2015. No information is available for the Edisto Glacier.

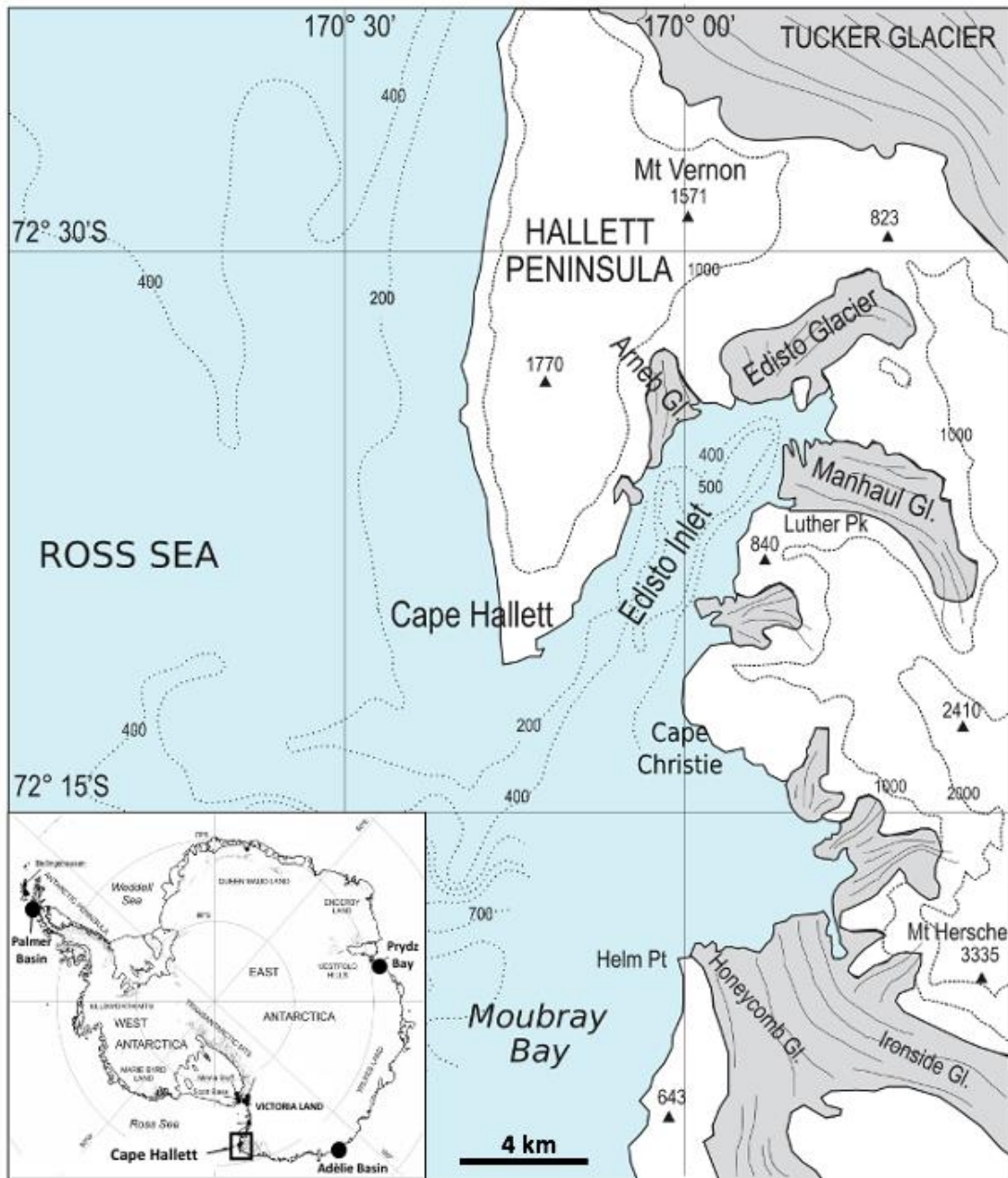


Fig. 4.1: Map of Edisto Inlet located between Cape Hallett and Cape Christie in the western Ross Sea (Antarctica). The lower left square shows the map of Antarctica with the location of the Adélie Basin and Prydz Bay in East Antarctica and the Palmer Basin in the Antarctic Peninsula (black dots). Bathymetric data and land morphology from map SS 58-60/2 (Cape Hallett), original scale 1:250,000 edited by U.S. Geological Survey. Modified after Di Roberto et al. (2019)

4.3 Data and Methods

The Edisto Inlet fjord is investigated by integrating different datasets acquired in the frame of several projects funded by PNRA (National Antarctic Research Program), including very high-resolution seismic profiles, multibeam swath bathymetry, gravity and piston sediment cores, Acoustic Doppler Current Profiles (ADCP) and a few Conductivity Temperature Pressure (CTD) measurements. ADCP water current velocity and direction, water temperature and salinity at 4 m depth were obtained on February 17th of 2017. CTD and LADCP profiles were obtained at 6 stations in the Edisto Inlet in February 2020.

The raw data supporting the findings of this study are the subject of a paper "*Early West Antarctic ice sheet retreat from a very high-resolution Holocene paleoclimate record*" Battaglia et al in preparation.

4.3.1 Geophysics Data

Sub-bottom profiles were acquired in the fjord entrance with a 3.5 kHz SBP on N/R Italice in 2005 and a hull-mounted Benthos CAP-6600 Chirp II Data Sonics on board of N/R OGS Explora in 2017 along the entire fjord (Fig 4.2). The two seismic datasets embrace a wide spectrum of penetration depth (up to ca. 100 meters below the sea floor, assuming a velocity of 1500 m/s) and vertical resolution between 100 and 20 cm, providing a good image of the geological setting beneath the seafloor and good potential for correlation with main density shift detected in the sediment cores.

The analysis of all dataset was conducted by using the IHS Kingdom Suite seismic interpretation software, to perform seismic stratigraphy, correlation of acoustic facies with sediment magnetic susceptibility and grain size logs and to obtain three dimensional, morpho-bathymetric images of the fjord.

Multibeam Swath Bathymetric data were acquired using a Teledyne Reson SeaBat 7150 Multibeam Echo Sounder, which has a system frequency of 12 kHz and 880 beams. These data sets were processed using PDS2000, then survey data were manually edited to remove anomalous readings and gridded to create relief maps. The optimal resolution of the data in most cases is a 10 m grid (Fig. 4.2).

The bathymetric data show that Edisto Inlet is a narrow basin, NNE-SSW elongated and landward deepening, with a step-like profile. The shallowest step, labelled as sectors 1 (fig. 4.2) has average water depth of 430 m, sector 2 of 460 m, sector 3 of 480 m, sector 4 is characterized by a deep depression that reaches a water depth of 700 m in the innermost area in front of the Edisto glacier.

4.3.2 Sediment cores

Fifteen sediment gravity and piston cores were acquired in the framework of four PNRA Projects near the entrance of the fjord in 2002, 2005 and in 2017 two other gravity cores were acquired in the central part of the fjord. In this thesis only ten cores are considered (BAY05 13c, 14c, 18c, 19c, 20c, 22c, ANTA02-CH41, HLF17-01, RS17-GC03, GC04) details about the analysis for the sediment cores are in the chapter 3 (tables 1). Fig. 4.2 shows the locations of the sediment cores, some of which were previously published by Finocchiaro et al. (2005), Mezgec et al. (2017), Di Roberto et al (2019), Tesi et al. (2020). In this work we describe ten of these cores (Table 1, paragraph 3.4.1).

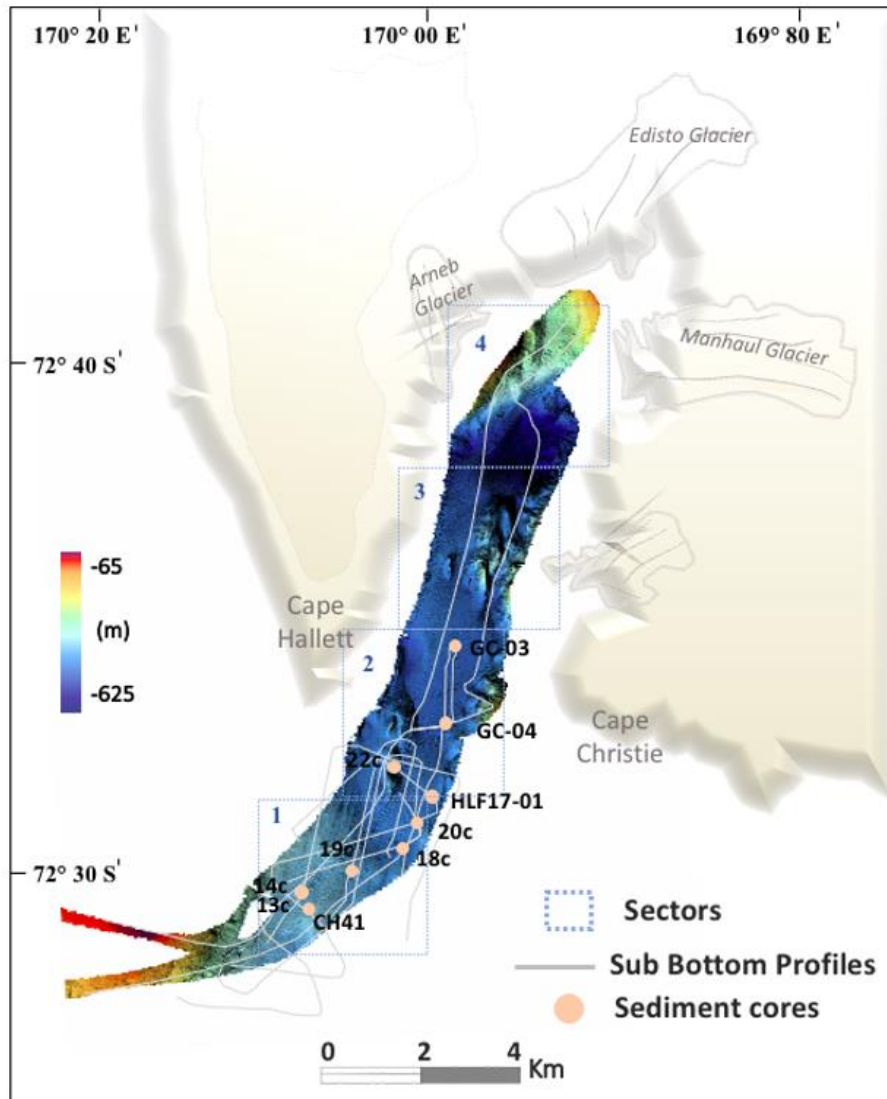


Fig. 4.2: Multibeam swath bathymetry of Edisto Inlet Fjord. Colors scale meters: High -65 m and Low – 625 m. Gray lines are the Sub-bottom seismic profiles acquired across the fjord. Orange points indicates the locations of the piston cores. The squares dashed in blue delimit the 4 sectors of the fjord respectively from 1 to 4 in a north-south direction.

4.3.3 Sedimentological analyses

In the frame of the BAY05 Project (2005) at University of Trieste on the cores 14c, 18c, 20c, and 22c the following analysis were made: X-ray analysis (Bartington MS2C), grain size analysis (the biogenic component is given mainly by diatoms), Multi-Sensor Core Logger (MSCL) measurements, such as density, the speed of the compression waves (P-wave velocity) and the amount of magnetically susceptible (MS) material present in the sediment. On core 13c (166 cm long) and 19c (75 cm long) only the MS has been measured. On the cores GC-03 and GC-04 only the Multi-Sensor Core Logger (MSCL) (Magnetic Susceptibility (MS), Density and P-wave Velocity) has been run at University of Trieste in

2019 in the frame of the PNRA Project ODYSSEA. Sedimentological analysis on cores CH41 and HL17F-01 were previously published by Finocchiaro et al. (2005), Di Roberto et al (2019), Tesi et al. (2020).

4.3.3.1 Grain size analysis

Grain size analyses were performed in 2005 by Prof. Ester Colizza (University of Trieste). Samples were treated with hydrogen peroxide to remove organic matter and sieved to separate the < 1mm fraction.

The grain size characterization of < 1 mm fraction was analysed using a Malvern MasterSizer 2000 laser. Sand, silt and clay were determined using the grainsize classification proposed by Friedman and Sanders (1978). Statistical parameters were determined according to Folk and Ward (1959).

4.3.3.2 Diatom analyses

The diatom analyses for the core BAY05_20c come from Mezgec et al 2017. The relative abundances of *Fragilariopsis curta* in the BAY05_20c increased from ~ 20% before 3.6 ka to ~ 70–80% over the last 1000 years. Between ~ 5.8 and ~ 3.6 ka the lowest relative abundances of *F. curta* are concomitant with high occurrences of *Chaetoceros Hyalochaete resting spores* (CRS) and *Thalassiosira antarctica resting spores* (TRS). The subsequent increase in the relative abundances of *F. curta*, together with the decrease in the occurrences of CRS and TRS, is marked by a centuries-old decline in the relative abundances of *F. curta* and a concomitant increased occurrence of CRS and TRS between 1.5 and 0.9 ka.

The diatom analyses for the CH41 and HLF17_01 cores come from Finocchiaro et al 2005 and Tesi et al 2020, respectively.

Both cores show that *Corethron pennatum*, *F. curta*, along with *Chaetoceros* resting spores account for up to 96% of the diatom assemblages throughout the cores. *C. pennatum* occurs only in the laminated layers starting from the bottom up to about 250 cm in core CH41, while *F. curta* and CRS are found in different percentages throughout the core. *F. curta* becomes dominant in the coarse-grained upper unit of the last few centuries in both cores with a percentage > 50%. The highest relative abundances of *F. curta* have been recorded in the last few centuries.

4.3.4 Oceanographic data

Ice concentrations in the Ross Sea are influenced by winds with ice remaining in the western region throughout the austral spring and generally melting in January due to local heating. This leads to extremely strong stratification and shallow mixed layers in the western Ross Sea.

During the 2017 survey, variations of currents along the route traveled inside the Edisto Inlet fjord have been marked, most likely influenced by the tide. However, it is not possible to highlight the contribution of the barotropic tide because the Tide Model Driver model (Padman & Erofeeva, 2005) does not cover the internal area of the Edisto Inlet fjord. At the mouth of the bay, it seems that the tidal currents (mainly diurnal tides) can locally reach 30-40 cm / s in the syzygous phases, while during the survey of 17/02/2017 the possible contribution of the tidal current did not exceed 5 -10 cm / s. At the bottom of the bay, low temperatures of around -1.6 ° C and relatively high salinity 34.27 were measured (taking into account the relative measurements at a depth of 4 m below sea level (bsl)).

The properties of the water masses in this small basin with a conspicuous variability of temperature and surface salinity are still poorly unknown, and future investigations are needed to have a better knowledge of the internal circulation as well as the water masses exchange with the ocean. These measurements will contribute to estimate the currents role in the morphobatimetry's configuration.

During the 2017 campaign on board R/V Explora, the following along-track data were acquired on the 17th of February: 1) surface temperature and salinity from thermosalinographer SBE21 and SBE38 at 4 m depth; 2) vertical profiles of currents from a 75 kHz Vessel Mounted-Acoustic Doppler Current Profiler (vmADCP), in the range 24-600 m depth with a vertical resolution of 16 m. ADCP data were then processed with the CODAS3 software developed by the University of Hawaii.

During the 2020 campaign on board R/V Laura Bassi, Conductivity-Temperature-Depth (CTD) profiles were acquired on the 6th of February along the whole water column at 6 stations in the Edisto bay. Temperature, salinity, oxygen and fluorescence profiles were obtained. Vertical profiles of currents were also measured by means of a Lowered-ADCP (LADCP) deployed together with the CTD.

4.4 Results

4.4.1 Seismic facies

The sedimentary succession within Edisto Inlet imaged with sub-bottom data has been divided into two main seismic facies, termed EI and EII (Fig. 4.3).

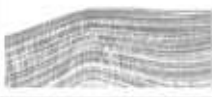

Seismic facies classification					
Facies Unit	Seismic Example	Internal configuration	Amplitude - Frequency	Lateral continuity	Occurrence
Facies EI		Sub horizontal to undulated stratified reflections	Moderate to high amplitude High Frequency	Good continuity reflections	Basin filled with biogenic ooze; No uniform rates of deposition; Low-energy ooze deposits
Facies EII		Transparent - poor reflections no internal organization	Low amplitude Low frequency	Low lateral continuity reflectors	High water content, possible presence of gas; Unconsolidated material rich in mud

Table 4.3 Seismic Facies classification. Facies EI: sub horizontal with high amplitude reflector mostly made of biogenic ooze. Facies EII: Transparent with poor reflections and low amplitude unconsolidated material rich in mud. The occurrence is inferred from the seismic facies and sediment cores.

The seismic facies EI, consists of laterally continuous, high amplitude, parallel, sub-horizontal or undulated reflectors that are generally conformable to the sea floor (Figure 4.4, 4.5, 4.7). In sectors 1 and 2, low angle truncational or onlap surfaces are observed within the seismic facies EI (Figure 4.4, 4.5).

Facies EI has an overall basin in-fill, tabular shape. Locally, near steep scarps, it has sigmoidal and mound-shape with internal reflectors pinching and/or downlapping on the lower unit in correspondence of sea floor depressions.

The seismic Facies EI is thin over sector 1 and reaches a maximum thickness of 180 ms (tw) in the central part of the fjord in sector 2 (see fig. 4.5 and 4.6 thickness map), where the sea floor appears to be flat.

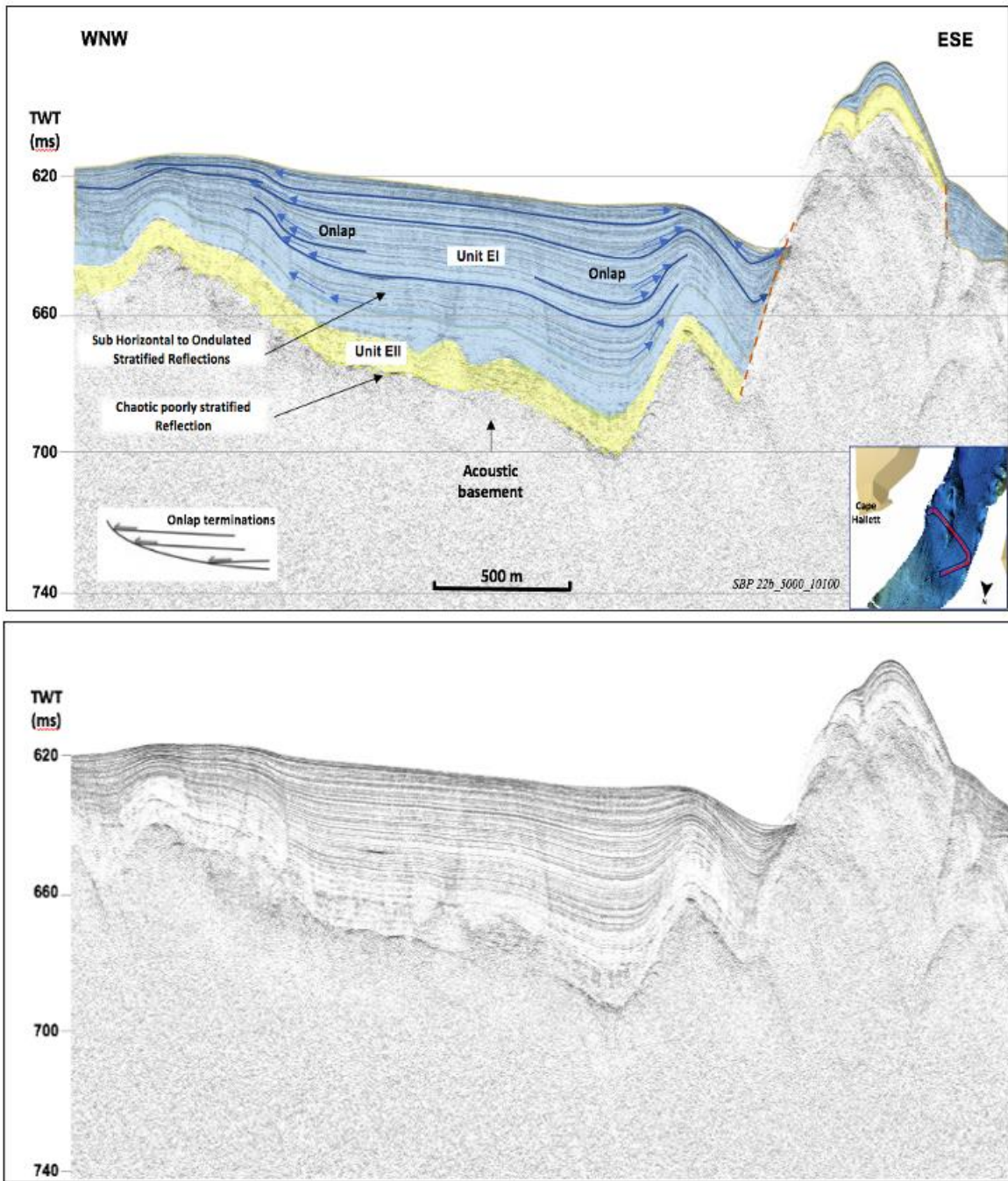


Figure 4.4: Interpreted and uninterpreted representative chirp record showing the general seismic stratigraphy of the survey area in Edisto Inlet fjord. The defined seismic units EI, EII are indicated based on characteristics of the reflectors. Depth labels in meters are based on 1500 ms^{-1} sound velocity. Colors on the chirp profiles mark interpreted seismic units. The blue arrows indicate the reflectors termination in onlap. Red dotted lines are two normal faults

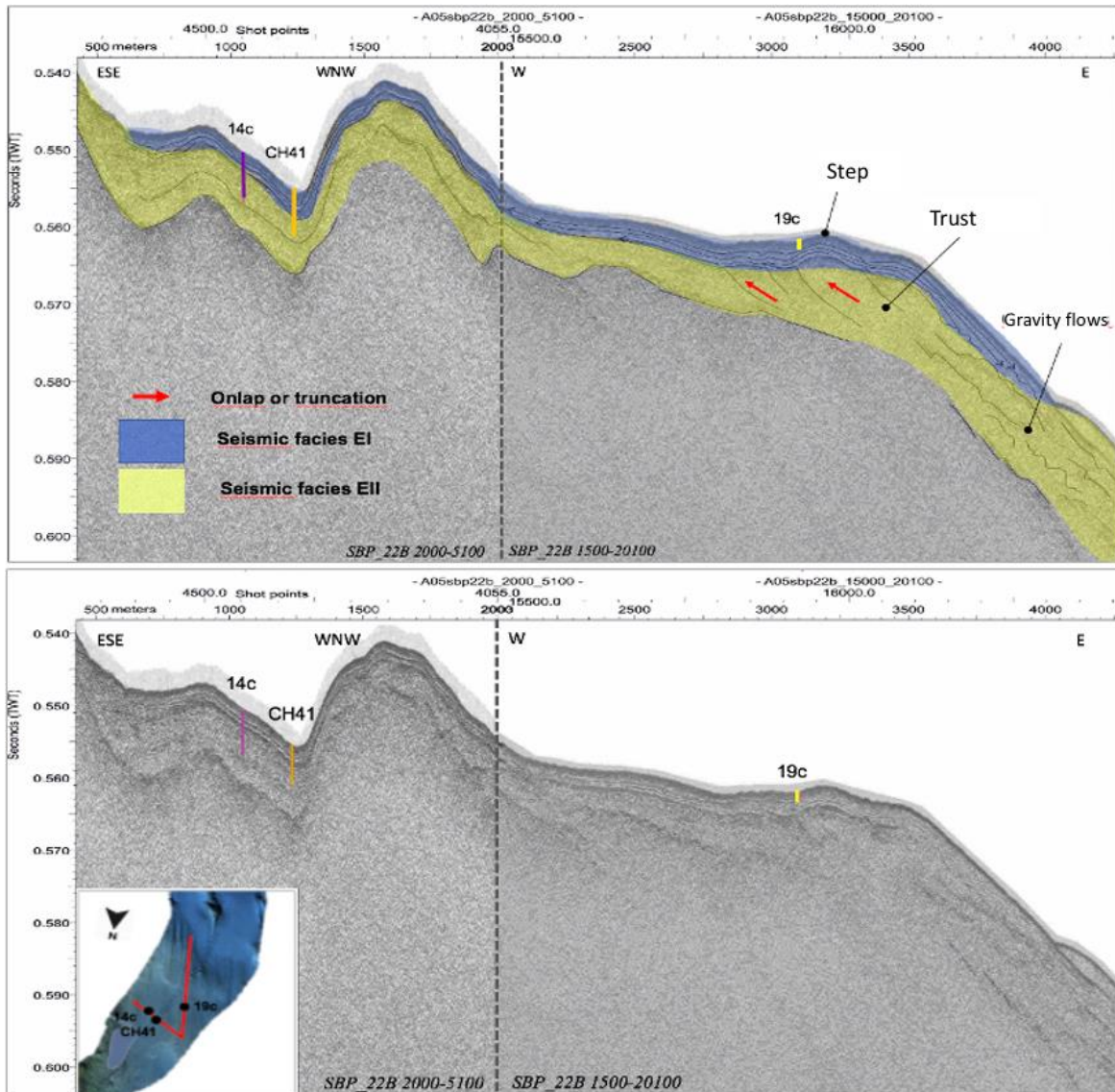


Figure 4.5: Interpreted and uninterpreted seismic lines showing a basin-floor succession with the two main seismic facies recognized: EI in blue, consists in laterally continuous, high amplitude parallel reflections and EII in yellow with an opaque or weakly stratified, sparse or discontinuous low amplitude reflections. Note the gradual progradation of gravity-flow deposits into the basin due to slope break. Evidence of thrust faults within the seismic facies EII. The pink, orange and green lines outline the location of the sediment cores.

In fig 4.6 the isopach map displays the stratigraphic thickness of the seismic facies EI between its upper and lower horizon. It is measured as the shortest distance between the two surfaces. The color bar is in two-way travel time (ms) and clearly shows maximum thickness (>160 ms twt) ~130 m in the central part of the fjord in sector 2.

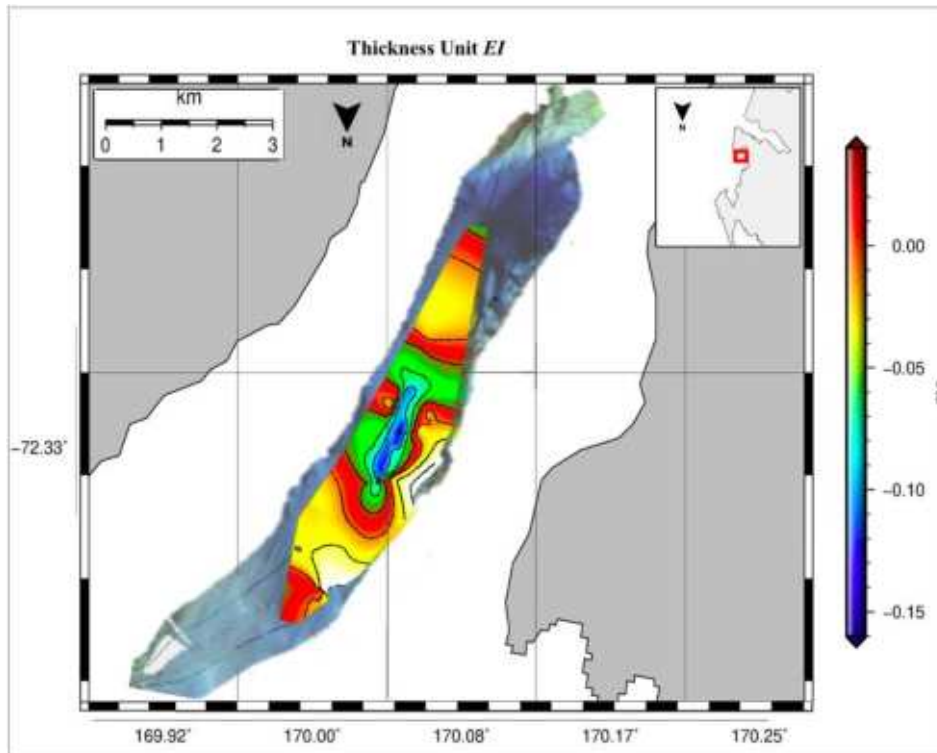


Figure 4.6 - Isopach map (based on 2D seismic reflection profiles) showing the thickness variations of the seismic unit EI. The color bar is in two-way travel time (ms).

The seismic Facies EII lies below EI and is opaque or weakly stratified, with sparse, discontinuous, low amplitude reflections (fig. 4.4, 4.5, 4.7). Some reflectors southwards inclined are observed near the southern edge of sector 1, where they appear to cut through at high angle and they upward displace a high amplitude reflector at the base of the seismic facies EI. The inclined seismic horizons converge on a flat, high amplitude reflector, toward south (fig. 4.5).

Along the slopes between sector 1 and 2 (fig. 4.4, 4.5, 4.7) reflectors of facies EII are irregular, discontinuous and southward dipping, locally showing with terminations in downlap on the deeper horizons.

Facies EII is blanketing the acoustic basement and is up to 50 ms (twt) thick in the northern and central sector of the fjord. It is not observed in the southern sector, because it is deeper than the penetration depth of the seismic data used in this work. Here Facies EII is locally visible on the top of acoustic basement highs, where it has a convex shape pinching on the edges (fig. 4.4, 4.5, 4.7).

Faults with normal offset of up to 50 ms (twt), dipping south, affect the lower part of the sedimentary section, in sector 2 and along the slopes between the four sectors (fig. 4.7).

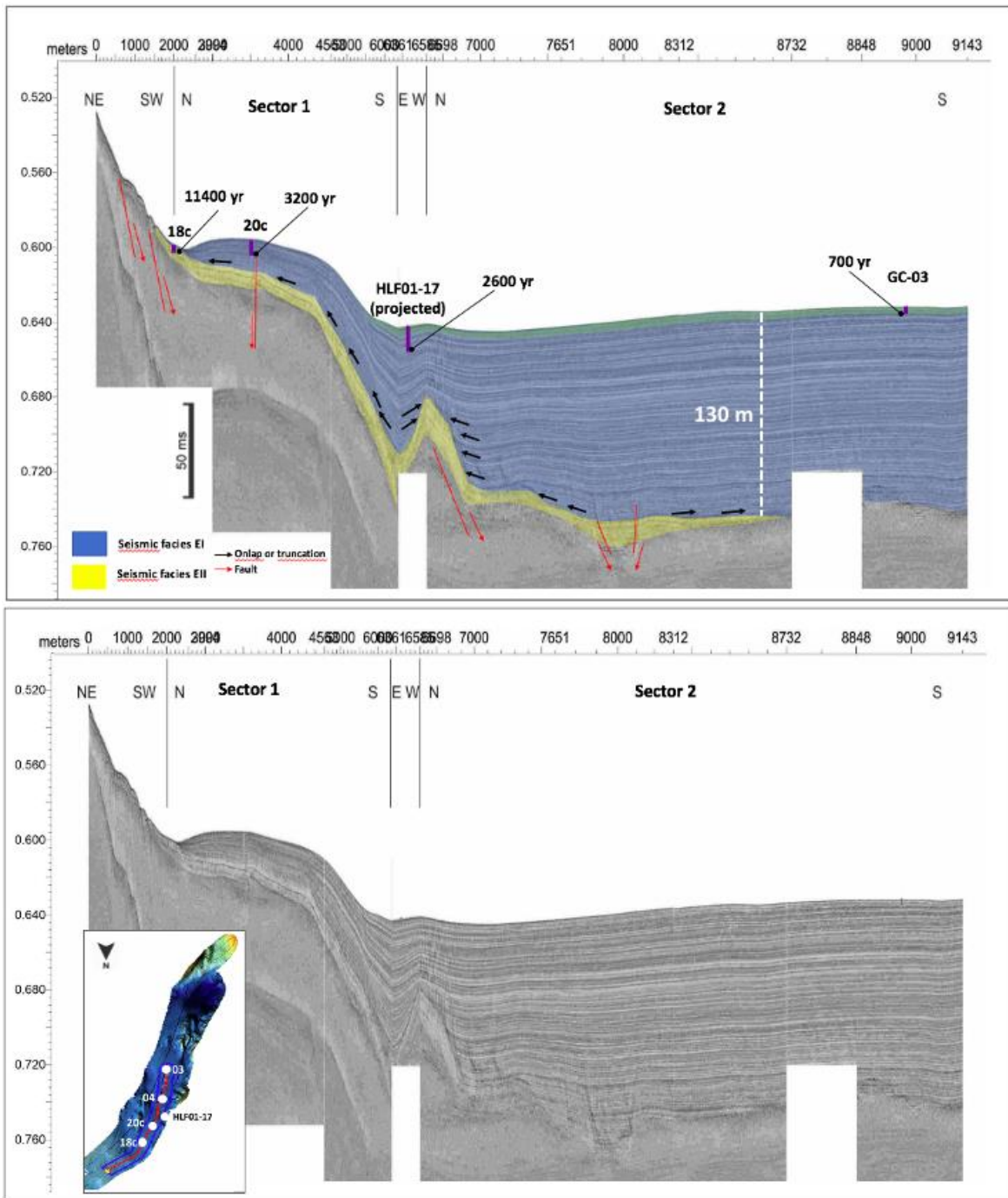


Figure 4.7 - Interpreted and uninterpreted sub bottom chirp profiles track lines show an elongated sediment drift in the sector 1 and a thick (up to 130 m) finely flat stratified unit in the sector 2. The well stratified parallel reflectors in blue indicate the first seismic facies EI with convex sigmoidal reflectors ending in onlap or pinch out (black arrows). The seismic facies EII in yellow is discontinuous with low amplitude reflections and is up to 35 m thick in the northern and central sector of the fjord with locally downlap terminations. The red arrows are associated with the propagation of a normal faults. Purple lines indicate the location of the sediment cores and the calibrated radiocarbon dates.

4.4.2 Bathymetry and Submarine Landforms

Smaller relief (~ 10 meters) elongated ridges, parallel to the fjord axis are visible on multibeam data in sector 1, in water depth of 410-470 meters (fig. 4.2, 4.8). The elongated ridges terminate to the north in correspondence of a morphological step, with relief of ~ 15 m and the steep slope facing north, that runs transversally across the fjord, with irregular, lobated trend (fig. 4.8). Sub bottom profiles show that the acoustic facies below the elongated ridges is opaque or weakly stratified, with reflectors draping or onlapping mounded features (seismic facies EI, fig. 4.4, 4.5, 4.7, 4.8).

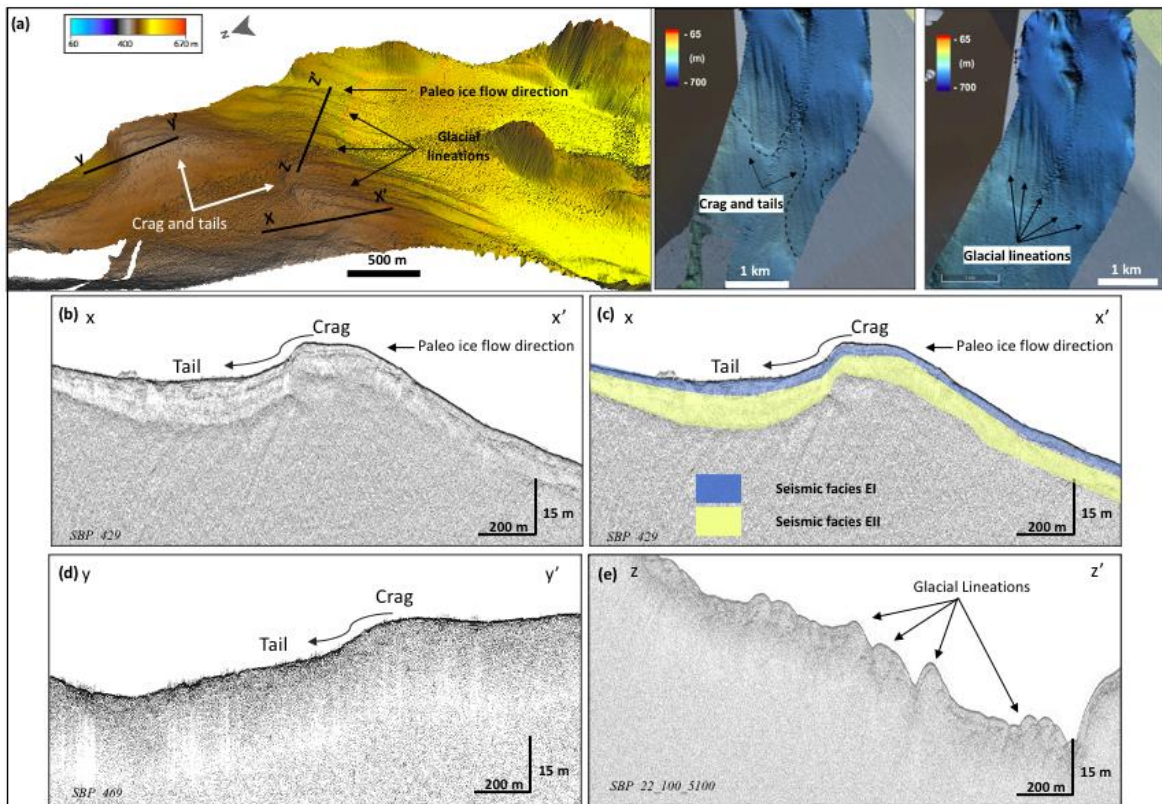


Figure 4.8: Multibeam swath bathymetry of Edisto Inlet in a 3D representation of the outer fjord showing the seafloor landforms (a). Paleo ice flow direction towards north (b, c). In (b) there is the representation of the two seismic facies EI in blue and EII in yellow. X – X' and Y – Y' show a crag and tail in the inner bay area (b,c,d), and Z-Z' (cross-section profile) shows glacial lineations (e). Vertical exaggeration is 4x in all images.

A smooth and almost flat seabed characterizes the sectors 2, in the middle of the Edisto Inlet Fjord with a thick (up to 130 meters) finely stratified unit record (fig. 4.7).

The southern sector of the fjord (sector 4), in front of the Edisto Glacier is characterized by a deep depression (fig. 4.9) up to 700 meters deep. Its western flank is cut by channels with size ranging from 100 to 300 meters of width and relief of up to 100 meters (channels A-D

in fig. 4.9). The eastern and northern flanks of the depression in sector 4 are steep and smooth (fig. 4.9) The seabed reflector in seismic profile across sector 4 is highly reflective, with no acoustic signal penetration below (Fig. 4.9a) with the exception of the smooth northeastern flank, where stratified reflectors are observed, like for sector 2 and 3 (Fig. 4.9 b).

The southernmost termination of the fjord shallows up to 300 meters. Here elongated ridges, trending N-S, tens of meter wide, bound small channels with relief of 15-20 meters between the ridge crest and the channel axis (channel C and D in fig. 4.9 c). The sea floor is generally reflective, allowing no penetration below, with the exception of stratified reflectors onlapping the flank of channel F (fig. 4.9).

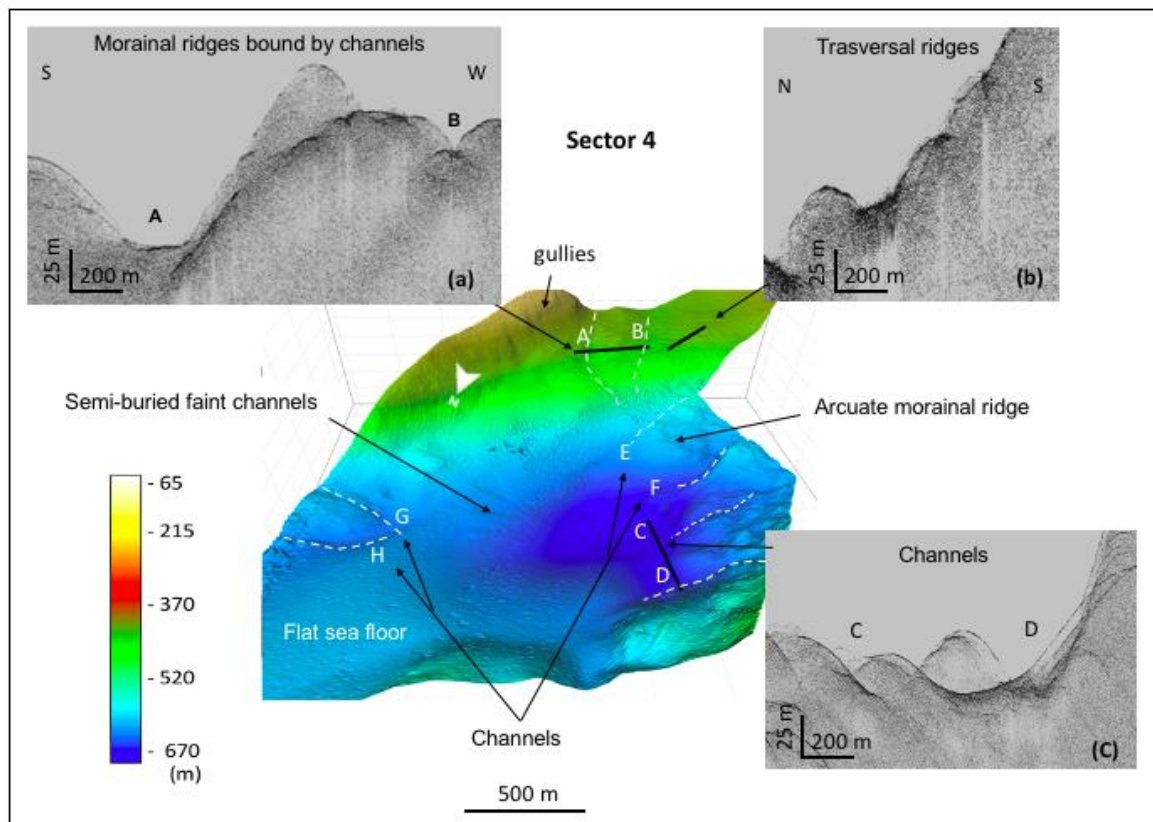


Figure 4.9 - 3D multibeam swath bathymetry of Edisto Inlet showing a broad and deep depression in the southernmost termination of the fjord up to 700 meters deep. Sub-bottom profiles show that the seabed of the southwestern flank is a strong high amplitude and irregular reflector, preventing any acoustic signal penetration below (a,b,c). White dotted lines outline the channel incisions (A to H). The smaller ridges represent morainal deposits. The color bar is in meters.

4.4.3 Stratigraphic data

Physical properties, grain size data, TOC, wt.% BSi and Xrays are partially published by Finocchiaro et al., 2005; Mezgec et al., 2017; Tesi et al., 2020 for most of the sediment cores collected in the Edisto Inlet fjord. The available measurements (table 4) document the presence of three main sedimentary facies and two subfacies deposited after the LGM in the sectors 1 and 2 of the fjord and provide direct lithological information for the acoustic facies identified on the seismic profiles. No samples exist from the sectors 3 and 4.

Table 4 summarizes all the physical characteristics and the average values of the geochemical analyzes distributed in the facies / subfacies recognized in each core (E. Colizza, unpublished).

core label	facies/subfacies	facies/subfacies depth (cm)	short description	Magnetic Susceptibility SI x10 ⁶ (avg)	water content % (avg)	Dry Density g/cm ³ (avg)	sand/silt/clay % (avg)	TOC % (avg)	SIBio % (avg)	calibrated age (BP)
ANTA02-CH41	SL-sf	304-406	strongly laminated	299	82	0,213	--	0,62	34	around 10 ka
	WL-sf	216-303	weakly laminated to massive	2756	62	0,502	23/60/17	0,76	19	>9 ka
	MBf	0-215	massive, +/- biturbated with gravel	4933	33	1,097	60/33/7	0,34	4	around 8 ka to present
BAY05-13c	MBf	0-166	massive, +/- biturbated with gravel	13082	--	--	--	--	--	--
BAY05-14c	Gdf	377-452	massive gravel rich sediment	7789	--	--	--	--	--	--
	SL-sf	308-376	strongly laminated	371	--	--	--	--	--	--
	WL-sf	208-307	weakly laminated to massive	1786	--	--	--	--	--	--
	MBf	0-207	massive, +/- biturbated with gravel	13259	--	--	--	--	--	--
BAY05-18c	Gdf	359-419	massive gravel rich sediment	3169	23	0,391	14/80/7	0,38	10	>36 ka
	SL-sf	289-349	strongly laminated	234	83	0,201	18/76/6	0,67	45	around 11 ka
	MBf	0-287	massive, +/- biturbated with gravel	6205	45	0,761	23/73/4	0,56	10	7200y to present
BAY05-19c	MBf	0-73	massive, +/- biturbated with gravel	8421	--	--	--	--	--	--
BAY05-20c	SL-sf	0-445	strongly to weakly laminated	223	76	0,286	13/82/5	0,55	22	3304 y to present
HLF17-01	SL-sf	0-1465	strongly laminated	329	77	0,246	11/84/5	0,65	30	4220 y to present
IT17RS_GC003	SL-sf	0-430	strongly laminated	339	--	--	--	--	--	base 810 y BP
IT17RS_GC004	SL-sf	0-406	strongly laminated	311	--	--	--	--	--	--
BAY05-22	WL-sf	0-389	weakly laminated to massive	4501	54	0,655	27/67/6	0,55	--	>8000 to present

Table 4: resume of the physical and geochemical characteristics distributed in the facies/subfacies recognized in each core (E. Colizza, unpublished). Facies/subfacies: *glaciomarine diamicton facies* (Gdf), *laminated facies* (Lf), *Strongly laminated sub-facies* (SL-sf), *weakly laminated sub-facies* (WL-sf).

4.4.3.1 Cores description

Data of core **ANTA02-CH41** come from Finocchiaro et al. (2005). The core was collected in 2002 at the entrance of the Edisto Inlet, along the conjunction between Cape Hallett and Cape Christie. The core, 406 cm long, is characterized at its base by one meter of rhythmic sequence of parallel light and dark diatom ooze laminae with little clastic material followed by one meter of massive dark olive-grey mud with wavy and irregular stratification. These sediments correspond to units A of Finocchiaro et al., 2005 and were deposited up to ~ 9400 ky BP. The more superficial portion of the core shows a massive feature and varies from a dark olive-grey muddy sand to a very dark grey, slightly muddy sand. These sediments correspond to unit B of Finocchiaro et al., 2005 and were deposited from ~ 8400 y BP to the present.

Core **BAY05-13c** is characterized by 166 cm of massive sediment with sparse pebble-size clasts. The X-ray image highlights an uneven sediment characterized by widespread pebbles, more concentrated at the base and at the middle-top core. The X-ray image and the MS average value (13082×10^{-6} SI) indicate a quite similar lithology of the BAY05-14c top core.

Core **BAY05-14c**, 452 cm long, has been collected at the entrance of the fjord, very close to core BAY05-13c. The sedimentary sequence is very similar to that recognized in core ANTA02-CH41 but an additional sediment facies was also recovered. In particular X-ray image data permits to recognize a massive and coarse (gravel) sediment at the bottom, overlying by the crudely laminated sediment passing to irregularly laminated to massive dense sediment with sparse pebbles at the top core.

BAY05-18c is a 419 cm long core, collected at the transition between sectors 1 and 2. The same massive gravel-rich sediment of core BAY05-14c characterizes the bottom core. The radiocarbon dating indicates an age >35 ky BP at its base. The overlying sediment passes from olive to dark olive grey planar to wavy laminated, and to black to very dark grey very weakly laminated to massive. Sparse gravel clasts are present. The lower boundary was dated around 11.4 ky old. The very weakly laminated and massive sediment, sometime

bioturbated, characterizes the top core. This sediment was deposited from 7200 y BP to the present.

Core **BAY05-19c** is characterized by 73 cm of massive pebbles-rich sediment at its base and massive to a very weakly laminated with sparse gravel clast toward the top core. X-ray and the MS measurement (mean value 8421×10^{-6} SI) suggest a sediment similar to that present at the top of core BAY05-18c.

Several data of core **BAY05-20c** have been published in Mezgec et al. (2017) and Di Roberto et al. (2019). The core is characterized by silt to sandy silt, light to dark laminae alternating with greenish fluffy diatomaceous mud. Light laminae are siltier with color spanning from olive-to-olive grey. Dark laminae are sandy silt, and the color varies from dark grey to black. Carbonate fragments and some millimetres clasts are present. The sediment covers a temporal range of about 3.2 ky (estimated by the lowest date). A tephra layer, dated 1254 C.E., has been recognized (Di Roberto et al., 2019) at 139-140 cm depth.

Core **BAY05-22c** was collected near the top of a sediment drift recognizable in the west flank of the fjord. The sediment is characterized by olive to dark olive grey sandy silt, weakly laminated to massive. The gravel fraction is sparse along the core and more concentrated at its base where also the sand fraction increases. The core bottom was dated as 8.1 ky old.

The piston core **HLF17-01** was published in Tesi et al. (2020), is characterized by 14.65 meters of soft biogenic (diatom) laminated sediment accumulated during the last 2.6 ky. A tephra layer was recognized at 136-137 cm depth and correlated to the 1254 C.E tephra of core BAY05-20c (Di Roberto et al., 2019).

IT17-RS-GC-003 and **IT17-RS-GC-004** (442 cm and 404 cm long, respectively) are the innermost cores collected by Italian expeditions. Both cores are thickly and regularly laminated. The low MS (avg 339×10^{-6} SI and 311×10^{-6} SI respectively) permits to suppose the sediment as a diatom ooze. The base of core IT17-RS-GC-003 was dated as 0.7 ky old.

4.4.3.2 Lithostratigraphic facies

The *glaciomarine diamicton facies (GDf)* is characterized by abundant pebbles in a sandy silt matrix high dry density (avg 1.388 g/cm³) and high magnetic susceptibility (MS, avg 5479 x 10⁻⁶ SI) (fig 4.10 b, c). Water content, TOC and wt% BSi contents (23%, 0.38%, 10% respectively), measured in core BAY05-18c are low. This facies is present at the bottom of cores BAY05-14c and BAY05-18c located in the sector 1 and its age is >35 ka BP (fig 4.10 c, table 4).

The *laminated facies (Lf)* is characterized by strongly to weakly laminated and massive diatom ooze with low clastic material. The different physical and geochemical characteristics from strongly laminated to weakly laminated permit us to distinguish two sub-facies:

Strongly laminated sub-facies (SL-sf) which presents the lowest MS (avg 301 x 10⁻⁶ SI)(fig 4.10 a), a high-water content (avg 80%), and wt% BSi (avg 33%). TOC content is 0.62% (medium value). The sediment presents a low dry density (avg 0.236). This sub-facies is present at the base of core ANTA02-CH41, overlays facies *GDf* in cores BAY05-14c and BAY05-18c and it is the only facies present in cores BAY05-20c (Figure 4.10), HLF17-01 (Figure 4.12). IT17RS-GC-003 and IT17RS-GC-004 (Figure 4.11). This sub-facies was deposited between c.a. 10 and 11.4 ka BP in sector 1 and at least since the last 4 ky BP in sector 2. The short coring tool available, has not allowed to sample the lower part of the subfacies *SL-sf* in sector 2, where it seems to exceeds more than 100 meters in thickness on the basis of seismic profiles.

Weakly laminated sub-facies (WL-sf) presents a higher MS than *SL-sf*, with average of 3014 x 10⁻⁶ SI (fig 4.10 a, b, d) with a water content and TOC around 58% and 0.65% respectively. The mean dry density that characterizes these sediments is 0.578 g/cm³. Sub-facies *WL-sf* overlies the *SL-sf* sub-facies in ANTA02-CH41 and BAY05-14c (Figure 4.10 a,b) and characterizes the entire core BAY05-22c. The sub-facies was deposited in a short time interval about 9000-8400 years ago in sector 1, while the age of sediment collected at Bay05-22c spans from 8.1 yr BP to the present (Figure 4.11)

Massive, bioturbated facies with gravel (MBf), (Unit B in Finocchiaro et al 2005) massive, sometime bioturbated silty sand to sandy silt sediment with dispersed gravel clasts characterizes this facies. The MS averages 9180×10^{-6} SI (fig 4.10 a, b, c), water content is 39%, TOC 0.45%, low wt% BSi (7%). The mean dry density is 0.929 g/cm³. This facies occurs at the top of cores (ANTA02-CH41, BAY05-14, BAY05-18c) (Fig 4.11). It is the only facies present in BAY05-13c in Sector 1. It has been deposited from 9 ky to the present.

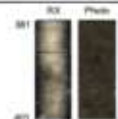
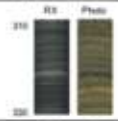
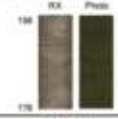

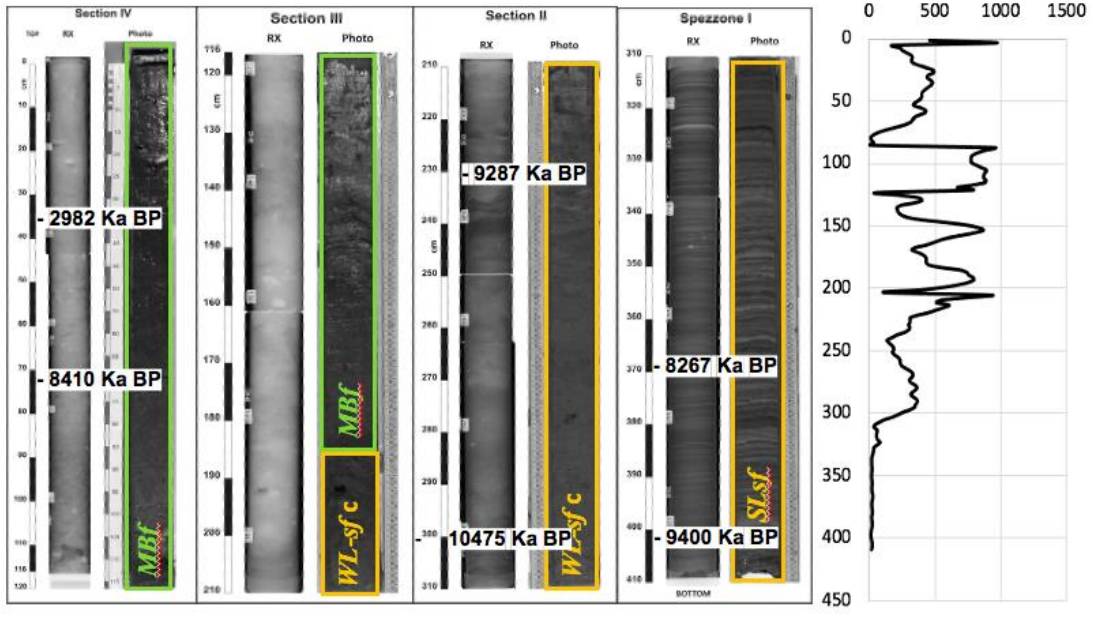
Facies association	Lithology	Sedimentary structure	Environmental Interpretation	Representative photos of facies association
<i>Gdf</i>	Gravel-rich dark olive sediment with abundant pebbles in a sandy silt matrix	Massive, chaotic	Subglacial till, Glacimarine Diamicton	
<i>SLsf</i>	Diatom ooze with low clastic material	Horizontally laminated	Low energy open marine condition with a seasonal alternation of productivity events	
<i>WL-Msf</i>	Sandy silt light to dark laminae of diatom ooze	Weakly laminated	Medium to low energy open marine conditions with more persistent sea ice cover	
<i>MBf</i>	Silty sand to sandy silt coarse grained sediment with dispersed gravel clasts	Massive, bioturbated	Meltwater facies linked to strong bottom tidal currents	

Table 5: Summary of the facies association and environmental interpretation from studied cores. Gdf facies is here represented by the interval 381-401 cm of core BAY05-18c, sub-facies SL-sf is represented by the interval 310-330 cm of core ANTA02-CH41(Finocchiaro et al 2005); sub-facies WL-sf is represented by the interval 158-178 cm of core BAY05-22c; facies MBf is represented by the interval 0-16 cm of core BAY05-18c.

(a)

ANTA02_CH41

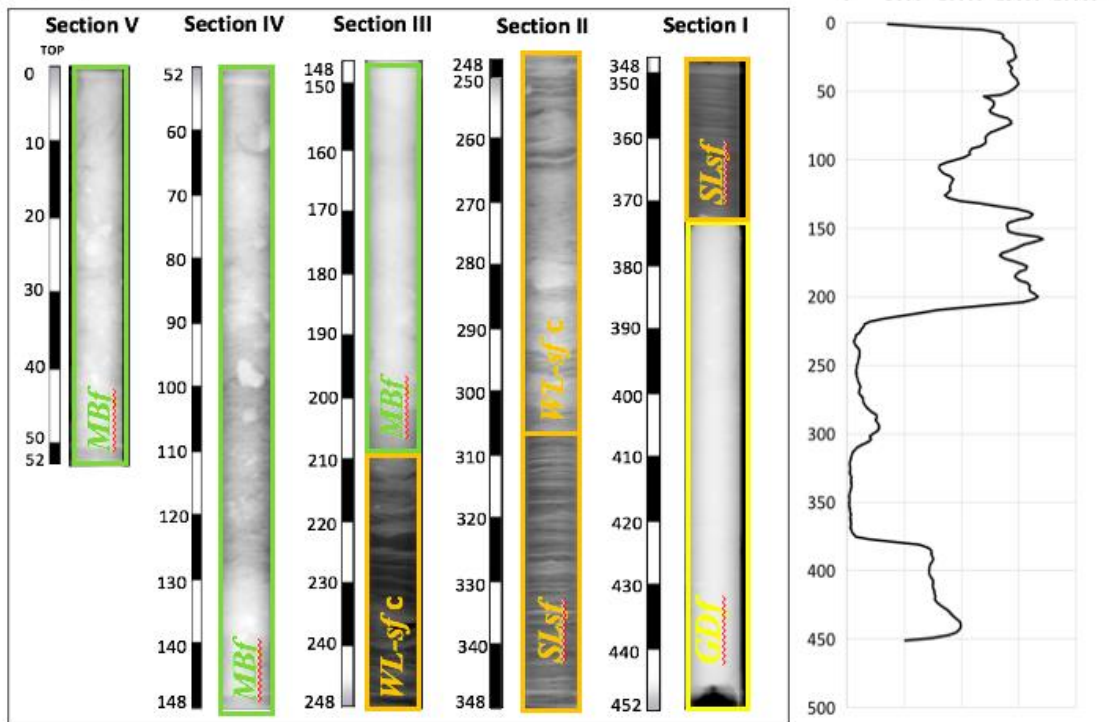
MS SI *10⁻⁶



(b)

BAY05_14c

MS SI *10⁻⁶



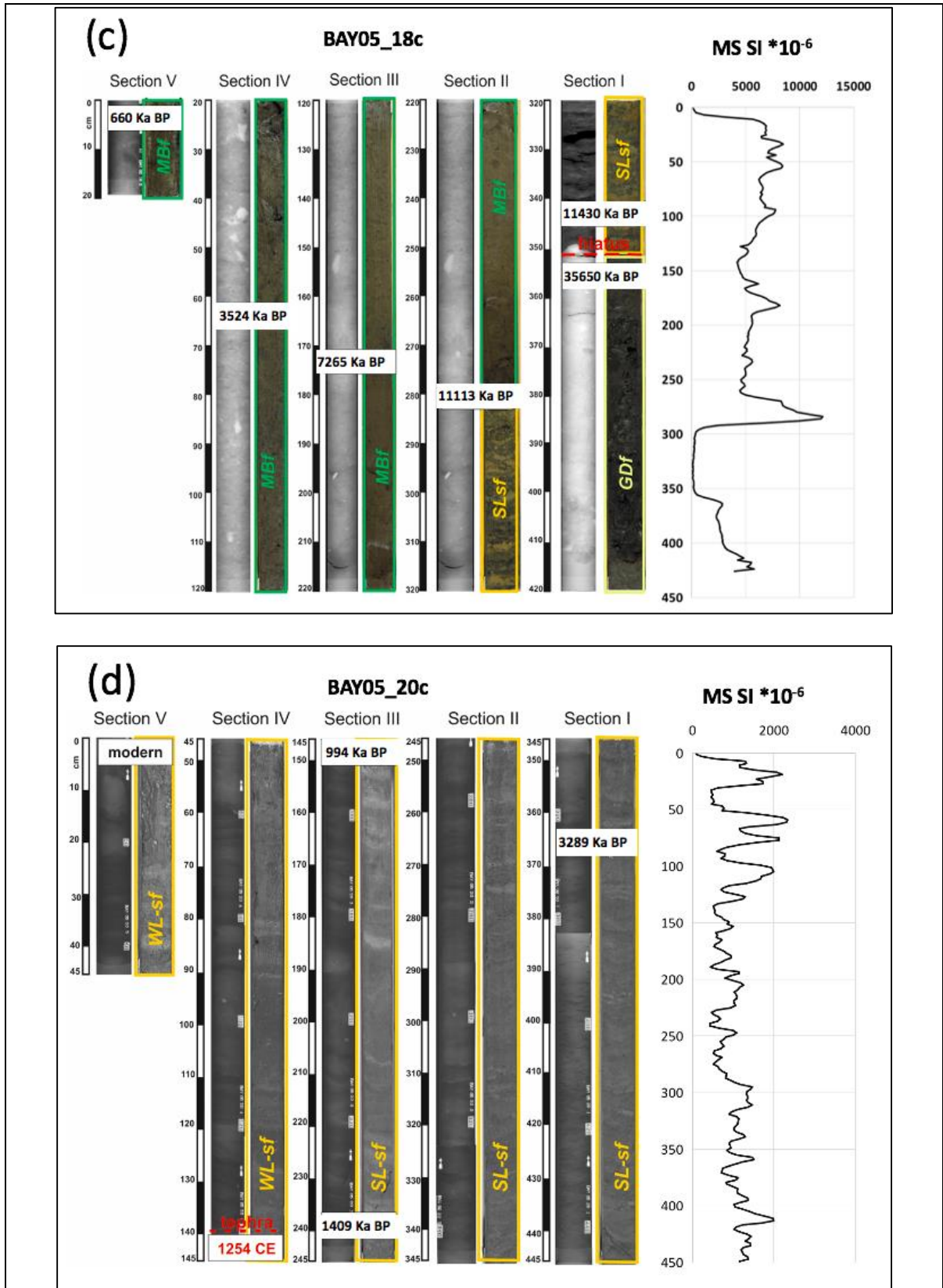


Figure 4.10: XRay, Photo and Magnetic Susceptibility (SI) curve for the core ANTA02-CH41 (a) BAY05-14c (b) BAY05-18c (c) and BAY05-20c (d). Each core is divided into the respective lithological facies indicated as: *Gdf* = glaciomarine diamicton facies (in yellow), *SL-sf* = strongly laminated sub-facies, *WL-sf* = weakly laminated sub-facies (orange) *MBf* = massive, bioturbated facies with gravel facies (green). The cores (a, c and d) report the depths with the radiocarbon calibrated dates.

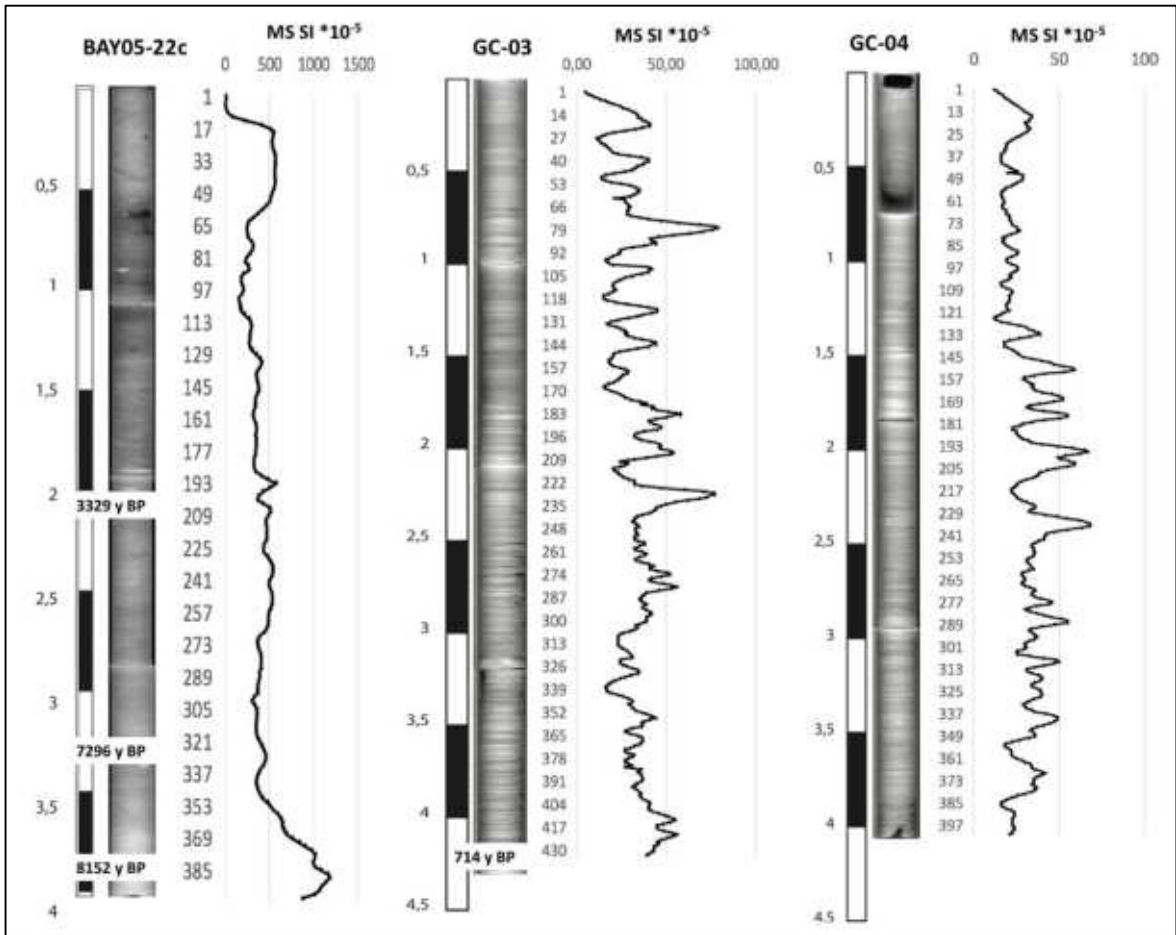


Figure 4.11: X-ray and Magnetic Susceptibility curve of the core BAY05-22c, GC-03 and GC-04. Core BAY05-22c spans from ~ 8.1 yr BP to the present and is characterized by the *Weakly laminated sub-facies (WL-sf)*. Core GC-03 has only one date made on benthic foraminifera from the core catcher (600 yr BP), is characterized by the *Strongly laminated sub-facies (SL-sf)*. Core GC-04 has not been dated and is characterized entirely by the *Strongly laminated sub-facies (SL-sf)*. The MS curve scale of the core BAY05-22c was multiplied by 10 to increase the visibility of the variations.

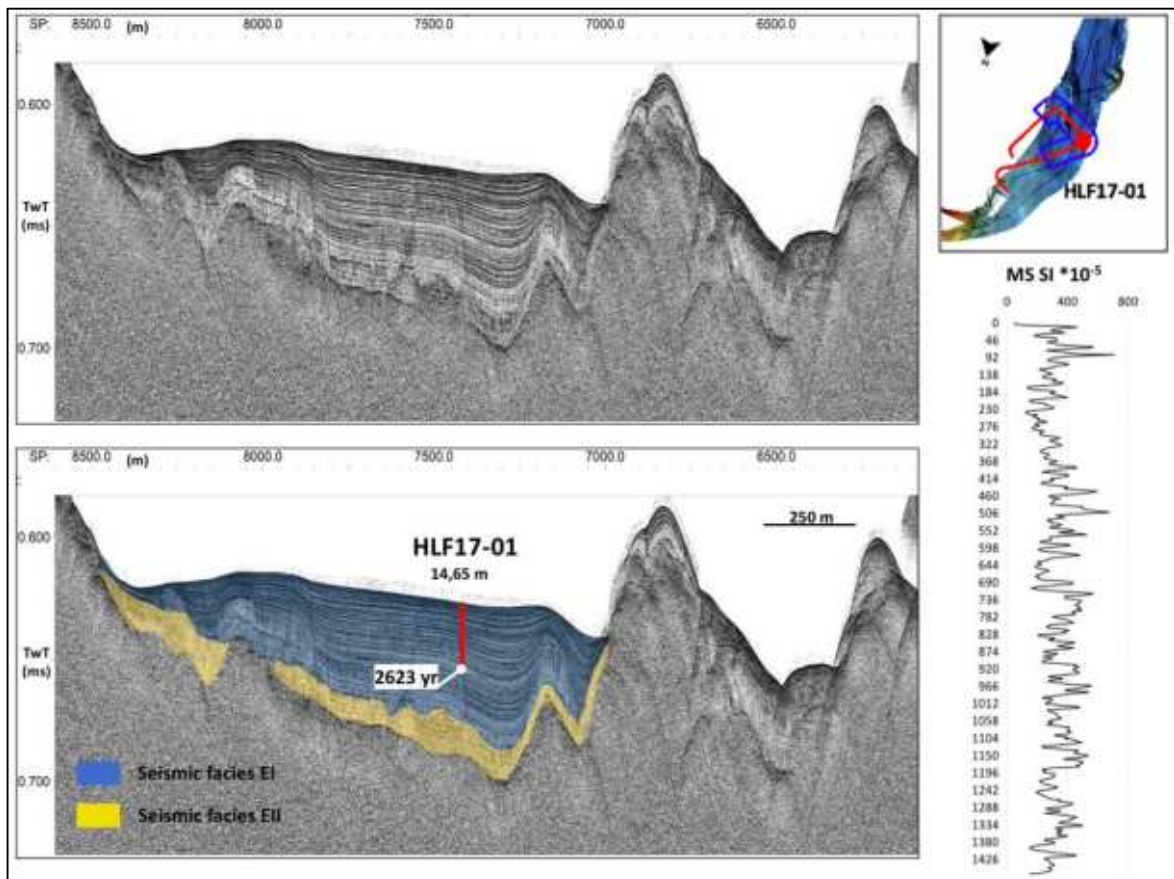


Figure 4.12: SBP showing core HLF17-01 (14,65m long) dated 2,6 ka at the bottom from Tesi et al (2019). The seismic facies EI (yellow), EII (blue) are indicated. On the top right map with the location of the core and on the bottom right curve of the magnetic susceptibility (MS).

4.4.3.3 Correlation between seismic data and sediment cores

Logging data provide the critical link between cores and seismic reflection profiles by measuring the in situ geophysical properties of borehole lithologies at a scale intermediate between the seismic and the core data. This linkage is essential because it allows detailed information obtained by core analysis to be extended to the entire seismic reflection data set. Correlations among the cores, logging data, and seismic profiles were made by importing the data of the physical properties of the cores into the Kingdom Suite software, creating a time to depth chart, i.e. a functional relationship between the velocity function and the times (two way travel time ms) observed in the seismic profiles and corresponding depths.

The lithological shift boundaries and the characteristics observed in each core appear to be related to the seismic reflections. Some of these shifts are also seen in the magnetic susceptibility curves. An example of this correlation is given by the figure 4.13 where the MS (from the core log data acquired onboard), grain size plotted on the seismic profiles of

core BAY05-18c are indicating that the diamicton at the base of cores 18c is overlain by a weakly laminated unit and topped by diatomaceous deposits with sparse ice rafted debris (MBf). The shift from strong to weakly laminated facies is at 11.1 yr BP from ¹⁴C dates is also marked by a shift in the magnetic susceptibility curve at 284 cm (Fig 4.10c and 4.13b)

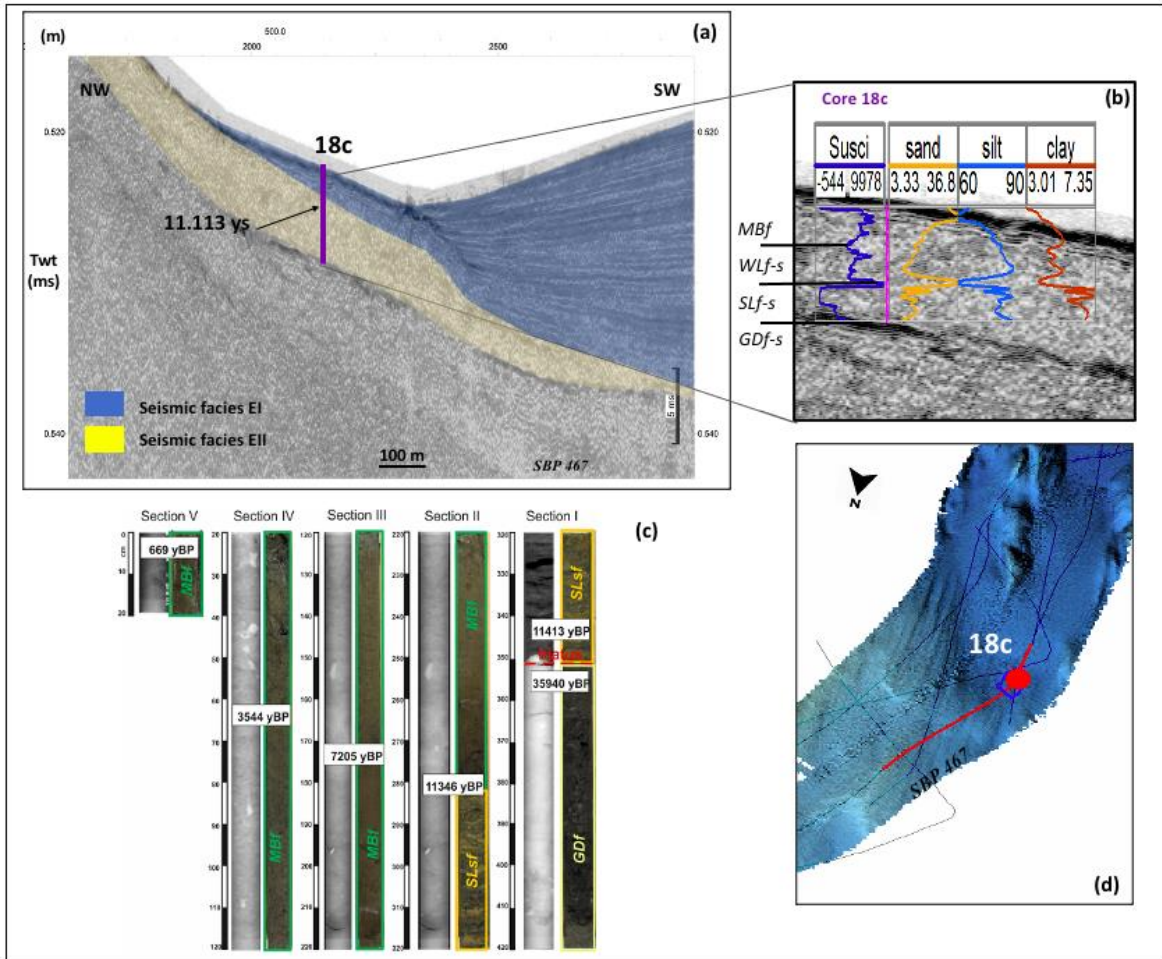


Figure 4.13: Representative correlation between seismic and sediment cores. (a) SBP showing the location of the core 18c. The seismic units EI, EII are indicated. (b) Core log physical properties of core 18c (MS and Gran size) plotted on the SBP. (c) Xray and photos of the core 18c with the stratigraphic facies highlighted and indication of the radiocarbon dates depth. *GDf* = *Glaciomarine diamicton facies*, *SL-sf* = *Strongly laminated sub-facies*, *WL-sf* = *Weakly laminated sub-facies* and *MBf* = *Massive, bioturbated facies with gravel facies*. (d) Bathymetric map with core's location (red dot) and SBP (red line).

4.4.4 Sediment drifts

The geophysical dataset combined with previous echo-sounding data collected in the outer sector of the fjord reveal the presence of sediment drifts. Sediment drifts are accumulations of hemipelagic mud and associated ice rafted debris which are formed and influenced by bottom currents and thus show evidence for being partially shaped by them. The most prominent of these features are usually to be found on the lower continental slope and rise or on the Antarctic continental shelf (Harris et al., 1997). They are characterized by a very high sedimentation rate and are potential excellent paleoclimatic archives for Holocene palaeoenvironmental change and glacial climate oscillations (Willmott et al., 2007; Domack et al., 2003). Paleoclimate records are crucial for understanding current changes taking place in Antarctica.

Drift types are significantly controlled by the physiographic and geological setting in which they develop and by different water masses that flow at different depths. Persistent bottom-current systems and associated oceanographic processes strongly affect the seafloor, conferring it erosional and depositional features. We considered the morphological pattern, and its interaction with bottom water, as the major factors that had controlled the style of sediment accumulation, in the classification systems for drifts our case is better represented by the *confined drift* (Rebesco et al. 2014). Confined drifts are usually mounded, with distinct moats in a relatively small confined basin. In the Edisto Inlet Fjord the drift has the typical form of a sigmoid clinoforme, with a length not exceeding 2 km and thicknesses from 30 to 100 m (figure 4.14).

They form a convex shape, with the predominance of sediment accumulation in the centre of the drift. These small drifts have an arcuate morphology and presents the shape of a separated elongated mounded drift. The Sub-Bottom Profiler (SBP) images show typical contouritic features: (1) an eroded slope characterised by truncated reflections; (2) chaotic acoustic facies of strong amplitude in the moat, and (3) mounded continuous reflections commonly found in muddy drifts with thin glacio-marine and pelagic layers (Fig. 4.14). In confined basins, gyres may transport sediment in suspension from a margin with a high sediment supply to an adjacent margin, favoring the development of fine-grained contourites in the latter. According to the coupled hydrodynamic models and geomorphological interpretations proposed for depositional, erosional and mixed contourite features by Miramontes et al 2019, separated elongated mounded drifts develop in the zone where

bottom currents are relatively weak, with mean velocities below 7 cm s^{-1} , although oceanographic measurements within the fjord are still few, these evidences make Edisto Inlet fall into this category.

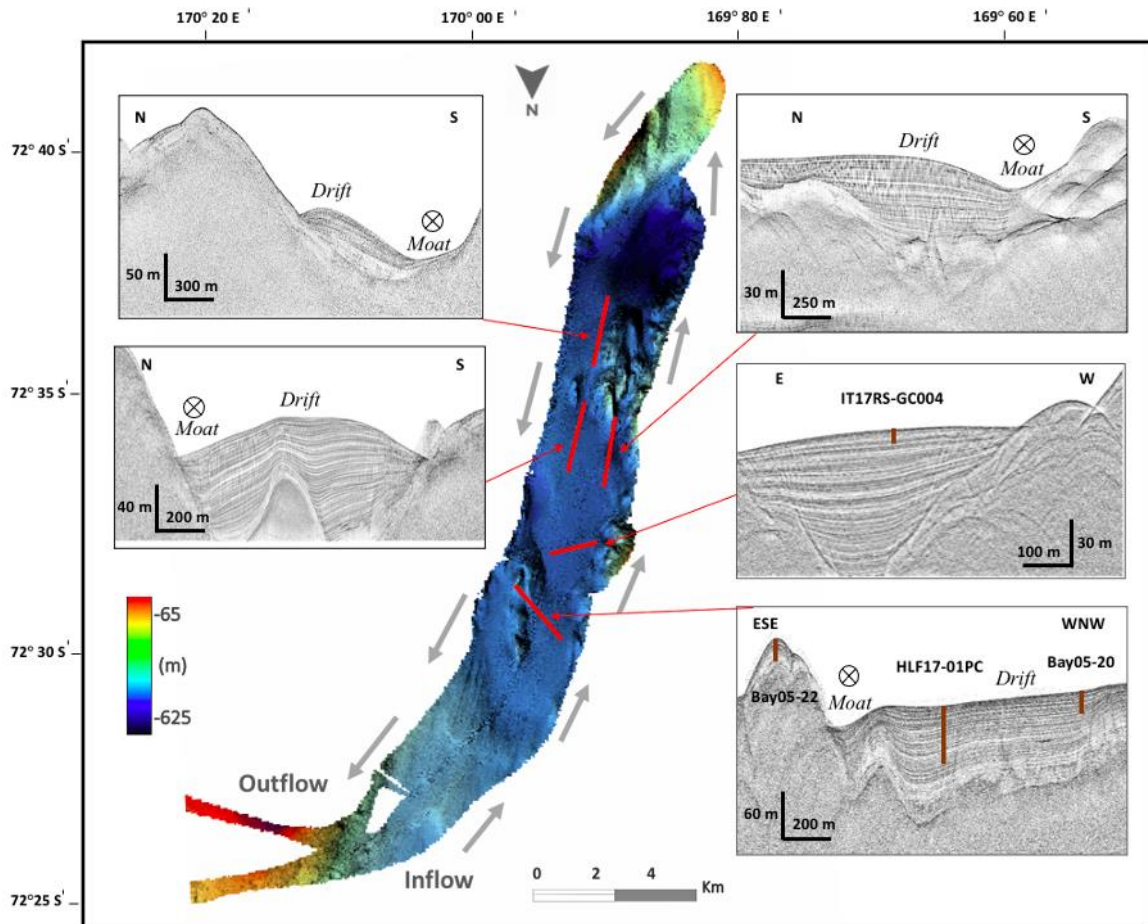


Fig. 4.14: The multibeam map shows the position of the sediment drift, represented by the SBP profiles (red lines) along the Edisto Inlet fjord. The gray arrows indicated the path and direction of the current in the fjord. Brown lines indicate the location of the sediment cores.

4.4.4.1 Sediment drift formation

The velocity measured by the ADCP in 2017 (during the acquisition of the morpho-bathymetric data) shows values ranging from 5 to 30 cm/s (Figure 4.15). Values are null over the areas with thickest sediment drifts in the middle of the Edisto Inlet Fjord (figure 4.15) Although this is not the current speed measured at the seabed but 100 meters above it, and although this is just one measure and cannot be used as representative of a long time period, we observe that these values are consistent with the geometry and type of sediment of the Edisto sediment drifts. Even a low-speed water current of 5 cm/s would be capable of

carrying suspended diatoms and prevent their deposition in the moats. Null bottom circulation velocity measured in the center of the Edisto Inlet Bay would explain the deposition and preservation of the thick soft diatom-ooze, comprising the sediment drifts. The oceanographic measurements inside the fjord are limited to the ADCP data collected PNRA cruise 2017 and a few CDT stations made in 2020 at the entrance of the bay (Figure 4.16). They show water stratification and an apparent gyre inside the bay, with south-southwestward current on the western flank and northeastward current on the eastern flank of the Bay. More measurements are needed to understand the circulation pattern and factors controlling it, like winds, sea ice and tides that in narrow fjords is generally significant. The available measures are too sparse and scarce to understand the present-day circulation and compare it with the location of the sediment drifts. However, the distribution of the drifts inside the Edisto fjord as observed in the seismic profiles, clearly shows that they are controlled by morphology, and would suggest the occurrence in the fjord of a persistent circulation pattern and high productivity conditions. All drifts-moats form on the flank or behind ridges and narrow bathymetric gateways. They developed their typical shape and stratified facies in the course of several thousands of years.

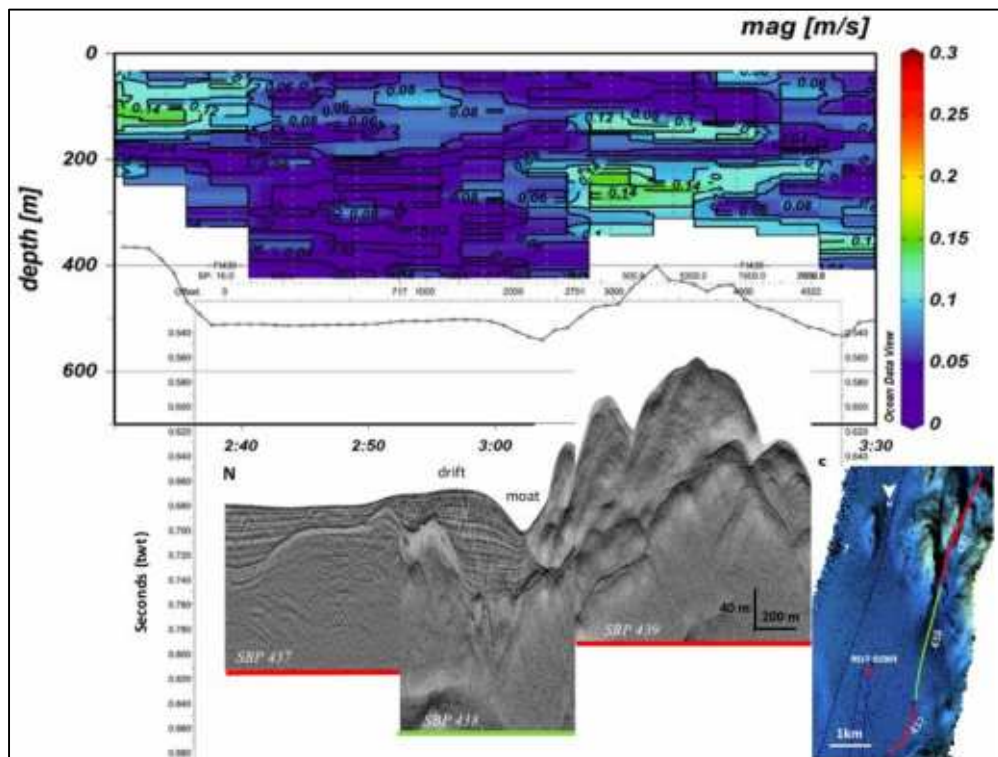


Figure 4.15: Sub-bottom profiles (437,438,439) with an elongated sediment drift and moat and the vertical transect of the currents from the vmADCP above that show that the speed increases in correspondence of the high morphological 0,10 cm/s on the side of which a moat has formed while where there is the drift the speed velocity is almost null.

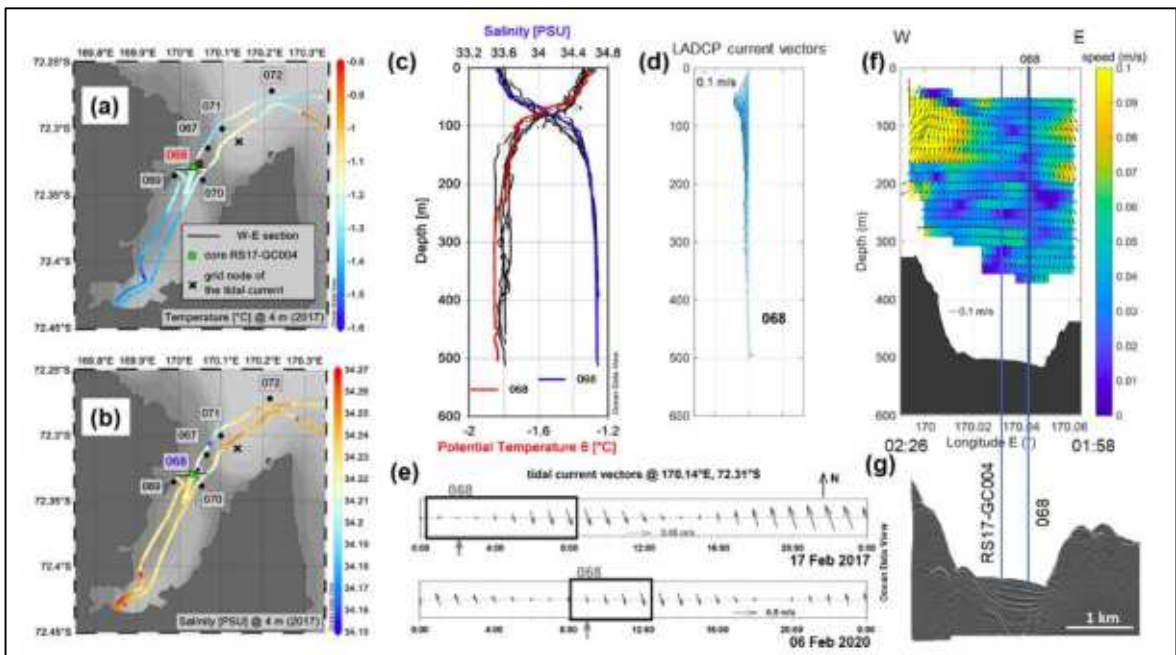


Figure 4.16: Oceanographic properties in the Edisto Inlet, based on data acquired in 2017 and 2020. Temperature (a) and salinity (b) along the ship track at 4 m depth during the survey in 2017; the locations of the gravity core RS17-GC004, the selected tidal grid node, the W-E section (shown in e, f, and g), and six CTD/LADCP (067-072) stations are displayed; potential temperature and salinity from the six CTD casts (in 2020) with emphasis on the 068 cast (c); current vectors from the LADCP at station 068 (d); hourly barotropic tidal current for the duration of the 2017 and 2020 surveys (black rectangles; note the speed scale change between 2017 and 2020) from TMD (Padman and Erofeeva, 2005), with the times (grey arrows) corresponding to the passage close to 068 station, (e); section W-E, showing a vertical transect of the currents from the VM-ADCP (f) and the sub-bottom profile, with positions of the gravity core and 068 CTD (g). All indicated dates and times are in UTC. Each current vector plot has a scale of referent velocity value. The northward (N) direction of the current vector is indicated in (e) and is valid for (d) and (f).

4.5 Discussion

4.5.1 Evidence of past glacial dynamics

Sea-floor landforms and accompanying acoustic and sediment stratigraphic records allow interpretation of the past ice stream in the Edisto Inlet coastal fjord.

Incised bedrock troughs in the coastal fjord are indicative of grounding ice erosion and expansion. Their formation must in some way also be related to bedrock influences and control, specifically in the form of faults.

The northern Victoria Land is characterized by a dense array of NW–SE trending fracture zones (Läufer et al 2011), apparently parallel to an intraplate dextral strike-slip fault system that cuts through the continental crust (Behrendt et al., 1991; Rocchi et al., 2002, 2005) and that seems to continue into the Ross Sea (Salvini et al., 1997). What becomes apparent on comparing geologic structure and tectonic zonation is that the NW–SE trending fracture zones in the northern Victoria Land must have a strong influence upon fjord orientation and upon distribution of fjord's ridges and depressions.

Different types of glacial landforms were identified on the seafloor in the different sectors of the fjord. Sector 1 (Figure 4.8) is located at the entrance of the fjord and presents the shallowest bathymetry (~430 m depth). There, glacial lineations are well visible, together with crag and tails, also found in Sector 2, with the stoss end pointing towards the outer bay. Those glacial features develop parallel to the main ice-sheet flow with the crag step (grounding line) and tails (ice proximal sediment deposition) being indicative of a fast-flowing outlet glacier or ice stream (Stokes and Clark, 2001; Shipp et al., 1999; Canals et al., 2000; Cofaigh et al 2016; Slabon et al. 2016; Halberstadt et al., 2016). The NE-SW orientation of those glacial features suggests that they were caused by glaciers advancing out of Edisto Inlet rather than by the nearby Ironside Glacier or the Honeycomb Glacier. In Sector 4, the bathymetry shows a deep depression (~700m depth) likely carved during repeated past advances and retreats of the Edisto Glacier and the Manhaul Glacier (Fig 4.9). In sector 4, at the very end of the fjord, subglacial and/or sub-cavity keel scours probably originate from grounded ice dynamics related to the past advances and retreats of the Edisto Glacier (Fig 4.9). A field of smaller ridges to the west of these features is interpreted as

morainal deposits (Fig 4.9 a), forming at the base of ice crevasses as a result of (1) either ploughing of linear furrows of basal diamicton during grounding ice still stands, while retreating (Greenwood et al., 2018), or (2) as the expression of grounded ice tidal lifting and settling of floating ice tongue or icebergs entrained in an ice melange (corrugation ridges, Smith et al., 2019) during keel scours formation. Altogether, those glacial landforms suggest that during past glaciations, and likely during the Last Glacial Maximum (LGM) as well, Edisto Inlet glaciers expanded, carved the seafloor and advanced outside of the fjord.

This scenario is also supported by a glacialmarine diamicton layer identified at the base of the sediment cores (*GDF* lithological facies ~ 65 cm) collected at the entrance of the fjord (cores BAY05 14c and 18c, Figure 4.10, 4.13) and dated back ~35 ka.

The *GDF* facies is characterised by gravel-rich sediments with pebbles in a sandy matrix, indicative of ice-proximal to subglacial environment, in analogy to what observed in other cores of the continental shelf of the Ross Sea, where the transition from glacial sediments (diamicton) to glacial-marine sediments and / or siliceous mud is characterized by a layer of sorted muddy sand. The presence of this layer was first reported by Kellogg et al. (1979) and later described as granulated facies by Domack et al. (1999). This coarse-grained sediment has been interpreted as a meltwater facies, related to the decoupling and uplift of a recessive melting line of the ice sheet.

The sediment cores collected in the innermost part of the fjord do not reach the diamicton. The top of the diamicton sampled at core Bay18c corresponds, however, to a high amplitude reflector in the acoustic facies EII (Figure 4.5, 4.10), that can be followed across the northern and central part of the fjord (Sector 1 and 2, Figure 4.7). This reflector lies at about 5-10 ms above the acoustic basement, that possibly correspond to compacted glacial till. The acoustic signal cannot penetrate deep enough to trace this reflector in the southern sector of the Edisto Bay. However, we can speculate that glacialmarine diamicton overlying compacted till and comprised in acoustic facies EII, likely characterises the sea floor until the southern end of the fjord.

4.5.2 Post-LGM progressive opening of the fjord

At the entrance of the fjord (core CH41, 14c, HLF17-01), a strongly laminated layer (*SL-sf*) made of a dense diatom ooze with a low clastic content (low magnetic susceptibility, Figure 4.10, 4.11) is found on top of the glacialmarine diamicton (Figure 4.10 b, c, 4.13).

Unfortunately, the resolution of seismic data does not allow us to follow this facies until the innermost part of the fjord. The lithology and the diatom analyses from Finocchiaro et al 2005, Mezgec et al 2017 and Tesi et al 2020 show that the diatoms assemblage and ecology indicates that low energy open-marine conditions associated with intervals of high productivity (seasonal sea ice) prevailed. This transition from glacial conditions to open-marine conditions is dated back to ~11 ka. This marks the reopening of the fjord and the resuming of oceanic circulation.

Subsequently, the deposition of sandy silt sediments and a low-density diatom ooze (*WL-sf*) at the entrance of the fjord (core 14c, CH41 fig 4.10 a, b) suggest a a brief phase of glacial advance forced by regional cooling from 9 to 8 ka.

The significant increase of *F. curta* and *Chaetoceros* in diatom assemblages, imply a climate cooling which is likely to be associated to a more persistent sea-ice covering (Finocchiaro et al 2005; Tesi et al 2020).

Similarly, reconstructions from Wilkes Land, Adelie Land and the Antarctic Peninsula suggest cooling between 10 and 8 ka. Cooling along Wilkes Land and Adelie Land has been correlated with advancing glaciers and sea ice expansion (Escuttia et al 2005, 2014), which has provided positive feedback on East Antarctica's atmospheric temperature. Along the Antarctic Peninsula, cooling of around 8 ka has been suggested to reflect a decrease in southwest wind (SWW), which led to a decrease in circumpolar deep water (CDW) intrusion on the continental shelf and subsequently to surface cooling (Shevenell et al., 2011). In contrast, diatom-based reconstructions of sea ice and ocean temperatures from Prydz Bay suggest that the surface waters off Princess Elizabeth Land were warmer at 8 ka than 10 ka (Barbara et al., 2010; Denis et al. al., 2010). It has been suggested that this regional warming was related to an increase in CDW intrusion into the shelf between 10 and 8 ka due to a more southerly location of the Antarctic Circumpolar Current (ACC).

In the Southern Ocean, in the area between the Antarctic Slope Front (ASF) and the Subtropical Front (STF), geological records generally show a large 10 to 8 ka cooling, similar to that estimated at the surface of the Antarctica (Bianchi and Gersonde, 2004; Hodell et al., 2001; Crosta et al., 2005; Panhke and Sachs, 2006; Nielsen et al., 2004). This shift is thought to be caused by a northward migration of ocean fronts (ACC South Front, Polar Front, Subantarctic Front or STF). Associated with this cooling event, diatom records in marine cores south of the polar front suggest a northward migration of the sea ice front

during the 10-8 ka period (Nielsen et al., 2004; Bianchi and Gersonde, 2004; Hodell et al., 2001).

The deposit in Edisto Inlet evidences an interval with more frequent and persistent sea ice conditions with icebergs transporting terrigenous material at the entrance of the bay (Finocchiaro et al 2005) (increasing magnetic susceptibility fig 4.10 a, b, c). A few thrusts, visible on seismic data (Figure 4.5) and cutting through both *WL-sf* facies and facies *SL-sf*, coincide with the occurrence of the first bathymetric step at the entrance of the fjord (Figure 4.5). Those features could potentially be attributed to soft sediment deformation from the keel of icebergs calved during the retreat of the glaciers and drifted away by oceanic currents. At last, the deposition of a massive bioturbated and sandy silt sediment layer with occurrence of gravels (*WL-sf*), marks the subsequent acceleration of the deglaciation of the fjord, from ~8-7.2 ka (CH41, 18c).

4.5.3 Preserved Late Holocene high-resolution sedimentary record

On top of the *WL-sf* facies, sub-bottom data from Sectors 1, 2 and 3 reveal exceptionally preserved, undisturbed bottom-current controlled sediment-drifts in the central part of the fjord, made of mounded bodies, acoustically stratified (acoustic facies EI) pinching toward moats (Figure 4.14). Their spatial distribution clearly shows that the deposition is controlled by the morphology of the fjord. All the drifts-moats, indeed, formed on the flank or behind ridges (Figure 4.14). During the austral summer 2017, LADCP measurements (~ 400 m depth) showed a good correspondence between the velocity of the bottom currents, the seabed morphology and the distribution of the sediment drifts inside the Edisto fjord (Figure 4.15, 4.16). Higher velocities (5 to 30 cm/s) were measured over moats, lower velocities (<5 cm/s) over the core of the sediment drifts, while almost no/very slow circulation occurred in the center of the fjord where the thickest sediment deposits, up to 130 meters, are observed (Fig. 4.6, 4.7).

Lithological analysis indicates that all drifts are made of laminated diatom ooze (*SL-sf* and *WL-sf* facies). The bottom of the longest core (HLF17-01) characterised by the *SL-sf* facies, in the upper section of the drift acoustic facies EI, is dated back to 2.62 ka (Tesi et al. 2020) (Figure 4.12). Drift typically forms on millennial timescale (Rebesco et al 2014) and our

data suggest that they start to deposit in the Edisto Inlet at least since 8 ka (based on the dated bottom of core 22c) or even earlier (ca. 11 ka, on the basis of the age of the *SL-sf* in core Bay18c) (Figure 4.11, 4.14). The deposition and preservation of the thick undisturbed sediment drifts of Edisto Inlet can only be explained if a modern-like oceanic circulation with periodic intervals of high productivity, fostered by the intrusion of warm waters, persisted over several thousands of years. Furthermore, this undisturbed sequence of soft sediment indicates that the glaciers never readvanced in the fjord after their retreat.

4.5.4 Edisto Inlet post-LGM evolution

[0] Glaciation: During the peak of the glaciation, Edisto Inlet glaciers advanced, merged and flowed out of the fjord as shown by all the glacial landforms found on the seafloor.

[1] Glacier retreat after the LGM: while the glaciers retreated, they dropped a subglacial melt-out till (*GD-f* facies) that currently drapes and fills the glacially eroded sea floor and is identified both in the sediment cores and in the seismic data. The *GD-f* facies is interpreted as deposited in front of a retreated glacier rather than subglacially because of its relatively soft character (that can be penetrated with high frequency seismic source). The retreat phase occurs between the LGM and at least 11 ka. Based on seismic lines, we found no evidence of glaciers re-advance, e.g. grounding-zone wedges. We thus infer that the retreat could have been gradual, with a progressive glacier thinning, but without any stationary phases of their grounding line. Deeper penetration seismic profiles will be crucial to define the type and morphology of the bottom of the current-controlled sediment drift, where it is thickest in the central sector of the bay. Higher energy seismic profiles could highlight whether grounding zone wedges or morainal banks occur along the fjord, documenting a step-like versus gradual grounding ice sheet retreat.

[2] Opening of the fjord and resuming of the oceanic circulation: In confined embayments, the gradual thinning of converging glaciers can lead to the formation of an ice shelf in the earlier stages of the retreat. The deposition of the biogenic-rich, stratified *SL-sf* on top of the subglacial melt-out till layer *GD-f* implies that until the core BAY05-18c, the fjord was glacier-free (no grounding ice) already ca. 11 ka ago. The lack of sediment cores reaching the *GD-f* facies in the central part of the fjord does not allow us to identify this

facies in the innermost sectors of Edisto. However the correlation of core Bay18c with the seismic data suggests that the *GD-f* lies over the entire sector 1, 2 and 3 of the fjord. Two scenarios are thus viable: (1) the *SF-f* facies deposited in the inner sectors 3 and 4 of the fjord directly over compacted till, with no melt-out till deposition and then no formation of an ice shelf, which implies a fast retreat of the glaciers; (2) the *SF-f* facies deposited over a *GD-f* facies also in the inner sectors 3 and 4 of the fjord, which implies a slower retreat of grounding ice, with the development of an ice shelf at its front, located further south in the fjord with respect to the location of BAY05-18c.

[3] Premise of deglaciation: the first scenario is ruled out by the deposition of weakly laminated and sandy material (*WL-sf*) on top of the *SL-sf* at the entrance of the fjord towards 9-8 ka. The sand fraction was likely transported by icebergs that mostly originated from Edisto glaciers, suggesting that glaciers front was floating. Further evidence supports the presence of an ice shelf at that stage. Thrusts identified in the *SL-sf* and *WL-sf* around 420 m depth, presumably caused by icebergs drifting. The bathymetry of the inner part of the fjord is larger than 420 m depth, implying that an ice shelf likely existed in the fjord until that stage. At last, the *WL-sf* is also found in the core BAY05-22c located within the fjord, implying that the ice shelf front was located further south relatively to the core BAY05-22c. During this period *Corethron* disappears, while *F. curta* becomes the prevailing species of diatoms. High percentages of *F. curta* > 50% have been associated with the presence of sea ice (Leventer et al., 1996; Cunningham et al., 1999). The high accumulation of terrigenous sediments could also document the rapid downward recession of local and / or regional glaciers and the onset of seasonal sea ice formation.

Persistent sea ice conditions could have been enhanced by the melting of icebergs, increasing the stratification of the oceanic waters within the fjord.

[4] Acceleration of the deglaciation and establishment of modern oceanic conditions: the disintegration of the ice shelf within Edisto Inlet started toward 8-7.2 ka and led to the deposition of the massive bioturbated and clast-rich layer (*MB-f*) in the outer sector of the bay, identified in the cores CH14 and BAY05-18c. Based on our evidence, we cannot constrain the duration of this final deglaciation phase.

However, core HLF17-01 suggest that open-marine (no ice shelf) condition was established in the central sector of the fjord earlier than 2.62 ka. At this time, a current-controlled sediment drift was already depositing in sectors 2 and 3 of the Edisto Inlet.

After the acceleration of the deglaciation, the drifts-moats in the sectors 2 and 3 of the Edisto Fjord developed in the course of several thousands of years, sometime between 7.2 ka and 2.6 ka. The undisturbed character of all the drifts found within Edisto Inlet indicates that no glaciers re-advance occurred at least since 7.2 ka as shown by the sediment drift morphology. During this period the lowest *F. curta* relative abundances, concomitant to high occurrences of CRS and TRS (Mezgec et al 2017) support the hypothesis of a more open oceanic conditions.

Implication for the deglaciation scenarios

The evidence of floating ice in the Edisto Bay since at least 11 ka would discount the occurrence of coeval grounding ice and ice shelf in this region of the north-western Ross Sea. At that time, if ice was grounding over the continental shelf, in deeper water and to the north of the Edisto Inlet, it would have necessarily implied both ice streams and coastal glaciers thickening. Even in the case that grounding ice was not present, but an ice shelf floated over the outer continental shelf, the Edisto fjord could not remain free of ice.

The geological perspective provided by these results demonstrate that the Edisto fjord preserves a unique sedimentary archive for investigating the response of Antarctic coastal glaciers to climatic and ocean circulation changes at millennial resolution since the LGM and that is an important site for future investigation on climate models that seek to predict dynamic of small glaciers system and their relationship with regional Antarctic ice sheet dynamics. Drilling the sediment drift in sector 3 of the Edisto fjord will then provide a continuous and expanded post-LGM record across the transition from the climatic optimum to the cooling, up to the recent times.

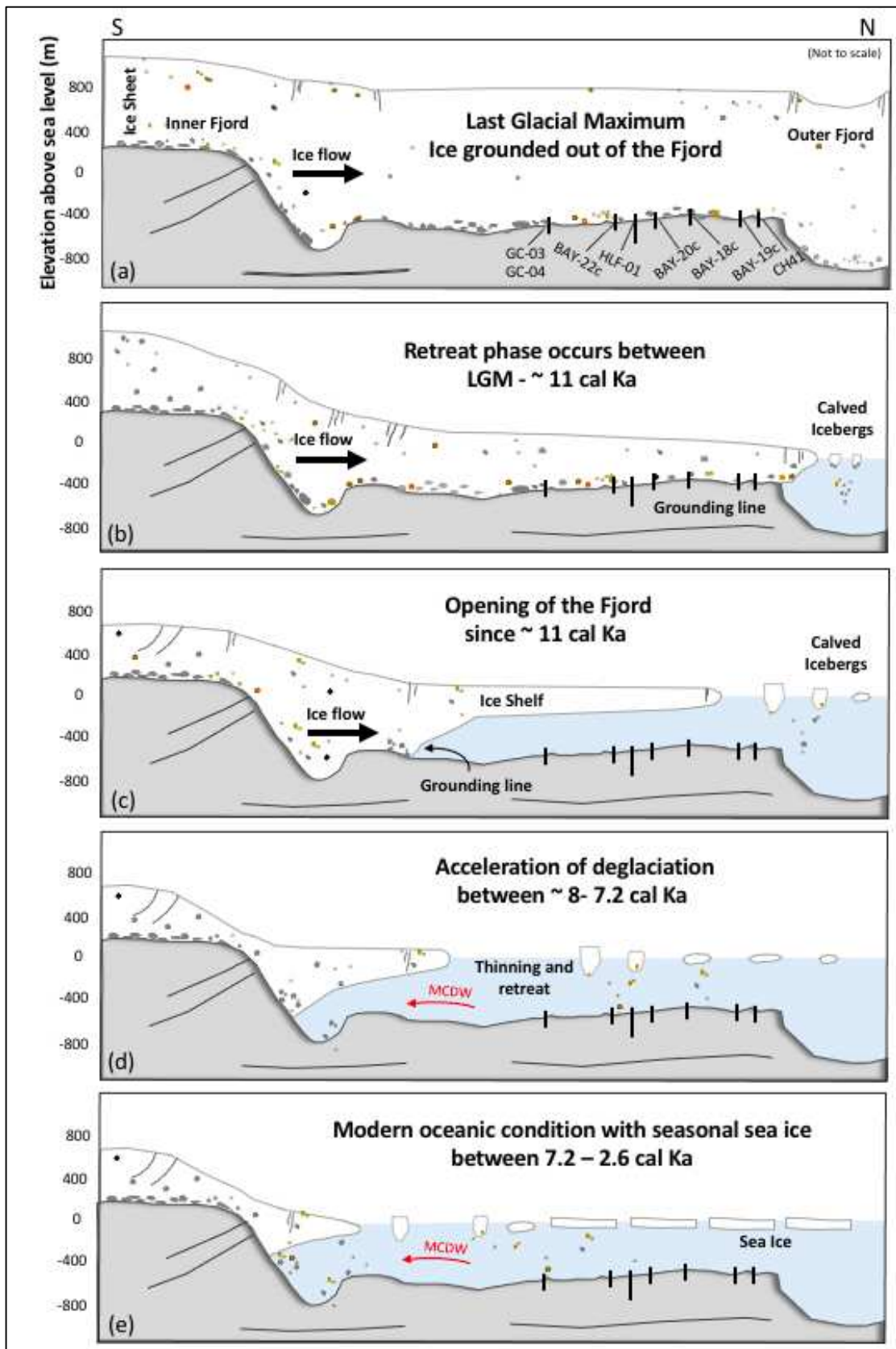


Figure 4.17: Cartoon of the Post-LGM Progressive opening phases of the Edisto Inlet Fjord.
 a. Advanced glacial phase (LGM), ice is grounded out of the Edisto Inlet Fjord. b. Opening of the Fjord between the LGM and 11 cal BP Ka. c. Acceleration of the deglaciation between 8 -7.2 Ka and intrusion of the mCDW d. Modern oceanic condition with seasonal sea ice something in between 7.2 cal ka and 2.6 ka.

4.6 Conclusions

The last deglaciation is the most recent, large-scale climate warming interval during which northern and southern hemispheres ice sheets retreated and sea level rise at a non-uniform rate. The Antarctic ice sheet is the main source of uncertainties upon future sea level rise, but little is known about its last deglaciation chronology in key marine-based sectors, such as the Ross Sea. We combine multibeam, reflection seismic data, and oceanographic measurements with the southernmost, first evidence of an expanded, ultrahigh resolution, Holocene sedimentary section deposited in the Edisto Inlet fjord (North Victoria Land, NVL). We find that post-glacial sedimentation resulted in an up to 130-meters-thick undisturbed diatom ooze (mainly), locally redistributed by bottom currents over confined drifts-moats in the inner part of the fjord. This line of evidence indicates that the fjord was not carved by grounding ice after the Holocene Climatic Optimum anymore and was subject to seasonal sea-ice free conditions with regular warm water intrusions. Those findings support an early retreat of coastal glaciers by ca. 11.1 ka from the NVL continental shelf after this period.

Chapter 5

5. ROBERTSON BAY

5.1 Introduction

The advance and retreat of the ice sheet during past climate glacials and interglacials has had a significant impact on the environmental condition of the continental margin (Domack et al 1999). Particularly, the Ross Sea is a key area for reconstructing the ice sheet dynamics from the geological records, as it drains a large sector of the most vulnerable West Antarctic Ice Sheet (Setti et al 2004). The grounding line advanced near the Ross Sea continental shelf edge at the end of the Last Glacial Maximum (LGM, ca. 20 ka) and now is located several hundreds of kms inland (Howat et al 2003; Anderson et al 2014).

Understanding sediment type and distribution is critical for studies reconstructing glacial and ice-sheet behaviour based on paleo-records (e.g., Naish et al. 2009; Anderson et al. 2011; Fernandez, Anderson, Wellner et al. 2011; Stokes et al. 2015). Previous study in the western Ross Sea continental shelf document that interglacial phases are characterized by deposition of diatom mud. The presence of this type of sediment in the geological record is interpreted as representing the establishment of seasonally sea ice open climatic conditions. However, interglacial diatom mud deposits are difficult to find, because they have been mostly eroded by grounding ice sheet, during subsequent glacial expansion, remoulded by icebergs or swept by bottom currents. Prothro et al. 2018 and Wellner et al. 2001, show the distribution of the sedimentary facies and glacial landforms, deposited after the LGM in the Ross Sea and Antarctic Peninsula, located mainly in inner shelf basins (where it is preserved from the action of icebergs and of strong bottom currents). Coastal bays and deep fjords are potentially good candidates to preserve expanded geological records of past interglacials. Tidewater glaciers generally respond more rapidly to climatic fluctuations than large ice sheet because they have small drainage areas and high accumulation rates (Anderson 1999). Rapid sediment accumulation generally is observed in temperate and subpolar fjords and coastal bays where tidewater glaciers are debouching and into which they carved deep depressions during maximum expansion. These depressions are now filled with high-

resolution sedimentary Holocene record, deposited after glacier retreat. Environmental variations are reflected in the cyclic alternations between glacial facies (e.g. sub-ice, melt-out, water-lain diamicton, Ice Rafted Debris - IRD) and open marine facies (biogenic mud) (Escutia et al., 2002, Maldonado et al., 2005, Close et al.2010). However, the characteristics of single bay can be widely variable, depending on the number and type of glaciers draining into the bay and to the processes carrying and depositing sediment in and out of the bay. Numerous factors control sedimentation including climate, seafloor bathymetry, bay geometry, oceanographic regime, the presence of sea ice, the size of ice drainage areas and proximity to sediment sources (Griffith & Anderson 1989; Domack & McClennen 1996; Ashley & Smith 2000). Each of these contributes differently to the distribution of sediment along the bays. Therefore, when applying any model of sediment distribution in a fjord or in a bay environment, we must take into account how local versus regional variations of bay systems variations affect sediment distribution.

The BAY project's cruise carried out by by PNRA (Programma Nazionale di Ricerca in Antartide) in 2005 and the following PNRA cruises in 2016 and in 2017 and the KOPRI cruise 2015 had the purpose of exploring several bays along the North Victoria Land to seek for: 1) post-LGM and possibly older interglacial records, 2) to verify the local versus regional response of the depositional system to climate changes; and 3) to investigate diachronicity of the Victoria Land system in response to the regional climatic oscillations. Expanded sedimentary sequence has been discovered in some of the fjords along the North Victoria Land (NVL, Finocchiaro et al., 2005, Mezgec et al., 2017). The present work is aimed at investigating the geological record from Robertson Bay and compare it with the Edisto Inlet record to study local versus regional response of the different glaciers to the post-LGM climatic change.

Robertson Bay lies between Cape Barrow and Cape Adare in the northern Victoria Land in the western Ross Sea. The seafloor morphology and seismic-stratigraphic characteristics of Robertson Bay have never been reported. In this thesis chapter, I constructed a new bathymetric map and some geological sections, obtained from multibeam, a grid of sub-bottom profiles (SBP) and sedimentological and geochemical analyses on two sediment cores collected inside the bay in 2005.

This multiproxy approach allowed reconstructing environmental changes in different morpho-bathymetric setting, from the Holocene to the present.

5.2 Regional Setting

Robertson Bay is located at the boundary between East and West Antarctica, at the Pacific termination of the Transantarctic Mountains. It's about 37 km wide and 40 km long, in Cape Adare region, a prominent cape of basaltic lavas and volcanoclastic deposits forming the northern tip of the Adare Peninsula and the north-easternmost extremity of Victoria Land. Figure 5.1

The geology of northern Victoria Land has received considerable attention in the past (Wright, 1981; Bradshaw et al., 1982; Field et al., 1983) and a more comprehensive study of volcanic rocks and tectonic significance is widely reported by Harrington 1958, Behrendt et al. 1991, Kyle 1990, Rocchi et al 2003, Nardini et al 2003.

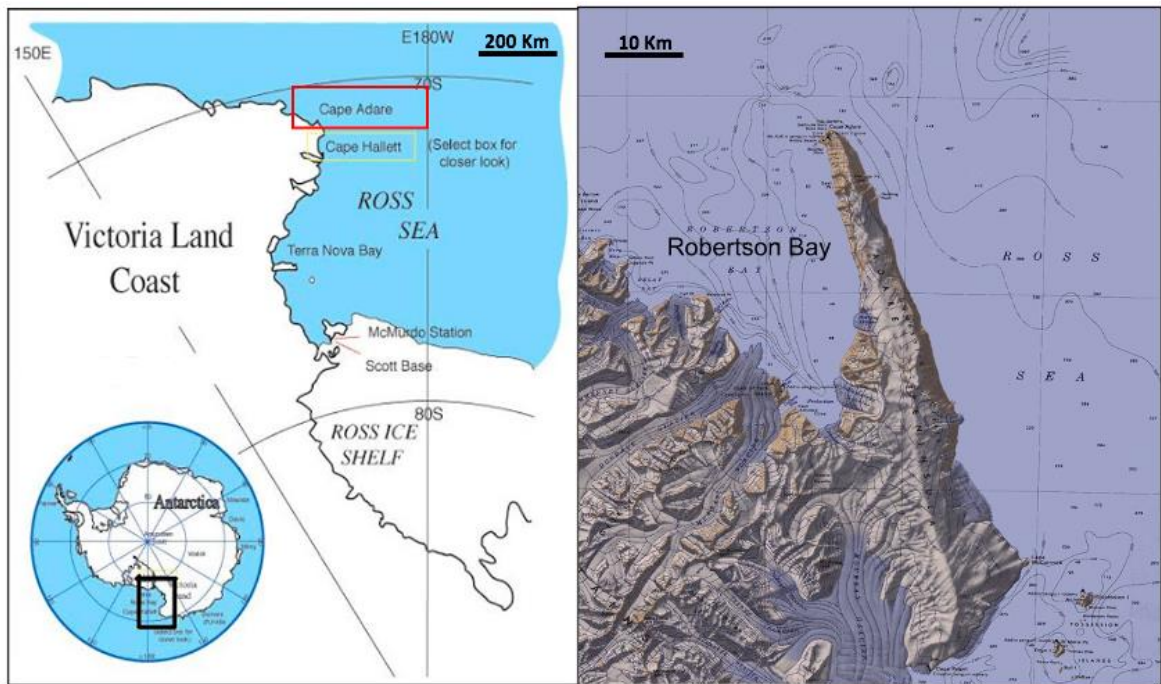


Figure 5.1 Map of Robertson Bay and the Adare Peninsula in the western Ross Sea. (U. S. Geological Survey)

The geological framework of NVL is commonly referred to the assembly and stabilization of three different NNW-trending, Neoproterozoic to Early Palaeozoic, fault-bound lithotectonic units or “terranes” onto the East Antarctic Craton during the Early Palaeozoic Ross orogeny (GANOVEX Team, 1987; Kleinschmidt and Tessensohn, 1987; Borg and Stump, 1987; Stump, 1995; Roland et al., 2004).

These terranes from west to east are: (i) the Wilson Terrane (WT), (ii) the Bowers Terrane (BT), and (iii) the Robertson Bay Terrane (RBT) (GANOVEX Team, 1987; Bradshaw, 1987, 1989; Tessensohn and Henjes-Kunst, 2005; Rocchi et al., 2011; Estrada et al., 2016). The latter comprises turbidites of the probable Cambrian Robertson Bay Group, which were metamorphosed and folded during the Ross Orogeny (approximately 500 Ma). These strata are intruded by granitoids of the Admiralty Intrusives (Borg et al. 1987, Rossetti et al. 2006) and local trachytic lavas of the McMurdo Volcanic Group (Kyle 1990).

5.3 Oceanography

The circulation of the Ross Sea is dominated by a polynya processes and by a wind-driven gyre. Near-freezing Ross Sea High Salinity Shelf Water (HSSW, with temperatures of c. -1.9°C) forms in the polynya, where prevailing katabatic winds drive intense sea ice production (Fig.5.2 an example of Terra Nova Bay polynya in the Victoria Land). Shelf Water originates from winter buoyancy loss of superficial waters due to sea-ice formation process that produces dense and salty water masses (Williams et al. 2010).

The Ross gyre involves the southernmost branch of the Circumpolar Deep Waters (CDW), that mixes with the surface and shelf waters forming on the continental shelf to create Modified Circumpolar Deep Waters (mCDW) (Williams et al. 2010) (Fig. 5.3).

At the shelf break, Antarctic Bottom Water (AABW) forms through modification of shelf water (SW) and HSSW via mixing with mCDW and AASW. Newly formed cold, saline AABW flows down the continental slope in cascading gravity currents into the abyssal ocean (Ohshima et al., 2013; Rintoul, 2000)

The change in the export of the Antarctic Bottom Water (AABW) strongly influences cooling and ventilation processes of deep oceans (Whitworth, T., Orsi, A.H., 2006). AABW is generated from vertical mixing events occurring between the modified Circumpolar Deep Water (mCDW) and Shelf Water.

The Modified Circumpolar Deep Water (mCDW) is a relatively warm, salty and nutrient-rich water mass that flows onto the continental shelf at certain locations in the Ross Sea. Through heat flux exchange, this water mass moderates the sea ice cover. It provides also nutrients to excite primary production (Ito et al. 2005). mCDW transport onto the shelf is known to occur at specific locations mainly influenced by bottom topography and depending

on the strength of the Antarctic Slope Front. The flow is considerable in spring and winter, due to influencing tides.

The Ross Sea is partially covered with sea ice for much of the year. In the south-central region little melting occurs (Holland et al. 2017). Sea ice concentration in the Ross Sea is influenced by wind with ice remaining in the western region throughout the austral spring and generally melting in January due to local heating (Holland et al. 2017). This leads to extremely strong stratification and shallow mixed layers in the western Ross Sea.

Cape Adare, in particular, provides a western boundary pathway for Ross Sea dense water exported from the central and western topographic troughs of the Ross Sea. The northward transport of bottom water observed in austral summer 2004 off Cape Adare was ~ 1.7 Sv, composed of $\sim 25\%$ HSSW (Gordon et al., 2015). Additional export of Ross Sea water into the deep ocean, composed mainly of Lower-Salinity Shelf Water (LSSW; including Ice Shelf Water) and modified Circumpolar Deep Water (mCDW), occurs east of Iselin Bank (Orsi and Wiederwohl, 2009).

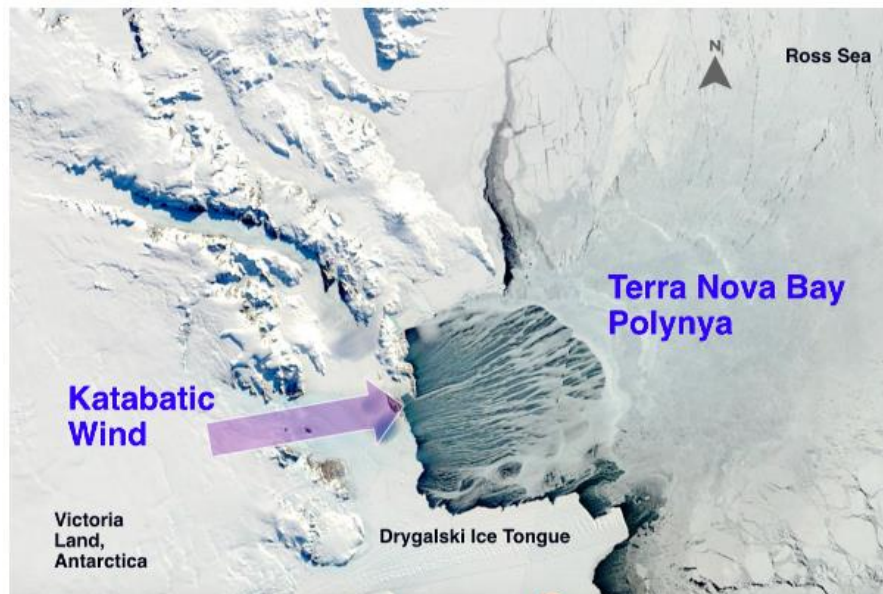


Figure 5.2 Satellite image courtesy of NASA of Terra Nova Bay Polynya in the Victoria Land.

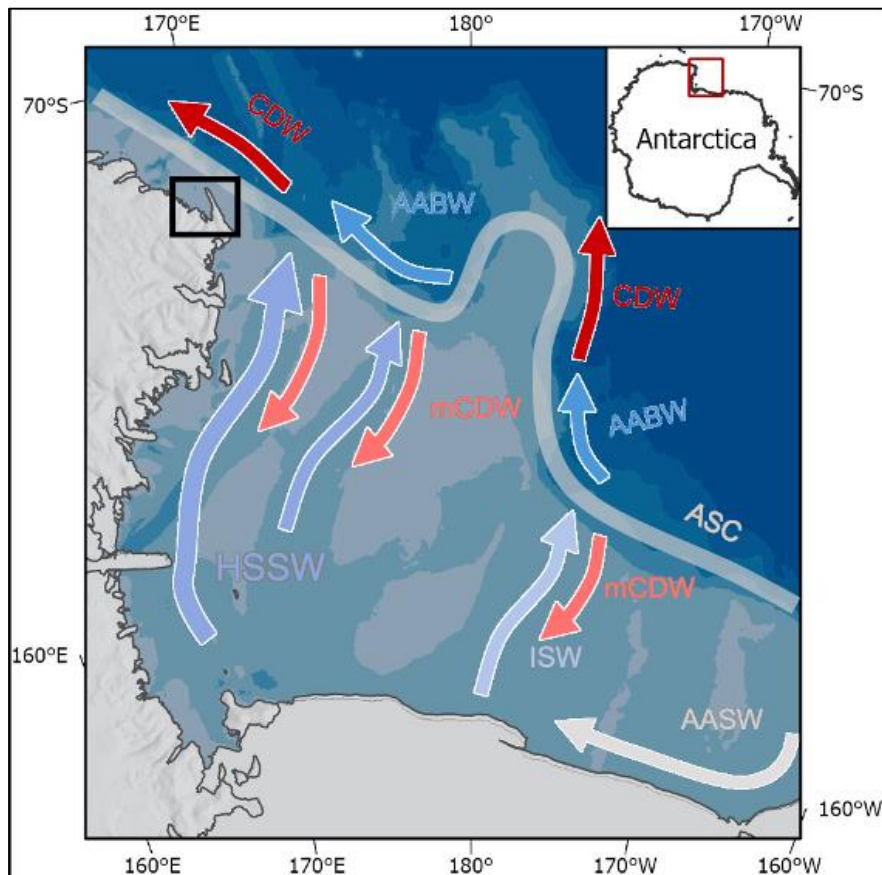


Figure 5.3 Schematic of the movement of water masses in the Ross Sea and along the marginal marine environment in East Antarctica. The diagram shows key water masses as defined from Whitworth et al., (1998). Main water masses include: Circumpolar Deep Water (CDW); Modified Circumpolar Deep Water (mCDW); Shelf Water (ISW); High Salinity Shelf Water (HSSW); Antarctic Surface Water (AASW); and Antarctic Bottom Water (AABW). The black rectangle indicates the location of Robertson bay in Cape Adare in the western Ross Sea.

5.4 Data and Methods

5.4.1 Multibeam Bathymetry and Sub-Bottom Profiles

The PNRA BAY Project took place in January 2005 along the Victoria Land coast and 100 miles of Sub-bottom profiles (SBP 3.5 kHz), 8 gravity cores (for a total of 30 meters) and one box corer were acquired in Robertson Bay. Only two of them, the **core 29c and 32c** have been used for this thesis Figure 5.4.

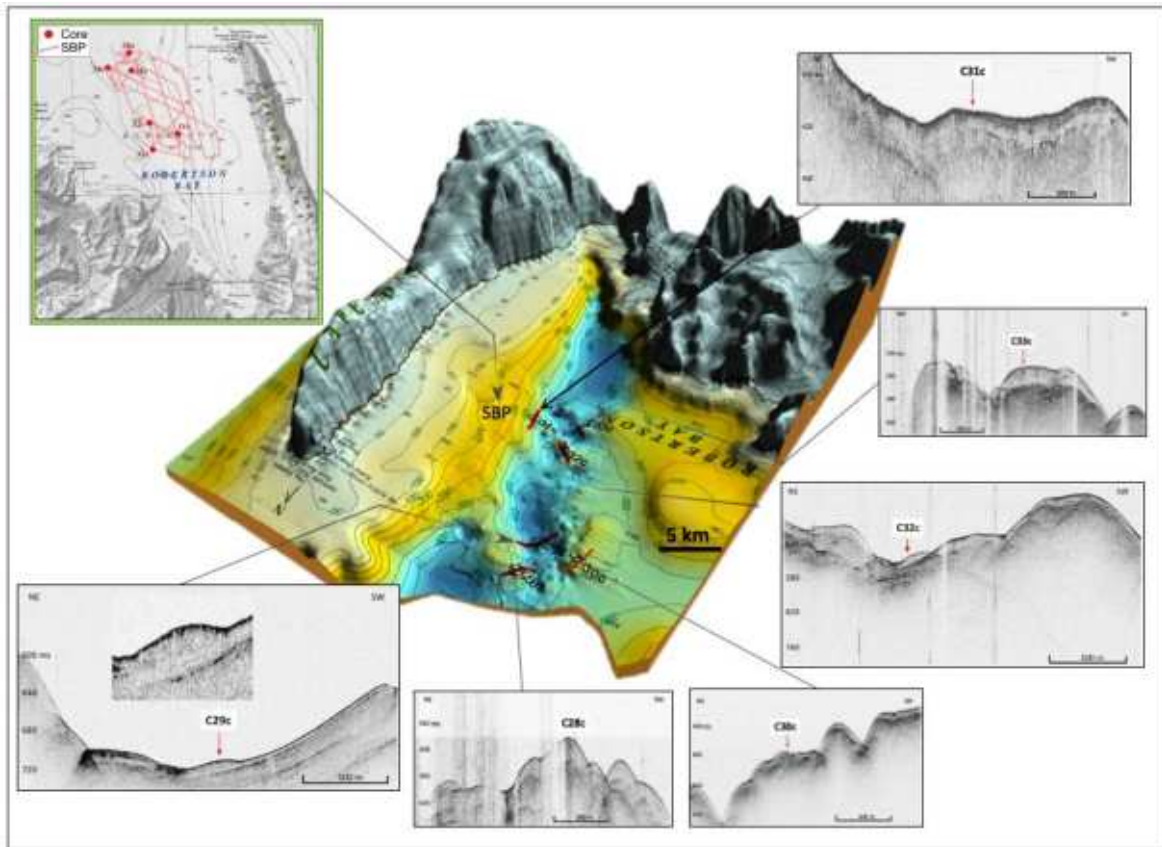


Figure 5.4. Bathymetric map of Robertson Bay with the location of the Sub-bottom profiles red lines and sediment cores red dots. Seismic profiles show the location of the sediment cores and the seafloor bathymetry (Morelli poster 2005).

The acquisition of the cores occurred along the continental slope off Cape Adare, at a depth between 150 m and 700 m. The choice of the sampling sites has been assisted by the aid of the high-resolution seismic profiles (SBP). The sediment cores, with an average length of about 4 meters, were sectioned into 100 cm lengths each and the magnetic susceptibility was measured on board. The cores were then stored at -4°C for the subsequent analysis.

The second geophysical data set for this study has been collected from a Korea Polar Research Institute (KOPRI) cruise in 2015 Figure 5.5. Shallow sub-bottom profiling data were collected using an SBP120 Sub-bottom profiler (12 kHz). The multibeam data was acquired using a hull-mounted Kongsberg-Simrad EM-122 multibeam echosounder, with a swath of 432 beams and an operating frequency of 12 kHz. Data acquired aboard the RV/IB Araon was manually edited to remove errant data with the multibeam editing software CARIS HIPS&SIPS 8.0, and gridded to 25×25 m.

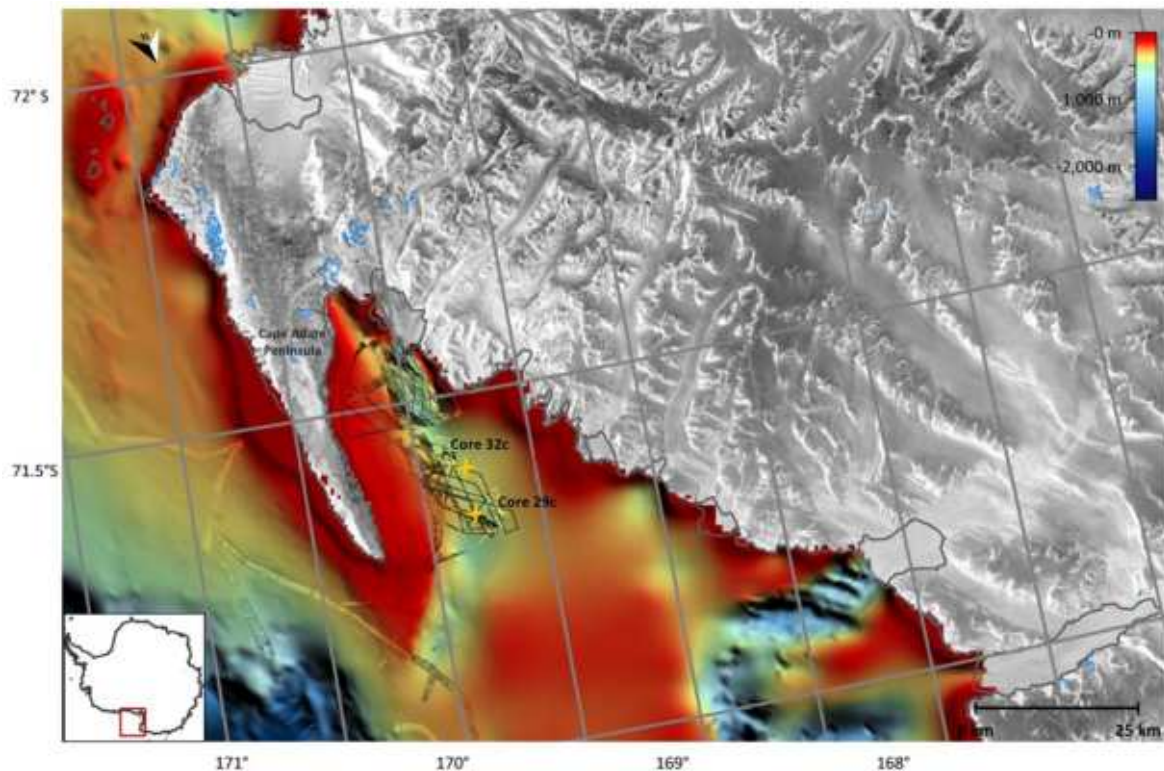


Figure 5.5. Geographic Map of Robertson Bay with the SBP and Multibeam data collected aboard the research vessel/ice breaker (RV/IB) Araon during a KOPRI expedition in 2015. Bathymetry collected aboard the research vessel *Italica* during a PNRA expedition in 2005 and SBP over it (Black lines). The two yellow stars indicate the location of the sediment core 29c and 32c. Colour bar shows heights/depths in metres.

The Sub-bottom profiles were taken to estimate rock and sediment types of the geomorphic assemblages and composition. Sub-bottom profile systems are successfully used in other similar glaciated areas to investigate the subsurface of the marine sedimentary sequence in poorly consolidated deposits and to characterize the sediment packages and bedrock up to 80-100 m below the seafloor (Anderson et al., 2001). Water depths and sediment thickness were calculated by converting the two-way travel time to meters using acoustic velocities of 1500 m s^{-1} for water and soft unconsolidated sediment. For interpretation of depositional mechanisms, the acoustic facies were correlated to the core (29c and 32c) sedimentology. The analysis of all the dataset was conducted by using the IHS Kingdom Suite seismic interpretation software.

All the data and methods used in this thesis are well detailed in the chapter 3.

5.4.2 Sedimentological analyses

On the cores BAY05 29c and 32c the following analysis were made: X-ray analysis (Bartington MS2C), grain size analysis (the biogenic component is given mainly by diatoms and spicules), Multi-Sensor Core Logger (MSCL) measurements, such as density, the speed of the compression waves (P-wave velocity) and the amount of magnetically susceptible material present in the sediment. Forams assemblage (by R. Melis, not published yet) and Diatom assemblage was made by PhD student F. Torricella at University of Pisa (not published yet).

5.4.2.1 Grain size analysis

Grain size analyses were performed in 2005 on 40 samples by Prof. Ester Colizza (University of Trieste). Samples were treated with hydrogen peroxide to remove organic matter and sieved to separate the < 1mm fraction.

The grain size characterisation of < 1 mm fraction was analysed using a Malvern MasterSizer 2000 laser. Sand, silt and clay were determined using the grainsize classification proposed by Friedman and Sanders (1978). Statistical parameters were determined according to Folk and Ward (1959).

5.4.2.2 Diatom Relative Abundance

Diatoms were identified to species or species group level based on a variety of Southern Ocean and Antarctic diatom resources (including Armand et al., 2005; Crosta et al., 2005; Scott, 2005; Romero et al., 2005). The relative abundance of each diatom species was determined as a percentage of total diatom valves counted for each sample.

The unpublished datasets presented in this thesis were provided by PhD student F. Torricella who performed diatom analysis at the University of Pisa.

A total of 209 samples were performed according to the methodology described in Rathburn et al., (1997) which avoids the use of centrifuge. A diatom count was performed under a microscope at a magnification of 1000x. For each sample at least 300 diatom valves in each sample were identified and counted following the counting method outlined by Armand (1999) and Crosta and Koc (2007). The relative abundance was determined for each taxon

as the ratio between the diatom species and the total diatom. The total absolute diatom abundance (ADA) in terms of the number of valves per gram of dry weight (nv gdw⁻¹) was determined using the formula described by Armand (1997).

5.4.2.2.1 Diatom Paleoecology

The distribution and assemblage of diatoms in the surface waters of the Southern Ocean is controlled by a variety of environmental factors. Light intensity, salinity, sea surface temperature, sea ice concentration and duration, nutrient availability, and water column stability (Armand et al., 2005; Beans et al., 2008; Crosta et al., 2005; Cunningham and Leventer, 1998; Romero et al., 2005). Sea ice extent, in particular, effects both total productivity - suppressing productivity when present and enhancing productivity as it retreats (Arrigo et al., 2010) and the nature of the diatom community. The diatom assemblage in Robertson Bay is dominated by sea ice (as opposed to open ocean) associated species with varying preferences regarding the nature and duration of ice extent (Torricella personal comment).

5.4.3 Geochemical analyses

Organic matter characterization (TOC), Carbon and Nitrogen isotopes ($\delta^{13}\text{C}$; $\delta^{15}\text{N}$) and Biogenic silica concentration (BSi) were made by myself at University of Otago and bulk radiocarbon dates were obtained at the Poznań Radiocarbon Laboratory located at Adam Mickiewicz University (Poland).

Sedimentary biogenic silica concentrations (BSi%) were measured at the Geochemical Preparation Laboratory, Geology Department, University of Otago. Measurements were carried out using an alkaline extraction spectrophotometric method modified from Strickland and Parsons (1972) and Mortlock and Froelich (1989).

Sediment samples for bulk carbon analyses were taken from core 29c and 32c at 5 cm resolution (211 samples in total). Sample preparation was conducted at the Geochemical Preparation Laboratory, Geology Department, University of Otago.

Carbon concentrations and isotopes were analysed using a Carlo Erba NA1500 Series 2 Elemental Analyzer interfaced with a DeltaPlus isotope ratio mass spectrometer via a ConFloII device at the Stable Isotope Laboratory at Stanford University, California, USA.

5.4.4 Chronology

To develop a chronology for core 29c e 32c, sediment samples for Ramped Pyrolysis (RP) radiocarbon analysis were taken from four depths for core 29c and from five depths from core 32c spanning the length of the cores. Samples were pre-treated by myself at the University of Otago and then sent to the Rafter Radiocarbon Lab AMS facility at GNS in Wellington for radiocarbon dating.

Due to the Covid-19 pandemic, the PR analyses suffered severe delays, as mentioned in chapter 3, therefore in this thesis the radiocarbon dates were calibrated with the Bayesian age model following Tesi et al 2020 (Table 3) with the latest version of OxCal software (see 3.6.5.1.3). For core BAY05_32c the limitation of the model due an inversion date showed a negative accumulation rates so in that case we used the unmodeled calibrated date.

5.5 Results

5.5.1 Glacial landforms

The bay was divided into two sectors (Figure 5.6): sector 1 was analysed by using a SBP dataset (PNRA 2005) correlated with the two sediment cores. Unfortunately, the lack of multibeam swath bathymetry did not allow the mapping of the glacial landforms in detail in sector 1. Instead, in sector 2, the swath bathymetry collected by KOPRI (2015) shows with more detail the occurrence of several glacial landform types: Streamline ridges, depressions, meltwater channels, Mega scale glacial lineations (MSGs), lateral moraine and other erosional features (Fig. 5.8).

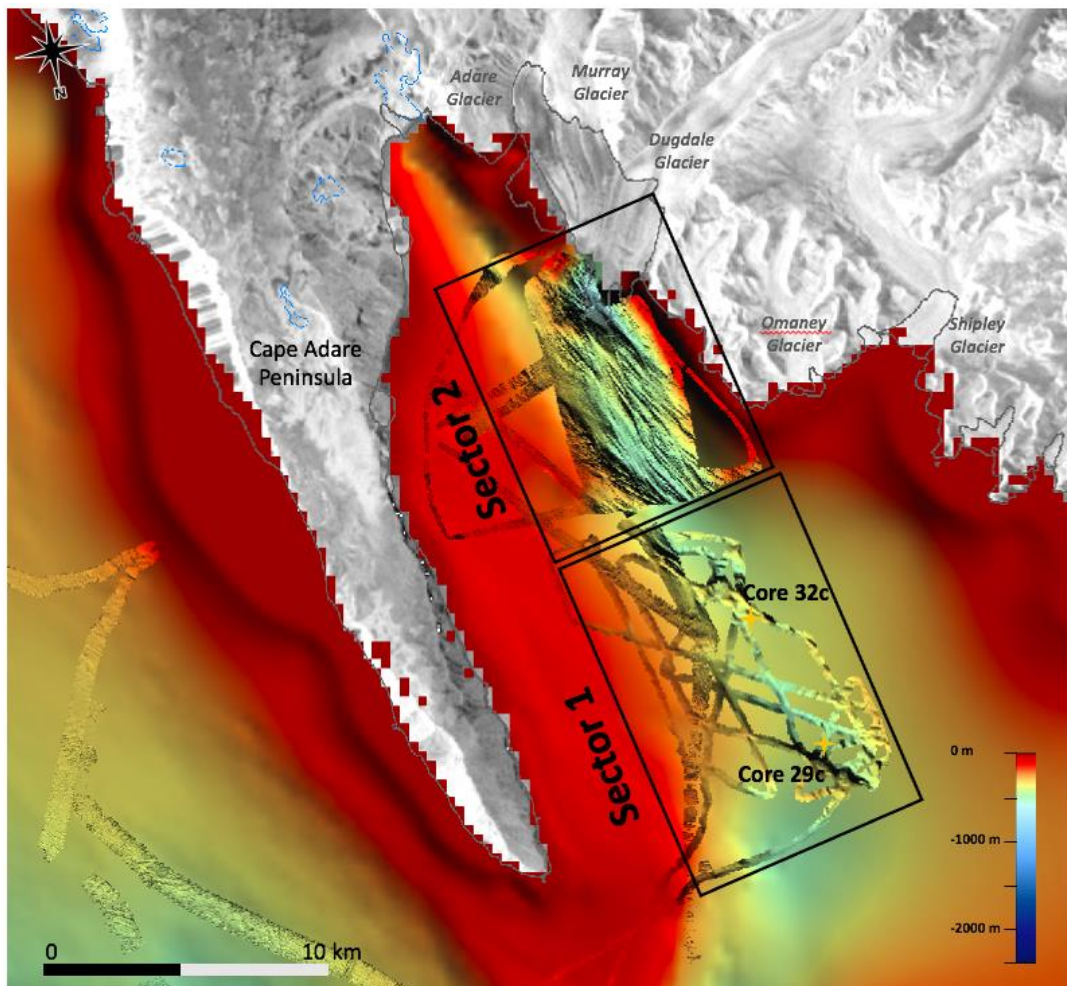


Figure 5.6: Sector 1 (outer shelf) the dataset is a bathymetric survey collected in 2005 (PNRA). Sector 2 (Inner shelf) the dataset is a high resolution multibeam swath bathymetry collected in 2015 (KOPRI).

The bathymetry in the sector 1, reconstructed using the SBP data, highlights the presence of three basins: the inner basin (up to 506 meters deep) is separated from the mid basin/ depression by a sill (Sill 2), at depth of 370. The mid-basin reaches a depth of 533 m and is separated by the outer basin by a sill (Sill 1) at 350 m. The outermost basin is 525 m deep (fig. 5.7)

The shape and orientation of the three basins must in some way reflect the main route of grounding ice erosion during past glacial maxima, although it is also influenced by bedrock lineations and substrate will in turn control the location of ice streams during glacial advances. NW–SE dextral faults have been identified in the North Victoria Land (Salvini et al 1997, Domack et al 1999, Howat et al 2003, Rocchi et al 2003), that likely continue offshore, and originate the two morphological steps, that separate the three basins, although there is no evidence of recent faulting in our SBP profiles.

Core 29c, is located at 450 m water depth, in the mid depression. Core 32c is located in the morphological sill between the mid and the inner basin (fig. 5.7).

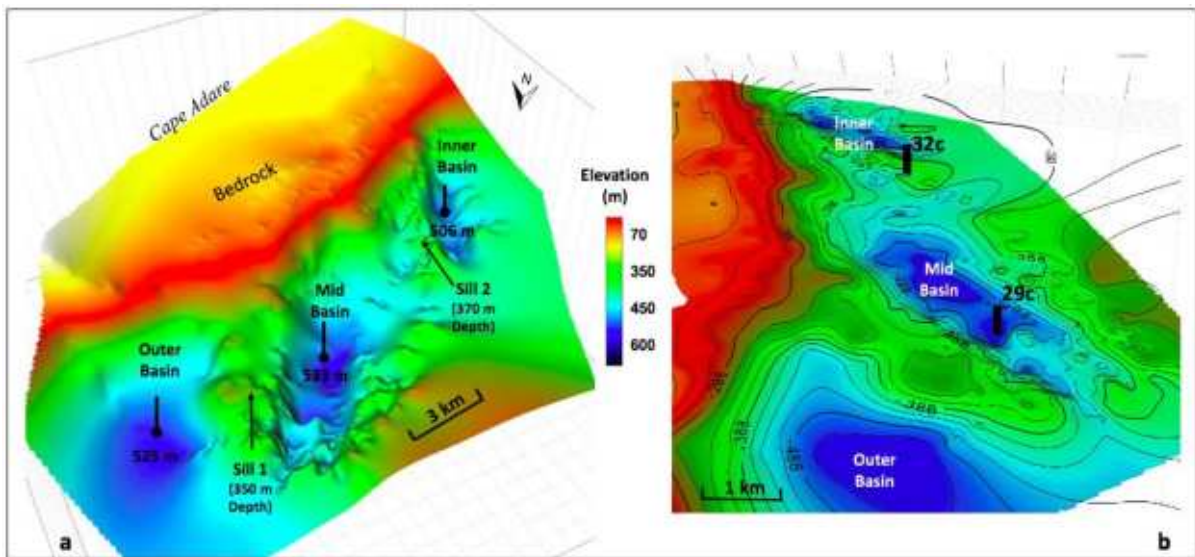


Figure 5.7 Bathymetric data collected from sector 1, aboard the research vessel *Italica*, during a PNRA expedition in 2005. The bathymetry highlights the presence of three basins ranging from 150 m to about 550 m. The inner depression (506 m) is separated from the outer depressions (533 m and 525 m) by two sills, at depth of 370 and 350 m (a). The black lines show the location of the sediment core 29 c and 32 c (b). Contour heights/depths are in metres.

5.5.1.1 Description of glacial landforms

The swath bathymetric data from sector 2 show a rugged crystalline substrate and elongated streamlined features overall parallel to the bay axis (Figures 5.8, 5.9).

The elongated ridges trend SE–NW, up to 7 km long, 1.5 km of width, and from 30 to 50 m high, have a slightly curved pattern with their convex sides to the SE. They exhibit a convergent pattern towards NE. Depressions within the elongated ridges are up to 6 km long, 2 km wide and 40 m deep, but are generally 1 km in width and have a V-shaped cross-sectional profile and are interpreted as glacial lineations. Some of them terminate with hills downstream (to the NE).

Channels (up to 4 Km long and 300 m wide and 8 m deep) are observed in innermost area of sector 2 and on the eastern side of the Bay (fig. 5.8). They likely originated from meltwater outwash during grounding ice retreat or belong to an old sub-glacial drainage system (fig. 5.8). Asymmetric mounds lying on the western and eastern side of Roberston Bay, in sector 2 (fig. 5.10) are interpreted as lateral moraine possibly formed during several glacier overriding stages. Linear incisions (2 Meters deep), oriented NW- SE, lying in the area between the channels and the elongate ridges are interpreted as glacial striations, possibly originated as Ice shelf melange scours or Sub-ice shelf keel scours (e.g. Smith et al., 2019), after lift-off of marine terminating glaciers and subsequent disintegration of floating ice with production of an iceberg armada.

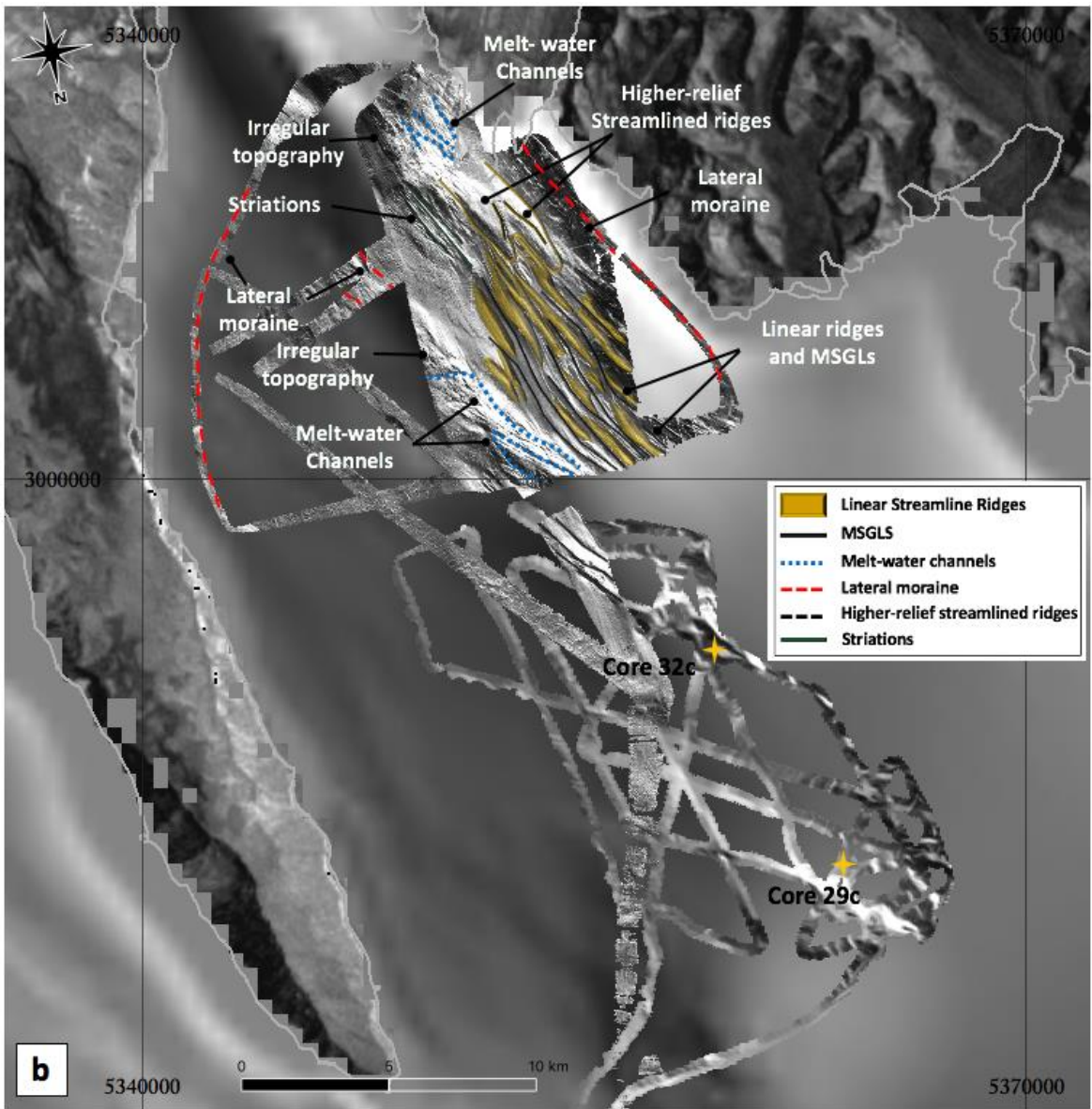
The character and dimensions of the bedforms observed in Robertson Bay match well to similar features described across a number of formerly glaciated regions in Antarctica, where they are carved in hard crystalline bedrock (e.g Graham et al 2009, Halberstadt et al., 2016, Simkins et al., 2017, Smith et al., 2019), and which are plastered by a till sheet at least several metres thick.

We are unable to determine the precise nature of the streamlined linear ridge (i.e., whether they are rock drumlins, roche moutonnées, or crag and tail). Between the bedforms, which are separated by less than 1 km in almost all cases, we observe the bed to be very flat, indicative of draping and infill sediments (Fig 5.9).

A high resolution three-dimensional (3D) map of the streamlined elongated ridges is provided in Figure 5.9 and a cross and longitudinal section in the seismic profile is provided in Figure 5,10, 5.11 (Transect XX' and YY'). In figure 5.11 the longitudinal section (ZZ') along the Sill 2 shows that the bedrock is cut by the marks of the glacial lineations.

These features suggest ice flow from southeast into Robertson Bay (Figures 5.8). Their orientation is opposite to that of present-day ice flow of the small coastal glaciers on the western flank of the bay Figure 5.6. Mineralogical analysis should be done in the future to reconstruct the provenance of sediment composing the elongated ridges. However, in analogy to what is observed on other Antarctic coastal regions (like Drygalsky Glacier and the Mertz Glacier), we suggest that during the Last Glacial Maximum the coastal glaciers (Adare, Murray and Dugdale) debouching into the Robertson Bay, expanded, merged and deviated westward.





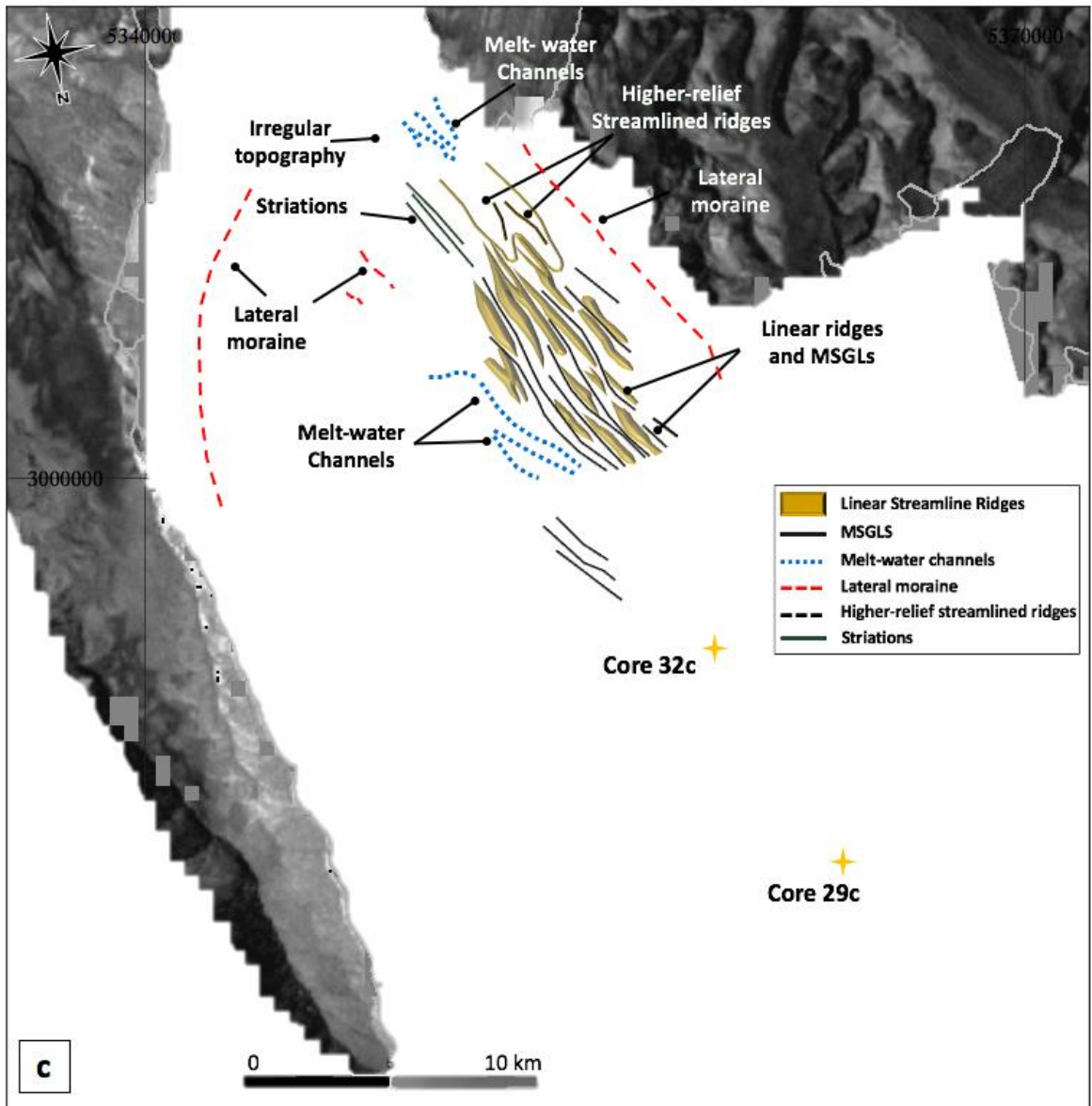


Figure 5.8 Robertson bay: (a) Relief shaded bathymetric map with no vertical exaggeration, (b) Mapped landforms on shaded relief, (c) Mapped landforms. Yellow stars are the location of the cores 29c and 32c.

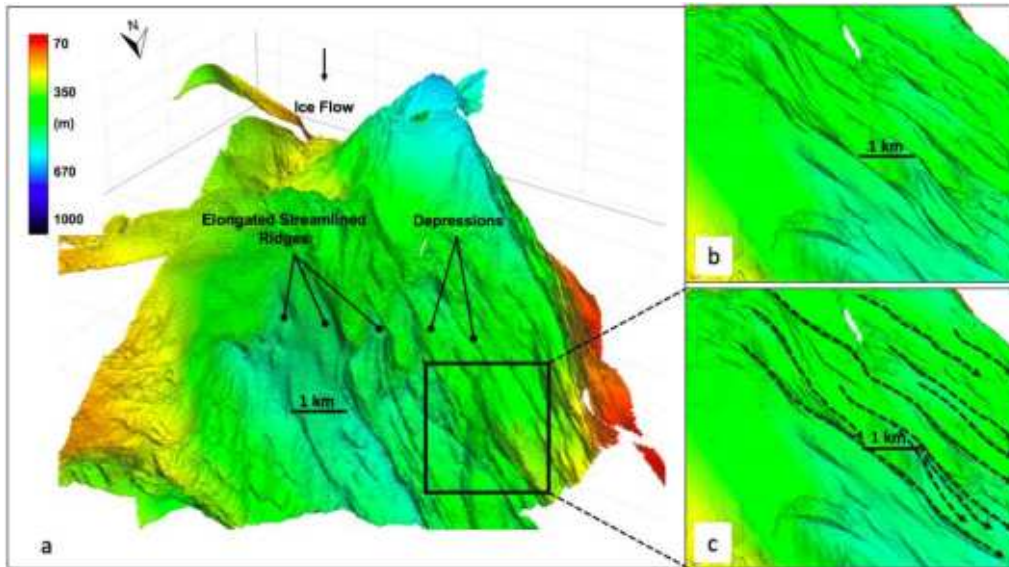


Figure 5.9 3D swath bathymetry of submarine elongate ridges at 25 m grid resolution (a) Zoom of the elongated streamlined bedforms uninterpreted oriented SE–NW (b) and interpreted, with Ice flow direction (black dotted arrows) (c). Figures b and c have been rotated by 15 ° degrees on the right. The colour bar (depths) is in metres.

In contrast, the areas with relatively smooth seafloor where the low reflectivity allows penetration of the acoustic signal below the seabed, is interpreted as the surface of recent soft sediment, filling and draping previous morphology, most probably made of hemipelagic diatomaceous ooze (in analogy with the Edisto Inlet Fjord) but no samples are available from this area.

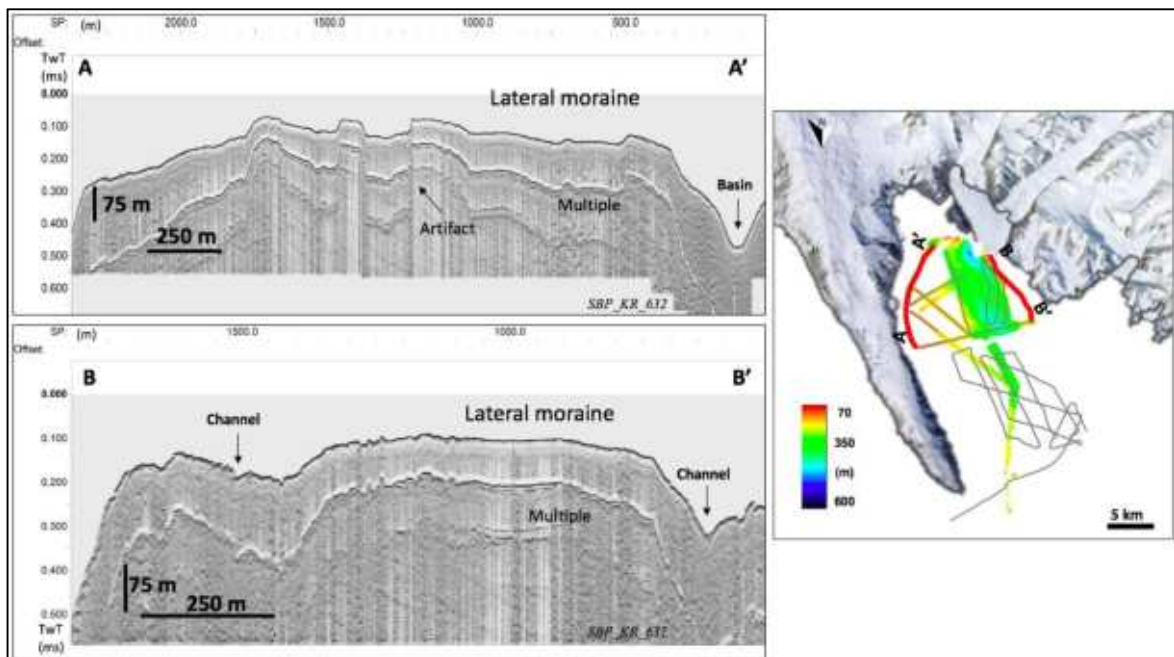


Figure 5.10: SBPs show in profile A A' and B B' two lateral moraines that could have formed during different phases of glacier stationing in the western and eastern flank of Robertson Bay.

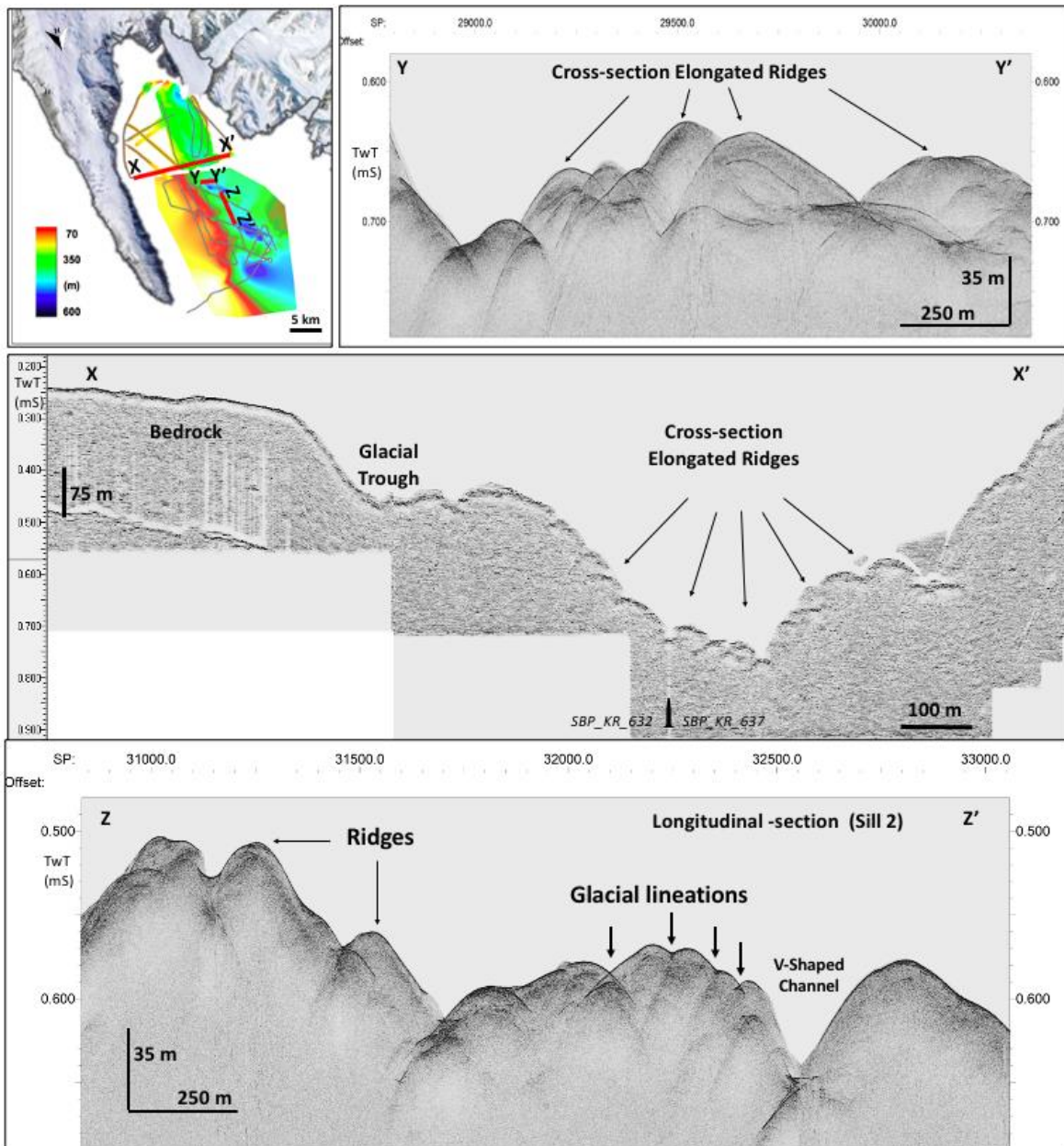


Figure 5.11: SBPs show in profile XX' and YY' two cross- sections of the elongated ridges. SBP ZZ' is the longitudinal section along the Sill 2, the bedrock shows the signs of glacial lineations, a V-shapes channel and few ridges.

5.5.2 Seismic facies

Acoustic lines were analysed using standard seismic stratigraphic techniques for glacial and glaciomarine deposystems. This procedure involves acoustic facies analysis. Three acoustic facies numbered from 1 to 3 Fig. 5.12 are defined on the basis of reflector geometry, amplitude and lateral continuity.

The acoustic basement is the limit of acoustic penetration, it is generally a high amplitude reflector sometimes discontinuous.

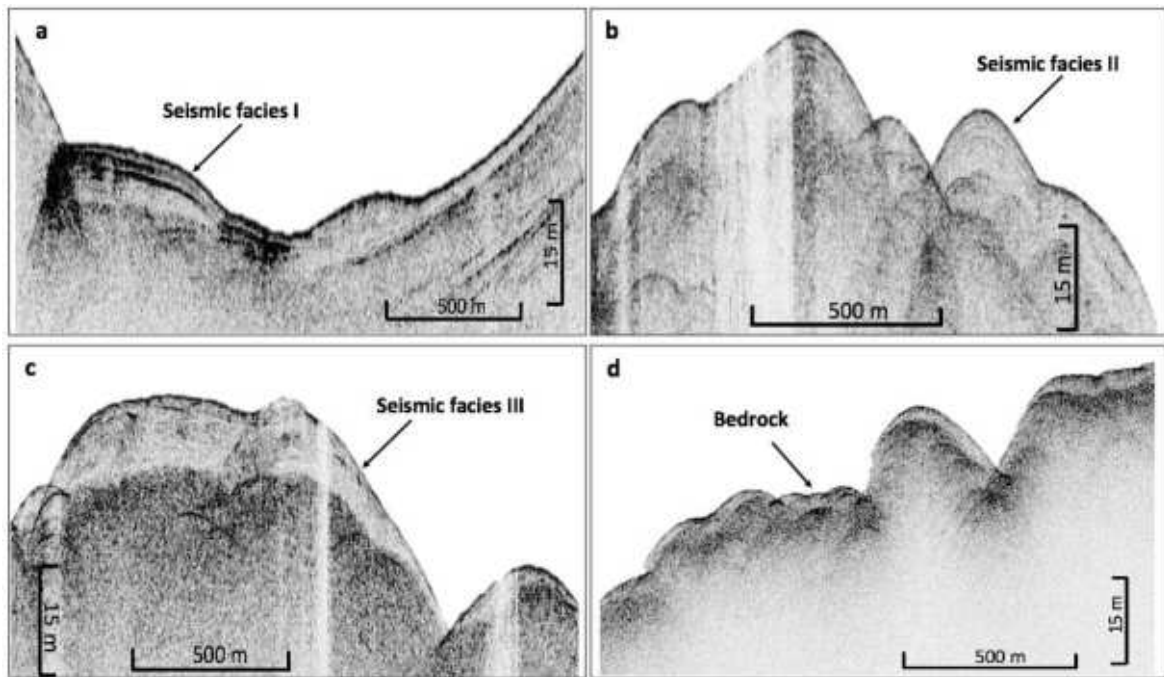
Seismic facies 1 consists of laterally continuous, high amplitude, parallel, sub-horizontal or undulated reflectors, generally conformable to the sea floor. *Facies 1* can be found as basin fill, onlapping the flank of a basin, or as sediment drift deposits (See paragraph 4.5.4 with details on geometry and internal facies of the sediment drift and references) (Figure 5.12a). The *seismic facies 1* reaches a maximum thickness of 100 ms (twl) in the inner part of the bay.

Seismic facies 2 shows medium to low amplitude, discontinuous reflectors. *Facies 2* can be found in asymmetric wedges or isolated mounds. Core 29 penetrated the acoustic facies 2 recovered diatomaceous mud and with poorly sorted muddy sand with IRD, deposited after the LGM.

The core 32c penetrated the acoustic facies 2 from 1 to 420 cm. (Figure 5.12b) recording marine post glacial sediment deposition.

Seismic facies 3 is transparent with low-amplitude reflectors that are found in asymmetric wedges or lenses overlying the acoustic basement (Figure 5.12c). Core 32 penetrated the acoustic facies 3 from 420 to 464cm, recovering normally- compacted glacial diamicton. Facies 3 can then be recording in of sub-glacial or ice proximal glacialmarine deposit.

The *acoustic basement* is the limit of acoustic penetration. It is generally a high amplitude reflector sometimes discontinuous with strong bowtie, hummocky reflections or diffraction (fig. 5.12d).



Seismic facies classification					
Facies Unit	Seismic Example	Internal configuration	Amplitude - Frequency	Lateral continuity	Occurrence
Facies I (a)		Sub horizontal to undulated stratified reflections	Moderate to high amplitude High Frequency	Good continuity reflections	Basin filled with biogenic ooze; No uniform rates of deposition; <u>Low-energy</u> ooze deposits
Facies II (b)		Undulated poorly stratified reflection	Medium to low amplitude Low frequency	Discontinuous reflectors	Marine post glacial <u>sediment deposition</u>
Facies III (c)		Chaotic, no stratified	Low amplitude Low frequency	Discontinuous (highly disrupted) Low lateral continuity	Possible diamicton - commonly applied to unsorted glacial deposits

Figure 5.12: Seismic Facies Classification; (a) Seismic facies 1, layered sediment or basin fill; (b) Seismic facies 2, asymmetric wedge with internal discontinuous reflections; (c) Seismic facies 3, asymmetric wedge with low amplitude and no internal reflections; (d) crystalline basement or bedrock.

Sub bottom profiles show that the acoustic facies below the elongated ridges is opaque or weakly stratified, with reflectors draping the ridges (Fig. 5.13).

Small depressions within the elongated ridges are filled with parallel stratified reflectors. One of these is shown in the Figure 5.13 with up to 15m of stratified sediments. In the innermost part of the bay a V-shaped valley is partially filled by sediment with high reflectivity (Fig. 5.13 c, d).

The thickness of the sediment was calculated using an acoustic velocity of 1500 m s^{-1} for the sediments.

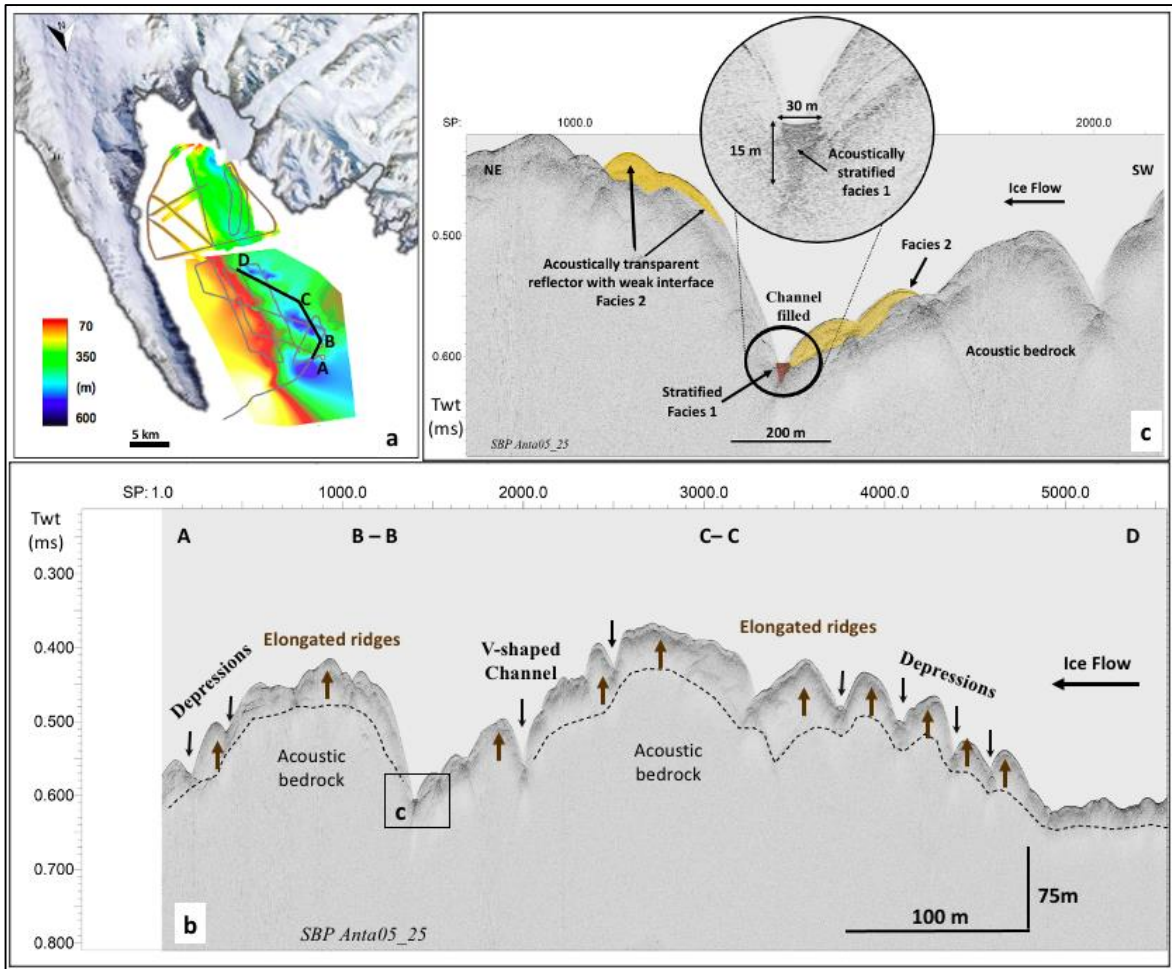


Figure. 5.13 Acoustic sub-bottom profiler data. (a) Map of the region and location of sub-bottom profiler surveys beneath Robertson Bay. Black boxes denote sections of data shown in the main figure (b). (c) Acoustically stratified basin (black circle) showing up to 15 m of stratified sediments. Sediment thickness was calculated using an acoustic velocity of 1500 m s⁻¹ for soft sediments. (b) Acoustically transparent seafloor reflector on the inland eastern slope of the bay with asymmetric ridges (brown arrows) and V-shape channels ((black arrows), dotted black line is the penetration limit of the acoustic bedrock.

5.5.3 Seismo - Stratigraphy

High resolution sub-bottom seismic profiles from Robertson Bay show that the seafloor is highly rugged and covered by a thin drape of weakly stratified sedimentary deposits.

The SBP in Sector 1, show that core 29c, located at the entrance of the bay, inside the mid basin, penetrates the upper 6 meters of a sediment drift, made of sandy material, locally

laminated. The core 29c penetrates *seismic facies 2*. The core doesn't penetrate *facies 1* that pinches out to the east of the core site (Fig. 5.14).

Core 32c located in the morphological sill, that is separating the inner basin from the mid basin. Core 32c penetrates the upper 5 meters of the seismic facies 2, composed of a marine sandy unit. The base of the core recovered a glacial marine diamicton corresponding to the facies 3 (fig. 5.14).

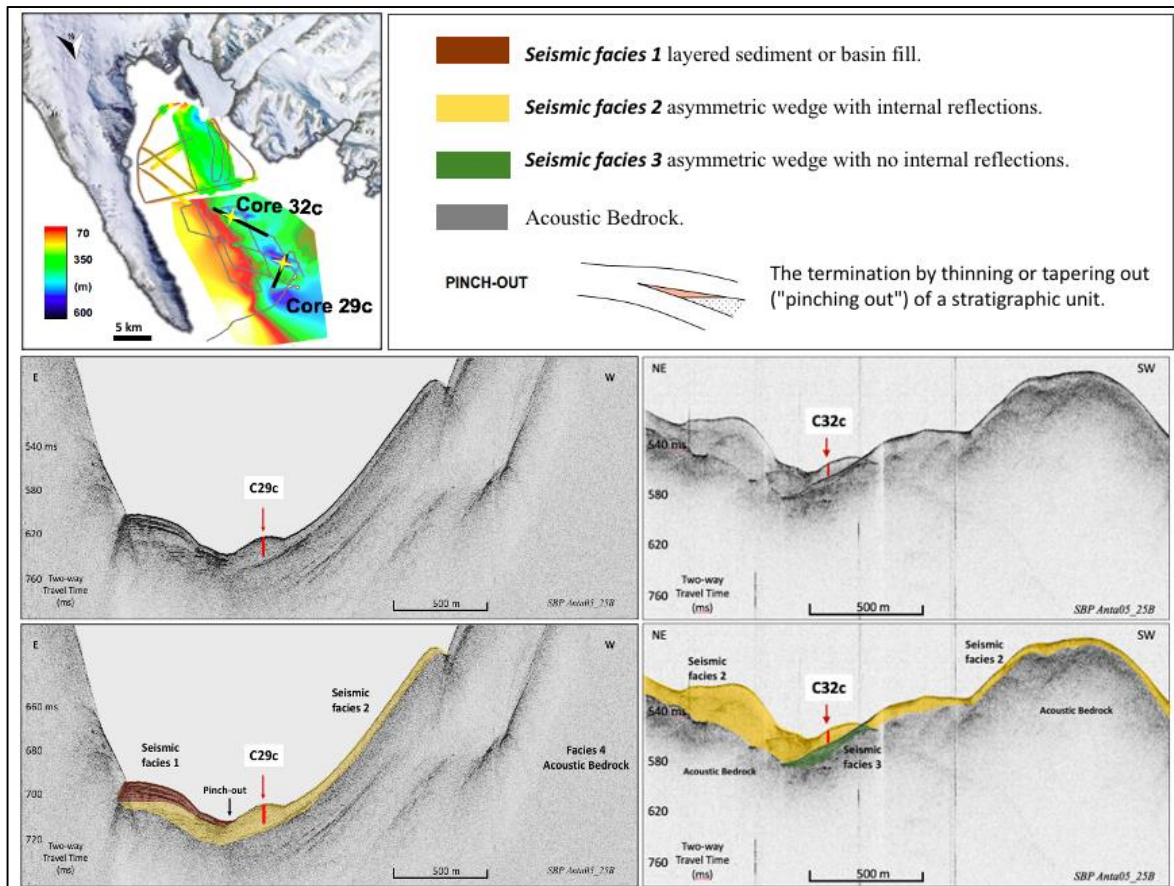


Figure 5.14. Top left map with the position of the SBP (red lines) and of the sediment cores (yellow stars). At the top right, the legend with the identification of the different colors with which the seismic facies are represented. Bottom left SBP uninterpreted and interpreted with location of core 29c and known seismic facies. Bottom right SBP uninterpreted and interpreted with location of core 32c and known seismic facies.

A NW-SE and E-W SBP CHIRP (fig. 5.15) transect shows:

- 1) a basement high with high acoustic reflectivity, on the eastern side of the bay, that can be the expression of the crystalline bedrock outcropping at the sea floor, or of a coarse residual lag, or of compacted subglacial till;
- 2) a rugged slope on the western flank of the basement high with terraces and mounded features approx. 15 m high, with high reflectivity, and chaotic facies with weak,

discontinuous internal reflectors (Figure 5.15 c). This facies suggest erosional processes here like from glacial scour, or slope failure.

The mounded feature could be a lateral moraine, since its internal reflector configurations resemble those characterizing the recessional moraines described elsewhere, (i.e. by Lodolo et al. 2020), although the lack of additional seismic data and sediment cores prevents us to constrain our hypothesis.

3) a basin filled with high amplitude, sub-horizontal, parallel reflections, at the base of the slope. The penetration of the signal (> 100 ms) below the sea floor suggest the relatively soft character of the basin infill, in contrast with the low signal penetration over the basement high. The undisturbed, sub-parallel geometry of the reflections filling the basin discounts the occurrence of large erosive events during the deposition. Therefore, a post-LGM age for the sediment infilling the basin can be reasonably inferred, because it would not have survived the LGM grounding ice expansion. However, the age of the basin infill is unknown due to the lack of sediment cores here (Figure 5.15 d)

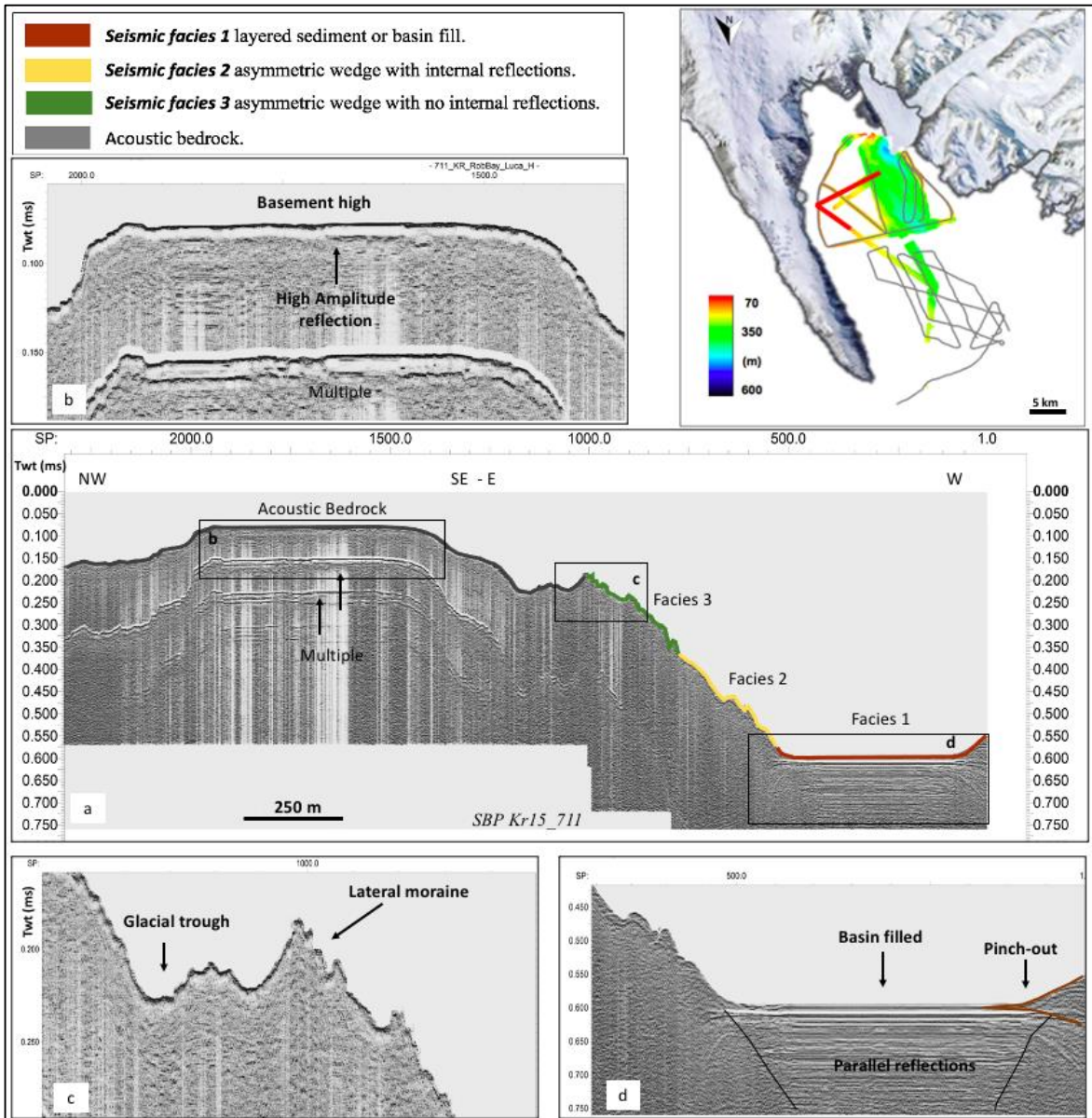


Figure 5.15. Top left map with the position of the SBP (red lines) At the top right, the legend with the identification of the different seismic facies. a) SBP oriented NW-SE and E-W with the recognized seismic facies indicated by the different colors (a). The black squares show the zoom of the basement high (b), glacial trough followed by a lateral moraine (c) and basin filled at the end of the slope (d).

In the sector 1 three SBP CHIRP (AA', BB', CC') (fig. 5.16) transect show several sediment drifts. As already detailed in section 4.5.4, sedimentary drifts are sedimentary bodies produced by the accumulation of sediments under the control of bottom currents (Rebesco and Stow, 2001, Stow et al., 2002, Rebesco, 2005, Rebesco et al., 2008, 2014).

Following the classification of Rebesco et al 2014, the sediment drifts in Robertson Bay are best represented by the *Elongated drift* and *Confined drift* usually mounded, with distinct moats in a relatively small confined basin. As in the Edisto Inlet Fjord the drifts have the

typical form of a sigmoid clinoform, characterized by a high-amplitude stratified seismic facies (Seismic Facies 1) with a length not exceeding 2 km but in Robertson Bay we have a much smaller thicknesses ranging from 3 to 10 meters (figure 5.16).

We do not have samples in this area to be able to constrain the lithology and the sedimentation rate, but the penetration of the acoustic signal below the seabed suggests a relatively soft character of the basin filling, in contrast to the scarce signal penetration in the basement high.

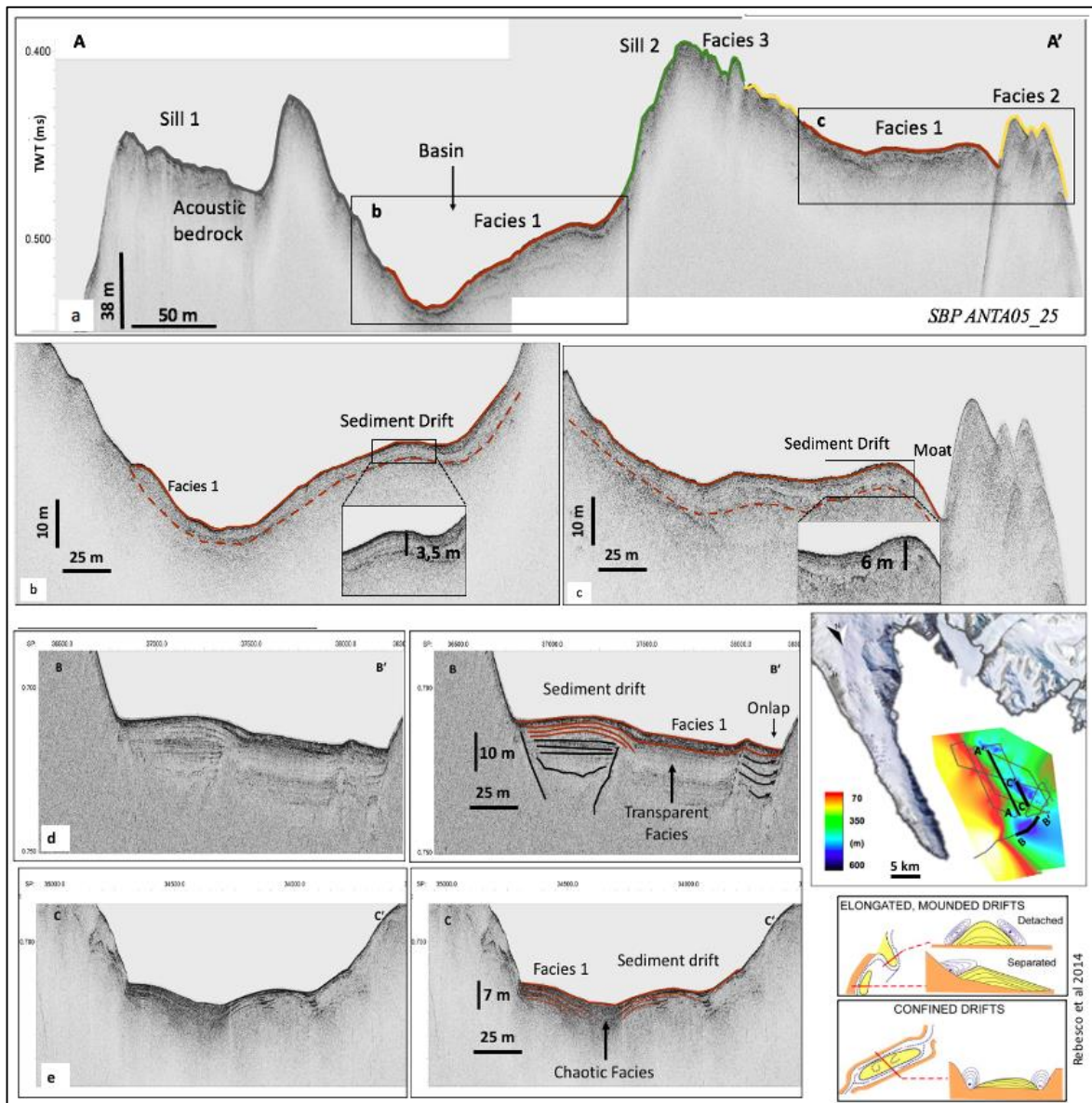


Figure 5.16: SBP CHIRP (AA', BB', CC') profile black lines in map. The two squares (b) and (c) are a zoom of sedimentary drifts characterized by acoustic facies 1 recognized in the SBP profile (a). SBP (d) and (e) show two more sediment drifts filling the basins. All sediment drift in Robertson Bay is represented by *elongated drift* and *confined drift* according to the classification by Rebesco et al 2014.

5.5.4 Stratigraphic data

Core 29c and 32c provide direct lithological information for the acoustic facies identified on the seismic profiles for the outer sector of the bay (sector 1). No samples are available from the inner sector 2 of the bay. Physical properties (water content, magnetic susceptibility), grain size data, diatom assemblage, biogenic silica (BiSi), total organic carbon (TOC) and X-rays document the presence of 4 main sedimentary facies (Fig 5.17 a, b). They generally consist of volcanoclastic sediment mixed with biogenic-rich mud and Ice Rafted Debris (IRD). The biogenic component consists mainly of diatoms and sponge spicules.

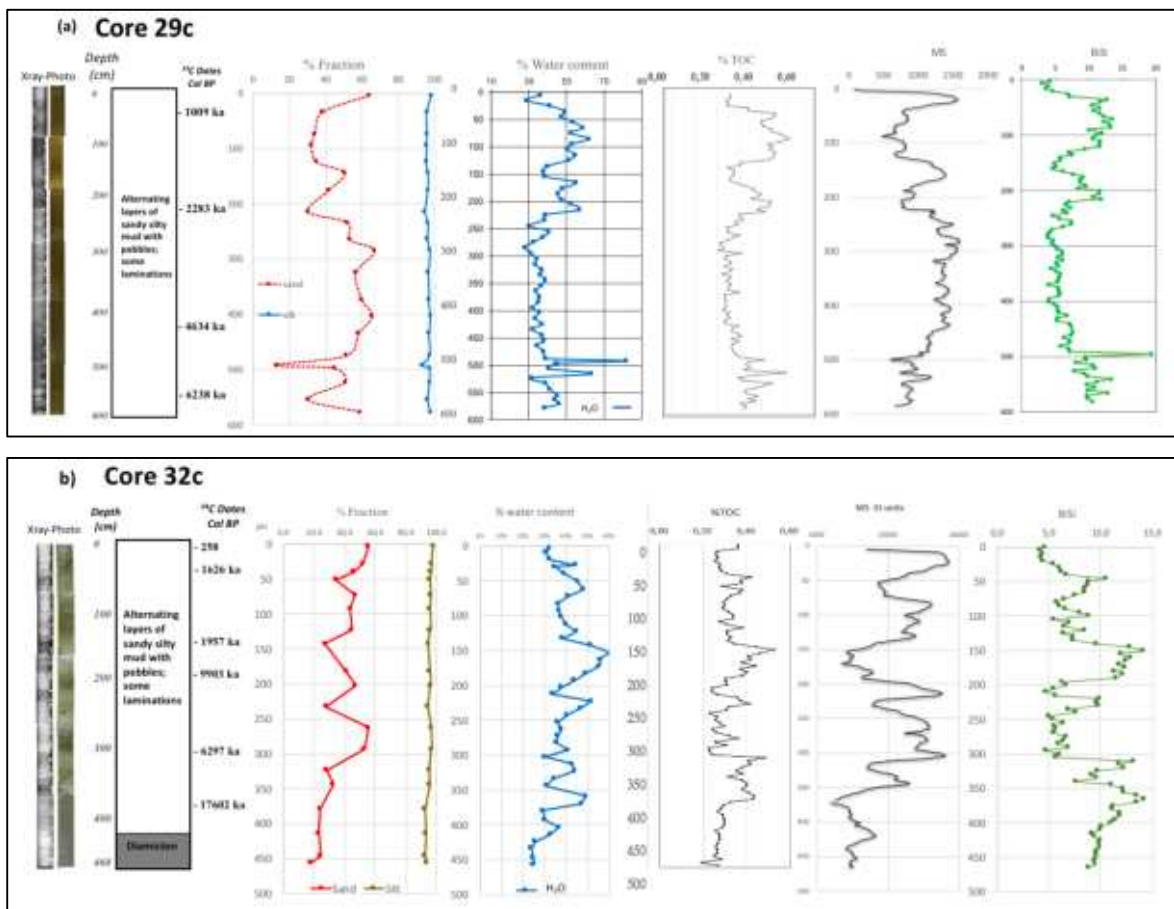


Figure 5.17: Xray, Photos, Radiocarbon dates (¹⁴C), grain size data (% fraction), water content, total organic carbon (TOC), magnetic susceptibility (MS), biogenic silica (BiSi) charts of the core 29c (a) and 32c (b)

5.5.4.1 Cores Description

Core BAY05-29c comprises a biogenic-rich lithological unit where the dominant grain size is silt with rare gravel clasts (color from dark olive to very dark gray) (Unit4). This lithological unit is moderately bioturbated and shows discontinuous dark laminae. Near the core bottom (420- 580 cm) there is an increased proportion of fine sand, slightly more distinct laminae. Sub-horizontal sandy pockets (very dark in color) occur at 510 cm and 516 cm (Unit 3).

Core BAY05-32c comprises three different lithological units. The top section of the core comprises a biogenic-rich lithological unit (Unit 4). From (0-400 cm) is made by a silty sand marine sediment with dispersed gravel clasts and sparse dark laminae (Unit3). The bottom (400 - 420 cm) is characterized by weakly stratified to massive silty sandy matrix with sparse Ice rafted debris (IRD) (Unit 2) and from 420 to 464 there is a glaciomarine diamicton characterized by abundant gravel and pebbles (from millimeter to centimetre) in a sandy silt matrix (Unit 1).

5.5.4.1.1 Lithostratigraphic facies

Weakly laminated silty sand marine facies (WLMf) (Unit 4) alternating layers silty sand to sandy silt sediment with dispersed gravel clasts characterizes this facies. The MS averages 491×10^{-5} SI, water content is 40%, TOC 0.32%, low wt% BSi 8.2%. The mean dry density is $1,650 \text{ g/cm}^3$. This facies occurs above the diamicton unit in core 32c and overall, in core 29c.

Laminated silty sand marine facies (Lmf) (Unit 3), diatomaceous mud with rare gravel clasts, moderately bioturbated and discontinuous dark laminae. The MS averages 742×10^{-5} SI, water content is 41%, TOC 0.32%, low wt% BSi 7,6%. The mean dry density is $1,650 \text{ g/cm}^3$. This facies occurs from 480 cm to the bottom in the core 29c and at the top 0 - 40 cm in core 32c

Silty sandy facies with pebbles and IRD (SSpf) (Unit 2) is characterized by weakly stratified to massive silty sandy matrix with sparse IRD (Ice rafted debris) with high dry density (avg

1.600 g/cm³) and high magnetic susceptibility (MS, avg 427 x 10⁻⁵ SI). Water content, TOC and wt% BSi contents (33%, 0.28%, 10% respectively) are low. This facies is present between 400 - 420 cm above the diamicton unit in core 32c.

Glacio Marine Diamicton facies (GmDf) (Unit 1) is characterized by abundant gravel and from millimeter to centimeter pebbles in a sandy silt matrix, high dry density (avg 1.500 g/cm³) and high magnetic susceptibility (MS, avg 371 x 10⁻⁵ SI). Water content, TOC and wt% BSi contents (24%, 0.26%, 9% respectively) are low. This facies is present at the bottom of cores BAY05-32c (420-464 cm).

5.5.5 Geochemical Proxies

Weight percent biogenic silica (wt% BSi), $\delta^{13}\text{C}$, and C:N ratio are discussed together. Five transitions (T6, T5, T4, T3, T2, T1) with prominent changes in the curves are highlighted in Figure 5.18 (core 29c) and Figure 5.19 (core 32c).

5.5.5.1 Core 29c

The upper section of the core 29c between 0 cm and 20 cm, wt% BSi averages 4% and $\delta^{13}\text{C}$ averages -22‰ (T1). Between 25 cm and 180 cm (T2), a step decrease occurs in $\delta^{13}\text{C}$ from -22‰ to -26‰; wt% BSi increases from 2% to 13%.

$\delta^{13}\text{C}$ values gradually increase with a peak at 158 cm (-23.8‰) accompanied by a corresponding decrease in wt% BSi, from 13% to 5% and a positive increase in the C:N ratio. However, a step increase in wt% BSi between 190 cm and 210 cm corresponded to a decrease in $\delta^{13}\text{C}$ profile (-26.3‰) (T3).

Between 220 cm and 520 cm high frequency variability in both wt% BSi and $\delta^{13}\text{C}$ decreases (T4). The C:N ratio in core 29c increases slightly except for a very high positive increase at 285 cm. A maximum peak in wt% BSi with the maxima at 495 cm (>18%) co-occur with minima in $\delta^{13}\text{C}$ (-27‰).

At the bottom of the core from 540 to 565 cm (T5) wt% BSi increase from 7% to 12% and that co-occur with decrease in $\delta^{13}\text{C}$ (-25‰).

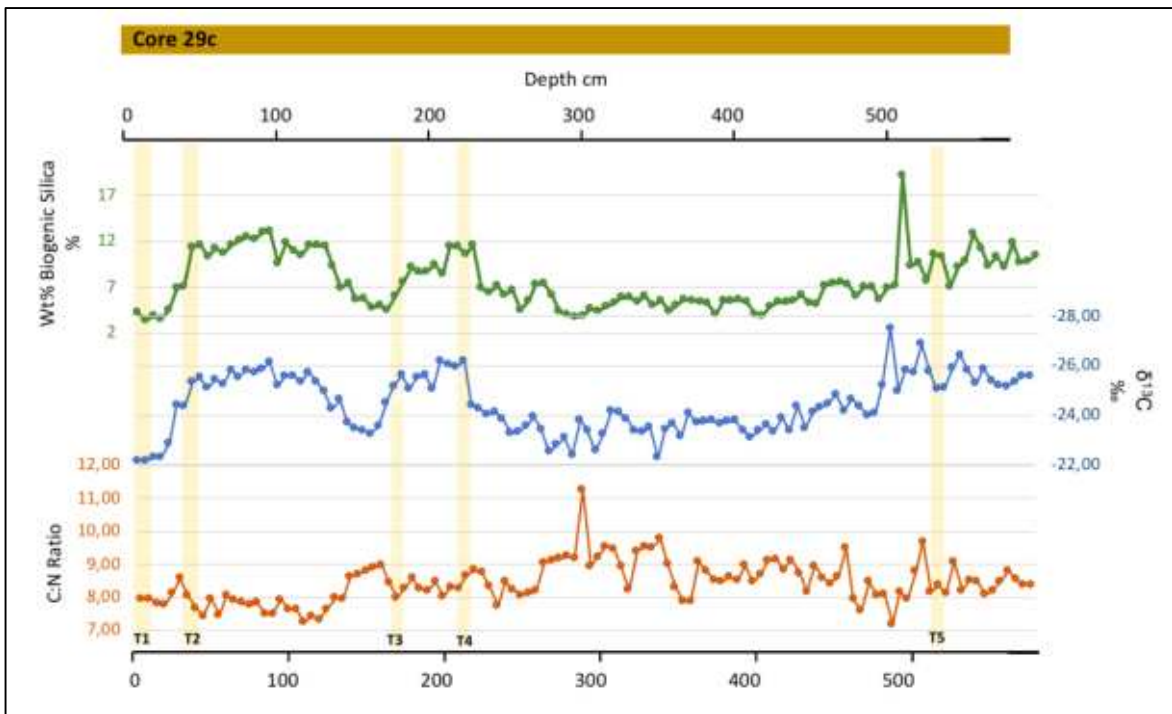


Figure. 5.18: Core 29c, weight percent biogenic silica, $\delta^{13}\text{C}$, and C:N ratio, highlighted five notable transitions (T1 to T5).

5.5.5.2 Core 32c

The upper section of the core 32c between 0 and 10 cm (T1) is characterized by wt% BSi (4%) and an increase in $\delta^{13}\text{C}$ (-23.5‰). Between 10 and 40 cm (T2), is characterized by minima in wt% BSi (4%) and maxima in $\delta^{13}\text{C}$ (-22‰). From 40 cm to 145 cm wt% BSi slightly increase up to 8% and $\delta^{13}\text{C}$ decrease (~ -25‰) (T3). From 135 to 190 cm (T4) there is a positive growth step in wt% BSi up to 13% and a decrease in $\delta^{13}\text{C}$ up to -27‰.

$\delta^{13}\text{C}$ values gradually increase with a peak at 295 cm (-23‰) accompanied by a corresponding decrease in wt% BSi, from 10% to 5%

Between 255 cm to 305 cm a positive increase trend in the C:N ratio is noted.

From 305 to 350 cm wt% BSi decrease from 12% to 7%, and then increase again up to 13%.

The $\delta^{13}\text{C}$ increase (from -26‰ to -24‰) to then decrease to a minimum of -28‰.

From 350 towards the bottom of the core but just before the diamicton (T6) wt% BSi slightly decrease, that co-occur with minima in $\delta^{13}\text{C}$ (-28‰).

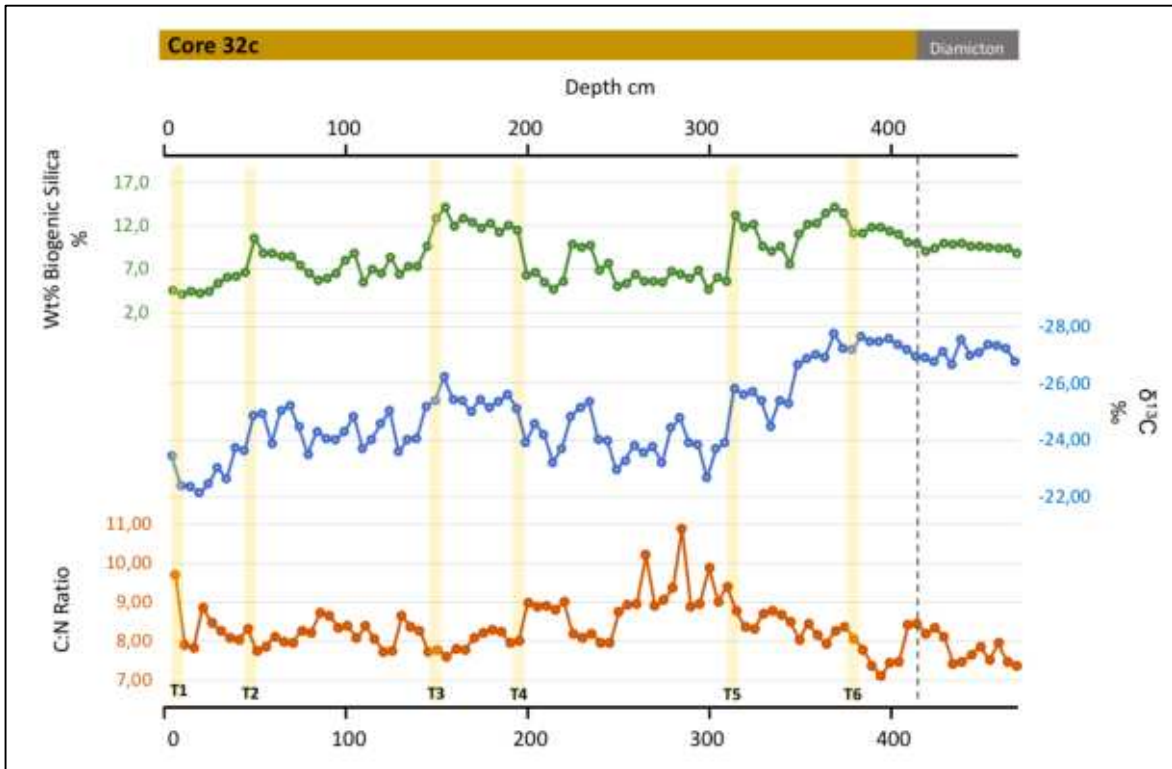


Figure 5.19: Core 32c, weight percent biogenic silica, $\delta^{13}\text{C}$, and C:N ratio, highlighted five notable transitions (T1 to T5).

This multi-proxy investigation highlights the importance of interpreting geochemical proxy data in the context of other paleoenvironmental proxies. This thesis will not take into consideration all the diatoms species found in the bay, but only the diatom species with well-established environmental preferences (Gersonde et al 2000; Leventer & Dunbar 1996; Haug & Myklestad 1976; Crosta et al 2004, 2009; Taylor -Silva et al 2018; Duncan et al 2022). I use the results from the unpublished diatom data provided by F. Torricella (Fig 5.20, 5.21). The combination of our proxies, once both theses will be reviewed, may reveal more detailed information and strengthen subsequent paleoenvironmental reconstructions of this region.

5.6 Discussion

5.6.1 Interpretation of glacial landforms and cores correlation

The sedimentary succession in Robertson Bay is composed of biogenic material produced in the water column and lithogenic material derived from terrigenous sources. Siliceous fossil diatoms dominate the biogenic component while terrigenous material is transported into the bay through erosion of the surrounding bedrock due to ice flow and the high-speed katabatic winds described by Harrowfield, DL (1996).

The distribution of depositional and morphological features in Robertson Bay reflect local geology, as well as glacial and circulation dynamics since the LGM.

Elongated ridges emerging from the sea floor and parallel to the bay axis, oriented SE-NW, and probably made by pre-Holocene sediments overlying crystalline bedrock, are interpreted as mega scale glacial lineations (MSGs) or streamline grooves (fig 5.8, 5.9, 5.11) formed under the ice flowing from south toward north, and grounding over a deformation layer, similar to the interpretations of Munoz, Y. P. and Wellner, J. S, 2018 and Batchelor, et al 2017 in the western Antarctic Peninsula.

These features have previously been described from a wide range of formerly glaciated terrestrial and marine environments where they are inferred to form sub-glacially and are used as indicators of fast-flowing outlet glaciers or ice streams (Stokes and Clark, 2001; Shipp et al., 1999; Canals et al., 2000; Ó Cofaigh et al 2016; Slabon et al. 2016; Halberstadt et al., 2016). Unfortunately, there are no samples from these ridges, therefore their composition is unknown, but the high seabed reflectivity on sub-bottom data with no or very little penetration below would suggest highly lithified or compacted character.

Sets of channels occur on bathymetric highs in innermost area of sector 2 and on the eastern side of the bay (fig. 5.8, 5.10). These channels are up to 4 km long, 300 m wide and 8 m deep. They are mainly flow-oriented and that often occur in-between ice-flow landforms.

Similar landforms were described in palaeo-ice stream tracks (e.g., Lowe and Anderson, 2003; Nitsche et al., 2013; Smith et al., 2009) and have been interpreted as the product of subglacial meltwater carrying sediments and eroding in hard bedrock. These channels are

interpreted as meltwater channels, which formed subglacially under ice-streaming conditions.

The swath bathymetric imagery reveals that distal-flanks accretion resulted in sequences of stacked tills lying on the western and eastern side of Robertson Bay, in sector 2 (fig. 5.10) oriented parallel to former ice flow.

On sub-bottom profiles, these ridges are represented by a strong reflection signal with no penetration, which indicates that they either consists of coarse sediments, massive till or bedrock. Those features are also characterized by longitudinal depressions (meltwater channels) with the near absence of postglacial sediments draping, suggests that these landforms are sediment bodies, most likely representing lateral moraines ridges deposited during standstills or re-advance of outlet glaciers during deglaciation.

Asymmetric smaller ridges no more than 15 m high, with a very weak internal stratification are interpreted as sedimentary mounds forming during the advance or the retreat of the glaciers from the bay (fig 5.10), however, the lack of additional seismic data and sediment samples prevents us to constrain our hypothesis.

Sub-bottom profiles show a variety of bottom current controlled sediment-drifts in sector 1 (Fig 5.16) typically made of mounded bodies with internal seismic facies 1, pinching toward moats. Sediment drifts have been found at all latitudes, including the lower continental slope and rise and on the Antarctic continental shelf (Harris et al., 1997; Escutia et al 2002; Presti et al., 2005, Close et al 2010; Maldonado 2015). They have a convex shape, with the predominance of sediment accumulation in the center of the drift and low or no deposition in the moat (Rebesco et al 2005). Sediment drift depocenter is characterized by suspended particle material settled from the water column in null or very low bottom current. Drift type and growth are controlled by the physiographic and geological setting in which they develop and by the supply of suspended material and the occurrence of persistent bottom-current circulation, conferring typical erosional and depositional typical features (pinching out toward the drift-moat). Following the classification for drifts by Rebesco et al. (2014) we suggest that the sediment drifts forming in Robertson Bay are *elongated drifts* and *confined drifts* (Rebesco et al. 2014) (fig 5.16).

In Robertson Bay, several basins act as depocentres but the thickness of the sedimentary records is not as high as for example in Edisto Inlet Fjord, considered a morphologically

protected fjord where bottom currents have allowed the formation of a very expanded sedimentary record. The thicknesses of the sedimentary drifts, in the northern part of Robertson Bay facing the mouth of the bay does not exceeding 10 m (Fig 5.16), suggesting a lower sedimentation rate, similar to Andvord Bay on the West Antarctic Peninsula (WAP) (Eidam et al 2019) where sediment accumulates at slow rates of millimeters per year, conditions which foster great biologic productivity in the coastal zone.

On the other hand, the deposition and preservation of the thicker (> 80 m) and undisturbed stratified sediment sequence (facies 1) in sector 2 (fig 5.15 d) of Robertson Bay can only be explained if a modern oceanic slow circulation with periodic intervals of high productivity, favored by intrusion of warm waters, persisted for several thousand years. Furthermore, this undisturbed sequence indicates that the glaciers never readvanced into the bay after their retreat.

Unfortunately, we do not have samples from Robertson Bay to constrain the age and sedimentation rate of the seismic facies 1.

The sediment deposited in the upper part of facies 2 and sampled at core Bay05_29c and Bay05_32c (fig. 5.14) has generally an opaque low amplitude acoustic facies and is draping or onlapping previous morphology (facies 2 in yellow in fig. 5.13, 5.14, 5.15, 5.16). Locally, facies 2 shows a geometry typical of confined sediment-drift inside the basin (fig. 5.14) or is forming on the top of morphological highs. Our interpretation is consistent with a hemipelagic origin and the establishment of a persistent, possibly tidally-fjord-driven circulation setting in Robertson Bay at least since 6.2 ka ago, dated at the base of core 29c, however, as suggested by the age of the sediments of seismic facies 2 in core Bay05-32c and the thickness of the facies 2 in sector 2 (fig 5.15 d) the onset of a shift in water masses circulation is clearly older than 6.2 ka.

The diamicton (sedimentary facies *GmDf*) sampled at the base of core Bay05-32c (fig 5.14) and dated 17.6 kyr BP, on the basis of the sedimentological and geochemical properties (TOC, MS, grain-size, water content, BiSi) is interpreted as glacial-marine sediment that has experienced variable inputs of sand resulting from pulses of iceberg rafted debris and/or meltwater from the retreating of the ice sheet in Robertson Bay right after the LGM.

The transition between the massive (glaciomarine, more terrigenous, less homogeneous and coarser sediments, with IRD) facies *GmDf* and facies *SSpf* just above the diamicton to a more biogenic-rich, stratified sub-facies (*Lmf*) lying over the *SSpf* facies, in sectors 1,

represents the transition to an open and stratified water, with the establishment of ocean circulation and seasonal sea ice condition inside Robertson Bay. This is supported by the higher percentage of BiSi > 12% and *F. obliquocostata*, *CRS* and *Chaetoceros spp* that dominate the diatom assemblage (F. Torricella unpublished) at the base of both cores from 17.5 ka to approximately 4.0 ka (Fig 5.20, 5.21). While *Fragilariopsis curta* is strongly associated with the modern summer sea ice edge and is observed in highest abundance close to melting sea ice, the *F. obliquocostata* is sometimes associated with both sea ice (Crosta et al. 2004, Armand et al. 2005) but also with cold open water and polynyas of the Antarctic Oceans (Taylor et al. 1997; Cunningham and Leventer 1998). This supports our interpretation of a general cooling trend during the early Holocene (Crosta et al. 2004; Armand et al. 2005; Leventer et al. 2007) possibly related to a reinvigoration of bottom circulation due to seasonal sea ice occurrence, meltwater discharge and coastal glaciers expansion and retreat.

The bathymetry in sector 1 highlights the presence of three basins separated by two sills (fig 5.7). The shape and orientation of the three basins reflect the main path of ice erosion during past glacial maxima, although it is also influenced by bedrock type and NVL's NW–SE dextral faults (Salvini et al 1997, Domack et al 1999, Howat et al 2003, Rocchi et al 2003), that likely continue offshore, although there is no evidence of faults in our SBP profiles.

The overall elongated ridges and MSGLs parallel to the bay axis suggest that the ice flow was flowing from southeast to northwest in Robertson Bay (Figure 5.8). Their orientation is opposite to that of the current ice flow of small coastal glaciers on the western side of the bay (fig 5.6), however, in analogy with what has been observed on other Antarctic coastal regions (such as the Drygalsky glacier and the Mertz Glacier), we suggest that during the LGM the coastal glaciers (Adare, Murray and Dugdale) that flow into Robertson Bay have expanded, melted and deviated westward into a single large ice sheet. This deviation is supported by a tectonic controlled features/trends (Harrington 1958; Behrendt et al. 1991; Kyle 1990; Rocchi et al 2003; Nardini et al 2003).

The sedimentology and geometry of the glacial landforms is consistent with the pattern that ice extended into Robertson Bay during the LGM but retreated in sector 1 at least 17.6 ka ago as shown by seismic facies 1 and 2 where the sediment drifts are preserved from glacial erosion, and strong bottom current winnowing, although a weak circulation was continuously occurring. Ice was grounded on shallower banks and ridges as shown by the

MSGs in both sector 1 and sector 2. Here the thicknesses, the IRD rich and massive facies of the sedimentary cover and the glacial lineations toward north would suggest ice pinning in the basement highs and on the sills (fig 5.11) and floating ice into the deepest depressions, the drift body of seismic facies 1 shows no signs of glacial erosion (fig. 5.16).

The retreat of the glaciers is also supported by the bloom of diatoms, in particular the dominance of *Chaetoceros* resting spores which peak at a relative abundance >40% just above the diamicton facies (*GmDf*) (approximately 17.6 ka) (F. Torricella unpublished data fig 5.21), represents a higher hydrodynamic regime after the retreat of the calving front of the Ross Sea Ice Shelf and the establishment of a more stratified water column.

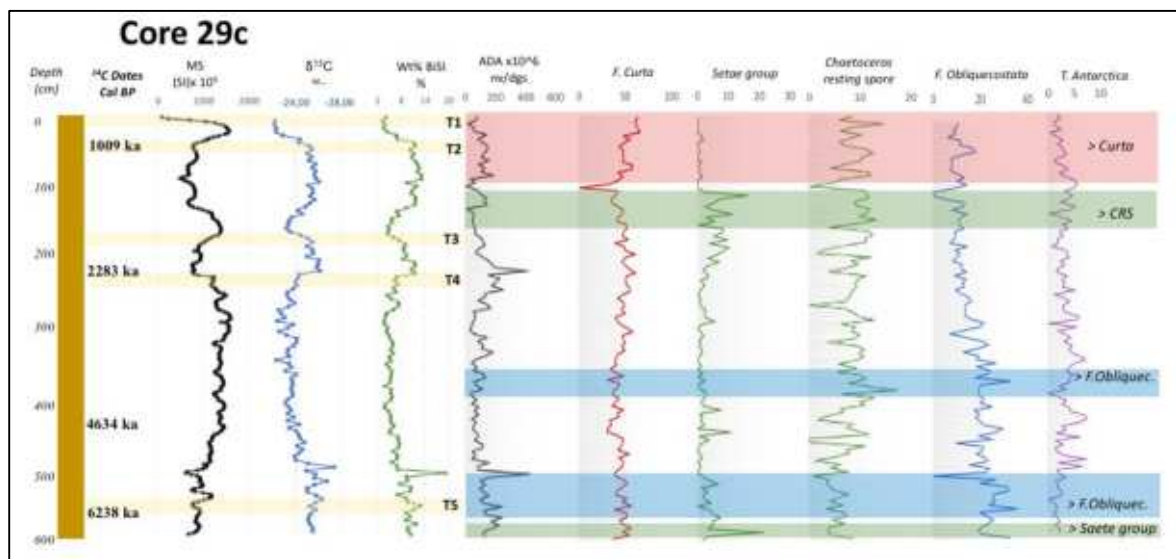


Figure 5.20: Summary results figure core 29c showing calibrated ¹⁴C dates, magnetic susceptibility (MS), weight percent biogenic silica (wt% BSi), and δ¹³C highlighting notable transitions (T1 to T5). ADA and relative abundances of *F. curta*, the setae group, *T. antarctica*; *Chaetoceros* resting spores (CRS), and *F. obliquecostata*; The bands of color highlight the dominant diatom species: red (*F. curta*), green (Setae group and CRS), blue (*F. obliquecostata*), pink, (*T. antarctica*) (F. Torricella unpublished data).

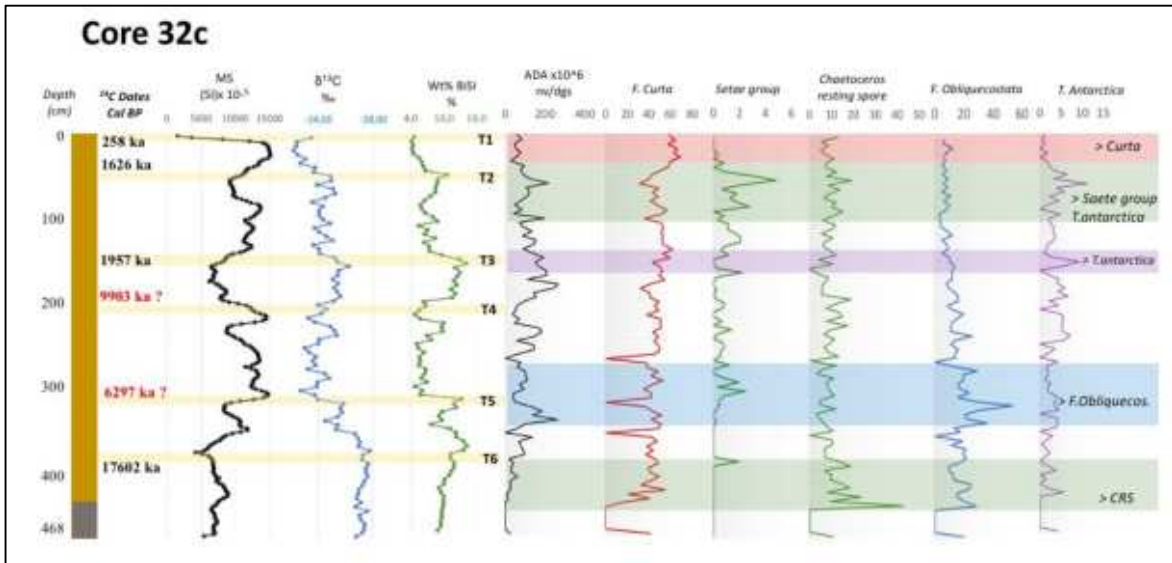


Figure 5.21: Summary results figure core 32c showing calibrated ^{14}C dates, magnetic susceptibility (MS), weight percent biogenic silica (wt% BSi), and $\delta^{13}\text{C}$ highlighting notable transitions (T1 to T6). The bands of color highlight the dominant diatom species: red (*F. curta*), green (setae group and CRS), blue (*F. obliquocostata*), pink, (*T. antarctica*) (F. Torricella unpublished data).

5.6.2 Core BAY05_29c and BAY05_32 Proxy data reconstruction

In the following sections we will discuss the Holocene environmental trends in Robertson Bay highlighting the environmental transitions (T6 17,600 – Early Holocene; T5, 17,600 – 6,500; T4 6,500, 2,400 – T3 2,400 – 2,000; T2 2,000 – 1,500; and T1 the last 1,000 cal yr BP) noted in core BAY05_29c and BAY05_32c (Fig 5.22, 5.23) through the main paleoenvironmental proxies such as:

- 1) The Magnetic susceptibility (MS), proxy for terrigenous flux;
- 2) Wt% BSi, proxy for biogenic flux, interpreted as a proxy for primary production;
- 3) $\delta^{13}\text{C}$: nutrient regime, interpreted as proxy for water column structure;
- 4) Ratio of *Chaetoceros* spp. / *Chaetoceros* resting spores (CRS), a proxy for nutrient availability in surface waters;
- 5) Relative abundance of *T. antarctica*, a proxy for water column structure;
- 6) Relative abundances of *F. curta*: a proxy for proximity and sea ice duration;

Weight percent biogenic silica (wt% BSi) and diatom absolute abundance (ADA) reflect the concentration of biogenic material relative to terrigenous material; variations in wt% BSi and ADA could reflect changes in (i) biogenic flux, (ii) terrigenous flux, or (iii) both processes operating simultaneously (Leventer et al., 1996; Mortlock and Froelich, 1989).

Like ADA and wt% BSi, bulk magnetic susceptibility (MS) is influenced by the variable dilution of magnetic terrigenous material from the continent by the diamagnetic shells of siliceous diatoms (cf. Leventer et al., 1996). However, bulk MS is also affected by any variations in the magnetic character (magnetic mineralogy, magnetic particle size, and any post-depositional diagenesis) of the sediment (Brachfeld and Banerjee, 2000; Brachfeld et al., 2002).

In cores BAY05_29c and BAY05_32c wt% BSi (biogenic flux) is inversely correlated with magnetic susceptibility (MS). The covariance trend between wt% BSi and MS indicates that MS reflects changes in terrigenous flux entering Robertson Bay.

As discussed in section 3.5.1, in the Antarctic environments, $\delta^{13}\text{C}$ is typically interpreted as a proxy for total primary production. This is because the effect of the fraction of the increase in primary production on $\delta^{13}\text{C}$ (surface water) is believed to dominate the effects of oceanographic change (stratification) and species-specific fractionation processes (Berg et al., 2013; Crosta et al., 2002; Panizzo et al., 2014; Villinski et al., 2000). Furthermore, since diatoms thrive in a stratified environment (Leventer et al., 1996), periods of high primary productivity typically occur with increases in stratification, such that both processes operate simultaneously to shift the $\delta^{13}\text{C}$ of surface waters to be more positive values (Fry, 1996; Villinski et al., 2000).

In Robertson Bay periods of high biogenic accumulation (higher wt% BSi and ADA) occur concomitant with more negative $\delta^{13}\text{C}$. Conversely, stratification (high $\delta^{13}\text{C}$) is correlated with lower primary productivity (wt% BSi and ADA) (Figure 5.22, 5.23). An inverse relationship between $\delta^{13}\text{C}$ and productivity indicates that the effect of a continually refreshed $\delta^{13}\text{C}$ pool in surface waters (decreased stratification) dominates the fractionation effect and may stimulate increased primary production. The correspondence of elevated $\delta^{13}\text{C}$ with lower biogenic flux (wt% BSi and ADA) may be due to nutrient limitation, as the micronutrients essential for primary production are supplied by terrigenous material from the continent and/or from upwelling deep waters (Graham et al., 2015; Sedwick et al., 2000).

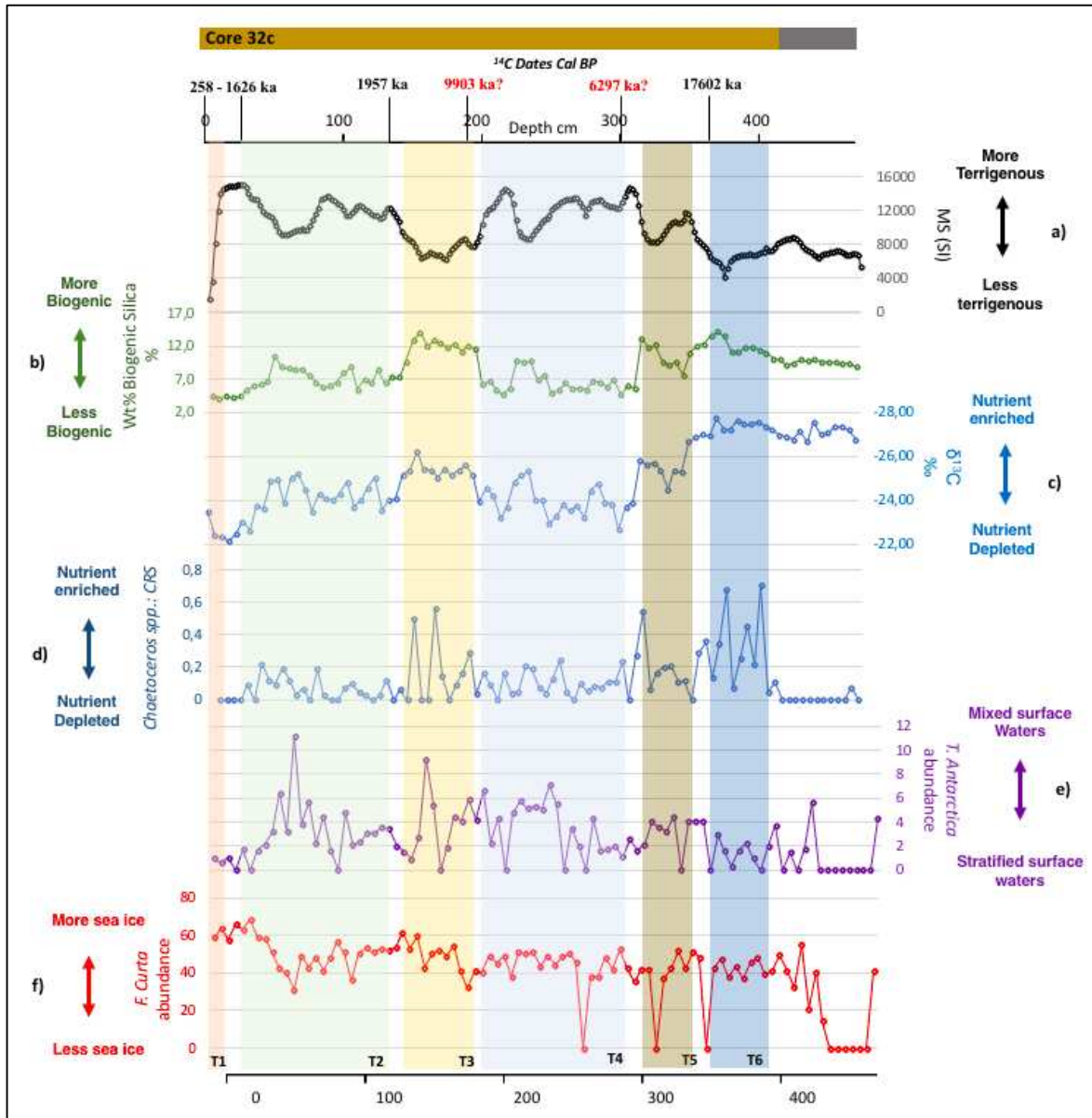


Figure 5.22: Holocene environmental trends in Robertson Bay core 32c highlighting environmental transitions (T6 17,500 – Early Holocene; T5, Late Holocene – 6,300; T4 6,300, 5,300 – T3 5,300 – 2,000; T2 2,000 – 1,500 and T1 the last 238 cal yr BP). (a) Magnetic susceptibility (MS), proxy for terrigenous flux. (b) Wt% BSi, proxy for biogenic flux, interpreted as a proxy for primary production. (c) $\delta^{13}\text{C}$, proxy for water column structure. (d) Ratio of *Chaetoceros* spp. / *Chaetoceros* resting spores (CRS), a proxy for nutrient availability in surface waters. (e) Relative abundance of *T. antarctica*, a proxy for water column structure. (f) Relative abundances of *F. curta*, a proxy for sea ice duration.

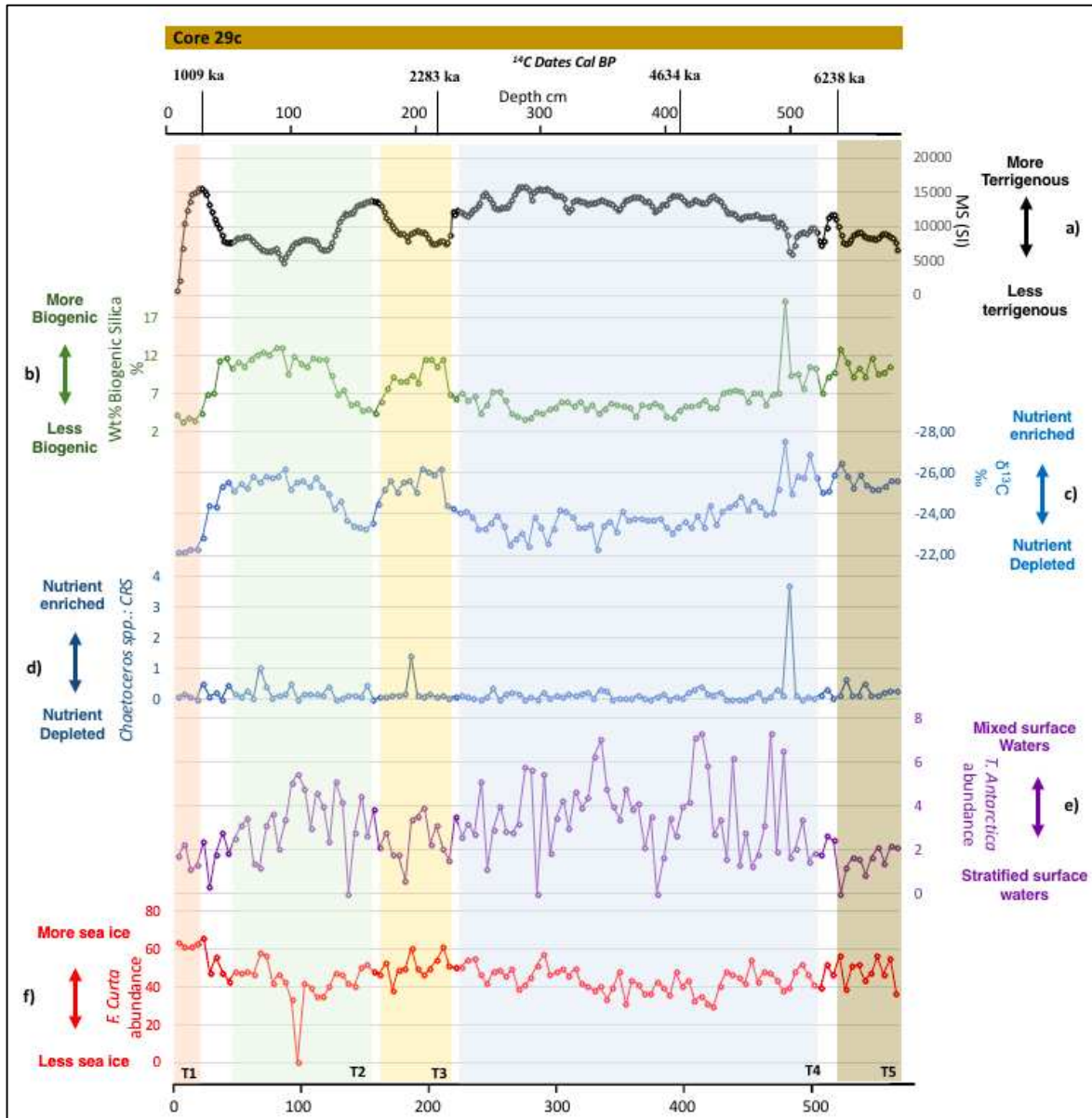


Figure 5.23: Holocene environmental trends in Robertson Bay core 29c highlighting environmental transitions ((T5, 17,000 – 6,200; T4 6,200, 2,200 – T3 2,200 – 2,000; T2 2,000 – 1,000 and T1 from 1000 yr BP to present day). (a) Magnetic susceptibility (MS), proxy for terrigenous flux. (b) Wt% BSi, proxy for biogenic flux, interpreted as a proxy for primary production. (c) $\delta^{13}\text{C}$, proxy for water column structure. (d) Ratio of *Chaetoceros* spp. / *Chaetoceros* resting spores (CRS), a proxy for nutrient availability in surface waters. (e) Relative abundance of *T. antarctica*, a proxy for water column structure. (f) Relative abundances of *F. curta*, a proxy for sea ice duration.

5.6.3 Robertson Bay post -LGM evolution

Variations in wt% BSi and $\delta^{13}\text{C}$ in the Robertson Bay sedimentary record reflect changes in both the isotopic composition ($\delta^{13}\text{C}$) and the nutrient concentration of surface waters.

Nutrient concentrations and $\delta^{13}\text{C}$ in Robertson Bay reflect variations in stratification which is affected by the strength of the katabatic winds inferred to drive water masses circulation such as the AASW, SW, and mCDW along the Antarctic slope front (ASF) (Miles et al., 2016; Schmidtko et al., 2014; Spence et al., 2014). Diatom species are sensitive to changes in sea ice, stratification, and nutrient concentration; thus, changes in the diatom assemblage can be used to differentiate between sea ice, stratification, and a water mass signal (Armand et al., 2005).

Deglacial Phase to Early Holocene

After ~17.6 ka when the onset of the reopening of the bay after LMG takes place, the **transition T6** (between ~17.6 ka and the Early Holocene) (Fig. 5.26) shows an increase in wt% BSi and ADA (primary productivity) and low MS (terrigenous input) and $\delta^{13}\text{C}$ (enrichment of nutrients and stratified surface water) and a more gradual shift in the sedimentary grain size.

In core BAY05_32c the end of the more intense glacial cover phase (LGM) was marked by a silty sand layer level (*Silty sandy facies with pebbles and IRD (SSpf)* (Unit 2) overlying the *glaciomarine diamicton facies (GmDf)*, which corresponded to the first deglacial phase, when the ice sheet detached from the seabed near the continental shelf edge and the oceanic current reactivated inside the bay.

The **transition T5** (between the Early Holocene and ~ 6 ka) (Fig 5.25, 5.26) shows the same trend in wt% BSi and ADA curves but with an increase in MS and $\delta^{13}\text{C}$.

This transition is marked by an increase in seasonal sea ice diatom species (*F. curta*, *F. obliquecostata*), and by an increased of the calving of icebergs (IRD level) and the bloom of the *Chaetoceros* resting spores species > 40% with a peak just above the diamicton facies (*GmDf*) (approximately 17.6 ka) (fig 5.21), representing a higher hydrodynamic regime. I presume that oceanic and continental shelf hydrological features evolved in this phase, leading to the establishment of seasonal sea ice cycles, cold and salty waters production (HSSW) and consistent mCDW input in Robertson Bay (Miles et al., 2016; Schmidtko et

al., 2014; Spence et al., 2014) after the retreat of the calving front of the Ross Sea Ice Shelf and the establishment of a more stratified water column.

Mid Holocene - Neoglacial

Transition T4 (from ~ 6.2 to ~ 2.2 ka in core 29c) (Fig 5.22) shows a decrease in primary productivity with lower values of wt% BSi and ADA and an increase in MS (terrigenous input) and $\delta^{13}\text{C}$. This reflects a nutrient depleted surface water. The lower abundance of *Chaetoceros spp./CRS* indicates an interruption of the stratification and the high abundance of *T. antarctica* reflects a well-mixed surface water.

This thesis proposes a decreased mCDW presence on the continental shelf during this phase with a weaker ocean masses circulation and a shorter sea ice free summer season. This hypothesis would justify the higher abundance of *F. curta* and would be consistent with the hypothesis of a general cooling trend.

In core 32c transition T4 shows the same geochemical pattern but in this case, we have an inversion date that does not allow to constrain an accurate age range.

Late Holocene

The Late Holocene can be divided into two different transitions: Across **Transition T3** (between 2.2 ka and 1.9) and **transition T2** (between ~ 2.0 and 1.0 ka) (Fig 5.22, 5.23) wt% BSi increase with a concomitant decline in $\delta^{13}\text{C}$ and MS. Depleted $\delta^{13}\text{C}$ and increased productivity during this interval is consistent with decreased stratification (increased surface wind stress and water column mixing). Increased abundance of *T. antarctica* indicates that the water column in Robertson Bay was well mixed and influenced by upwelling mCDW during the interval relative to the period between 2.0 and 1.9 ka (Denis et al., 2010). The ratio of *Chaetoceros spp.* and CRS is also consistent with inferred nutrient enrichment of surface waters (Leventer, 1992). A decline in *F. curta* from ~50% to ~40% indicates that sea ice was less prevalent in Robertson Bay (warmer period).

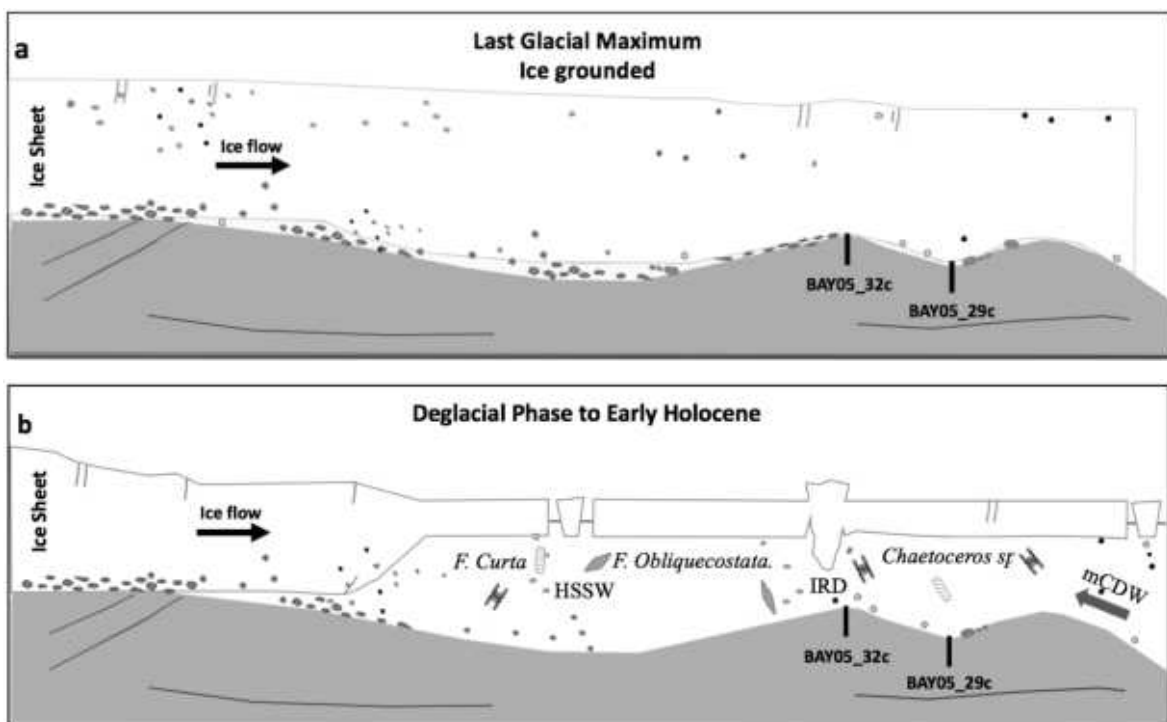
Marine reconstructions from Adélie Land and the Ross Sea also record resurgence of mid-Holocene-like conditions (Denis et al., 2009). The interval between 2.4 and 1.5 ka is associated with a decrease in sea ice extent, and increase in productivity, glacial meltwater, and stratification in marine records from Adélie Land (Johnson et al 2021; Ashley et al 2021; Newton, 2015; Panizzo et al., 2014; Crosta et al., 2007, Denis et al., 2009). In the Ross Sea,

a decrease in coastal sea ice extent and polynya efficiency occurs concomitant with terrestrial records that indicate warming (Mezgec et al., 2017).

Transition T1 (1.0 ka to Present). Between 1.0 ka to Present (Fig 5.22, 5.23), lower primary production and rising abundance of *F. curta* in Robertson Bay indicates increasing sea ice extent. The total absence of both *Chaetoceros* spp. and CRS, lower wt% BSi, and increased $\delta^{13}\text{C}$ also indicate a stratified environment associated with nutrient limitation in the surface layer. High $\delta^{13}\text{C}$ in Robertson Bay during the late Holocene may also indicate that decreased mCDW presence on the continental shelf after 258 cal yr BP.

After the contraction of the Ross Sea polynya at ~1.0 ka, increased sea ice extent and colder conditions persisted in the Ross Sea up to the modern period (Mezgec et al., 2017).

Records from ice in cores from eastern Victoria Land, East Antarctica (Talos Dome, Taylor Dome, and Mt. Erebus Saddle) and West Antarctica (Siple Dome) also indicate increased sea ice production and katabatic wind intensity (Bertler et al., 2011; Kreutz et al., 1998; Mezgec et al., 2017; Rhodes et al., 2012). Late-Holocene cooling, associated with decreased primary productivity, may also have occurred on the Antarctic Peninsula beginning at ~700 cal yr BP (Domack et al., 2001).



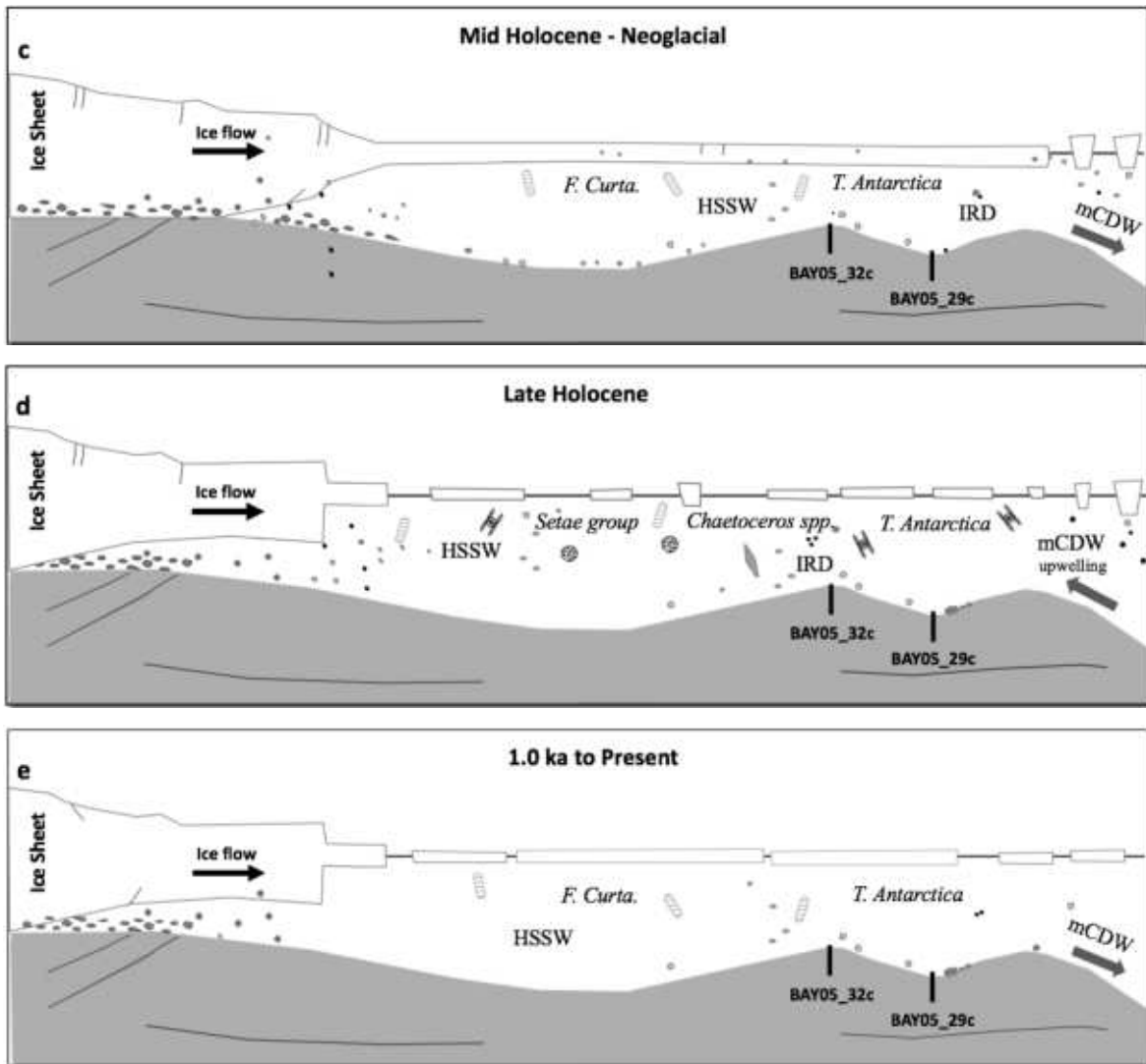


Figure 5.24: Proposed palaeoenvironmental evolution model. a. Advanced glacial phase (LGM) with total covering from ice shelf, grounded in Robertson Bay. b. Transitional phase from glacial to interglacial environment (transition T6 and T5) with seasonal sea ice conditions with high productivity of diatom blooms and consistent mCDW input. The arrows represent intrusion of mCDW current. c. A Mid Holocene – Neoglacial phase with more sea ice and (general cooling trend) with well-mixed surface water and a decrease of the mCDW (Transition T4). d. A Late Holocene phase of seasonal sea ice conditions with high productivity of seasonal diatom blooms and water column mixing influenced by upwelling mCDW (Transition T3). e. From 1.0 ka to Present, lower primary production and increased sea ice extent and colder conditions with decrease of the mCDW (Transition T1).

5.7 Conclusions

Reconstruction of the paleo-glaciomarine environment

Some inferences concerning sedimentary environment can be made from the marine geology and glacial landforms of Robertson Bay.

Geomorphic features present in Robertson Bay were identified, mapped in detail, and interpreted in order to reconstruct ice sheet configuration since the LGM, and to define ice flow style and streaming activity.

During the LGM, an ice sheet covered the region with grounded ice, extending out to the shelf break off of Robertson Bay. During this and perhaps previous glaciation, the bedrock was scoured by the ice streams (glacial lineations) with steep slope ridges (fig. 5.8, 5.9.).

The bay is not regular, but it is divided in three basins: the inner basin (up to 506 meters deep) is separated from the mid depression by a sill (Sill 2), at depth of 370. The mid-basin reaches a depth of 533 m and is separated by the outer basin by a sill (Sill 1) at 350 m respectively. The outermost basin is 525 m deep (fig. 5.7)

The thickness of the well-stratified sequence (seismic facies 1) averages between 3 and 10 m in the sector 1, but evidences of a higher sedimentation rate are noted in the sector 2 (fig 5.15 d) with thickness up to 75 m, while the thickness of the opaque facies with weak internal stratification (seismic facies 2) averages between 3 and 50 m based on the interpretation of the SBP profile and the two sediment cores 29c and 32c (fig 5.14) this is indicating that the postglacial sedimentation has been dominated by hemipelagic sedimentation as well as into Edisto Inlet Fjord.

Even though we were not able to extrapolate the sedimentation rate in Robertson Bay, initiation of these sequences deposition is estimated to be around 17.6 ka based on AIO radiocarbon dating.

During deglaciation the ice sheet retreated through Robertson Bay depositing lateral and frontal recessional moraines.

As climate conditions became warmer with resultant sea-level rise, stratified hemipelagic mud accumulated, draping over the deep basins.

The occurrence of ice proximal or sub-ice-shelf, glaciomarine diamicton at the base of the core 32c dated to 17.6 ka makes it possible to postulate that the subglacial till is clearly older.

This would mean that Robertson Bay was ice covered during the LGM at least until 17.6 ka ago. As the tidewater glacier retreated landward, the bay experienced a marine transgression. During this period, subglacial meltwater streams may have been present at the ice front. As glaciers continue to retreat, energy conditions became lower in response to increasing distance to the tidewater glaciers. Consequently, pebbly mud accumulated at the results of both vertical settling of mud and from overflow plumes and deposition of gravel from drifting icebergs (Unit 2). Sediment-laden melt water plumes from the streams deposited interlaminated sand and mud (Unit 3) by rapid suspension settling. During this time the glacier was likely ablated by active calving dumping gravel, and other sediment into Unit 4

Marine Proxy data reconstruction

The Holocene paleoenvironment of Robertson Bay is reconstructed using geochemical and physical proxies for primary productivity (wt% BSi, $\delta^{13}\text{C}$) relative terrigenous contribution (MS); terrigenous source (grain size); and oceanography ($\delta^{13}\text{C}$). These interpretations are complemented by supporting evidence from unpublished diatom abundance and assemblage data provided by F. Torricella. The work on diatoms is still under revision and for this reason is not presented here.

Holocene surface water conditions are recorded in the sedimentary record by biogenic sediments. In most Antarctic sedimentary environments, stratification is associated with increased primary productivity; however, in core BAY05_29c and BAY05_32c, wt% BSi, ADA, MS, and $\delta^{13}\text{C}$ co-vary with maxima in the MS and $\delta^{13}\text{C}$ records corresponding to minima in the wt% BSi and ADA records. Therefore, stratification (high $\delta^{13}\text{C}$, low *Chaetoceros spp.* relative to CRS) co-occurs with lower biogenic flux (wt% BSi).

In Robertson Bay, the ecological benefits of stratification appear to be outweighed by associated nutrient limitation in the surface layer. Thus, periods of higher primary production are linked to a continually refreshed $\delta^{13}\text{C}$ reservoir in the surface ocean layer by either increased water masses circulation or increased presence of nutrient-rich mCDW on the continental shelf at the mouth of Robertson Bay. Periods of enhanced mCDW inflow and mixing result in an upwelling-associated diatom assemblage, increased primary

productivity, and more negative bulk sedimentary $\delta^{13}\text{C}$ values because both mixing and mCDW refresh the surface reservoir of ^{12}C and nutrients.

The same paleoenvironmental transitions were recognized in both cores and divided into six phases from the post LGM (deglaciation phase) to the early Holocene (T1 to T6) closely related to the dynamics of the Ross ice shelf and to the regional oceanographic and ice-affected environments.

[a] Advanced glacial phase (LGM) with total coverage by the ice shelf, grounded on the bay (fig.5.24 a)

[b] Deglacial Phase to Early Holocene - Transition T6 (between ~17.6 ka and the Early Holocene) (Fig. 5.23) shows an increase in wt% BSi and ADA (primary productivity) and low MS (terrigenous input) and $\delta^{13}\text{C}$ (enrichment of nutrients and stratified surface water). **Transition T5** (between the Early Holocene and ~ 6.2 ka) (Fig 5.22, 5.23) shows the same trend in wt% BSi and ADA curves but with an increase in MS and $\delta^{13}\text{C}$.

This transition marked by seasonal sea ice diatom species (*F. curta*, *F. obliquecostata*), increased together with the calving of icebergs (IRD level) and the bloom of the *Chaetoceros* resting spores species represents a higher hydrodynamic regime.

It is considered a deglacial phase during which the hydrodynamic situation restored with the influence of the mCDW, which gradually expanded over the continental slope, and the formation of HSSW on the continental shelf (fig.5.24 b).

[c] Mid Holocene Transition T4 (between ~ 6.2 ~ 2.2 ka) (Fig 5.25, 5.26) shows a decrease in primary productivity with lower values of wt% BSi and ADA and an increase in MS (terrigenous input) and $\delta^{13}\text{C}$. During the mid-Holocene, more positive $\delta^{13}\text{C}$ values and lower primary productivity in Robertson Bay are attributed to inhibited mCDW inflow and nutrient limitation in the surface layer (fig.5.24 c)

Marine sedimentary records from Adélie Land (Crosta et al., 2007), the Ross Sea (Mezgec et al., 2017), and the Antarctic Peninsula (Leventer et al., 2002; Taylor and Sjunneskog, 2002) indicate that the mid-Holocene was a climatic optimum associated with stratification, high primary productivity, and decreased sea ice extent. Inferred nutrient limitation and

decreased presence of mCDW in Robertson Bay during the mid-Holocene is interpreted to be the result of an enhanced regional oceanographic conditions.

[d] Late Holocene -Transition T3 (between 2.2 and 1.9 ka) and **Transition T2** (between 1.9 and 1.0 ka) (Fig 5.22, 5.23) mark increased primary production and more negative in $\delta^{13}\text{C}$ are interpreted to indicate a decreased stratification and an increased surface water column mixing. Nutrient-rich surface waters in Robertson Bay are interpreted to reflect increased presence of mCDW on the continental shelf in East Antarctica (fig.5.24 d).

[e]Transition T1 (1.0 ka to Present) (Fig 5.22, 5.23) lower primary production and increased $\delta^{13}\text{C}$ indicate a stratified environment associated with nutrient limitation in the surface layer, decreased mCDW presence on the continental shelf rising abundance of *F. curta* in Robertson Bay indicates increasing sea ice extent. Colder conditions persisted in the Ross Sea from 1000 ka into the modern period (fig.5.24 e).

Chapter 6

6. CONCLUSIONS

Models on continental-scale reconstructions of the Antarctic ice sheet (AIS) retreat during the last deglaciations (Golledge et al 2021) show that the AIS experienced substantial changes after the Last Glacial Maximum (LGM, ~21 kiloyears ago, ka). In the Ross Sea, where the ice sheet mostly advanced up to the continental shelf edge (Bentley et al 2014), the deglacial history remains, however, still debated. In this sector, the ice sheet grounds below sea level (Leong et al 2020) and as such, it is sensitive not only to atmospheric warming, but also to oceanic warming (Lowry et al., 2020). Compilations of marine data indicate that the retreat was not contemporaneous between the Eastern (early retreat, Bart et al 2018) and the Western Ross Sea (e.g. Halberstad et al., 2016), with periods of grounding-line stability interrupted by episodes of rapid retreat. This has generally been attributed to differences in pinning areas in the seafloor bathymetry (e.g. Anderson et al., 2019). In the Western Ross Sea, marine data suggest that by 15 ka, the ice sheet had largely retreated (Prothro, 2020). But the grounding line position along the coasts of Victoria Land is unknown and tentatively located offshore until about 8-4 ka (Prothro, 2020).

To fill this knowledge gap I studied two coastal bays of North Victoria Land (NVL) as ideal environments where to retrieve highly resolved archives as they act as natural sediment traps. Rapid and high sediment accumulation have, indeed, been observed in other Antarctic fjords and coastal bays (Sjunneskog et al., 2002; Rebesco et al., 1998; Cunningham et al., 1999; Domack et al., 1999; 2001; Domack et al 2003; Mosola and Anderson, 2006; McGlannan et al., 2017, Escutia et al., 2014; Munoz, Y. P., & Wellner, J. S. (2016), Crosta et al 2021, Asley et al., 2020) where tidewater glaciers are debouching and carving deeply the fjord sea floor during ice expansions.

6.1 Edisto Inlet Fjord

In this thesis I report the southernmost, first evidence of an expanded, ultrahigh resolution, Holocene sedimentary section in Antarctica, deposited in the Edisto Inlet fjord (NVL), to advance the knowledge about post-LGM - AIS retreat from the western Ross Sea. Multibeam bathymetry and echosounding subbottom data, combined with geological records and present-day oceanographic measurements document that the most of the post-LGM sedimentation has been influenced by the deposition of biogenic material (mainly diatom ooze), locally redistributed by bottom water currents. The interplay of high sediment rate due to high productivity and of fjord-type persistent circulation, resulted in the formation of confined drifts-moats and in the accumulation of an up to 130 meters thick sedimentary section in the inner part of the fjord. This analysis shows that the sediment drift in the central sectors of the fjord have remained undisturbed since at least 11 ka. I infer that the fjord was not carved by grounding ice since the Holocene Climatic Optimum, and that glaciers remained mostly terrestrial. The continuous deposit of diatom ooze suggests seasonal sea ice free conditions, with regular warm water intrusions supporting that the NVL coastal glaciers retreated by ca. 11 ka. This would discount the occurrence of expanded grounding ice over the north western Ross Sea continental shelf after the Holocene Climatic Optimum.

The Holocene sedimentary section (130 m) in central sector of the Edisto fjord is very similar to that one found in the Adélie Basin where the sediment accumulation has been particularly high (averaging 2 cm/y) after the Last Glacial Maximum (Denis et al., 2009) as documented by the IODP site U1357 (Escutia et al., 2011). Here the thick (183 m) Holocene sedimentary section above the last glacial diamicton deposited since 10,000 y.

6.2 Robertson Bay

In Robertson Bay I developed a conceptual model of paleoenvironmental evolution of the processes that drove environmental changes during the Holocene integrating geophysical and geological data with geochemical proxies for primary productivity (weight percent biogenic silica, wt% BSi, absolute diatom abundance (ADA); relative terrigenous contribution (magnetic susceptibility MS); terrigenous source (grain size); oceanography

($\delta^{13}\text{C}$); My results are complemented with absolute diatom abundance (ADA) and diatom assemblage analysis performed by another PhD student (under revision).

I reported the first geophysical characterization and morphologic mapping of the bay compared radiocarbon dates with a lithological and geochemical proxy to provide a first-order constraint of ice sheet retreat in the western Ross Sea. The glacio-marine diamicton dated 17.6 ka at the base of core 32c suggests that the ice expanded into Robertson Bay during the LGM, but ice was not grounding in the middle of the bay after that time. This hypothesis is based on a shift in the depositional environment from a glaciomarine diamicton facies (*GmDf*) to silty sandy facies with pebbles and IRD (*SSpf*).

Paleoenvironmental transitions were recognized in the two sediment cores studied in the Bay and divided into six phases from the post LGM (deglaciation phase) to the early Holocene (T1 to T6) closely related to the dynamics of the Ross ice shelf and to the regional oceanographic and ice-affected environments.

- a) Glacial phase (LGM) with the occurrence of floating and grounding ice in the inner sector of the Robertson Bay
- b) Transitional phase from glacial to interglacial environment (transition T6 and T5) with seasonal sea ice conditions, high productivity of diatom blooms and incursion of mCDW in the Bay.
- c) A Mid Holocene – Neoglacial phase with more sea ice (cooling trend) and a decrease of the mCDW influence (transition T4)
- d) A Late Holocene phase of seasonal sea ice conditions with high productivity of seasonal diatom blooms and water column mixing influenced by mCDW (transition T3)
- e) From 1.0 ka to Present, lower productivity and increased sea ice extent and colder conditions with decrease of the mCDW influence (Transition T1).

In Robertson Bay the postglacial sedimentation has been characterised by hemipelagic sedimentation as well as into Edisto Inlet Fjord. However, the Holocene record in Robertson Bay is less expanded than in the Edisto Inlet Fjord or in the Adelie Basin.

Edisto Inlet and the Adelie Basin are confined protected areas with a slow circulation, while Robertson Bay's is a wider bay more exposed to ocean current. Elongated and confined sediment drift features have been recognized in Robertson bay, like in the Edisto Fjord. However, the lack of oceanographic measurement series do not allow to compare the

location of the sediment drift with modern circulation and water masses distribution in the Bays.

The high-resolution marine sediments paleoclimatic records revealed significant variations in the extent and duration of sea ice cover and in primary productivity from the Early Holocene to present.

6.3 Evolution post LGM: comparison between Edisto Inlet fjord and Robertson Bay

During the peak of the glaciation, the glaciers in both bays advanced, merged and flowed across the bays, as evidenced by the glacial landforms found on the seabed.

The retreat phase of the glaciers in Edisto Inlet fjord occurred between the LGM and about ~11 ka while in Robertson Bay it took place between the LGM and 17.6 ka. This is based on the radiocarbon dates of sediments lying above the diamicton facies in the cores BAY05_18c (Edisto Bay) and BAY05_32c (Robertson Bay) and the seismic facies. There is no evidence of glaciers re-advance, e.g. post-LGM grounding-zone wedges. I therefore deduce that the retreat could have been gradual with a progressive glacier thinning, without any stationary or ice re-advancing phases. The grounding ice retreat with no floating ice and open water circulation establishment in Edisto Inlet occurred about 11 ka ago, while in Robertson Bay during the Early Holocene deglaciation phase glaciers front was floating.

In Edisto Inlet the deposition of the massive sediment (*MB-f*, whose base is dated at 7.2 ka in BAY05-18c) indicate a cooling event.

In Robertson Bay a change to a higher hydrodynamic regime occurred at ~ 6.0 ka. Based on geochemical proxies I presume that oceanic and continental shelf hydrological condition evolved in this phase, leading to the establishment of seasonal sea ice cycles, with cold and salty water production (HSSW) and with more mCDW incursion into the bay.

The T4 transition appears to be characterised by a general cooling in the Robertson bay core data. This assumption is based on decrease in primary productivity (BSi and ADA) and an increase in terrigenous input (MS) and $\delta^{13}\text{C}$. This reflects a nutrient depleted surface water. My hypothesis is consistent with a decreased mCDW presence on the continental shelf during this phase with a weaker ocean masses circulation and a shorter ice free summer season.

In the Late Holocene between 2.2 and 1.6 ka the water column in Robertson Bay was well mixed and influenced by upwelling mCDW during this interval and sea ice was less prevalent suggesting a warmer period.

From 1.0 ka to present, there has been an increase in sea ice and lower primary production associated with nutrient limitation in the surface layer. A high $\delta^{13}\text{C}$ in Robertson Bay may also indicate a decrease in the presence of mCDW on the continental shelf after 1.0 ka.

Increased sea ice extent and colder conditions persisted in the Ross Sea to the modern period are consistent with other ice core records from East Victoria Land, East Antarctica (Talos Dome, Taylor Dome, and Mt. Erebus Saddle) and West Antarctica (Siple Dome) which also indicate increased sea ice production and katabatic wind intensity (Bertler et al., 2011; Kreutz et al., 1998; Mezgec et al., 2017; Rhodes et al., 2012).

This is a first reconstruction based on the available data on the two bays, but I expect the Ramped Pyrolysis dating to return younger ages than those measured on AIOM, so when all ages are finalized this paleoenvironmental reconstruction could be revised.

These results obtained in the Edisto Inlet Fjord and Robertson Bay will then be compared with the results of the thesis obtained by two other PhD students F. Torricella (University of Pisa) and Olivia Truax (University of Otago) (still ongoing) focusing on diatom paleoecology and paleoceanographic reconstruction in the same region.

This will help to better understand the role played by subglacial and seafloor morphology in influencing ice circulation and dynamics, and thus the interaction between ocean and ice sheet during the transition from glaciers to interglacials.

6.4 Forward look

The geological perspective provided by the results obtained by this thesis are an important framework for future sediment coring and investigation on climate models that seek to predict dynamic of small glaciers system. Such unique expanded paleoclimate and palaeoceanographic record, in combination with the Adelie Deep similar record, and in comparison, with Talos Dome ice core can help to understand how the polar southern hemisphere system reacts to rapid climatic impulses such as those occurring during

meltwater pulses. This will also provide insight into how Victoria Land's glaciers are in phase with other regions of the Antarctic ice sheet in response to regional and global climate change.

This work has demonstrated that a good knowledge on regional ice and ocean dynamics will allow to reconstruct the different response of the ice sheet perimeter to climate variability. It is necessary to sample further sites in both regions and along longitudinal transects in order to understand to what extent of confidence our paleoenvironmental interpretations can be extrapolated on a spatial and longer time scale and what will be the impact of climate teleconnection variability from low to high latitude. Such kind of data set are needed to estimate polar amplification of global climate changes.

There is a need for new radiocarbon dating to overcome the problem of dating reversals and to have a more accurate age depth model. The occurrence of tephra and cryptotephra have been reported from both the Edisto and from the Robertson bay sediments (Di Roberto and Torricella personal communication). Future work on the volcanic component will then shed further light into age model and provenance of the clastic material.

The geophysical and geomorphological study carried out on the Edisto Inlet fjord and Robertson Bay provides a crucial baseline for interpreting the sediment core records, consistently with the morphological setting and ocean circulation. Correct and detailed quantitative analysis provided by such multidisciplinary studies are needed to constrain modelling of paleo-ice streams and outlet glaciers dynamics. The systematic mapping of submarine landforms in sparsely mapped areas such as the bays along the North Victoria Land should be the focus of future studies in order to provide robust databases for analysing and understanding the past history dynamics of marine-based ice sheets.

7. Bibliography

- Aario, R. (1977). Associations of flutings, drumlins, hummocks and transverse ridges. *GeoJournal*, 1(6), 65-72.
- Ablain, M., Legeais, J. F., Prandi, P., Marcos, M., Fenoglio-Marc, L., Dieng, H. B., ... & Cazenave, A. (2017). Satellite altimetry-based sea level at global and regional scales. In *Integrative study of the mean sea level and its components* (pp. 9-33). Springer, Cham.
- Ackley, S. F., & Sullivan, C. W. (1994). Physical controls on the development and characteristics of Antarctic sea ice biological communities— a review and synthesis. *Deep Sea Research Part I: Oceanographic Research Papers*, 41(10), 1583–1604. [https://doi.org/10.1016/0967-0637\(94\)90062-0](https://doi.org/10.1016/0967-0637(94)90062-0)
- Adie, R.J. (1962). The Geology of Antarctica. In *Antarctic Research: The Matthew Fontaine Maury Memorial Symposium* (eds W.E. Smith, H. Wexler, M.J. Rubin and J.E Caskey). <https://doi.org/10.1029/GM007p0026>
- Ainley, D. G. (2002). The Ross Sea, Antarctica, where all ecosystem processes still remain for study, but maybe not for long. *Marine Ornithology*, 30, 55-62.
- Alley R.B., Blankenship D.D., Rooney S.T., Bentley C.R. (1989), Sedimentation beneath ice shelves - the view from ice stream B., *Marine Geology*, vol. 85, pp. 101-120.
- Alley R.B., Whillans I.M. (1991), Changes in the West Antarctic Ice Sheet, *Science*, vol. 254, pp. 959-963, DOI: 10.1126/science.254.5034.95
- Alley, R. B., Anandakrishnan, S., Christianson, K., Horgan, H. J., Muto, A., Parizek, B. R., ... & Walker, R. T. (2015). Oceanic forcing of ice-sheet retreat: West Antarctica and more. *Annual Review of Earth and Planetary Sciences*, 43, 207-231.
- Alley, R. B., Cuffey, K. M., Evenson, E. B., Strasser, J. C., Lawson, D. E., & Larson, G. J. (1997). How glaciers entrain and transport basal sediment: physical constraints. *Quaternary Science Reviews*, 16(9), 1017-1038.
- Alley, R. B., Mayewski, P. A., Sowers, T., Stuiver, M., Taylor, K. C., & Clark, P. U. (1997). Holocene climatic instability: A prominent, widespread event 8200 yr ago. *Geology*, 25(6), 483-486.
- Altabet M.A., Francois R. (1994) The Use of Nitrogen Isotopic Ratio for Reconstruction of Past Changes in Surface Ocean Nutrient Utilization. In: Zahn R., Pedersen T.F., Kaminski M.A., Labeyrie L. (eds) *Carbon Cycling in the Glacial Ocean: Constraints on the Ocean's Role in Global Change*. NATO ASI Series (Series I: Global Environmental Change), vol 17. Springer, Berlin, Heidelberg. https://doi.org/10.1007/978-3-642-78737-9_12
- Amante C, Eakins BW. ETOPO11 arc-minute global relief model: Procedures, data sources and analysis. NOAA Technical Memorandum NESDIS NGDC-24. Boulder, CO, USA: National Geophysical Data Center; 2009. DOI: 10.7289/V5C8276M
- Anderson et al., 1980a J.B. Anderson, D.D. Kurtz, E.W. Domack, K.M. Balshaw Glacial and glacial marine sediments of the Antarctic Continental shelf *J. Geol.*, 88 (1980), pp. 399-414
- Anderson et al., 1980b J.B. Anderson, E.W. Domack, D.D. Kurtz Observations of sediment laden icebergs in Antarctic waters: Implications to glacial erosion and transport *J. Glaciol.*, 25 (1980), pp. 387-396
- Anderson et al., 1982 J.B. Anderson, D. Kurtz, F. Weaver, M. Weaver Sedimentation on the West Antarctic Continental Margin C. Craddock (Ed.), *Antarctic Geoscience*, Univ. of Wisconsin Press, Madison, Wisc (1982), pp. 1003-1012

- Anderson, J. B., Conway, H., Bart, P. J., Witus, A. E., Greenwood, S. L., McKay, R. M., ... & Stone, J. O. (2014). Ross Sea paleo-ice sheet drainage and deglacial history during and since the LGM. *Quaternary Science Reviews*, 100, 31-54.
- Anderson, J. B., Simkins, L. M., Bart, P. J., De Santis, L., Halberstadt, A. R. W., Olivo, E., & Greenwood, S. L. (2019). Seismic and geomorphic records of Antarctic Ice Sheet evolution in the Ross Sea and controlling factors in its behaviour. *Geological Society, London, Special Publications*, 475(1), 223-240.
- Anderson, J. B., Warny, S., Askin, R. A., Wellner, J. S., Bohaty, S. M., Kirshner, A. E., ... & Majewski, W. (2011). Progressive Cenozoic cooling and the demise of Antarctica's last refugium. *Proceedings of the National Academy of Sciences*, 108(28), 11356-11360.
- Anderson, J. B.: *Antarctic Marine Geology*, Cambridge University Press, New York, (1999).
- Anderson, J.B., Shipp, S., Lowe, A., Wellner, J.S., Mosola, A.B. (2002). The Antarctic Ice Sheet during the Last Glacial Maximum and its subsequent retreat history: a review. *Quat. Sci. Rev.*, 21, 49–70.
- Anderson, J.B.; Conway, H.; Bart, P.J.; Witus, A.E.; Greenwood, S.L.; McKay, R.M.; Hall, B.L.; Ackert, R.P.; Licht, K.; Jakobsson, M. Ross Sea paleo-ice sheet drainage and deglacial history during and since the LGM. *Quat. Sci. Rev.* (2014), 100, 31–54. [CrossRef]
- André, M.F. (2017), Ice Sheets. *International Encyclopedia of Geography: People, the Earth, Environment and Technology*, pp. 1–5. doi:10.1002/9781118786352.wbieg0819
- Andresen, C.S., Straneo, F., Ribergaard, M.H., Bjørk, A.A., Andersen, T.J., Kuijpers, A., Nørgaard-Pedersen, N., Kjær, K.H., Schjøth, F., Weckström, K., Ahlstrøm, A.P. (2011). Rapid response of Helheim Glacier in Greenland to climate variability over the past century. *Nat. Geosci.*, 5, 37–41. doi:10.1038/ngeo1349
- Andrews, J. T., E. W. Domack, W. L. Cunningham, A. Leventer, K. J. Licht, A. Jull, D. J. Demaster, and A. E. Jennings (1999), Problems and possible solutions concerning radiocarbon dating of surface marine sediments, Ross Sea, Antarctica, *Quat. Res.*, 52(2), 206– 216.
- Andrews, J. T., Stein, R., Moros, M., & Perner, K. (2016). Late Quaternary changes in sediment composition on the NE Greenland margin (~ 73 N) with a focus on the fjords and shelf. *Boreas*, 45(3), 381-397.
- Archer, D., & Brovkin, V. (2008). The millennial atmospheric lifetime of anthropogenic CO₂. *Climatic Change*, 90(3), 283-297.
- Archer, D., Eby, M., Brovkin, V., Ridgwell, A., Cao, L., Mikolajewicz, U., ... & Tokos, K. (2009). Atmospheric lifetime of fossil fuel carbon dioxide. *Annual review of earth and planetary sciences*, 37, 117-134.
- Armand Nees, S., L., De Deckker, P., Labracherie, M., & Passlow, V. (1999). A diatom and benthic foraminiferal record from the South Tasman Rise (southeastern Indian Ocean): implications for palaeoceanographic changes for the last 200,000 years. *Marine Micropaleontology*, 38(1), 69-89.
- Armand, L. K., & Zielinski, U. (2001). Diatom species of the genus *Rhizosolenia* from Southern Ocean sediments: distribution and taxonomic notes. *Diatom Research*, 16(2), 259-294.
- Armand, L. K., Crosta, X., Romero, O., & Pichon, J. J. (2005). The biogeography of major diatom taxa in Southern Ocean sediments: 1. Sea ice related species. *Palaeogeography, Palaeoclimatology, Palaeoecology*, 223(1-2), 93-126.
- Arndt, J. E., Schenke, H. W., Jakobsson, M., Nitsche, F. O., Buys, G., Goleby, B., ... & Wigley, R. (2013). The International Bathymetric Chart of the Southern Ocean (IBCSO) Version 1.0—A new bathymetric compilation covering circum-Antarctic waters. *Geophysical Research Letters*, 40(12), 3111-3117.

- Arnold, J. R., & Libby, W. F. (1949). Age Determinations by Radiocarbon Content: Checks with Samples of Known Age. *Science*, 110(2869), 678–680. <http://www.jstor.org/stable/1677049>
- Arrigo, K. R., Dunbar, R. B., Lizotte, M. P., & Robinson, D. H. (2002). Taxon-specific differences in C/P and N/P drawdown for phytoplankton in the Ross Sea, Antarctica. *Geophysical Research Letters*, 29(19), 44-1.
- Arrigo, K. R., Mills, M. M., Kropuenske, L. R., van Dijken, G. L., Alderkamp, A. C., & Robinson, D. H. (2010). Photophysiology in two major Southern Ocean phytoplankton taxa: photosynthesis and growth of *Phaeocystis antarctica* and *Fragilariopsis cylindrus* under different irradiance levels. *Integrative and Comparative Biology*, 50(6), 950-966.
- Arrigo, K. R., van Dijken, G. L., and Bushinsky, S. (2008), Primary production in the Southern Ocean, 1997–2006, *J. Geophys. Res.*, 113.
- Ashley, G. M., & Smith, N. D. (2000). Marine sedimentation at a calving glacier margin. *Geological Society of America Bulletin*, 112(5), 657-667.
- Ashley, K. E., McKay, R., Etourneau, J., Jimenez-Espejo, F. J., Condrón, A., Albot, A., ... & Bendle, J. A. (2021). Mid-Holocene Antarctic sea-ice increase driven by marine ice sheet retreat. *Climate of the Past*, 17(1), 1-19.
- Assmy, P., Smetacek, V., Montresor, M., Klaas, C., Henjes, J., Strass, V. H., ... & Wolf-Gladrow, D. (2013). Thick-shelled, grazer-protected diatoms decouple ocean carbon and silicon cycles in the iron-limited Antarctic Circumpolar Current. *Proceedings of the National Academy of Sciences*, 110(51), 20633-20638.
- Bamber J.L., Vaughan D.G., and Joughin I. (2000), Widespread Complex Flow in the Interior of the Antarctic Ice Sheet, *Science*, vol. 287, pp. 1248-1250.
- Bamber, J. L., Oppenheimer, M., Kopp, R. E., Aspinall, W. P., & Cooke, R. M. (2019). Ice sheet contributions to future sea-level rise from structured expert judgment. *Proceedings of the National Academy of Sciences*, 116(23), 11195-11200.
- Banwell, A. F., MacAyeal, D. R., & Sergienko, O. V. (2013). Breakup of the Larsen B Ice Shelf triggered by chain reaction drainage of supraglacial lakes. *Geophysical Research Letters*, 40(22), 5872-5876.
- Banwell, A. F., Willis, I. C., Macdonald, G. J., Goodsell, B., & MacAyeal, D. R. (2019). Direct measurements of ice-shelf flexure caused by surface meltwater ponding and drainage. *Nature communications*, 10(1), 1-10.
- Baradello, L. (2014) An improved processing sequence for uncorrelated Chirp sonar data. *Marine Geophysical Volume 35* (4), pp 337-344.
- Baradello, L., Battaglia, F. & Vesnaver, A. Fast method to transform chirp envelope data into pseudo-seismic data. *Mar Geophys Res* 42, 14 (2021).
- Barbara, L., Crosta, X., Massé, G., & Ther, O. (2010). Deglacial environments in eastern Prydz Bay, East Antarctica. *Quaternary Science Reviews*, 29(19-20), 2731-2740.
- Barchyn, T. E., Dowling, T. P., Stokes, C. R., & Hugenholtz, C. H. (2016). Subglacial bed form morphology controlled by ice speed and sediment thickness. *Geophysical Research Letters*, 43(14), 7572-7580.
- Bareille, G., Labacherie, M., Labeyrie, L., Pichon, J. J., & Turon, J. L. (1991). Biogenic silica accumulation rate during the Holocene in the southeastern Indian Ocean. *Marine Chemistry*, 35(1-4), 537-551.
- Barker P., Camerlenghi, A., Acton G.D. (1998), Antarctic glacial history and sea-level change: Leg 178 samples Antarctic Peninsula margin sediments. *Joides Journal*, vol. 24, pp. 7-10

- Baroni, C. (2001). *Antartide*. Terra di Scienza e Riserva Naturale (pp. 1-280). Terra Antartica Publication.
- Baroni, C., Noti, V., Ciccacci, S., Righini, G., & Salvatore, M. C. (2005). Fluvial origin of the valley system in northern Victoria Land (Antarctica) from quantitative geomorphic analysis. *Geological Society of America Bulletin*, 117(1-2), 212-228.
- Bart P.J. (2001), Did the Antarctic Ice Sheets expand during the early Pliocene?, *Geology*, vol. 29, pp. 67-70, <https://doi.org/10.1130/0091-7613>
- Bart, P. J., & Tulaczyk, S. (2020). A significant acceleration of ice volume discharge preceded a major retreat of a West Antarctic paleo-ice stream. *Geology*, 48(4), 313-317.
- Bart, P. J., and J.B. Anderson (1996), Seismic expression of depositional sequences associated with expansion and contraction of ice sheets on the northwestern Antarctic Peninsula continental shelf, *Geological Society, London, Special Publications*, 117 (1), 171-186.
- Bart, P. J., Mullally, D., & Golledge, N. R. (2016). The influence of continental shelf bathymetry on Antarctic Ice Sheet response to climate forcing. *Global and Planetary Change*, 142, 87-95.
- Bart, P.J., and L. De Santis. (2012). Glacial intensification during the Neogene: A review of seismic stratigraphic evidence from the Ross Sea, Antarctica, continental shelf. *Oceanography* 25(3):166–183
- Bartek, L. R., Andersen, J., & Oneacre, T. (1997). Ice stream troughs and variety of Cenozoic seismic stratigraphic architecture from a high southern latitude section: Ross Sea Antarctica. In *Glaciated Continental Margins* (pp. 250-254). Springer, Dordrecht.
- Bassis, J. N., & Jacobs, S. (2013). Diverse calving patterns linked to glacier geometry. *Nature Geoscience*, 6(10), 833-836.
- Bassis, J. N., & Walker, C. C. (2012). Upper and lower limits on the stability of calving glaciers from the yield strength envelope of ice. *Proceedings of the Royal Society A: Mathematical, Physical and Engineering Sciences*, 468(2140), 913-931.
- Batchelor, C. L., & Dowdeswell, J. A. (2014). The physiography of High Arctic cross-shelf troughs. *Quaternary Science Reviews*, 92, 68-96.
- Batchelor, C. L., & Dowdeswell, J. A. (2015). Ice-sheet grounding-zone wedges (GZWs) on high-latitude continental margins. *Marine Geology*, 363, 65-92.
- Batchelor, C. L., Dowdeswell, J. A., & Rignot, E. (2018). Submarine landforms reveal varying rates and styles of deglaciation in North-West Greenland fjords. *Marine Geology*, 402, 60-80.
- Batchelor, C. L., Ottesen, D., & Dowdeswell, J. A. (2017). Quaternary evolution of the northern North Sea margin through glacial debris-flow and contourite deposition. *Journal of Quaternary Science*, 32(3), 416-426.
- Bates R.L., and Jackson J.A., editors, (1987), *Glossary of Geology*: American Geological Institute, Alexandria, VA, 3rd edition, 788 pages
- Beaman R.J., O'Brien P. E., Post A. L., De Santis L. A new high-resolution bathymetry model for the Terre Adélie and George V continental margin, East Antarctica. *Antarctic Science* pp 1-9 (2010)
- Beans, C., Hecq, J. H., Koubbi, P., Vallet, C., Wright, S., & Goffart, A. (2008). A study of the diatom-dominated microplankton summer assemblages in coastal waters from Terre Adélie to the Mertz Glacier, East Antarctica (139 E–145 E). *Polar Biology*, 31(9), 1101-1117.
- Behrendt J.C., LeMasurier W.E., Cooper A.K., Tessensohn F., Tréhu A. & Damaske D., 1991. Geophysical studies of the West Antarctic Rift System. *Tectonics*, 10, 1257-1273.

- Behrendt J.C., Saltus R., Damaske D., McCafferty A., Finn C.A., Blankenship D. & Bell R.E., 1996. Patterns of late Cenozoic volcanic and tectonic activity in the West Antarctic Rift System revealed by aeromagnetic surveys. *Tectonics*, 15, 660-676.
- Behrendt, J. C., LeMasurier, W. E., Cooper, A. K., Tessensohn, F., Trehu, A., & Damaske, D. (1991). Geophysical studies of the West Antarctic rift system. *Tectonics*, 10(6), 1257-1273.
- Bendle, J. Core data from the Antarctic margin. *Nature* 470, 181–182 (2011). <https://doi.org/10.1038/470181a>
- Benn, D., & Evans, D. J. (2014). *Glaciers and glaciation*. Routledge.
- Benn, D.I., and D.J.A. Evans (1998), *Glaciers and Glaciation*, 2nd ed., 784 pp., Routledge, New York.
- Benn, Douglas, and David JA Evans. *Glaciers and glaciation*. Routledge, 2014.
- Bennett, M. M., & Glasser, N. F. (Eds.). (2011). *Glacial geology: ice sheets and landforms*. John Wiley & Sons.
- Bennett, M. R., & Boulton, G. S. (1993). A reinterpretation of Scottish ‘hummocky moraine’ and its significance for the deglaciation of the Scottish Highlands during the Younger Dryas or Loch Lomond Stadial. *Geological magazine*, 130(3), 301-318.
- Bennett, M.R. (2003), Ice streams as the arteries of an ice sheet: their mechanics, stability and significance. *Earth Science Reviews*, vol. 61, pp. 309-339, [http://doi.org/10.1016/S00128252\(02\)00130-7](http://doi.org/10.1016/S00128252(02)00130-7)
- Bentley C. (1987), Antarctic Ice Streams: a review, *Journal of Geophysical Research*, vol. 92, pp. 8843-8858, <https://doi.org/10.1029/JB092iB09p08843>
- Bentley, M. J., Cofaigh, C. Ó., Anderson, J. B., Conway, H., Davies, B., Graham, A. G., ... & RAISED Consortium. (2014). A community-based geological reconstruction of Antarctic Ice Sheet deglaciation since the Last Glacial Maximum. *Quaternary Science Reviews*, 100, 1-9.
- Berg, G. M., Mills, M. M., Long, M. C., Bellerby, R., Strass, V., Savoye, N., Röttgers, R., Croot, P. L., Webb, A., and Arrigo, K. R. (2011), Variation in particulate C and N isotope composition following iron fertilization in two successive phytoplankton communities in the Southern Ocean, *Global Biogeochem. Cycles*, 25, GB3013, doi:10.1029/2010GB003824.
- Berger W.H., Herguera J.C. (1992) Reading the Sedimentary Record of the Ocean’s Productivity. In: Falkowski P.G., Woodhead A.D., Vivirito K. (eds) *Primary Productivity and Biogeochemical Cycles in the Sea*. Environmental Science Research, vol 43. Springer, Boston, MA. https://doi.org/10.1007/978-1-4899-0762-2_24
- Berkman, Paul Arthur Forman, Steven L., Pre-bomb radiocarbon and the reservoir correction for calcareous marine species in the Southern Ocean *Geophysical Research Letters Geophys. Res. Lett.* 23- 40094-8276 <https://doi.org/10.1029/96GL00151>
- Bertler, N. A. N., Mayewski, P. A., & Carter, L. (2011). Cold conditions in Antarctica during the Little Ice Age—Implications for abrupt climate change mechanisms. *Earth and Planetary Science Letters*, 308(1-2), 41-51.
- Bianchi, C., & Gersonde, R. (2004). Climate evolution at the last deglaciation: the role of the Southern Ocean. *Earth and Planetary Science Letters*, 228(3-4), 407-424.
- Bindschadler, R., Choi, H., Wichlacz, A., Bingham, R., Bohlander, J., Brunt, K., ... & Young, N. (2011). Getting around Antarctica: new high-resolution mappings of the grounded and freely-floating boundaries of the Antarctic ice sheet created for the International Polar Year. *The Cryosphere*, 5(3), 569-588.
- Bird P. An updated digital model of plate boundaries. *Geochemistry, Geophysics, Geosystems*. 2003;4:1027.

- Birks H.j.b., Braak C.j.f. Ter, Line J. M., Juggins S. and Stevenson A. C. 1990 Diatoms and pH reconstruction *Phil. Trans. R. Soc. Lond.* B327263–278
- Blaauw Maarten, Methods and code for ‘classical’ age-modelling of radiocarbon sequences, *Quaternary Geochronology*, Volume 5, Issue 5, 2010, Pages 512-518, ISSN 1871-1014.
- Boldt, K. V., Nittrouer, C. A., Hallet, B., Koppes, M. N., Forrest, B. K., Wellner, J. S., & Anderson, J. B. (2013). Modern rates of glacial sediment accumulation along a 15° S-N transect in fjords from the Antarctic Peninsula to southern Chile. *Journal of Geophysical Research: Earth Surface*, 118(4), 2072-2088.
- Böning, C., Dispert, A., Visbeck, M. *et al.* The response of the Antarctic Circumpolar Current to recent climate change. *Nature Geosci* **1**, 864–869 (2008).
- Borg, S. G., Stump, E., Chappell, B. W., McCulloch, M. T., Wyborn, D., Armstrong, R. L., & Holloway, J. R. (1987). Granitoids of northern Victoria Land, Antarctica: implications of chemical and isotopic variations to regional crustal structure and tectonics. *American journal of science*, 287(2), 127-169.
- Borg, S.G., 1984. Granitoids of Northern Victoria Land, Antarctica. PhD. thesis. Arizona State University.
- Borg, S.G., Stump, E., 1987. Paleozoic magmatism and associated tectonic problems of Northern Victoria Land, Antarctica. McKenzie, G. (Ed.), *Gondwana Six: Structure, Tectonics and Geophysics*. Amer. Geophys. Union, Geophys. Monogr., vol. 40, 67–76.
- Borstad, C. P., Rignot, E., Mouginot, J., & Schodlok, M. P. (2013). Creep deformation and buttressing capacity of damaged ice shelves: theory and application to Larsen C ice shelf. *The Cryosphere*, 7(6), 1931-1947.
- Boulton, G.S. & Eyles, N. (1979) Sedimentation by valley glaciers: a model and genetic classification. In: *Moraines and Varves* (Ed. by C. Schluchter), pp. 11-23. A. A. Balkema, Rotterdam.
- Brachfeld, S. A., Banerjee, S. K., Guyodo, Y., & Acton, G. D. (2002). A 13200-year history of century to millennial-scale paleoenvironmental change magnetically recorded in the Palmer Deep, western Antarctic Peninsula. *Earth and Planetary Science Letters*, 194(3-4), 311-326.
- Brachfeld, S., Acton, G. D., Guyodo, Y., & Banerjee, S. K. (2000). High-resolution paleomagnetic records from Holocene sediments from the Palmer Deep, Western Antarctic Peninsula. *Earth and Planetary Science Letters*, 181(3), 429-441.
- Bradshaw, J. D., Laird, M. G., and Wodzicki, A., 1982, Structural style and tectonic history in northern Victoria Land, in Craddock, Campbell, ed., *Antarctic geoscience: Madison, Wisconsin*, International Union of Geological Sciences, ser. B, no. 4, p. 809-816.
- Bradshaw, J. D., Weaver, S. D., & Laird, M. G. (1985). Suspect terranes and Cambrian tectonics in northern Victoria Land, Antarctica.
- Bradshaw, J.D., 1987. Terrane boundaries and terrane displacement in Northern Victoria Land, Antarctica: some problems and constraints. In: In: Leitch, E., Scheibner, E. (Eds.), *Terrane Accretion and Orogenic Belts*, Geodynamics Series, vol. 19. AGU, Washington, D. C, pp. 199–206.
- Bradshaw, J.D., 1989. Terrane boundaries in north Victoria land. *Memor. Soc. Geol. Ital.* 33, 9–15.
- Briner, J.P. (2007), Supporting evidence from the New York drumlin field that elongate subglacial bedforms indicate fast flow, *Boreas*, 36, 143-147.
- Broecker W.S., T.-H. Peng *Tracers in the Sea*, Eldgo Press, Palisades, NY (1982) 690 pp
- Broecker, W. S., Peng, T.-H., Ostlund, G., and Stuiver, M. (1985), The distribution of bomb radiocarbon in the ocean, *J. Geophys. Res.*, 90(C4), 6953– 6970.

- Bromwich, D. H., and Kurtz, D. D. (1984). Katabatic wind forcing of the Terra Nova Bay polynya. *J. Geophys. Res.* 89, 3561–3572.
- Brunelle, B. G., Sigman, D. M., Cook, M. S., Keigwin, L. D., Haug, G. H., Plessen, B., Schettler, G., and Jaccard, S. L. (2007), Evidence from diatom-bound nitrogen isotopes for subarctic Pacific stratification during the last ice age and a link to North Pacific denitrification changes, *Paleoceanography*, 22, PA1215.
- Brunt, K.M.; Fricker, H.A.; Padman, L.; Scambos, T.A.; O’Neel, S. Mapping the grounding zone of the Ross Ice Shelf, Antarctica, using ICESat laser altimetry. *Ann. Glaciol.* 2010, 51, 71–79.
- Budillon G., Castagno P., Aliani S., Spezie G., Padman L. (2011), Thermohaline variability and Antarctic bottom water formation at the Ross Sea shelf break. *Deep Sea Research Part I: Oceanographic Research Papers*, vol. 58, pp. 1002–1018.
- Buffen, A., Leventer, A., Rubin, A., & Hutchins, T. (2007). Diatom assemblages in surface sediments of the northwestern Weddell Sea, Antarctic Peninsula. *Marine Micropaleontology*, 62(1), 7-30.
- Butzin Martin, Matthias Prange, Gerrit Lohmann, Radiocarbon simulations for the glacial ocean: The effects of wind stress, Southern Ocean sea ice and Heinrich events, *Earth and Planetary Science Letters*, Volume 235, Issues 1–2,
- Campbell, A. J., Hulbe, C. L., & Lee, C. K. (2018). Ice stream slowdown will drive long-term thinning of the Ross ice shelf, with or without ocean warming. *Geophysical Research Letters*, 45(1), 201-206.
- Catania, G. A., Scambos, T. A., Conway, H., & Raymond, C. F. (2006). Sequential stagnation of Kamb ice stream, West Antarctica. *Geophysical Research Letters*, 33(14).
- Cazenave, A., Meyssignac, B., Ablain, M., Balmaseda, M., Bamber, J., Barletta, V., ... & Wouters, B. (2018). Global sea-level budget 1993-present. *Earth System Science Data*, 10(3), 1551-1590.
- Chapman, W. L., & Walsh, J. E. (2007). A synthesis of Antarctic temperatures. *Journal of Climate*, 20, 4096–4117
- Chemical Geology*, Volume 114, Issues 3–4, 1994, Pages 289-302, ISSN 0009-2541.
- Christoffersen P., Tulaczyk S., Carsey F.D., Behar A. E. (2006), A quantitative framework for interpretation of basal ice facies formed by ice accretion over subglacial sediment. *Journal of Geophysical Research*.
- Church, J. A., Clark, P. U., Cazenave, A., Gregory, J. M., Jevrejeva, S., Levermann, A., ... & Unnikrishnan, A. S. (2013). *Sea level change*. PM Cambridge University Press.
- Clark, C.D. (1993), Mega-scale glacial lineations and cross-cutting ice-flow landforms, *Earth Surface Processes and Landforms*, 18, 1-29.
- Clark, C.D., A.L.C. Hughes, S.L. Greenwood, M. Spagnolo, and F.S.L. Ng (2009), Size and shape characteristics of drumlins, derived from a large sample and associated scaling laws, *Quaternary Science Reviews*, 28, 677-692.
- Clark, C.D., and R.T. Meehan (2001), Subglacial bedform geomorphology of the Irish Ice Sheet reveals major configuration changes during growth and decay, *Journal of Quaternary Science*, 16 (5), 483-496.
- Close, D. I. (2010). Slope and fan deposition in deep-water turbidite systems, East Antarctica. *Marine Geology*, 274(1-4), 21-31.
- Close, D. I., Stagg, H.M.J., O’Brien, P.E., (2007). Seismic stratigraphy and sediment distribution on the Wilkes Land Terre Adélie margins, East Antarctica. *Marine Geology* 239, pp. 33–57

- Close, D. I., Watts A. B. and Stagg H. M. J., (2009). A marine geophysical study of the Wilkes Land rifted continental margin, Antarctica. *Marine Geoscience, Geophys. J. Int.* 177, 430–450
- Cofaigh, C. Ó., Hogan, K. A., Dowdeswell, J. A., & Streuff, K. (2016). Stratified glacimarine basin-fills in West Greenland fjords. *Geological Society, London, Memoirs*, 46(1), 99-100.
- Comiso J. C., Kwok R., Martin S., and Gordon A. L. (2011), Variability and trends in sea ice extent and ice production in the Ross Sea, *J. Geophysical Research*, 116, C04021, doi: 10.1029/2010JC006391
- Comiso, J. C., & Nishio, F. (2008). Trends in the sea ice cover using enhanced and compatible AMSR-E, SSM/I, and SMMR data. *Journal of Geophysical Research*, 113(C2).
- Comiso, J.C. and F. Nishio. (2008) Trends in the sea ice cover using enhanced and compatible AMSR-E, SSM/I, and SMMR data. *J. Geophys. Res.*, 113(C2).
- Conway, H., Hall, B. L., Denton, G. H., Gades, A. M., & Waddington, E. D. (1999). Past and future grounding-line retreat of the West Antarctic Ice Sheet. *Science*, 286(5438), 280-283.
- Cook, A. J., Fox, A. J., Vaughan, D. G., & Ferrigno, J. G. (2005). Retreating glacier fronts on the Antarctic Peninsula over the past half-century. *Science*, 308(5721), 541–544.
- Cook, A. J., Holland, P. R., Meredith, M. P., Murray, T., Luckman, A., & Vaughan, D. G. (2016). Ocean forcing of glacier retreat in the western Antarctic Peninsula. *Science*, 353(6296), 283–286.
- Cook, A. J., Vaughan, D. G., Luckman, A. J., & Murray, T. (2014). A new Antarctic Peninsula glacier basin inventory and observed areachanges since the 1940s. *Antarctic Science*, 26(6), 614–624.
- Cook, C. P., Van De Fliedrt, T., Williams, T., Hemming, S. R., Iwai, M., Kobayashi, M., ... & Yamane, M. (2013). Dynamic behaviour of the East Antarctic ice sheet during Pliocene warmth. *Nature Geoscience*, 6(9), 765-769.
- Cooper, A.K.; Barrett, P.J.; Hinz, K.; Traube, V.; Letichenkov, G.; Stagg, H.M. Cenozoic prograding sequences of the Antarctic continental margin: A record of glacio-eustatic and tectonic events. *Mar. Geol.* 1991, 102, 175–213.
- Costa, R. R., Mendes, C. R. B., Tavano, V. M., Dotto, T. S., Kerr, R., Monteiro, T., ... & Secchi, E. R. (2020). Dynamics of an intense diatom bloom in the Northern Antarctic Peninsula, February 2016. *Limnology and Oceanography*, 65(9), 2056-2075.
- Cowan, E. A., & Powell, R. D. (1990). Suspended sediment transport and deposition of cyclically interlaminated sediment in a temperate glacial fjord, Alaska, USA. *Geological Society, London, Special Publications*, 53(1), 75-89.
- Cowan, E. A., Powell, R. D., & Anderson, J. B. (1991). Ice-proximal sediment accumulation rates in a temperate glacial fjord, southeastern Alaska. *Glacial marine sedimentation*, 61-73.
- Cowan, E. A., Seramur, K. C., Powell, R. D., Willems, B. A., Gulick, S. P., & Jaeger, J. M. (2010). Fjords as temporary sediment traps: History of glacial erosion and deposition in Muir Inlet, Glacier Bay National Park, southeastern Alaska. *Bulletin*, 122(7-8), 1067-1080.
- Cowan, E., Seramur, K., Cai, J., Powell, R.D. (1999). Cyclic sedimentation produced by fluctuations in meltwater discharge, tides and marine productivity in an Alaskan fjord. *Sedimen.*, 46, 1109–1126.
- Cowan, E.A. 1988. Sediment transport and deposition in a temperate glacial fjord, Glacier Bay, Alaska. Ph.D. Thesis, Northern Illinois University.
- Cowan, E.A., Cai, J., Powell, R.D., Clark, J.D., Pitcher J.N. (1997). Temperate glacimarine varies, an example from Disenchantment Bay, Southern Alaska. *J. Sed. Res.*, 67(3), 536– 549.

- Cowan, E.A., Powell, R.D. (1990). Suspended sediment transport and deposition of cyclically interlaminated sediment in a temperate glacial fjord, Alaska, U.S.A, in *Glacimarine 144 Environments: Processes and Sediments*, edited by J. A. Dowdeswell and J. D. Scourse, Geological Society Special Publication, p. 75-89.
- Cridland, A.A. (1963), A *Glossopteris* flora from the Ohio Range, Antarctica. *American Journal of Botany*, 50: 186-195. <https://doi.org/10.1002/j.1537-2197.1963.tb07194.x>
- Crosta, X., & Koç, N. (2007). Chapter eight diatoms: From micropaleontology to isotope geochemistry. *Developments in marine geology*, 1, 327-369.
- Crosta, X., Etourneau, J., Orme, L. C., Dalaiden, Q., Campagne, P., Swingedouw, D., ... & Ikehara, M. (2021). Multi-decadal trends in Antarctic sea-ice extent driven by ENSO–SAM over the last 2,000 years. *Nature Geoscience*, 14(3), 156-160.
- Crosta, X., Pichon, J. J., & Burckle, L. H. (1998). Application of modern analog technique to marine Antarctic diatoms: Reconstruction of maximum sea-ice extent at the Last Glacial Maximum. *Paleoceanography*, 13(3), 284-297.
- Crosta, X., Romero, O., Armand, L. K., & Pichon, J. J. (2005). The biogeography of major diatom taxa in Southern Ocean sediments: 2. Open ocean related species. *Palaeogeography, Palaeoclimatology, Palaeoecology*, 223(1-2), 66-92.
- Crosta, X., Romero, O., Armand, L. K., & Pichon, J. J. (2005). The biogeography of major diatom taxa in Southern Ocean sediments: 2. Open ocean related species. *Palaeogeography, Palaeoclimatology, Palaeoecology*, 223(1-2), 66-92.
- Crosta, X., Romero, O., Armand, L. K., & Pichon, J. J. (2005). The biogeography of major diatom taxa in Southern Ocean sediments: 2. Open ocean related species. *Palaeogeography, Palaeoclimatology, Palaeoecology*, 223(1-2), 66-92.
- Crosta, X., Shemesh, A., Salvignac, M. E., Gildor, H., & Yam, R. (2002). Late Quaternary variations of elemental ratios (C/Si and N/Si) in diatom-bound organic matter from the Southern Ocean. *Deep Sea Research Part II: Topical Studies in Oceanography*, 49(9-10), 1939-1952.
- Crosta, X., Sturm, A., Armand, L., & Pichon, J. J. (2004). Late Quaternary sea ice history in the Indian sector of the Southern Ocean as recorded by diatom assemblages. *Marine Micropaleontology*, 50(3-4), 209-223.
- Cuffey, K. M., & Paterson, W. S. B. (2010). *The physics of glaciers*. Academic Press.
- Cuffey, K. M., Conway, H., Hallet, B., Gades, A. M., & Raymond, C. F. (1999). Interfacial water in polar glaciers and glacier sliding at -17° C. *Geophysical Research Letters*, 26(6), 751-754.
- Cunningham, W. L., & Leventer, A. (1998). Diatom assemblages in surface sediments of the Ross Sea: relationship to present oceanographic conditions. *Antarctic Science*, 10(2), 134-146.
- Cunningham, W. L., Leventer, A., Andrews, J. T., Jennings, A. E., & Licht, K. J. (1999). Late Pleistocene-Holocene marine conditions in the Ross Sea, Antarctica: evidence from the diatom record. *The Holocene*, 9(2), 129-139.
- Curtis, M. L. (2001). Tectonic history of the Ellsworth Mountains, West Antarctica: reconciling a Gondwana enigma. *Geological Society of America Bulletin*, 113(7), 939-958.
- DaSilva, J., Anderson, J., Stravers J. (1997). Seismic facies changes along a nearly continuous 24 latitudinal transect: the fjords of Chile and the northern Antarctic Peninsula. *Mar. Geol.*, 143, 103-123.

- De Santis, L., Brancolini, G., Donda, F., (2003). Seismo-stratigraphic analysis of the Wilkes Land continental margin (East Antarctica): influence of glacially driven processes on the Cenozoic deposition. *Deep-Sea Res., Part II* 50 (8–9), 1563–1594
- De Santis, L., Prato, S., Brancolini, G., Lovo, M., & Torelli, L. (1999). The Eastern Ross Sea continental shelf during the Cenozoic: implications for the West Antarctic ice sheet development. *Global and Planetary Change*, 23(1-4), 173-196.
- Deacon G. E. R. (1937), *The hydrography of the Southern Ocean.*, 'Discovery' Reports, vol. 19, pp. 124
- DeConto, R. M., & Pollard, D. (2016). Contribution of Antarctica to past and future sea-level rise. *Nature*, 531(7596), 591-597.
- DeMaster, D. J. (1981). The supply and accumulation of silica in the marine environment. *Geochimica et Cosmochimica acta*, 45(10), 1715-1732.
- Denis, D., Crosta, X., Barbara, L., Massé, G., Renssen, H., Ther, O., & Giraudeau, J. (2010). Sea ice and wind variability during the Holocene in East Antarctica: insight on middle–high latitude coupling. *Quaternary Science Reviews*, 29(27-28), 3709-3719.
- Di Roberto, A., Colizza, E., Del Carlo, P. et al. First marine cryptotephra in Antarctica found in sediments of the western Ross Sea correlates with englacial tephra and climate records. *Sci Rep* 9, 10628 (2019). <https://doi.org/10.1038/s41598-019-47188-3>
- Dieng, H. B., Cazenave, A., Meyssignac, B., & Ablain, M. (2017). New estimate of the current rate of sea level rise from a sea level budget approach. *Geophysical Research Letters*, 44(8), 3744-3751.
- DiFiore, P. J., Sigman, D. M., and Dunbar, R. B. (2009), Upper ocean nitrogen fluxes in the Polar Antarctic Zone: Constraints from the nitrogen and oxygen isotopes of nitrate, *Geochem. Geophys. Geosyst.*, 10, Q11016, doi:10.1029/2009GC002468.
- DiFiore, P. J., Sigman, D. M., Trull, T. W., Lourey, M. J., Karsh, K., Cane, G., and Ho, R. (2006), Nitrogen isotope constraints on subantarctic biogeochemistry, *J. Geophys. Res.*, 111, C08016, doi:10.1029/2005JC003216.
- Diviacco P., Rebesco M., Camerlenghi A. (2006), Late Pliocene Mega Debris Flow Deposit and Related Fluid Escapes Identified on the Antarctic Peninsula Continental Margin by Seismic Reflection Data Analysis. *Marine Geophysical Researches*, vol. 27, pp. 109–128. doi:10.1007/s11001-005-3136-8
- Doake, C. S. M., & Vaughan, D. G. (1991). Rapid disintegration of the Wordie Ice Shelf in response to atmospheric warming. *Nature*, 350(6316), 328-330.
- Domack Eugene W., David J.P. Foss, James P.M. Syvitski, Charles E. McClennen, Transport of suspended particulate matter in an Antarctic fjord, *Marine Geology*, Volume 121, Issues 3–4, 1994, Pages 161-170, ISSN 0025-3227.
- Domack, E. W., Jacobson, E. A., Shipp, S., & Anderson, J. B. (1999). Late Pleistocene–Holocene retreat of the West Antarctic Ice-Sheet system in the Ross Sea: Part 2—sedimentologic and stratigraphic signature. *Geological Society of America Bulletin*, 111(10), 1517-1536.
- Domack, E.W. and Williams, C.R. (1990). Fine Structure and Suspended Sediment Transport in Three Antarctic Fjords. In *Contributions to Antarctic Research I*, C.R. Bentley (Ed.).
- Domack, E.W., Ishman, S.E. (1993). Oceanographic and physiographic controls on modern sedimentation within Antarctic fjords. *Geol. Soc. Am. Bull.*, 105(9), 1175–1189, doi:10.1130/0016-7606(1993)105<1175.
- Domack, E.W., McClennen, C.E. (1996). Accumulation of glacial marine sediments in fjords of the Antarctic Peninsula and their use as late Holocene paleoenvironmental indicators. *Ant. Res. Ser.*, 70, 135–154.

- Donda, F., O'Brien, P. E., De Santis, L., Rebesco, M., & Brancolini, G. (2008). Mass wasting processes in the Western Wilkes Land margin: possible implications for East Antarctic glacial history. *Palaeogeography, Palaeoclimatology, Palaeoecology*, 260(1-2), 77-91.
- Dowdeswell, J. A., & Fugelli, E. M. G. (2012). The seismic architecture and geometry of grounding-zone wedges formed at the marine margins of past ice sheets. *Bulletin*, 124(11-12), 1750-1761.
- Dowdeswell, J. A., Hogan, K. A., Arnold, N. S., Mugford, R. I., Wells, M., Hirst, J. P. P., & Decalf, C. (2015). Sediment-rich meltwater plumes and ice-proximal fans at the margins of modern and ancient tidewater glaciers: Observations and modelling. *Sedimentology*, 62(6), 1665-1692.
- Dowdeswell, J. A., Ottesen, D., Evans, J., Cofaigh, C. Ó., & Anderson, J. B. (2008). Submarine glacial landforms and rates of ice-stream collapse. *Geology*, 36(10), 819-822.
- Dowdeswell, J.A. and J.L. Bamber (2007), Keel depths of modern Antarctic icebergs and implications for sea-floor scouring in the geological record, *Marine Geology*, 243, 120-131.
- Dowdeswell, J.A., Fugelli, E.M.G. (2012), The seismic architecture and geometry of grounding-zone wedges formed at the marine margins of past ice sheets. *Geological Society of America Bulletin*, doi:10.1130/B30628.1
- Ducklow, H. W., Baker, K., Martinson, D. G., Quetin, L. B., Ross, R. M., Smith, R. C., et al. (2007). Marine pelagic ecosystems: The west Antarctic Peninsula. *Philosophical Transactions of the Royal Society, B: Biological Sciences*, 362(1477), 67.
- Dunbar, R. B., Anderson, J. B., Domack, E. W., & Jacobs, S. S. (1985). Oceanographic influences on sedimentation along the Antarctic continental shelf. *Oceanology of the Antarctic continental shelf*, 43, 291-312.
- Duncan, R. J., Nielsen, D. A., Sheehan, C. E., Deppeler, S., Hancock, A. M., Schulz, K. G., ... & Petrou, K. (2022). Ocean acidification alters the nutritional value of Antarctic diatoms. *New Phytologist*.
- Dupont, T. K., & Alley, R. B. (2005). Assessment of the importance of ice-shelf buttressing to ice-sheet flow. *Geophysical Research Letters*, 32(4).
- Dutrieux, P., De Rydt, J., Jenkins, A., Holland, P. R., Ha, H. K., Lee, S. H., ... & Schröder, M. (2014). Strong sensitivity of Pine Island ice-shelf melting to climatic variability. *Science*, 343(6167), 174-178.
- Edwards, T. L., Nowicki, S., Marzeion, B., Hock, R., Goelzer, H., Seroussi, H., ... & Zwinger, T. (2021). Projected land ice contributions to twenty-first-century sea level rise. *Nature*, 593(7857), 74-82.
- Eidam, E. F., Nittrouer, C. A., Lundesgaard, Ø., Homolka, K. K., & Smith, C. R. (2019). Variability of sediment accumulation rates in an Antarctic Fjord. *Geophysical Research Letters*, 46(22), 13271-13280.
- Elverhøi, A., Lønne, Ø., & Seland, R. (1983). Glaciomarine sedimentation in a modern fjord environment, Spitsbergen. *Polar Research*, 1(2), 127-150.
- Ely, J. C., Clark, C. D., Spagnolo, M., Hughes, A. L., & Stokes, C. R. (2018). Using the size and position of drumlins to understand how they grow, interact and evolve. *Earth Surface Processes and Landforms*, 43(5), 1073-1087.
- Escutia, C., & Brinkhuis, H. (2014). From greenhouse to icehouse at the Wilkes Land Antarctic margin: IODP Expedition 318 synthesis of results. In *Developments in marine geology* (Vol. 7, pp. 295-328). Elsevier.
- Escutia, C., De Santis, L., Donda, F., Dunbar, R. B., Cooper, A. K., Brancolini, G., & Eitrem, S. L. (2005). Cenozoic ice sheet history from East Antarctic Wilkes Land continental margin sediments. *Global and Planetary Change*, 45(1-3), 51-81.

- Escutia, C., Eitrem, S. L., Cooper, A. K., & Nelson, C. H. (2000). Morphology and acoustic character of the Antarctic Wilkes Land turbidite systems: ice-sheet-sourced versus river-sourced fans. *Journal of Sedimentary Research*, 70(1), 84-93.
- Escutia, C., Nelson, C. H., Acton, G. D., Eitrem, S. L., Cooper, A. K., Warnke, D. A., & Jaramillo, J. M. (2002). Current controlled deposition on the Wilkes Land continental rise, Antarctica. *Geological Society, London, Memoirs*, 22(1), 373-384.
- Estrada, S., Läufer, A., Eckelmann, K., Hofmann, M., Gärtner, A., Linnemann, U., 2016. Continuous neoproterozoic to ordovician sedimentation at the east Gondwana margin - implications from detrital zircons of the Ross orogen in Northern Victoria Land, Antarctica. *Gondwana Res.* 37, 426–448.
- Etourneau, J., Sgubin, G., Crosta, X., Swingedouw, D., Willmott, V., Barbara, L., ... & Kim, J. H. (2019). Ocean temperature impact on ice shelf extent in the eastern Antarctic Peninsula. *Nature Communications*, 10(1), 1-8.
- Evans, D. J., & Hiemstra, J. F. (2005). Till deposition by glacier submarginal, incremental thickening. *Earth surface processes and landforms*, 30(13), 1633-1662.
- Evans, D., & Gooster, L. (2014). *Glacial landsystems*. Routledge.
- Evans, J., Ó Cofaigh, C., Dowdeswell, J. A., & Wadhams, P. (2009). Marine geophysical evidence for former expansion and flow of the Greenland Ice Sheet across the north-east Greenland continental shelf. *Journal of Quaternary Science: Published for the Quaternary Research Association*, 24(3), 279-293.
- Farmer, D. M., & Freeland, H. J. (1983). The physical oceanography of fjords. *Progress in oceanography*, 12(2), 147-219.
- Farmer, D.M., Freeland, H.J., 1983. The physical oceanography of fjords. *Prog. Oceanogr.* 12, 147-220.
- Favier, L., Durand, G., Cornford, S. L., Gudmundsson, G. H., Gagliardini, O., Gillet-Chaulet, F., ... & Le Brocq, A. M. (2014). Retreat of Pine Island Glacier controlled by marine ice-sheet instability. *Nature Climate Change*, 4(2), 117-121.
- Fernandez, R. A., Anderson, J. B., Wellner, J. S., & Hallet, B. (2011). Timescale dependence of glacial erosion rates: A case study of Marinelli Glacier, Cordillera Darwin, southern Patagonia. *Journal of Geophysical Research: Earth Surface*, 116(F1).
- Fernandez, R. A., Anderson, J. B., Wellner, J. S., Minzoni, R. L., Hallet, B., & Smith, R. T. (2016). Latitudinal variation in glacial erosion rates from Patagonia and the Antarctic Peninsula (46 S–65 S). *Bulletin*, 128(5-6), 1000-1023.
- Field, B. D., Findlay, R. H., & Oliver, R. L. (1983). The sedimentology of the Robertson Bay Group, northern Victoria Land. *Antarctic Earth Science*, 102-106.
- Finocchiaro, F., Langone, L., Colizza, E., Fontolan, G., Giglio, F., & Tuzzi, E. (2005). Record of the early Holocene warming in a laminated sediment core from Cape Hallett Bay (Northern Victoria Land, Antarctica). *Global and Planetary Change*, 45(1-3), 193-206.
- Fogwill, C. J., Phipps, S. J., Turney, C. S. M., & Golledge, N. R. (2015). Sensitivity of the Southern Ocean to enhanced regional Antarctic ice sheet meltwater input. *Earth's Future*, 3(10), 317– 329.
- Folk, R. L., & Ward, W. C. (1959). Brazor River Bar: A study in the significant of grain size parameter. *Journal sed. Petrol*, 41, 45-1058.
- Freeman, N. M., Lovenduski N.S., and Gent P.R. (2016), Temporal variability in the Antarctic Polar Front (2002– 2014), *Journal of Geophysical Research, Oceans*, vol. 121, pp. 7263–7276.

- Fretwell, P., Pritchard, H. D., Vaughan, D. G., Bamber, J. L., Barrand, N. E., Bell, R., ... & Zirizzotti, A. (2013). Bedmap2: improved ice bed, surface and thickness datasets for Antarctica. *The Cryosphere*, 7(1), 375-393.
- Friedman, G. M., & Sanders, J. E. (1978). *Principles of sedimentology*. Wiley.
- Fritz, S., Juggins, S., Battarbee, R. et al. Reconstruction of past changes in salinity and climate using a diatom-based transfer function. *Nature* 352, 706–708 (1991).
- Fry, B., Hopkinson Jr, C. S., Nolin, A., Norrman, B., & Zweifel, U. L. (1996). Long-term decomposition of DOC from experimental diatom blooms. *Limnology and Oceanography*, 41(6), 1344-1347.
- Fürst, J. J., Durand, G., Gillet-Chaulet, F., Tavard, L., Rankl, M., Braun, M., & Gagliardini, O. (2016). The safety band of Antarctic ice shelves. *Nature Climate Change*, 6(5), 479-482.
- Gagliardini, O., Durand, G., Zwinger, T., Hindmarsh, R. C. A., & Le Meur, E. (2010). Coupling of ice-shelf melting and buttressing is a key process in ice-sheets dynamics. *Geophysical Research Letters*, 37(14).
- GANOVEX Team, 1987. Geological map of North Victoria land, Antarctica, 1:500,000 —explanatory notes. *Geol. Jahrb.* B66, 7–79.
- Garner, A. J., Weiss, J. L., Parris, A., Kopp, R. E., Horton, R. M., Overpeck, J. T., & Horton, B. P. (2018). Evolution of 21st century sea level rise projections. *Earth's Future*, 6(11), 1603-1615.
- Gersonde, R., & Zielinski, U. (2000). The reconstruction of late Quaternary Antarctic sea-ice distribution—the use of diatoms as a proxy for sea-ice. *Palaeogeography, Palaeoclimatology, Palaeoecology*, 162(3-4), 263-286.
- Godfred-Spenning, C. R., & Simmonds, I. (1996). An Analysis of Antarctic Sea-Ice and Extratropical Cyclone Associations. *International Journal of Climatology*, 16(12), 1315–1332.
- Golledge, N. R., Clark, P. U., He, F., Dutton, A., Turney, C. S. M., Fogwill, C. J., ... & Carlson, A. E. (2021). Retreat of the Antarctic Ice Sheet during the Last Interglaciation and implications for future change. *Geophysical Research Letters*, 48(17), e2021GL094513.
- Golledge, N. R., Kowalewski, D. E., Naish, T. R., Levy, R. H., Fogwill, C. J., & Gasson, E. G. (2015). The multi-millennial Antarctic commitment to future sea-level rise. *Nature*, 526(7573), 421-425.
- Gordon, A. L., A. Bergamasco, and L. Padman (2009b), Southern ocean shelf slope exchange, *Deep Sea Res., Part II*, 56(13–14), 775–777.
- Gordon, A. L., Huber, B. A., & Busecke, J. (2015). Bottom water export from the western Ross Sea, 2007 through 2010. *Geophysical Research Letters*, 42(13), 5387-5394.
- Graham, A. G., Larter, R. D., Gohl, K., Hillenbrand, C. D., Smith, J. A., & Kuhn, G. (2009). Bedform signature of a West Antarctic palaeo-ice stream reveals a multi-temporal record of flow and substrate control. *Quaternary Science Reviews*, 28(25-26), 2774-2793.
- Grange, L. J., & Smith, C. R. (2013). Megafaunal communities in rapidly warming fjords along the West Antarctic Peninsula: hotspots of abundance and beta diversity. *PloS one*, 8(12), e77917.
- Granger, Julie, Sigman, Daniel M., Needoba, Joseph A., Harrison, Paul J., (2004), Coupled nitrogen and oxygen isotope fractionation of nitrate during assimilation by cultures of marine phytoplankton, *Limnology and Oceanography*, 5, doi: 10.4319/lo.2004.49.5.1763.
- Greenwood, S. L., Simkins, L. M., Halberstadt, A. R. W., Prothro, L. O., & Anderson, J. B. (2018). Holocene reconfiguration and readvance of the East Antarctic Ice Sheet. *Nature communications*, 9(1), 1-12.

- Greenwood, S.L.; Gyllencreutz, R.; Jakobsson, M.; Anderson, J.B. Ice-flow switching and East/West Antarctic Ice Sheet roles in glaciation of the western Ross Sea. *Bulletin* 2012, 124, 1736–1749. [CrossRef]
- Greer Gilmer PhD, 2020, Late Quaternary Southern Hemisphere westerly wind variability in the mid-to high latitude southwest Pacific (thesis)
- Griffith, T. W., & Anderson, J. B. (1989). Climatic control of sedimentation in bays and fjords of the northern Antarctic Peninsula. *Marine Geology*, 85(2-4), 181-204.
- Gulley, J. D., Benn, D. I., Screamon, E., & Martin, J. (2009). Mechanisms of englacial conduit formation and their implications for subglacial recharge. *Quaternary Science Reviews*, 28(19-20), 1984-1999.
- Halberstadt, A.R.W.; Simkins, L.M.; Greenwood, S.L.; Anderson, J.B. Past ice-sheet behaviour: Retreat scenarios and changing controls in the Ross Sea, Antarctica. *Cryosphere* 2016, 10, 1003–1020.
- Hall, B. L., Henderson, G. M., Baroni, C., & Kellogg, T. B. (2010). Constant Holocene Southern-Ocean 14C reservoir ages and ice-shelf flow rates. *Earth and Planetary Science Letters*, 296(1-2), 115-123.
- Hallet, B. (1979). A theoretical model of glacial abrasion. *J. Glaciol.*, 23, 39-50.
- Hallet, B. (1996). Glacial quarrying: a simple theoretical model, *Ann. Glaciol.*, 22, 1-8
- Hallet, B., Hunter, L., & Bogen, J. (1996). Rates of erosion and sediment evacuation by glaciers: A review of field data and their implications. *Global and Planetary Change*, 12(1-4), 213-235.
- Hallet, B., Hunter, L., Bogen, J. (1996). Rates of erosion and sediment evacuation by glaciers: A review of field data and their implications. *Glob. Planet. Change*, 12(1-4), 213–235, doi: 10.1016/0921-8181(95)00021-6.
- Hamilton, W., 1972, The Hallett Volcanic Province, Antarctica. U. S. Geol. Survey Prof. Paper 456-C, p. C1–C62.
- Hanessian J., The International Antarctic Treaty (1959). *The International and Comparative Law Quarterly* Vol. 9, No. 3 (Jul., 1960), pp. 436-480
- Hanna E., Navarro F., Pattyn F., Domingues C.M., Fettweis X., Ivins E.R., Nicholls R.J., Ritz C., Smith B., Tulaczyk S., Whitehouse P.L., Zwally H.J. (2013), Ice-sheet mass balance and climate change, *Nature*, vol. 498, pp. 51–59.
- Harbor Jonathan M.; Numerical modeling of the development of U-shaped valleys by glacial erosion. *GSA Bulletin* 1992;; 104 (10): 1364–1375.
- Harbor, J. (1992). Numerical modeling of the development of U-shaped valleys by glacial erosion. *Geol. Soc. Am. Bull.*, 104, 1364-1375.
- Harbor, J.M. and Wheeler, D.A. (1992), On the mathematical description of glaciated valley cross sections. *Earth Surf. Process. Landforms*, 17: 477-485.
- Harrington H.J. (1965) *Geology and Morphology of Antarctica*. In: van Miegheem J., van Oye P. (eds) *Biogeography and Ecology in Antarctica*. Monographiae Biologicae, vol 15. Springer, Dordrecht.
- Harrington, H. J., & McKellar, I. C. (1958). A radiocarbon date for penguin colonization of Cape Hallett, Antarctica. *New Zealand Journal of Geology and Geophysics*, 1(3), 571-576.
- Harris, P. T., Brancolini, G., Armand, L., Busetti, M., Beaman, R. J., Giorgetti, G., ... & Trincardi, F. (2001). Continental shelf drift deposit indicates non-steady state Antarctic bottom water production in the Holocene. *Marine Geology*, 179(1-2), 1-8.

- Harris, P. T., Domack, E., Manley, P. L., Gilbert, R., & Leventer, A. (1999). Andvord drift: A new type of inner shelf, glacial marine deposystem from the Antarctic Peninsula. *Geology*, 27(8), 683–686
- Harris, P. T., Taylor, F., Domack, E., DeSantis, L., Goodwin, I., Quilty, P. G., & O'Brien, P. E. (1997). Glacimarine siliciclastic muds from Vincennes Bay, East Antarctica; preliminary results of an exploratory cruise in 1997. *Terra Antarctica*, 4(1), 11-20.
- Harrowfield, D. L. (1996). The role of the wind in the destruction of an historic hut at Cape Adare in Antarctica. *Polar Record*, 32(180), 3-18.
- Hauber E., Sassenroth, C., De Vera J.P., Schmitz N., Jaumann R., Reiss D., Hiesinger H., Johnsson A. (2018), Debris flows and water tracks in northern Victoria Land, continental East Antarctica: a new terrestrial analogue site for gullies and recurrent slope lineae on Mars. Geological Society, London, Special Publications, SP467.12. doi:10.1144/sp467.12
- Haug, A., & Myklestad, S. (1976). Polysaccharides of marine diatoms with special reference to *Chaetoceros* species. *Marine Biology*, 34(3), 217-222.
- Haughton P., Davis C., McCaffrey W., Barker S. (2009), Hybrid sediment gravity flow deposits - Classification, origin and significance, *Marine and Petroleum Geology*, vol. 26, pp. 1900- 1918.
- Hay, C. C., Morrow, E., Kopp, R. E., & Mitrovica, J. X. (2015). Probabilistic reanalysis of twentieth-century sea-level rise. *Nature*, 517(7535), 481-484.
- Hayes J.M, Factors controlling ^{13}C contents of sedimentary organic compounds: Principles and evidence, *Marine Geology*, Volume 113, Issues 1–2, 1993, Pages 111-125, ISSN 0025-3227.
- Heather L. Selley, Anna E. Hogg, Stephen Cornford, Pierre Dutrieux, Andrew Shepherd, Jan Wuite, Dana Floricioiu, Anders Kusk, Thomas Nagler, Lin Gilbert, Thomas Slater, Tae-Wan Kim. Widespread increase in dynamic imbalance in the Getz region of Antarctica from 1994 to 2018. *Nature Communications*, 2021; 12 (1)
- Henley, S. F., Annett, A. L., Ganeshram, R. S., Carson, D. S., Weston, K., Crosta, X., Tait, A., Dougans, J., Fallick, A. E., and Clarke, A.: Factors influencing the stable carbon isotopic composition of suspended and sinking organic matter in the coastal Antarctic sea ice environment, *Biogeosciences*, 9, 1137–1157.
- Heywood K.J., Schmidtko S., Heuzé C., Kaiser J., Jickells T.D., Queste B.Y., Stevens D.P., Wadley M., Thompson A.F., Fielding S., Guihen D., Creed E., Ridley J.K. and Smith W. (2014), Ocean processes at the Antarctic continental slope, *Philosophical Transactions of the Royal Society A: Mathematical, Physical and Engineering Sciences*, vol. 372.
- Hillenbrand C.D., Baesler, A., Grobe H. (2005), The sedimentary record of the last glaciation in the western Bellingshausen Sea (West Antarctica): Implications for the interpretation of diamictons in a polar-marine setting. *Marine Geology*, vol. 216, pp. 191–204.
- Hillenbrand, CD., Smith, J., Hodell, D. et al. West Antarctic Ice Sheet retreat driven by Holocene warm water incursions. *Nature* 547, 43–48 (2017). <https://doi.org/10.1038/nature22995>
- Hillier, J. K., Kougioumtzoglou, I. A., Stokes, C. R., Smith, M. J., Clark, C. D., & Spagnolo, M. S. (2016). Exploring explanations of subglacial bedform sizes using statistical models. *Plos one*, 11(7), e0159489.
- Hodell, D. A., Kanfoush, S. L., Shemesh, A., Crosta, X., Charles, C. D., & Guilderson, T. P. (2001). Abrupt cooling of Antarctic surface waters and sea ice expansion in the South Atlantic sector of the Southern Ocean at 5000 cal yr BP. *Quaternary Research*, 56(2), 191-198.
- Hogan, K. A., Larter, R. D., Graham, A. G., Arthern, R., Kirkham, J. D., Totten Minzoni, R., ... & Wellner, J. (2020). Revealing the former bed of Thwaites Glacier using sea-floor bathymetry: implications for warm-water routing and bed controls on ice flow and buttressing. *The Cryosphere*, 14(9), 2883-2908.

- Hogg, A., Hua, Q., Blackwell, P., Niu, M., Buck, C., Guilderson, T., . . . Zimmerman, S. (2013). SHCal13 Southern Hemisphere Calibration, 0–50,000 Years cal BP. *Radiocarbon*, 55(4), 1889-1903. doi:10.2458/azu_js_rc.55.16783
- Holland, M. M., Landrum, L., Kostov, Y., & Marshall, J. (2017). Sensitivity of Antarctic sea ice to the Southern Annular Mode in coupled climate models. *Climate Dynamics*, 49(5), 1813-1831.
- Holland, M.M., Landrum, L., Raphael, M. et al. Springtime winds drive Ross Sea ice variability and change in the following autumn. *Nat Commun* 8, 731 (2017). <https://doi.org/10.1038/s41467-017-00820-0>
- Hollister C.D., Heezen B.C. (1972), Geological effects of ocean bottom currents, A.L. Gordon (Ed.), *Studies in Physical Oceanography*, vol. 2, Gordon and Breach, New York, N.Y, pp. 37- 66
- Hooke, R. L., & Elverhøi, A. (1996). Sediment flux from a fjord during glacial periods, Isfjorden, Spitsbergen. *Global and Planetary Change*, 12(1-4), 237-249.
- Hooke, R., Elverhøi, A. (1996). Sediment flux from a fjord during glacial periods, Isfjorden, Spitsbergen. *Glob. Planet. Change*, 12, 237-249.
- Horn Matthew G., Charlotte P. Beucher, Rebecca S. Robinson, Mark A. Brzezinski, Southern ocean nitrogen and silicon dynamics during the last deglaciation, *Earth and Planetary Science Letters*, Volume 310, Issues 3–4, 2011, Pages 334-339, ISSN 0012-821X, <https://doi.org/10.1016/j.epsl.2011.08.016>.
- Howat, I. M., & Domack, E. W. (2003). Reconstructions of western Ross Sea palaeo-ice-stream grounding zones from high-resolution acoustic stratigraphy. *Boreas*, 32(1), 56-75.
- Howe, J. A., Austin, W. E., Forwick, M., Paetzel, M., Harland, R. E. X., & Cage, A. G. (2010). Fjord systems and archives: a review. Geological Society, London, Special Publications, 344(1), 5-15.
- Hua, Q., Barbetti, M., & Rakowski, A. (2013). Atmospheric Radiocarbon for the Period 1950–2010. *Radiocarbon*, 55(4), 2059-2072. doi:10.2458/azu_js_rc.v55i2.16177
- Hulbe, C. L., Scambos, T. A., Youngberg, T., & Lamb, A. K. (2008). Patterns of glacier response to disintegration of the Larsen B ice shelf, Antarctic Peninsula. *Global and planetary change*, 63(1), 1-8.
- Hulbe, C., & Fahnestock, M. (2007). Century-scale discharge stagnation and reactivation of the Ross ice streams, West Antarctica. *Journal of Geophysical Research: Earth Surface*, 112(F3).
- Hunter, L. E., Powell, R. D., & Lawson, D. E. (1996). Flux of debris transported by ice at three Alaskan tidewater glaciers. *Journal of Glaciology*, 42(140), 123-135.
- Ingólfsson Ó., Hjort C., Berkman P., Björck, S., Colhoun E., Goodwin I.D., Hall B., Hiraakawa, K. Melles, M. Möller P. and Prentice M. (1998), Antarctic glacial history since the Last Glacial Maximum: an overview of the record on land, *Antarctic Science*, vol. 10, pp. 326-344.
- Ito, T., Parekh, P., Dutkiewicz, S., & Follows, M. J. (2005). The Antarctic circumpolar productivity belt. *Geophysical research letters*, 32(13).
- Jabour, J., & Smith, D. (2018). The Ross Sea Region Marine Protected Area: Can It be Successfully Managed? *Ocean Yearbook Online*, 32(1), 190-205.
- Jacobs S.S. (2002), Freshening of the Ross Sea during the Late 20th Century. *Science*, vol. 297(5580), pp. 386–389. doi:10.1126/science.1069574
- Jacobs S.S. (2004), Bottom water production and its links with the thermohaline circulation. *Antarctic Science*, vol. 16, pp. 427–437.

- Jacobs, S. S., Hellmer, H. H., & Jenkins, A. (1996). Antarctic ice sheet melting in the Southeast Pacific. *Geophysical Research Letters*, 23(9), 957-960.
- Jacobs, S.S., H.H. Hellmer, C.S.M. Doake, A. Jenkins (1992) Melting of ice shelves and the mass balance of Antarctica. *J. Glaciol.*, 38(130), 375–387.
- Jacot Des Combes, H., Esper, O., De La Rocha, C. L., Abelmann, A., Gersonde, R., Yam, R., & Shemesh, A. (2008). Diatom $\delta^{13}\text{C}$, $\delta^{15}\text{N}$, and C/N since the Last Glacial Maximum in the Southern Ocean: Potential impact of species composition. *Paleoceanography*, 23(4).
- Jaeger John M. r v, Nittrouer Charles A.; Sediment deposition in an Alaskan fjord; controls on the formation and preservation of sedimentary structures in Icy Bay. *Journal of Sedimentary Research* 1999;; 69 (5): 1011–1026.
- Jaeger, J. M., & Koppes, M. N. (2016). The role of the cryosphere in source-to-sink systems. *Earth-Science Reviews*, 153, 43-76.
- Jaeger, J. M., & Nittrouer, C. A. (1999). Marine record of surge-induced outburst floods from the Bering Glacier, Alaska. *Geology*, 27(9), 847-850.
- Jaeger, J.M., Nittrouer, C.A. (1999). Sediment deposition in an Alaskan fjord; controls on the formation and preservation of sedimentary structures in Icy Bay. *J. Sed. Res.*, 69(5), 1011– 1026.
- Jakobsson, M., Gyllencreutz, R., Mayer, L. A., Dowdeswell, J. A., Canals, M., Todd, B. J., ... & Larter, R. D. (2016). Mapping submarine glacial landforms using acoustic methods. *Geological Society, London, Memoirs*, 46(1), 17-40.
- Jakobsson, M., Todd, B. J., Dowdeswell, E. K., & Hogan, K. (2016). *Atlas of Submarine Glacial Landforms: Modern, Quaternary and Ancient*.
- Jeffries, M.O. (2002), Ellesmere Island ice shelves and ice islands, U.S. Geological Survey Professional Paper 1386-J147-J163
- Jenkins, A., Dutrieux, P., Jacobs, S. *et al.* Observations beneath Pine Island Glacier in West Antarctica and implications for its retreat. *Nature Geosci* 3, 468–472 (2010).
- Jenkins, A., Shoosmith, D., Dutrieux, P., Jacobs, S., Kim, T. W., Lee, S. H., ... & Stammerjohn, S. (2018). West Antarctic Ice Sheet retreat in the Amundsen Sea driven by decadal oceanic variability. *Nature Geoscience*, 11(10), 733-738.
- Johnson, K.M., McKay, R.M., Etourneau, J. et al. Sensitivity of Holocene East Antarctic productivity to subdecadal variability set by sea ice. *Nat. Geosci.* 14, 762–768 (2021).
- Jordan, T. A., Riley, T. R., & Siddoway, C. S. (2020). The geological history and evolution of West Antarctica. *Nature Reviews Earth & Environment*, 1(2), 117-133.
- Joughin I., Tulaczyk S., Bindschadler R., Price S. F. (2002), Changes in west Antarctic ice stream velocities: Observation and analysis. *Journal of Geophysical Research: Solid Earth*, 107(B11), EPM 3–1–EPM 3–22.
- Joughin, I., & Alley, R. B. (2011). Stability of the West Antarctic ice sheet in a warming world. *Nature Geoscience*, 4(8), 506-513.
- Joughin, I., Shapero, D., Smith, B., Dutrieux, P., & Barham, M. (2021). Ice-shelf retreat drives recent Pine Island Glacier speedup. *Science Advances*, 7(24), eabg3080.
- Joughin, I., Smith, B. E., & Medley, B. (2014). Marine ice sheet collapse potentially under way for the Thwaites Glacier Basin, West Antarctica. *Science*, 344(6185), 735-738.

- K.L. Karsh, T.W. Trull, D.M. Sigman, P.A. Thompson, J. Granger, The contributions of nitrate uptake and efflux to isotope fractionation during algal nitrate assimilation, *Geochimica et Cosmochimica Acta*, Volume 132, 2014, Pages 391-412, ISSN 0016-7037.
- Kellogg, T. B., & Truesdale, R. S. (1979). Ross Sea diatoms: Modern assemblage distributions and their relationship to ecologic, oceanographic, and sedimentary conditions — Reply. *Marine Micropaleontology*, 4, 401–404.
- Kellogg, T. B., Truesdale, R. S., & Osterman, L. E. (1979). Late Quaternary extent of the West Antarctic ice sheet: new evidence from Ross Sea cores. *Geology*, 7(5), 249-253.
- Khim, B. K., Colizza, E., Lee, J. I., Giglio, F., Ha, S., & Bak, Y. S. (2021). Biological productivity and glaciomarine sedimentation in the Central Basin of the northwestern Ross Sea since the last glacial maximum. *Polar Science*, 28, 100682.
- Kim, S., Lee, J. I., McKay, R. M., Yoo, K. C., Bak, Y. S., Lee, M. K., ... & Hyun, C. U. (2020). Late pleistocene paleoceanographic changes in the Ross Sea—Glacial-interglacial variations in paleoproductivity, nutrient utilization, and deep-water formation. *Quaternary Science Reviews*, 239, 106356.
- King, E. C., Hindmarsh, R. C., & Stokes, C. R. (2009). Formation of mega-scale glacial lineations observed beneath a West Antarctic ice stream. *Nature Geoscience*, 2(8), 585-588.
- King, E. C., Woodward, J., & Smith, A. M. (2007). Seismic and radar observations of subglacial bed forms beneath the onset zone of Rutford Ice Stream, Antarctica. *Journal of Glaciology*, 53(183), 665-672.
- Kingslake, J., Ely, J. C., Das, I., & Bell, R. E. (2017). Widespread movement of meltwater onto and across Antarctic ice shelves. *Nature*, 544(7650), 349-352.
- Kingslake, J., Scherer, R. P., Albrecht, T., Coenen, J., Powell, R. D., Reese, R., ... & Whitehouse, P. L. (2018). Extensive retreat and re-advance of the West Antarctic Ice Sheet during the Holocene. *Nature*, 558(7710), 430-434.
- Klassen, R. A. (1994). A preliminary interpretation of glacial history derived from glacial striations, central Newfoundland. *Current Research, Part D. Geological Survey of Canada, Paper*, 117-143.
- Kleinschmidt, G., & Tessensohn, F. (1987). Early Paleozoic westward directed subduction at the Pacific margin of Antarctica. *Gondwana Six: Structure, tectonics, and geophysics*, 40, 89-105.
- Koehlin, R. (1947). The Formation of Fjords. *Journal of Glaciology*, 1(2), 66-68. d
- Konrad, H., Shepherd, A., Gilbert, L., Hogg, A. E., McMillan, M., Muir, A., & Slater, T. (2018). Net retreat of Antarctic glacier grounding lines. *Nature Geoscience*, 11(4), 258-262.
- Kopp, R. E., DeConto, R. M., Bader, D. A., Hay, C. C., Horton, R. M., Kulp, S., ... & Strauss, B. H. (2017). Evolving understanding of Antarctic ice-sheet physics and ambiguity in probabilistic sea-level projections. *Earth's Future*, 5(12), 1217-1233.
- Koppes, M., Hallet, B., Rignot, E., Mouginot, J., Wellner, J. S., & Boldt, K. (2015). Observed latitudinal variations in erosion as a function of glacier dynamics. *Nature*, 526(7571), 100-103.
- Koppes, M., Sylwester, R., Rivera, A., & Hallet, B. (2010). Variations in Sediment yield Over the Advance and Retreat of a Calving Glacier, Laguna San Rafael, North Patagonian Icefield. *Quaternary Research*, 73(1), 84-95.
- Koppes, M.N., Hallet, B. (2002). Influence of rapid glacial retreat on the rate of erosion by tidewater glaciers. *Geology*, 30(1), 47.

- Kreutz, K. J., Mayewski, P. A., Pittalwala, I. I., Meeker, L. D., Twickler, M. S., & Whitlow, S. I. (2000). Sea level pressure variability in the Amundsen Sea region inferred from a West Antarctic glaciochemical record. *Journal of Geophysical Research: Atmospheres*, 105(D3), 4047-4059.
- Kruger, J. (1996). Moraine ridges formed from subglacial frozen-on sediment slabs and their differentiation from push moraines. *Boreas*, 25(1), 57-64.
- Krupnik I, Allison I, Bell R, Cutler P, Hik D, Lopez-Martinez J, et al. Understanding Earth's Polar Challenges: International Polar Year 2007-2008– Summary by the IPY Joint Committee. Edmonton, Alberta: Art Design Printing Inc; 2011. pp. 457-476
- Kurtz DD, Bromwich DH (1985) A recurring, atmospherically-forced polynya in Terra Nova Bay. *Antarctic Research Series, Oceanology of the Antarctic Continental Shelf*, 43, edited by Jacobs SS, A.G.U., Washington, D. C., pp. 177-201
- Kyle P.R., 1990. McMurdo Volcanic Group-Western Ross Embayment: Introduction. In: W.E. LeMasurier & J.W. Thomson, *Volcanoes of the Antarctic Plate and Southern Oceans*, Amer. Geophys. Union, Washington, D.C., 19-25.
- Kyle, P. R., Meeker, K., & Finnegan, D. (1990). Emission rates of sulfur dioxide, trace gases and metals from Mount Erebus, Antarctica. *Geophysical Research Letters*, 17(12), 2125-2128.
- Kyrke-Smith T.M., Katz R.F., Fowler A.C. (2013), Subglacial hydrology and the formation of ice streams. *Proceedings of the Royal Society A: Mathematical, Physical and Engineering Sciences*, vol. 470(2161), pp. 20130494–20130494. doi:10.1098/rspa.2013.0494
- Laird, M.G., 1987. Evolution of the cambrian-early ordovician Bowers basin, north Victoria land, and its relationships with the adjacent Wilson and Robertson Bay terrane. *Memor. Soc. Geol. Ital.* 33, 25–34.
- Laird, M.G., Bradshaw, J.D., 1982. Uppermost proterozoic and lower paleozoic geology of the transantarctic mountains. In: Craddock, C. (Ed.), *Antarctic Geosciences*. Univ. Wisconsin Press, Madison, pp. 525–533.
- Larter R.D., Barker P.F. (1989), Seismic stratigraphy of the Antarctic Peninsula Pacific margin: A record of Pliocene-Pleistocene ice volume and paleoclimate, *Geology*, vol. 17, pp. 731-734.
- Läufer A.L., Damaske D. and Lisker F. (2011) Neogene Tectonics in the Edisto and Tucker Inlet Region and Its Correlation with Offshore Magnetic Anomalies North of Cape Adare, Northern Victoria Land, Antarctica. *Polarforschung* 80 (2), 111 – 126, 2011
- Lear, C. H., Elderfield, H., & Wilson, P. A. (2000). Cenozoic deep-sea temperatures and global ice volumes from Mg/Ca in benthic foraminiferal calcite. *Science*, 287(5451), 269-272.
- Ledford-Hoffman P.A, D.J Demaster, C.A Nittrouer, Biogenic-silica accumulation in the Ross Sea and the importance of Antarctic continental-shelf deposits in the marine silica budget, *Geochimica et Cosmochimica Acta*,
- Lee, J.I.; McKay, R.M.; Gollidge, N.R.; Yoon, H.I.; Yoo, K.-C.; Kim, H.J.; Hong, J.K. Widespread persistence of expanded East Antarctic glaciers in the southwest Ross Sea during the last deglaciation. *Geology* 2017, 45, 403–406.
- Leong, W. J., & Horgan, H. J. (2020). DeepBedMap: a deep neural network for resolving the bed topography of Antarctica. *The Cryosphere*, 14(11), 3687-3705.
- Leventer, A., & Dunbar, R. B. (1996). Factors influencing the distribution of diatoms and other algae in the Ross Sea. *Journal of Geophysical Research: Oceans*, 101(C8), 18489-18500.
- Leventer, A., Domack, E. W., Ishman, S. E., Brachfeld, S., McClennen, C. E., & Manley, P. (1996). Productivity cycles of 200–300 years in the Antarctic Peninsula region: understanding linkages

- among the sun, atmosphere, oceans, sea ice, and biota. *Geological Society of America Bulletin*, 108(12), 1626-1644.
- Leventer, A., Domack, E., Barkoukis, A., McAndrews, B., & Murray, J. (2002). Laminations from the Palmer Deep: A diatom-based interpretation. *Paleoceanography*, 17(3), PAL-3.
- Leventer, A., Dunbar, R. B., and DeMaster, D. J. (1993), Diatom Evidence for Late Holocene Climatic Events in Granite Harbor, Antarctica, *Paleoceanography*, 8(3), 373– 386.
- Levermann, A., Clark, P. U., Marzeion, B., Milne, G. A., Pollard, D., Radic, V., & Robinson, A. (2013). The multimillennial sea-level commitment of global warming. *Proceedings of the National Academy of Sciences*, 110(34), 13745-13750.
- Libes, S. M., *An Introduction to Marine Biogeochemistry*, Wiley & Sons, N.Y., 1992.
- Lisitzin A.P. (2003), *Sea-Ice and Iceberg Sedimentation in the Ocean: Recent and Past*, Springer, Heidelberg, Germany, 562 pages.
- Lisitzin, A. P. (1985). The silica cycle during the last ice age. *Palaeogeography, Palaeoclimatology, Palaeoecology*, 50(1), 241-270.
- Livingstone, S. J., Cofaigh, C. Ó., Hogan, K. A., & Dowdeswell, J. A. (2016). Submarine glacial-landform distribution along an Antarctic Peninsula palaeo-ice stream: a shelf-slope transect through the Marguerite Trough system (66–70° S). *Geological Society, London, Memoirs*, 46(1), 485-492.
- Lodolo, E. et al. Late-glacial fluctuations of two southern Patagonia outlet glaciers revealed by high-resolution seismic surveys. *Quat. Res.*
- Lowe, A. L., & Anderson, J. B. (2003). Evidence for abundant subglacial meltwater beneath the paleo-ice sheet in Pine Island Bay, Antarctica. *Journal of Glaciology*, 49(164), 125-138.
- Lowry, D. P., Golledge, N. R., Bertler, N. A., Jones, R. S., McKay, R., & Stutz, J. (2020). Geologic controls on ice sheet sensitivity to deglacial climate forcing in the Ross Embayment, Antarctica. *Quaternary Science Advances*, 1, 100002.
- Lucchi, R. G., Rebesco, M., Camerlenghi, A., Busetti, M., Tomadin, L., Villa, G., ... & Giorgetti, G. (2002). Mid-late Pleistocene glacial-marine sedimentary processes of a high-latitude, deep-sea sediment drift (Antarctic Peninsula Pacific margin). *Marine Geology*, 189(3-4), 343-370.
- Lurton, X. (2010). *An Introduction to Underwater Acoustics: Principles and Applications*. Berlin: Springer.
- MacAyeal D, Okal EA, Aster RC, Bassis JN. Seismic and hydroacoustic tremor generated by colliding icebergs. *Journal of Geophysical Research*. 2008;113:F03011.
- MacAyeal, D. R., & Sergienko, O. V. (2013). The flexural dynamics of melting ice shelves. *Annals of Glaciology*, 54(63), 1-10.
- Mackiewicz Nancy E., Ross D Powell, Paul R Carlson, Bruce F Molnia, *Interlaminated ice-proximal glacial-marine sediments in Muir Inlet, Alaska, Marine Geology, Volume 57, Issues 1–4, (1984)*
- Maldonado, A., Barnolas, A., Bohoyo, F., Escutia, C., Galindo-Zaldívar, J., Hernández-Molina, J., ... & Vázquez, J. T. (2005). Miocene to recent contourite drifts development in the northern Weddell Sea (Antarctica). *Global and Planetary Change*, 45(1-3), 99-129.
- Marschalek, J. W., Zurli, L., Talarico, F., van de Flierdt, T., Vermeesch, P., Carter, A., ... & McKay, R. M. (2021). A large West Antarctic Ice Sheet explains early Neogene sea-level amplitude. *Nature*, 600(7889), 450-455.

- Martin, D. F., Cornford, S. L., & Payne, A. J. (2019). Millennial-scale vulnerability of the Antarctic ice sheet to regional ice shelf collapse. *Geophysical Research Letters*, 46(3), 1467-1475.
- Matsuoka, K., Hindmarsh, R. C., Moholdt, G., Bentley, M. J., Pritchard, H. D., Brown, J., ... & Whitehouse, P. L. (2015). Antarctic ice rises and rumples: Their properties and significance for ice-sheet dynamics and evolution. *Earth-science reviews*, 150, 724-745.
- McGlannan, A. J., Bart, P. J., Chow, J. M., & DeCesare, M. (2017). On the influence of post-LGM ice shelf loss and grounding zone sedimentation on West Antarctic ice sheet stability. *Marine Geology*, 392, 151-169.
- McKay, R. (2008) Retreat of the Ross Ice Shelf since the Last Glacial Maximum derived from sediment cores in deep basins surrounding Ross Island. *Palaeogeogr. Palaeoclimatol. Palaeoecol.* 260, 245–261
- McMillan, M., Shepherd, A., Sundal, A., Briggs, K., Muir, A., Ridout, A., ... & Wingham, D. (2014). Increased ice losses from Antarctica detected by CryoSat-2. *Geophysical Research Letters*, 41(11), 3899-3905.
- McMinn, A., Heijnisj, H., Harle, K., & McOrist, G. (2001). Late-Holocene climatic change recorded in sediment cores from Ellis Fjord, eastern Antarctica. *The Holocene*, 11(3), 291-300.
- McMullen K., Domack E., Leventer A., Dunbar R., and Brachfeld S. (2006), Glacial morphology and marine stratigraphy of the Mertz Trough, East Antarctica, *Palaeogeography, Palaeoclimatology, Palaeoecology*, vol. 231, pp. 169–180.
- Meier, M., Lundstrom, S., Stone, D., Kamb, B., Engelhardt, H., Humphrey, N.F., Dunlap, W.W., Fahnestock, M., Krimmel, R.M., Walters, R. (1994). Mechanical and hydrologic basis for the rapid motion of a large tidewater glacier, 1. Observations. *J. Geophys. Res.* 99, 15219 15229.
- Menzies, J., & Ross, M. (2020). *Glacial Processes and Landforms—Transport and Deposition*.
- Menzies, J., van der Meer, J. J., & Shilts, W. W. (2018). Subglacial processes and sediments. In *Past glacial environments* (pp. 105-158). Elsevier.
- Menzies, J., van der Meer, J. J., & Shilts, W. W. (2018). Subglacial processes and sediments. In *Past glacial environments* (pp. 105-158). Elsevier.
- Meredith, M. P., & King, J. C. (2005). Rapid climate change in the ocean west of the Antarctic Peninsula during the second half of the 20th century. *Geophysical Research Letters*, 32, L19604
- Meyers MA, KK Chawla – 2008 *Mechanical behavior of materials*
- Meyers Philip A., Preservation of elemental and isotopic source identification of sedimentary organic matter,
- Mezgec, K., Stenni, B., Crosta, X. et al. Holocene sea ice variability driven by wind and polynya efficiency in the Ross Sea. *Nat Commun* 8, 1334 (2017).
- Miles, B. W. J., Stokes, C. R., Vieli, A., & Cox, N. J. (2013). Rapid, climate-driven changes in outlet glaciers on the Pacific coast of East Antarctica. *Nature*, 500(7464), 563-566.
- Miles, B. W., Stokes, C. R., & Jamieson, S. S. (2016). Pan-ice-sheet glacier terminus change in East Antarctica reveals sensitivity of Wilkes Land to sea-ice changes. *Science Advances*, 2(5), e1501350.
- Milliken, K.T., Anderson, J.B., Wellner, J.S., Bohaty, S.M., Manley, P.L. (2009). High resolution Holocene climate record from Maxwell Bay, South Shetland Islands, Antarctica. *Geol. Soc. Am. Bull.*, 121(11-12), 1711–1725.
- Minzoni, R. T., Anderson, J. B., Fernandez, R., & Wellner, J. S. (2015). Marine record of Holocene climate, ocean, and cryosphere interactions: herbert sound, James Ross island, Antarctica. *Quaternary Science Reviews*, 129, 239-259.

- Molnia, B. F. (1983). Subarctic glacial-marine sedimentation: a model. In *Glacial-marine sedimentation* (pp. 95-144). Springer, Boston, MA.
- Morlighem, M., Rignot, E., Binder, T., Blankenship, D., Drews, R., Eagles, G., ... & Young, D. A. (2020). Deep glacial troughs and stabilizing ridges unveiled beneath the margins of the Antarctic ice sheet. *Nature Geoscience*, 13(2), 132-137.
- Mortlock, R. A., & Froelich, P. N. (1989). A simple method for the rapid determination of biogenic opal in pelagic marine sediments. *Deep Sea Research Part A. Oceanographic Research Papers*, 36(9), 1415-1426.
- Mosher, D. C., & Simpkin, P. G. (December 1999). Status and Trends of Marine High-Resolution Seismic Reflection Profiling: Data Acquisition. *Geoscience Canada*, ss. 174-188.
- Mosola, A.B.; Anderson, J.B. Expansion and rapid retreat of the West Antarctic Ice Sheet in eastern Ross Sea: Possible consequence of over-extended ice streams? *Quat. Sci. Rev.* 2006, 25, 2177–2196.
- Mouginot, J., Rignot, E., & Scheuchl, B. (2014). Sustained increase in ice discharge from the Amundsen Sea Embayment, West Antarctica, from 1973 to 2013. *Geophysical Research Letters*, 41(5), 1576-1584.
- Mulder, T., Syvitski, J.P.M., Migeon, S., Faugeres, J.-C., Savoye, B. (2003). Marine hyperpycnal flows: initiation, behavior and related deposits. A review. *Mar. Pet. Geol.* 20, 861–882,
- Munoz Y.P., Wellner J.S. (2018). Seafloor geomorphology of western Antarctic Peninsula bays: a signature of ice flow behaviour. *The Cryosphere*, 12, vol. 1, pp. 205–225.
- Munoz, Y. P., & Wellner, J. S. (2016). Local controls on sediment accumulation and distribution in a fjord in the West Antarctic Peninsula: implications for palaeoenvironmental interpretations. *Polar Research*, 35(1), 25284.
- Naish, T. R. Constraints on the amplitude of late Pliocene eustatic sea-level fluctuations: new evidence from the New Zealand shallow-marine sediment record. *Geology* 25, 1139–1142 (2007)
- Naish, T. R., Wilson G. (2009) - Obliquity-paced Pliocene West Antarctic ice sheet oscillations. *Nature* Vol 458.
- Naish, T., Powell, R., Levy, R., Wilson, G., Scherer, R., Talarico, F., ... & Williams, T. (2009). Obliquity-paced Pliocene West Antarctic ice sheet oscillations. *Nature*, 458(7236), 322-328.
- Napieralski, J., Harbor, J., & Li, Y. (2007). Glacial geomorphology and geographic information systems. *Earth-Science Reviews*, 85(1-2), 1-22.
- Nardini I, P. Armienti, S. Rocchi, S. Burgess 40Ar–39Ar Chronology and petrology of the Miocene rift-related volcanism Daniell Peninsula (northern Victoria Land, Antarctica) *Terra Antartica*, 10 (2003), pp. 39-62
- Nelson, A. E., Smellie, J. L., Hambrey, M. J., Williams, M., Vautravers, M., Salzmann, U., ... & Regelous, M. (2009). Neogene glacial debris flows on James Ross Island, northern Antarctic Peninsula, and their implications for regional climate history. *Quaternary Science Reviews*, 28(27-28), 3138-3160.
- Nengye L, 2018, "The European Union and the establishment of marine protected areas in Antarctica" *International Environmental Agreements: Politics, Law and Economics* Vol. 18, No. 6, pp 861, 1573-1553
- Nerem, R. S., Chambers, D. P., Choe, C., & Mitchum, G. T. (2010). Estimating mean sea level change from the TOPEX and Jason altimeter missions. *Marine Geodesy*, 33(S1), 435-446.
- Nesje, A. (2009). Fjords of Norway: Complex Origin of a Scenic Landscape. In *Geomorphological Landscapes of the World* (pp. 223-234). Springer, Dordrecht.

- Nick, F.M., van der Veen, C.J., Oerlemans, J. (2007). Controls on advance of tidewater glaciers: Results from numerical modeling applied to Columbia Glacier. *J. Geophys. Res.*, 112(F3), 1–11.
- Nielsen, S. H., Koç, N., & Crosta, X. (2004). Holocene climate in the Atlantic sector of the Southern Ocean: controlled by insolation or oceanic circulation?. *Geology*, 32(4), 317-320.
- Nitsche, F. O., Gohl, K., Larter, R. D., Hillenbrand, C. D., Kuhn, G., Smith, J. A., ... & Jakobsson, M. (2013). Paleo ice flow and subglacial meltwater dynamics in Pine Island Bay, West Antarctica. *The Cryosphere*, 7(1), 249-262.
- Nitsche, F. O., Larter, R. D., Gohl, K., Graham, A. G., & Kuhn, G. (2016). Crag-and-tail features on the Amundsen Sea continental shelf, West Antarctica. *Geological Society, London, Memoirs*, 46(1), 199-200.
- Nygaard, A., Sejrup, H. P., Haflidason, H., Lekens, W. A. H., Clark, C. D., & Bigg, G. R. (2007). Extreme sediment and ice discharge from marine-based ice streams: New evidence from the North Sea. *Geology*, 35(5), 395-398.
- Ó Cofaigh C., Larter R.D., Dowdeswell J.A., Hillenbrand C.D., Pudsey C.J., Evans J., Morris P. (2005), Flow of the West Antarctic Ice Sheet on the continental margin of the Bellingshausen Sea at the Last Glacial Maximum. *Journal of Geophysical Research: Solid Earth*, vol. 110, doi:10.1029/2005jb003619
- O'Brien, P. E., De Santis, L., Harris, P. T., Domack, E., & Quilty, P. G. (1999). Ice shelf grounding zone features of western Prydz Bay, Antarctica: sedimentary processes from seismic and sidescan images. *Antarctic Science*, 11(1), 78-91.
- O'Leary, T., Trull, T. W., Griffiths, F. B., Tilbrook, B., and Revill, A. T. (2001), Euphotic zone variations in bulk and compound-specific $\delta^{13}C$ of suspended organic matter in the Subantarctic Ocean, south of Australia, *J. Geophys. Res.*, 106(C12), 31669– 31684, doi:10.1029/2000JC000288.
- Oeschger, H., Siegenthaler, U., Schotterer, U. and Gugelmann, A. (1975), A box diffusion model to study the carbon dioxide exchange in nature. *Tellus*, 27: 168-192. <https://doi.org/10.1111/j.2153-3490.1975.tb01671.x>
- Ohshima, K. I., Fukamachi, Y., Williams, G. D., Nishishi, S., Roquet, F., Kitade, Y., ... & Wakatsuchi, M. (2013). Antarctic Bottom Water production by intense sea-ice formation in the Cape Darnley polynya. *Nature Geoscience*, 6(3), 235-240.
- Olivia Truax MSc, 2018, Antarctic Holocene paleoceanographic evolution at the Ross Sea-Southern Ocean interface (thesis)
- Orombelli G. (1986) La prima spedizione del Programma Nazionale di Ricerche in Antartide. Osservazioni geomorfologiche. *Rivista Geografica Italiana* 93: 129-169
- Orsi, A. H., & Wiederwohl, C. L. (2009). A recount of Ross Sea waters. *Deep Sea Research Part II: Topical Studies in Oceanography*, 56(13-14), 778-795.
- Padman L., Howard S.L., Orsi A.H., Muench, R.D. (2008), Tides of the northwestern Ross Sea and their impact on dense outflows of Antarctic Bottom Water. *Deep Sea Research Part II: Topical Studies in Oceanography*, vol. 56, pp. 818–834.
- Padman, L., & Erofeeva, S. (2005). Tide model driver (TMD) manual. Earth and Space research.
- Pagani, M., Huber, M., Liu, Z., Bohaty, S. M., Henderiks, J., Sijp, W., ... & DeConto, R. M. (2011). The role of carbon dioxide during the onset of Antarctic glaciation. *science*, 334(6060), 1261-1264.
- Pahnke, K., & Sachs, J. P. (2006). Sea surface temperatures of southern midlatitudes 0–160 kyr BP. *Paleoceanography*, 21(2).

- Pan, B. J., Vernet, M., Reynolds, R. A., & Mitchell, B. G. (2019). The optical and biological properties of glacial meltwater in an Antarctic fjord. *PLoS one*, 14(2), e0211107.
- Panizzo, V., Crespin, J., Crosta, X., Shemesh, A., Masse, G., Yam, R., ... & Cardinal, D. (2014). Sea ice diatom contributions to Holocene nutrient utilization in East Antarctica. *Paleoceanography*, 29(4), 328-343.
- Paolo, F. S., Fricker, H. A., & Padman, L. (2015). Volume loss from Antarctic ice shelves is accelerating. *Science*, 348(6232), 327-331.
- Passchier, S., Ciarletta, D. J., Henao, V., & Sekkas, V. (2019). Sedimentary processes and facies on a high-latitude passive continental margin, Wilkes Land, East Antarctica. *Geological Society, London, Special Publications*, 475(1), 181-201.
- Patterson S.L., Whitworth T. (1990), *Physical oceanography*, Elsevier Oceanographic Series, vol. 51, New York, pp. 55-93
- Pattyn, F. (2018). The paradigm shift in Antarctic ice sheet modelling. *Nature communications*, 9(1), 1-3.
- Pattyn, F., Ritz, C., Hanna, E., Asay-Davis, X., DeConto, R., Durand, G., ... & Van den Broeke, M. (2018). The Greenland and Antarctic ice sheets under 1.5 C global warming. *Nature climate change*, 8(12), 1053-1061.
- Pérez, L. F., Jakobsson, M., Funck, T., Andresen, K. J., Nielsen, T., O'Regan, M., & Mørk, F. (2020). Late Quaternary sedimentary processes in the central Arctic Ocean inferred from geophysical mapping. *Geomorphology*, 369, 107309.
- Pérez, L. F., Martos, Y. M., García, M., Weber, M. E., Raymo, M. E., Williams, T., ... & Zheng, X. (2021). Miocene to present oceanographic variability in the Scotia Sea and Antarctic ice sheets dynamics: Insight from revised seismic-stratigraphy following IODP Expedition 382. *Earth and Planetary Science Letters*, 553, 116657.
- Pérez, L. F., Santis, L. D., McKay, R. M., Larter, R. D., Ash, J., Bart, P. J., ... & International Ocean Discovery Program Expedition 374 Scientists. (2022). Early and middle Miocene ice sheet dynamics in the Ross Sea: Results from integrated core-log-seismic interpretation. *Bulletin*, 134(1-2), 348-370.
- Peters, J. L., Benetti, S., Dunlop, P., Cofaigh, C. Ó., Moreton, S. G., Wheeler, A. J., & Clark, C. D. (2016). Sedimentology and chronology of the advance and retreat of the last British-Irish Ice Sheet on the continental shelf west of Ireland. *Quaternary Science Reviews*, 140, 101-124.
- Pezza, A. B., Rashid, H. A., & Simmonds, I. (2012). Climate links and recent extremes in antarctic sea ice, high-latitude cyclones, Southern Annular Mode and ENSO. *Climate Dynamics*, 38(1–2), 57–73.
- Pichon J.-J., M. Labracherie, L.D. Labeyrie, J. Duprat Transfer functions between assemblages and surface hydrology in the Southern Ocean Palaeogeogr. *Palaeoclimatol. Palaeoecol.*, 61 (1987), pp. 79-95
- Pollard, D., DeConto, R. M., & Alley, R. B. (2015). Potential Antarctic Ice Sheet retreat driven by hydrofracturing and ice cliff failure. *Earth and Planetary Science Letters*, 412, 112-121.
- Pour A.B., Park Y., Hashim M. and Hong J. K. (2018) Regional geological mapping in Northern Victoria Land, Antarctica using multispectral remote sensing satellite data.
- Powell R. D. (1990), *Glaciomarine processes at grounding-line fans and their growth to icecontact deltas*. Geological Society, London, Special Publications, vol. 53, pp.53–73.
- Powell, R. D., & Molnia, B. F. (1989). Glaciomarine sedimentary processes, facies and morphology of the south-southeast Alaska shelf and fjords. *Marine Geology*, 85(2-4), 359-390.
- Powell, R.D. (1991). Grounding-line systems as second-order controls on fluctuations of tidewater termini of temperate glaciers, in *Glacial Marine Sedimentation: Paleoclimatic Significance*, edited by J.B.

- Anderson and G.M. Ashley, Geological Society of America Special Paper 261, Boulder, CO, p. 75–93.
- Powell, R.D., Dawber, M., McInnes, J.N., Pyne, A.R. (1996). Observations of the grounding-line area at a floating glacier terminus. *Ann. Glaciol.*, 22, 217-223
- Presti, M., De Santis, L., Brancolini, G., & Harris, P. T. (2005). Continental shelf record of the East Antarctic Ice Sheet evolution: seismo-stratigraphic evidence from the George V Basin. *Quaternary Science Reviews*, 24(10-11), 1223-1241.
- Priddle, J., Heywood, R.B. & Theriot, E. Some environmental factors influencing phytoplankton in the Southern Ocean around South Georgia. *Polar Biol* 5, 65–79 (1986). <https://doi.org/10.1007/BF00443379>
- Pritchard, H., Ligtenberg, S. R., Fricker, H. A., Vaughan, D. G., van den Broeke, M. R., & Padman, L. (2012). Antarctic ice-sheet loss driven by basal melting of ice shelves. *Nature*, 484(7395), 502-505.
- Pritchard, H.D., R.J. Arthern, D.G. Vaughan, and L.A. Edwards (2009), Extensive dynamic thinning on the margins of the Greenland and Antarctic ice sheets, *Nature*, 461 (7266), 971-975, doi: 10.1038/nature08471.
- Prothro, L. O., Simkins, L. M., Majewski, W., & Anderson, J. B. (2018). Glacial retreat patterns and processes determined from integrated sedimentology and geomorphology records. *Marine Geology*, 395, 104-119.
- Purkey, S. G., & Johnson, G. C. (2013). Antarctic Bottom Water Warming and Freshening: Contributions to Sea Level Rise, Ocean Freshwater Budgets, and Global Heat Gain. *Journal of Climate*, 26(16), 6105–6122.
- Quinn, R., Bull, J. M. and Dix, J. K., 1997, Imaging wooden artefacts using Chirp sources, *Archaeological Prospection* 4 (1), 25–35.
- R. McKay, N.R. Golledge, S. Maas, T. Naish, R. Levy, G. Dunbar, G. Kuhn; Antarctic marine ice-sheet retreat in the Ross Sea during the early Holocene. *Geology* 2016; 44 (1): 7–10.
- Raphael, M. N. (2003). Impact of observed sea-ice concentration on the Southern Hemisphere extratropical atmospheric circulation in summer. *Journal of Geophysical Research*, 108(D22).
- Rathburn, A. E., Pichon, J. J., Ayress, M. A., & De Deckker, P. (1997). Microfossil and stable-isotope evidence for changes in Late Holocene palaeoproductivity and palaeoceanographic conditions in the Prydz Bay region of Antarctica. *Palaeogeography, Palaeoclimatology, Palaeoecology*, 131(3-4), 485-510.
- Ray, Y., Sen, S., Sen, K., & Beg, M. J. (2021). Quantifying the past glacial movements in Schirmacher Oasis, East Antarctica. *Polar Science*, 30, 100733.
- Rebecca Parker MSc, 2017, Sea-ice and diatom primary productivity in the Ross Sea, Antarctica: the response to post glacial warming (thesis)
- Rebesco M. (2005), Contourites. In: Selley, R.C., Cocks, L.R.M., Plimer, I.R. (Eds.), *Encyclopedia of Geology*. Elsevier, Oxford, pp. 513–527
- Rebesco M., Hernández-Molina F. J., Van Rooij D., Wåhlin A. (2014), Contourites and associated sediments controlled by deep-water circulation processes: State-of-the-art and future considerations, *Marine Geology*, vol. 352, pp. 111-154.
- Rebesco, M., & Stow, D. (2001). Seismic expression of contourites and related deposits: a preface. *Marine Geophysical Researches*, 22(5), 303-308.

- Rebesco, M., Camerlenghi, A., De Santis, L., Domack, E., & Kirby, M. (1998). Seismic stratigraphy of Palmer Deep: a fault-bounded late Quaternary sediment trap on the inner continental shelf, Antarctic Peninsula Pacific margin. *Marine Geology*, 151(1-4), 89-110.
- Rebesco, M., Camerlenghi, A., Geletti, R., & Canals, M. (2006). Margin architecture reveals the transition to the modern Antarctic ice sheet ca. 3 Ma. *Geology*, 34(4), 301-304.
- Rebesco, M., E. Domack, F. Zgur, C. Lavoie, A. Leventer, S. Brachfeld, V. Willmott, G. Halverson, M. Truffer, T. Scambos, J. Smith, and E. Pettit (2014), Boundary Condition of Grounding Lines Prior to Collapse, Larsen-B Ice Shelf, Antarctica, *Science*, 345, 1354-1358.
- Reimer, P. (2021). Evolution of Radiocarbon Calibration. *Radiocarbon*, 1-17.
- Reimer, P., Bard, E., Bayliss, A., Beck, J., Blackwell, P., Ramsey, C., . . . Van der Plicht, J. (2013). IntCal13 and Marine13 Radiocarbon Age Calibration Curves 0–50,000 Years cal BP. *Radiocarbon*, 55(4), 1869-1887.
- Reinardy, B. T. I., Escutia, C., Iwai, M., Jimenez-Espejo, F. J., Cook, C., van de Flierdt, T., & Brinkhuis, H. (2015). Repeated advance and retreat of the East Antarctic Ice Sheet on the continental shelf during the early Pliocene warm period. *Palaeogeography, Palaeoclimatology, Palaeoecology*, 422, 65-84.
- Reinardy, B. T., Booth, A. D., Hughes, A. L., Boston, C. M., Åkesson, H., Bakke, J., ... & Pearce, D. M. (2019). Pervasive cold ice within a temperate glacier—implications for glacier thermal regimes, sediment transport and foreland geomorphology. *The Cryosphere*, 13(3), 827-843.
- Rhodes, R. H., Bertler, N. A. N., Baker, J. A., Steen-Larsen, H. C., Sneed, S. B., Morgenstern, U., & Johnsen, S. J. (2012). Little Ice Age climate and oceanic conditions of the Ross Sea, Antarctica from a coastal ice core record. *Climate of the Past*, 8(4), 1223-1238.
- Rignot E., Mouginot J., Scheuchl B. (2011), Ice Flow of the Antarctic Ice Sheet, *Science*, vol. 333, pp. 1427-1430.
- Rignot, E., J. Mouginot, M. Morlighem, H. Seroussi, and B. Scheuchl (2014), Widespread, rapid grounding line retreat of Pine Island, Thwaites, Smith, and Kohler glaciers, West Antarctica, from 1992 to 2011.
- Rignot, E., Jacobs, S., Mouginot, J., & Scheuchl, B. (2013). Ice-shelf melting around Antarctica. *Science*, 341(6143), 266-270.
- Rintoul, S. R. (1998). On the origin and influence of Adélie land bottom water. In S. S. Jacobs & R. F. Weiss (Eds.), *Antarctic Research Series* (Vol. 75, pp. 151–171). Washington, D. C.: American Geophysical Union. <https://doi.org/10.1029/AR075p0151>
- Rintoul, S. R. (2000). Southern Ocean currents and climate. In *Papers and proceedings of the Royal Society of Tasmania* (Vol. 133, No. 3, pp. 41-50).
- Rintoul, S. R. (2011). The Southern Ocean in the earth system. *Science diplomacy: Antarctica, science, and the governance of international spaces*.
- Ritz, C., Edwards, T. L., Durand, G., Payne, A. J., Peyaud, V., & Hindmarsh, R. C. (2015). Potential sea-level rise from Antarctic ice-sheet instability constrained by observations. *Nature*, 528(7580), 115-118.
- Robel, A. A., Seroussi, H., & Roe, G. H. (2019). Marine ice sheet instability amplifies and skews uncertainty in projections of future sea-level rise. *Proceedings of the National Academy of Sciences*, 116(30), 14887-14892.
- Robinson R.S. , Daniel M. Sigman, Nitrogen isotopic evidence for a poleward decrease in surface nitrate within the ice age Antarctic, *Quaternary Science Reviews*, Volume 27, Issues 9–10, 2008, Pages 1076-1090, ISSN 0277-3791.

- Robinson, R. S., Brunelle, B. G., and Sigman, D. M. (2004), Revisiting nutrient utilization in the glacial Antarctic: Evidence from a new method for diatom-bound N isotopic analysis, *Paleoceanography*, 19, PA3001, doi:10.1029/2003PA000996.
- Robinson, R. S., et al. (2012), A review of nitrogen isotopic alteration in marine sediments, *Paleoceanography*, 27, PA4203, doi:10.1029/2012PA002321.
- Rocchi, S., Armienti, P., D'Orazio, M., Tonarini, S., Wijbrans, J. R., & Di Vincenzo, G. (2002). Cenozoic magmatism in the western Ross Embayment: Role of mantle plume versus plate dynamics in the development of the West Antarctic Rift System. *Journal of Geophysical Research: Solid Earth*, 107(B9), ECV-5.
- Rocchi, S., Bracciali, L., Di Vincenzo, G., Gemelli, M., & Ghezzi, C. (2011). Arc accretion to the early Paleozoic Antarctic margin of Gondwana in Victoria Land. *Gondwana Research*, 19(3), 594-607.
- Rocchi, S., Di Vincenzo, G., Armienti, P., 2005. Plates, plumes and paradigms. In: Foulger, G.R., Anderson, D.L., Natland, J.H., et al. (Eds.), *Geological Society of America Special Paper*, 388, pp. 435-447.
- Rocchi, S., Storti, F., Di Vincenzo, G., & Rossetti, F. (2003). Intraplate strike-slip tectonics as an alternative to mantle plume activity for the Cenozoic rift magmatism in the Ross Sea region, Antarctica. *Geological Society, London, Special Publications*, 210(1), 145-158.
- Rodriguez A.B. , Anderson J.B. (2004), Contourite origin for shelf and upper slope sand sheet, offshore Antarctica, *Sedimentology*, vol. 51 , pp. 699-711.
- Roland, N. W., Läufer, A. L., & Rossetti, F. (2004). Revision of the terrane model of northern Victoria Land (Antarctica). *Terra Antarctica*, 11(1), 55-65.
- Romero, O. E., Armand, L. K., Crosta, X., & Pichon, J. J. (2005). The biogeography of major diatom taxa in Southern Ocean surface sediments: 3. Tropical/Subtropical species. *Palaeogeography, Palaeoclimatology, Palaeoecology*, 223(1-2), 49-65.
- Rosenheim, B. E., Day, M. B., Domack, E., Schrum, H., Benthien, A., and Hayes, J. M. (2008), Antarctic sediment chronology by programmed-temperature pyrolysis: Methodology and data treatment, *Geochem. Geophys. Geosyst.*
- Rosenheim, B., Santoro, J., Gunter, M., & Domack, E. (2013). Improving Antarctic Sediment ¹⁴C Dating Using Ramped Pyrolysis: An Example from the Hugo Island Trough. *Radiocarbon*, 55(1), 115-126.
- Rossetti, F., Storti, F., Busetti, M., Lisker, F., Di Vincenzo, G., Läufer, A. L., ... & Salvini, F. (2006). Eocene initiation of Ross Sea dextral faulting and implications for East Antarctic neotectonics. *Journal of the Geological Society*, 163(1), 119-126.
- Rossetti, F., Tecce, F., Aldega, L., Brilli, M., Faccenna, C., 2006. Deformation and fluid flow during orogeny at the palaeo-pacific active margin of Gondwana: the early palaeozoic Robertson Bay accretionary complex (north Victoria land, Antarctica). *J. Metamorph. Geol.* 24, 33-53.
- Röthlisberger, H. (1972). Water pressure in intra-and subglacial channels. *Journal of Glaciology*, 11(62), 177-203.
- Salvini, F., Brancolini, G., Busetti, M., Storti, F., Mazzarini, F., & Coren, F. (1997). Cenozoic geodynamics of the Ross Sea region, Antarctica: Crustal extension, intraplate strike-slip faulting, and tectonic inheritance. *Journal of Geophysical Research: Solid Earth*, 102(B11), 24669-24696.
- Sangiorgi, F., Bijl, P. K., Passchier, S., Salzmann, U., Schouten, S., McKay, R., ... & Brinkhuis, H. (2018). Southern Ocean warming and Wilkes Land ice sheet retreat during the mid-Miocene. *Nature Communications*, 9(1), 1-11.

- Santos, G. M., J. R. Southon, S. Griffin, S. R. Beaupre, and E. R. M. Druffel (2007), Ultra small-mass AMS ¹⁴C sample preparation and analyses at KCCAMS/UCI Facility, *Nucl. Instrum. Methods Phys. Res., Sect. B*, 259(1), 293–302.
- Scambos, T. A., Hulbe, C., Fahnestock, M., & Bohlander, J. (2000). The link between climate warming and break-up of ice shelves in the Antarctic Peninsula. *Journal of Glaciology*, 46(154), 516-530.
- Scambos, T., Fricker, H. A., Liu, C. C., Bohlander, J., Fastook, J., Sargent, A., ... & Wu, A. M. (2009). Ice shelf disintegration by plate bending and hydro-fracture: Satellite observations and model results of the 2008 Wilkins ice shelf break-ups. *Earth and Planetary Science Letters*, 280(1-4), 51-60.
- Schannwell, C., Barrand, N. E., & Radić, V. (2016). Future sea-level rise from tidewater and ice-shelf tributary glaciers of the Antarctic Peninsula. *Earth and Planetary Science Letters*, 453, 161-170.
- Scheuchl B., Mouginit J., Rignot E. (2012), Twelve years of ice velocity change in Antarctica observed by RADARSAT-1 and 2-satellite radar interferometry. *The Cryosphere Discussions*. 6. 1715-1738. 10.5194/tcd-6-1715-2012.
- Schmidtko, S., Heywood, K. J., Thompson, A. F., & Aoki, S. (2014). Multidecadal warming of Antarctic waters. *Science*, 346(6214), 1227-1231.
- Schock, S. G., LeBlanc, L. R., & Mayer, L. A. (1989). Chirp subbottom profiler for quantitative sediment analysis. *Geophysics*, 445-450.
- Schoof C. (2007), Ice sheet grounding line dynamics: Steady states, stability, and hysteresis., *Journal of Geophysical Research: Earth Surface*, pp. 2003–2012.
- Scott, F. J., Marchant, H. J., Australian Biological Resources Study, & Australia (Eds.). (2005). *Antarctic Marine Protists*. Canberra: Australian Biological Resources Study and Australian Antarctic Division.
- Sedwick, P. N., DiTullio, G. R., & Mackey, D. J. (2000). Iron and manganese in the Ross Sea, Antarctica: Seasonal iron limitation in Antarctic shelf waters. *Journal of Geophysical Research: Oceans*, 105(C5), 11321-11336.
- Seroussi, H., Nakayama, Y., Larour, E., Menemenlis, D., Morlighem, M., Rignot, E., & Khazendar, A. (2017). Continued retreat of Thwaites Glacier, West Antarctica, controlled by bed topography and ocean circulation. *Geophysical Research Letters*, 44(12), 6191-6199.
- Setti, M., Marinoni, L., & Lopez-Galindo, A. (2004). Mineralogical and geochemical characteristics (major, minor, trace elements and REE) of detrital and authigenic clay minerals in a Cenozoic sequence from Ross Sea, Antarctica. *Clay Minerals*, 39(4), 405-421.
- Shapiro G.I., Huthnance J.M., Ivanov V.V., (2003), Dense water cascading off the continental shelf. *Journal of Geophysical Research*, vol. 108.
- Shemesh A., L.H. Burckle, P.N. Froelich Dissolution and preservation of Antarctic diatoms and the effect on sediment thanatocoenoses *Quaternary Res.*, 31 (1989), pp. 288-308
- Shemesh, A., Mortlock, R. A., & Froelich, P. N. (1989). Late Cenozoic Ge/Si record of marine biogenic opal: Implications for variations of riverine fluxes to the ocean. *Paleoceanography*, 4(3), 221-234.
- Shepherd, A., D. Wingham and E. Rignot. (2004) Warm ocean is eroding West Antarctic Ice Sheet. *Geophys. Res. Lett.*, 31(23).
- Shepherd, A., Ivins, E., Rignot, E., Smith, B., Van Den Broeke, M., Velicogna, I., ... & Wouters, B. (2018). Mass balance of the Antarctic Ice Sheet from 1992 to 2017. *Nature*, 558, 219-222.

- Shevenell, A. E., Domack, E. W., & Kernan, G. M. (1997). Record of Holocene palaeoclimate change along the Antarctic Peninsula: evidence from glacial marine sediments, Lallemand Fjord. *Oceanographic Literature Review*, 6(44), 552.
- Shevenell, A. E., Ingalls, A. E., Domack, E. W., & Kelly, C. (2011). Holocene Southern Ocean surface temperature variability west of the Antarctic Peninsula. *Nature*, 470(7333), 250-254.
- Shipp, S. S. (1999). Retreat history of the last glacial maximum ice sheet in Ross Sea, Antarctica. Rice University.
- Sigman, D. M., Altabet, M. A., Francois, R., McCorkle, D. C., and Gaillard, J.-F. (1999), The isotopic composition of diatom-bound nitrogen in Southern Ocean sediments, *Paleoceanography*, 14(2), 118–134.
- Silvano, A., Foppert, A., Rintoul, S. R., Holland, P. R., Tamura, T., Kimura, N., ... & Macdonald, A. M. (2020). Recent recovery of Antarctic Bottom Water formation in the Ross Sea driven by climate anomalies. *Nature Geoscience*, 13(12), 780-786.
- Simkins, L. M., Greenwood, S. L., & Anderson, J. B. (2018). Diagnosing ice sheet grounding line stability from landform morphology. *The Cryosphere*, 12(8), 2707-2726.
- Simms Alexander R., Kristy T. Milliken, John B. Anderson, Julia S. Wellner, The marine record of deglaciation of the South Shetland Islands, Antarctica since the Last Glacial Maximum, *Quaternary Science Reviews*, Volume 30, Issues 13–14, 2011, Pages 1583-1601, ISSN 0277-3791.
- Sjunneskog, C., & Taylor, F. (2002). Postglacial marine diatom record of the Palmer deep, Antarctic Peninsula (ODP Leg 178, Site 1098) 1. Total diatom abundance. *Paleoceanography*, 17(3), PAL-4.
- Slabon, P., Dorschel, B., Jokat, W., Myklebust, R., Hebbeln, D., & Gebhardt, C. (2016). Greenland ice sheet retreat history in the northeast Baffin Bay based on high-resolution bathymetry. *Quaternary Science Reviews*, 154, 182-198.
- Smith, A. M., & Murray, T. (2009). Bedform topography and basal conditions beneath a fast-flowing West Antarctic ice stream. *Quaternary Science Reviews*, 28(7-8), 584-596.
- Smith, J. A., Graham, A. G., Post, A. L., Hillenbrand, C. D., Bart, P. J., & Powell, R. D. (2019). The marine geological imprint of Antarctic ice shelves. *Nature Communications*, 10(1), 1-16.
- Smith, R. C., Fraser, W. R., & Stammerjohn, S. E. (2003). Climate variability and ecological response of the marine ecosystem in the western Antarctic Peninsula (WAP) region. *Climate variability and ecosystem response at longterm ecological research sites*. Oxford University Press, New York, New York, USA, 158-173.
- Smith, W. O., Dinniman, M. S., Hofmann, E. E., & Klinck, J. M. (2014). The effects of changing winds and temperatures on the oceanography of the Ross Sea in the 21st century: Modeled Future Ross Sea Changes. *Geophysical Research Letters*, 41(5), 1624–1631.
- Spagnolo, M., Clark, C. D., Ely, J. C., Stokes, C. R., Anderson, J. B., Andreassen, K., ... & King, E. C. (2014). Size, shape and spatial arrangement of mega-scale glacial lineations from a large and diverse dataset. *Earth Surface Processes and Landforms*, 39(11), 1432-1448.
- Speer K., Rintoul S.R., Sloyan B. (2000), The Diabatic Deacon Cell. *J. Physical Oceanography*, vol. 30, pp. 3212–3222.
- Spence, P., Griffies, S. M., England, M. H., Hogg, A. M., Saenko, O. A., & Jourdain, N. C. (2014). Rapid subsurface warming and circulation changes of Antarctic coastal waters by poleward shifting winds. *Geophysical Research Letters*, 41(13), 4601-4610.

- Steig, E.J., D.P. Schneider, S.D. Rutherford, M.E. Mann, J.C. Comiso (2009) Warming of the Antarctic ice-sheet surface since the 1957. *Nature*, 457(7228), 459–462
- Stephen R. Rintoul, Chris W. Hughes, Dirk Olbers, 2001, The antarctic circumpolar current system, *International Geophysics*
- Stern, A. A., Dinniman, M. S., Zagorodnov, V., Tyler, S. W., and Holland, D. M. (2013), Intrusion of warm surface water beneath the McMurdo Ice Shelf, Antarctica, *J. Geophys. Res. Oceans*, 118, 7036– 7048, doi:10.1002/2013JC008842.
- Steven D. Boger, Antarctica — Before and after Gondwana, *Gondwana Research*, Volume 19, Issue 2, 2011.
- Stokes, C. R. (2017). Deglaciation of the Laurentide Ice Sheet from the Last Glacial Maximum. *Cuadernos de investigación geográfica.*, 43(2), 377-428.
- Stokes, C. R. (2018). Geomorphology under ice streams: moving from form to process. *Earth Surface Processes and Landforms*, 43(1), 85-123.
- Stokes, C. R., & Clark, C. D. (2001). Palaeo-ice streams. *Quaternary Science Reviews*, 20(13), 1437-1457.
- Stokes, C. R., & Clark, C. D. (2002). Are long subglacial bedforms indicative of fast ice flow?. *Boreas*, 31(3), 239-249.
- Stokes, C. R., & Clark, C. D. (2002). Ice stream shear margin moraines. *Earth Surface Processes and Landforms*, 27(5), 547-558.
- Stokes, C. R., Fowler, A. C., Clark, C. D., Hindmarsh, R. C., & Spagnolo, M. (2013). The instability theory of drumlin formation and its explanation of their varied composition and internal structure. *Quaternary Science Reviews*, 62, 77-96.
- Stokes, C. R., Spagnolo, M., Clark, C. D., Cofaigh, C. Ó., Lian, O. B., & Dunstone, R. B. (2013). Formation of mega-scale glacial lineations on the Dubawnt Lake Ice Stream bed: 1. size, shape and spacing from a large remote sensing dataset. *Quaternary Science Reviews*, 77, 190-209.
- Stokes, C. R., Tarasov, L., Blomdin, R., Cronin, T. M., Fisher, T. G., Gyllencreutz, R., ... & Teller, J. T. (2015). On the reconstruction of palaeo-ice sheets: recent advances and future challenges. *Quaternary Science Reviews*, 125, 15-49.
- Stokes, C.R., and C.D. Clark (1999), Geomorphological criteria for identifying Pleistocene ice streams, *Annals of Glaciology*, 28 (1), 67-74.
- Storey, B. C., & Granot, R. (2021). Tectonic history of Antarctica over the past 200 million years. *Geological Society, London, Memoirs*, 55(1), 9-17.
- Stow D.A.V., Kahler G., and Reeder M., (2002), Fossil contourites: type example from an Oligocene palaeoslope system, Cyprus. In: Stow, D.A.V., Pudsey, C.J., Howe, J.A., Faugères, J.-C., Viana, A.R. (Eds.), *Deep-water Contourite Systems: Modern Drifts and Ancient Series*
- Straneo, F., & Heimbach, P. (2013). North Atlantic warming and the retreat of Greenland's outlet glaciers. *Nature*, 504(7478), 36-43.
- Straneo, F., et al. (2013). Challenges to Understanding the Dynamic Response of Greenland's Marine Terminating Glaciers to Oceanic and Atmospheric Forcing. *Bull. Am. Meteorol. Soc.*, 94(8), 1131–1144, doi:10.1175/BAMS-D-12-00100.1.159
- Strickland, J. D. H., & Parsons, T. R. (1972). *A practical handbook of seawater analysis*.
- Stuiver, M. P., G. W. Pearson, and T. Braziunas (1986), Radiocarbon age calibration of marine samples back to 9000 cal yr BP, *Radiocarbon*, 28(2), 980– 1021.

- Stuiver, M., and H. A. Polach (1977), Discussion; Reporting of C-14 data, *Radiocarbon*, 19(3), 355– 363.
- Stump, E. (1995). *The Ross Orogen of the transantarctic mountains*. Cambridge University Press.
- Subt C, Fangman KA, Wellner JS, Rosenheim BE. Sediment chronology in Antarctic deglacial sediments: Reconciling organic carbon 14C ages to carbonate 14C ages using Ramped PyrOx. *The Holocene*. 2016;26(2):265-273. doi:10.1177/0959683615608688
- Syvitski, J. (1989). On the deposition of sediment within glacier-influenced fjords: oceanographic controls. *Mar. Geol.*, 85, 301–329.
- Syvitski, J. P., & Farrow, G. E. (1989). Fjord sedimentation as an analogue for small hydrocarbon-bearing fan deltas. *Geological Society, London, Special Publications*, 41(1), 21-43.
- Syvitski, J.P.M. (1991). Towards an understanding of sediment deposition on glaciated continental shelves. *Cont. Shelf Res.*, 11, 897-937.
- Syvitski, J.P.M., Burrell, D.C., Skei, J.M., 1987. *Fjords: Processes and Products*. Springer.
- Szczucinski, W., Zajaczkowski, M. (2012). Factors controlling downward fluxes of particulate matter in glacier-contact and non-glacier contact settings in a subpolar fjord (Billefjorden, Svalbard), in *Sediments, Morphology and Sedimentary Processes on Continental Shelves*, vol. 44, edited by M.Z. Li, C.R. Sherwood, and P.R. Hill, International Association of Sedimentologists, Wiley-Blackwell, Oxford, UK, p. 369-386.160
- Szczuciński, W., Zajaczkowski, M., & Scholten, J. (2009). Sediment accumulation rates in subpolar fjords— Impact of post-Little Ice Age glaciers retreat, Billefjorden, Svalbard. *Estuarine, Coastal and Shelf Science*, 85(3), 345-356.
- Taylor-Silva, B. I., & Riesselman, C. R. (2018). Polar frontal migration in the warm late Pliocene: Diatom evidence from the Wilkes Land margin, East Antarctica. *Paleoceanography and Paleoclimatology*, 33(1), 76-92.
- Tesi, T., Belt, S. T., Gariboldi, K., Muschitiello, F., Smik, L., Finocchiaro, F., ... & Langone, L. (2020). Resolving sea ice dynamics in the north-western Ross Sea during the last 2.6 ka: From seasonal to millennial timescales. *Quaternary Science Reviews*, 237, 106299.
- Tessensohn, F., & Henjes-Kunst, F. (2005). Northern Victoria Land terranes, Antarctica: far-travelled or local products?. *Geological Society, London, Special Publications*, 246(1), 275-291.
- Thomas, I. D., King, M. A., Bentley, M. J., Whitehouse, P. L., Penna, N. T., Williams, S. D., ... & Koivula, H. (2011). Widespread low rates of Antarctic glacial isostatic adjustment revealed by GPS observations. *Geophysical Research Letters*, 38(22).
- Tinto, K. J., Padman, L., Siddoway, C. S., Springer, S. R., Fricker, H. A., Das, I., ... & Bell, R. E. (2019). Ross Ice Shelf response to climate driven by the tectonic imprint on seafloor bathymetry. *Nature Geoscience*, 12(6), 441-449.
- Tolotti, R., Salvi, C., Salvi, G., & Bonci, M. C. (2013). Late Quaternary climate variability as recorded by micropalaeontological diatom data and geochemical data in the western Ross Sea, Antarctica. *Antarctic Science*, 25(6), 804-820.
- Turner, J., Lu, H., White, I., King, J. C., Phillips, T., Hosking, J. S., et al. (2016). Absence of 21st century warming on Antarctic Peninsula consistent with natural variability. *Nature*, 535(7612), 411–415.
- Van de Vijver, B., & Beyens, L. (1999). Biogeography and ecology of freshwater diatoms in Subantarctica: a review. *Journal of biogeography*, 26(5), 993-1000.

- Van der Meer, J. J., Menzies, J., & Rose, J. (2003). Subglacial till: the deforming glacier bed. *Quaternary Science Reviews*, 22(15-17), 1659-1685.
- Vanessa Lucieer, Geoffroy Lamarche, 2011, Unsupervised fuzzy classification and object-based image analysis of multibeam data to map deep water substrates, Cook Strait, New Zealand, *Continental Shelf Research*, Volume 31, Issue 11, 2011, Pages 1236-1247, ISSN 0278-4343.
- Vaughan, D., Doake, C. Recent atmospheric warming and retreat of ice shelves on the Antarctic Peninsula. *Nature* 379, 328–331 (1996).
- Vaughan, D.G., Marshall, G.J., Connolley, W.M. *et al.* Recent Rapid Regional Climate Warming on the Antarctic Peninsula. *Climatic Change* **60**, 243–274 (2003).
- Velicogna, I., Sutterley, T. C., & Van Den Broeke, M. R. (2014). Regional acceleration in ice mass loss from Greenland and Antarctica using GRACE time-variable gravity data. *Geophysical Research Letters*, 41(22), 8130-8137.
- Villinski, J. C., Dunbar, R. B., & Mucciarone, D. A. (2000). Carbon 13/Carbon 12 ratios of sedimentary organic matter from the Ross Sea, Antarctica: A record of phytoplankton bloom dynamics. *Journal of Geophysical Research: Oceans*, 105(C6), 14163-14172.
- Viseras, C., & Maldonado, A. (1999). Facies architecture, seismic stratigraphy and development of a high-latitude basin: the Powell Basin (Antarctica). *Marine geology*, 157(1-2), 69-87.
- Watts A. *International Law and the Antarctic Treaty System* 1992
- Weertman, J. (1974). Stability of the junction of an ice sheet and an ice shelf. *Journal of Glaciology*, 13(67), 3-11.
- Wellner, J., Lowe, A., Shipp, S., & Anderson, J. (2001). Distribution of glacial geomorphic features on the Antarctic continental shelf and correlation with substrate: Implications for ice behavior. *Journal of Glaciology*, 47(158), 397-411.
- Wellner, J.S., D.C. Heroy, and J.B. Anderson (2006), The death mask of the Antarctic ice sheet: comparison of glacial geomorphic features across the continental shelf, *Geomorphology*, 75, 157-171.
- Wenta, M., & Cassano, J. J. (2020). The atmospheric boundary layer and surface conditions during katabatic wind events over the Terra Nova Bay Polynya. *Remote Sensing*, 12(24), 4160.
- Whillans I.M., and C.J. Van der Veen (1993), New and improved determinations of velocity of Ice Streams B and C, West Antarctica, in *Journal of Glaciology*, pp. 483-490
- Whitworth, T., & Orsi, A. H. (2006). Antarctic Bottom Water production and export by tides in the Ross Sea. *Geophysical Research Letters*, 33(12).
- Whitworth, T., Orsi, A. H., Kim, S.-J., Nowlin, W. D., & Locarnini, R. A. (1998). Water masses and mixing near the Antarctic slope front. In S. S. Jacobs & R. F. Weiss (Eds.), *Antarctic Research Series* (Vol. 75, pp. 1–27). Washington, D. C.: American Geophysical Union.
- Williams, G. D., Aoki, S., Jacobs, S. S., Rintoul, S. R., Tamura, T., & Bindoff, N. L. (2010). Antarctic bottom water from the Adélie and George V Land coast, East Antarctica (140–149 E). *Journal of Geophysical Research: Oceans*, 115(C4).
- Wilson, D. J., Bertram, R. A., Needham, E. F., van de Flieddt, T., Welsh, K. J., McKay, R. M., ... & Escutia, C. (2018). Ice loss from the East Antarctic Ice Sheet during late Pleistocene interglacials. *Nature*, 561(7723), 383-386.
- Wise, M. G., Dowdeswell, J. A., Jakobsson, M., & Larter, R. D. (2017). Evidence of marine ice-cliff instability in Pine Island Bay from iceberg-keel plough marks. *Nature*, 550(7677), 506-510.

- Wright R., Anderson J.B., Fisco P.P. (1983), Distribution and Association of Sediment Gravity Flow Deposits and Glacial/Glacial-Marine Sediments around the Continental Margin of Antarctica. In: Molnia B.F. (Eds.) *Glacial-Marine Sedimentation*. Springer, Boston, MA, pp. 265-300.
- Wright, T. O., 1981, Sedimentology of the Robertson Bay Group, north Victoria Land, Antarctica: *Geologisches Jahrbuch*, v. B41, p. 127-138.
- Wright, T. O., Ross Jr, R. J., & Repetski, J. E. (1984). Newly discovered youngest Cambrian or oldest Ordovician fossils from the Robertson Bay terrane (formerly Precambrian), northern Victoria Land, Antarctica. *Geology*, 12(5), 301-305.
- Yilmaz O (2001) *Seismic data analysis*. IG N.10 Society of Exploration Geophysicists, Tulsa.
- Yokoyama, Y., Anderson, J. B., Yamane, M., Simkins, L. M., Miyairi, Y., Yamazaki, T., ... & Ohkouchi, N. (2016). Widespread collapse of the Ross Ice Shelf during the late Holocene. *Proceedings of the National Academy of Sciences*, 113(9), 2354-2359.
- Yuan, X., & Martinson, D. G. (2000). Antarctic sea ice extent variability and its global connectivity. *Journal of Climate*, 13(10), 1697-1717.
- Zachos, J. C., Quinn, T. M., & Salamy, K. A. (1996). High-resolution (104 years) deep-sea foraminiferal stable isotope records of the Eocene-Oligocene climate transition. *Paleoceanography*, 11(3), 251-266.
- Zecchin M., Octavian C., Rebesco M. (2015), High-resolution sequence stratigraphy of clastic shelves IV: High-latitude settings. *Marine and Petroleum Geology*, vol. 68, pp. 427-437.
- Zickfeld, K., Solomon, S., & Gilford, D. M. (2017). Centuries of thermal sea-level rise due to anthropogenic emissions of short-lived greenhouse gases. *Proceedings of the National Academy of Sciences*, 114(4), 657-662.